The Thesis Committee for Stephen Michael Stacey
Certifies that this is the approved version of the following thesis:

Evaluation of ASTM C 494 Procedures for Polycarboxylate Admixtures used in Precast Concrete Elements

APPROVED BY
SUPERVISING COMMITTEE:

Supervisor:

Raissa Ferron

Kevin Folliard

Evaluation of ASTM C 494 Procedures for Polycarboxylate Admixtures used in Precast Concrete Elements

by

Stephen Michael Stacey

BSCE

Thesis

Presented to the Faculty of the Graduate School of

The University of Texas at Austin

in Partial Fulfillment

of the Requirements

for the Degree of

Master of Science in Engineering

The University of Texas at Austin

May 2016

Acknowledgements

I would like to extend my most sincere thanks to my advisors Dr. Raissa Ferron and Dr. Kevin Folliard for their leadership and encouragement towards research in the field of concrete materials. Dr. Ferron, thank you for your incredible support and trust that you instilled in my work over the past 2 years. Dr. Folliard, thank you for your infections spirit and interest towards research in concrete as well as encouragement towards improving my understanding of my work over the past 4 years. I am also extremely grateful to have such a great mentor and close friend in Dr. Thano Drimalas, who has been there for me in every project venture and through all of my good and "less" good ideas. Dr. Drimalas, you have been instrumental in my academic and career achievements at the University of Texas and I know we will continue working together in the future.

I have to thank my colleague and partner Dr. Fred Aguayo for all of his help with my research. It's been great experience to learn from and work with one of my best friends on something we both love, "concrete." Thank you Gwen for stepping in at the lab, I know the project and research is in good hands! Thank you to everyone at the lab for your help and advice throughout my fellowship there. Thank you Nick, Jose, Racheal, Esteban, Pam, Ricky, Morgan for all of your help with the seemingly endless mixtures and measurements.

Thank you Mike Rung and Sherian Williams for you help and advice! Mike, thank you for your sound advice and experience with all of the lab equipment. Sherian, thank you for still loving me, despite my countless mistakes when it comes to orders and payments.

Thank you to everyone at the 18B CMRG laboratory. For the past 4 years I have felt to know our lab as a family. The friendship and support from each and everyone of you made the work and time spent at the University of Texas one of the greatest times of my life. Thank you.

Lastly, I have to thank my parents, Eric and Becky Stacey. Thank you for all of your endless support over the last 5 years. None of this would have been remotely possible without your prayers and encouragement. Dad, thank you for instilling in me, my technical know how, to build, and always look to build better. Mom, thank you for teaching me that there is never a compromise to hard work. I could never ask for better parents, and I will always continue to make you proud. Love always, ProudUTSon.

Abstract

Evaluation of ASTM C 494 Procedures for Polycarboxylate Admixtures used in Precast Concrete Elements

Stephen Michael Stacey, M.S.E

The University of Texas at Austin, 2016

Supervisor: Raissa Ferron

This thesis presents the investigation towards increasing the understanding of the effect of polycarboxylate (PCE) High-Range Water-Reducers (HRWRs) on the performance of concrete mixtures, with a special focus on concrete mixtures that will be used in precast concrete beam applications. Since the mid-2000's, precast concrete elements at several major precast plants throughout Texas have displayed extensive micro-cracking along their exposed surfaces despite never being subjected to service load conditions. The precast industry's transition from naphthalene based HRWRs to polycarboxylate based HRWRs was identified as a potential culprit for inducing the cracking phenomenon. The admixture qualification standard, ASTM C494, was closely investigated for its relevancy in passing and failing HRWR agents with respect to a mixture's propensity towards the latent observed cracking effect. Key testing procedures

of ASTM C494 were investigated by subjecting mixture designs that had performed both good and bad in the field with respect to micro-cracking. Testing proved that ASTM C494 testing protocols were insufficient and lacking towards predicting the micro-cracking behavior. Therefore, an additional parametric study through concrete and paste testing was created to investigate precast concrete mixture designs and their polycarboxylate admixture influences. The testing program focused on autogenous shrinkage through concrete restrained ring testing and paste analysis via the corrugated tube test. Tests were carried out by introducing different HRWR types and dosages, and quantifying their outlying observed strain effects with respect to one anther. Results have shown that HRWR type and dosage play a vital role in the delay of final set and extent of autogenous shrinkage observed. In addition to the parametric study, a field study was performed in order to correlate the laboratory testing back to the micro-cracking development on concrete elements exposed to natural conditions.

Table of Contents

List of Tables

List of Figures

CHAPTER 1: INTRODUCTION

1.1 DESCRIPTION OF THE PROBLEM

Over the past few decades surface cracking has become more and more apparent on girders produced at precast plants all throughout the state of Texas. Originally the concern was that the cracking was a result of alkali-silica reaction (ASR) and delayed ettringite formation (DEF), yet that theory was dismissed when the cracking did not initiate expansion in field or laboratory cast exposure blocks. The type of cracking seen has been perceived as a map and or micro-cracking pattern, and analogous to all cracks in concrete, it is due to volumetric change; the exact mechanism causing the volumetric changes is not fully understood. The cracks have been labeled as "micro-cracks" as they do not appear to increase in crack width, but rather prove to densify and scatter across the concrete structure. The cracking appears to intensify as the concrete is exposed to the environment (typically apparent in 18 to 24 months after casting). The cracking became a cause for concern when TxDOT's quality control noticed that the map cracking would develop even prior to the girders being put in service, occurring simply by sitting in the precast yard. Although this indicates that the cause of cracking is highly due to a material-related issue, there is still concern that the cracks could lead to the degradation to the beams reinforcement through corrosion and impair the durability, structural performance and service life of the girders.

As a result of the latent cracking that had developed on the girders were subsequently rejected and terminated from future service. These finding have resulted in sizable expenses to the precast producers as well as the state DOT, who has been

responsible for inspecting and researching with regards to the cracking issue on the existing girders currently in service. With ASR and DEF showing not to be the likely cause of the cracking, the investigation began to look at the concrete pathology, in order to see if something had been altered to cause the material related cracking issue. The investigation showed that with precast plants' goal of releasing pre-stressed strands and stripping molds on girders at earlier and earlier times the water-to-cementitious ratio (w/cm) threshold continued to be lowered. This lowering of water addition and increase in cement content called for an even greater increase in water reducing admixture of polycarboxylate superplasticizer agents. Currently, 3/4 of the major precast plants in the state of Texas have begun to experiment and utilize self consolidating concrete (SCC) mixture designs. The incorporation of viscosity-modifying admixtures (VMAs) which are used to minimize segregation has prompted new developments in superplasticizers and therefore created an additional cause for concern with respect to the micro-cracking seen in the field. Despite the wealth of changes that have occurred in mixture designs in the recent decade the course of this research conducted at The University of Texas has targeted the analysis of superplasticizers, specifically polycarboxylate admixtures, addition as the culprit of the volumetric change that are later observed.

The goal of this research was to increase our understanding of the role that superplasticizers, particularly polycarboxylate-based superplasticizers, have on the micro-cracking in precast concrete. A key aspect of this project was to determine the suitability of ASTM C494, Standard Specification for Chemical Admixtures for Concrete, to be used as a tool to screen mixtures containing superplasticizers in order to determine their micro-cracking susceptibility of the mixture (2013). Additionally, an extensive investigation in shrinkage mechanisms, especially autogenous shrinkage, was

conducted. Field surveys of full-scale girders as well as concrete specimens cast at two different exposure sites was also conducted and the impact of exposure conditions on the micro-cracking problem was also taken into account.

1.2 BACKGROUND AND SCOPE

From the second that water is introduced to concrete, the mixture undergoes volumetric changes that will continue to develop over the concrete's lifetime. In the very initial stages of the concrete the volume change is mainly attributed to autogenous and thermal changes. Delayed shrinkage of the concrete is induced by the concrete's exposure to the environment, through drying shrinkage and to a lesser extent, carbonation shrinkage.

The rising concern is that these volumetric changes are occurring far beyond the fresh and fluid state of the mixture and are causing tensile stresses to develop in the concrete much later into the final set state of the mixture. Unfortunately, predicting and modeling the cracking phenomenon in considering all of the concrete system's mechanical properties, creep, size and restrain conditions has yet to be fully understood. In addition, the present knowledge on free deformation effects have yet to be fully understood, as mixture designs and admixtures are continually changing to meet the growing needs of the precast industry.

Since the 1970's, the development of high-performance concrete (HPC) has been a focal point of the concrete industry, allowing designers and contractors to enter an entirely new regime of structural performance. The increasing high cement content mixture designs in conjunction with low w/cm (0.28 to 0.33) and high range water

reducing admixtures made high early strength and long-term durability attainable. Precast production plants continue to develop increasing higher early strengths permitting a shorter timeline for form stripping and and strand release. Concerns for material based onset concrete deterioration was originally thought to have been subsided due to the highly stringent guidelines placed on mixture designs such as with approved aggregate suppliers that have been documented in the Concrete Related Source Quality Catalog [TxDOT 2016].

Despite meeting TxDOT's qualification standards for the prevention of concrete deterioration or cracking related issues the micro-cracking problem persisted. A brief investigation proved that the cracks were not causing any volumetric expansion, and therefore could not be ASR or DEF related. Despite the amount of effort that was put into improving the HPC mixture designs, the drastically decreasing w/cm content and implementation of new portland cements (PC) and high range water reducers has proven to be the ultimate pitfall as it drastically increased the concrete's susceptibility to early age cracking. The micro-cracking issue is still prevalent in the most up to date HPC mixtures. Concrete cast at precast plants less than a year ago shows the develop the micro-cracking all along the concrete's exposed surfaces.

Results have confirmed that the typical 0.28 to 0.33 w/cm ratio ranges implemented at precast plants paired with the need to increase the use of high range water reducers has had a direct influence the high early age shrinkage of concrete. The investigation led by the The Texas Department of Transportation (TxDOT) in conjunction with work performed by The Construction Materials Research Group (CMRG) at the University of Texas at Austin has guided research to target the superplasticizers and specifically the polycarboxylate admixtures as the subject of focus

for eliminating the cracking issue. In this project we examine the performance of actual precast plant mixtures as well as examine the effect of superplasticizer admixture dosage on volumetric changes with respect to shrinkage. The work program was performed in two phases:

- Phase 1 consisted of casting concrete and paste mixtures and testing them against current testing protocol for qualifying admixtures.
- Phase 2 consisted of implementing a series of additional tests with the hopes of better quantifying an admixture's potential for provoking shrinkage cracking.

1.3 CONTENT

The study composed in this thesis has sought out to quantify the precast field observations along with the observed cracking seen at both UT and TxDOT concrete exposure sites in order to distinguish the potential shrinkage causing mechanisms. The research outlined in the following sections has been performed in order to better guide a build of a testing matrix that is capable of testing high range water reducing admixtures and discerning if they are appropriate for future field use according to their shrinkage effects.

This thesis has been segmented into 7 unique chapters. Chapter 2 presents a literature review on the history, development and the potential factors that contribute to the cracking phenomenon. Chapter 2 consists of Task 1, which focused upon gathering information about (1) the use and qualification of polycarboxylates in precast elements, especially precast girders, and (2) cracking observed in precast girders. Chapter 3 describes the materials that were used throughout this project. Chapter 3 outlines the

selections based on Task 2, which focused on the selection of materials and mixture proportions that will be used for ASTM C494 testing and other tests related to the project, and assess key physical, chemical, and mineralogical properties of the constituent materials. Materials were selected based upon their past and continued use at two major pre-cast plants in Texas.

Chapter 4 outlines Tasks 3-4, testing procedures performed in the laboratory to identify and single out the driving proponent of the cracking phenomenon with respect to the different admixture dosages and actual precast plant mixture designs. The work performed made use of the existing protocol for testing admixtures qualification, ASTM C494, in concrete mixtures through drying shrinkage, compression, time of set, and water content measurements.

Chapter 5 describes the testing program and equipment employed for testing pastes and concrete mixtures through an amended testing procedure series that quantifies a mixture's shrinkage and cracking response. Paste testing included autogenous shrinkage through volumetric, linear and visual inspection, and concrete testing included restrained autogenous shrinkage testing.

Chapter 6 presents the research related to field exposure specimens including precast plant visits, exposure site visits, large cast exposure blocks and carbonation front ingress for long term monitoring. Mixtures were either cast in the lab conditions or in the field and selected to mimic actual precast mixtures as well as mixtures with varying admixture dosages to identify superplasticizer's potential cracking effect in the field. Similar mixtures were also selected and monitored at the TxDOT exposure site and a visual examination and scale of cracking deterioration was developed.

Chapter 7 summarizes key findings in this thesis and makes recommendations for future research and testing.

CHAPTER 2: LITERATURE REVIEW

2.1 INTRODUCTION

The following chapter provides a history as well as a literature review with regards to concerning shrinkage mechanisms that may be leading to the development of the map cracking phenomenon plaguing precast elements in the state of Texas.

2.2 CRACKING HISTORY

Since the 1990's TxDOT has been working intensely to create a prescriptive based means of preventing ASR and DEF in concrete structures. Since the early 2000's, TxDOT, along with research based out of the University of Texas at Austin helped to develop a matrix to identify aggregates prone to ASR as well as setup a system for mitigating ASR in concrete. Yet even after the introduction of the ASR mitigation techniques a map cracking pattern type of distress still developed on several girders in TxDOT's producer pre-cast plant yards.

The cracking was originally discovered by TxDOT's quality control department that had been directed to monitor pouring and handling of precast girders at a New Braunfels plant. While several girders that were left in the "bone yard" waiting to be put into service significant map cracking had developed on the surface on both the flange and web sections of the girders. Figure 1 from a precast plant in Waco shows a sever case of micro-cracking seen in the field.

Figure 1: Micro-cracking focused on the top flange of a precast girder at a Waco Plant

The girders were subsequently rejected and a funded investigation was setup by the Federal Highway Administration (FWHA) ASR Development and Deployment Program. This investigation was led by Dr. Kevin Folliard with the University of Texas at Austin, Dr. Michael D.A Thomas with the University of New Brunswick, and Dr. Benoit Fournier with Laval University in order to determine the root cause behind the observed cracking. While the cracking pattern showed to be indicative of ASR the conclusions

based upon petrographic analysis of cores pulled from several girders indicated no significant signs of ASR deterioration mechanisms.

Recently more rejected girders for other TxDOT projects have emerged in various precast plants across Texas, but the original 4 that led to this study were composed of straight cement mixtures ranging from 0.33 to 0.35 w/cm apart from one that contained 20% replacement of the cement with Class F fly ash. ASR lab analysis paired with field exposure blocks indicates that the observed cracking was not the result of ASR. Although the testing ruled out ASR as the deleterious mechanism the same distinct micro-cracking developed on the ASR exposure blocks as pictured in Figures 2-3. Through standard ASR casting procedure ASTM C1293, Standard Test Method for Determination of Length Change of Concrete Due to Alkali-Silica Reaction, the exposure blocks were cast as straight cement mixtures ranging from 0.42 to 0.45 w/cm (2015).

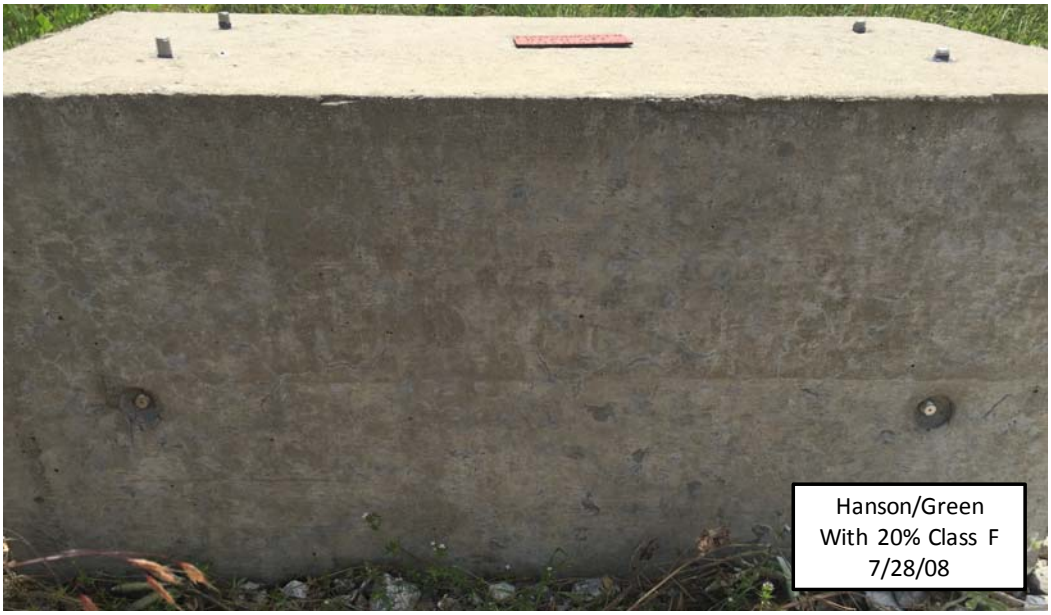

Figure 2: Precast plant exposure block replicate cast according to ASTM C1293 0.42 w/cm and 20% Class F fly ash

Figure 3: Precast plant straight cement exposure block replicate cast according to ASTM C1293 0.45 w/cm

Replicate exposure blocks were cast at UT using concrete mixtures ranging from 0.28 to 0.42 w/cm through graduate researcher Nicolas Tiburzi's work outlined in his master's thesis, "Evaluation of volume changes and cracking potential of low water-to-cementitious material ratio concrete mixtures" (Tiburzi 2015).

Currently, the work performed at the University of Texas has stemmed from the visual observation reported over the last several years at nearly all of the high production precast plants in Texas. Research led by Dr. Folliard and Dr. Drimalas has been focused on evaluating the volumetric changes the concrete related to the use of varying superplasticizers and dosages employed at precast plants.

2.3 SHRINKAGE TESTING

Shrinkage and expansion of concrete after final set is the main driving force that leads to cracking. Stresses associated with volume changes are even further exacerbated when the concrete is set in a fixed or restrained system. Since the micro-cracking issue ensued on un-serviced girders and exposure blocks without any external loading or restrain the list of testing procedures purely target material based issues based on early and latent shrinkage of concrete. The following section outlines the four main mechanisms responsible for shrinkage according to their differential effects and period: chemical, plastic, drying and carbonation shrinkage (Grube 1991).

2.3.1 DRYING SHRINKAGE

2.3.1.1 Definition and Mechanisms

Drying shrinkage is the volume change in concrete induced by external evaporation of internal water in hardened concrete, and can take place over the lifetime of the structure. Where shrinkage onset by the internal evaporation of water in the concrete's fresh state due to the heat of hydration is referred to as autogenous shrinkage (see Section 2.3.2), drying shrinkage is only applicable in an unsealed system. Drying shrinkage will only occur if the concrete is exposed to an environment exhibiting a relative humidity lower than the one in the concrete's pore system (Mehta and Monteiro 2006). Drying shrinkage is exacerbated when the amount of water introduced into the mixture is much greater than the amount needed for hydration of the concrete (Neville 2002). This is because the excess water that is added for workability does not contribute to creating hydration products. Thus this water is not chemically bound and therefore is

susceptible to drying induced shrinkage for the bulk of the concrete (Mehta and Monteiro 2006).

Following the curing period, the exposure temperature and relative humidity acts in a wicking action, drawing water out of the concrete until an equilibrium between the concrete and holding environment is met. Concrete is a porous material; when water is added to the system shrinkage or swelling will occur depending if there is the water that can leave or enter the pores (Acker 2004). The extent of drying shrinkage is not only dependent on the evaporable water in the system but also to the pore size distribution as this governs the different transportation mechanisms for moisture migration. These mechanisms may act simultaneously within the drying material (Kropp et al. 1995) and include permeation due to a pressure head, diffusion due to a concentration gradient, capillary suction due to surface tension acting in the capillaries, or adsorption-desorption phenomena, involving fixation and liberation of molecules on the solid surface due to mass forces. The capillary tension, surface tension, disjoining pressures, and movement of interlayer water mechanisms are described in detail in Section 2.3.2.1. These different mechanisms can act simultaneously and will occur depending on which requires the least amount of work.

Aggregates in concrete are less effected by the drying effect in the system. Therefore, a greater aggregate content mixture will limit the total shrinkage of the system (except in the instance of lightweight concrete). Aggregate acts further to reduce the drying shrinkage effect by restricting shrinkage of the overall concrete, however the extent of restricting shrinkage is dependent on the aggregate's creep resistance, permeability and stiffness (Bisschop and van Mier 2002) (Lura & Bisschop 2004).

2.3.1.2 Testing

ASTM C157, Length Change of Hardened Hydraulic-Cement Mortar and Concrete, was utilized as per requirements of ASTM C494 to determine the length change in concrete as a result of drying shrinkage (2014). The test provides comparative measurements for volumetric expansion or contraction of concrete due to causes other than physically applied forces or fluctuations in environmental temperature. ASTM C494 mandates that the admixture in testing does not meet ASTM C494's specifications if the length change of the specimen at 14 days of drying relative to the reference bar is greater than 0.010 percentage units. This testing procedure was used as a means of approving certain admixtures and concrete mixtures for further testing.

ASTM C192, standard practice for making and curing concrete test specimens in the laboratory, procedures consists casting samples in rigid prism molds, where two lifts are performed (continuous pour in the case of an SCC mixture design) and gage studs are fixed at both ends of mold. After casting is complete the prisms are set in a curing room that is in accordance with ASTM C511, standard specification for mixing rooms, moist cabinets, moist rooms, and water storage tanks used in the testing of hydraulic cements and concretes, until 23½ ± ½ hour and subsequently demolded (2013). After demolding, the specimens are placed into a 23 ± 0.5 °C saturated lime water bath for approximately 30 min to aid in eliminating length change associated with thermal variation. At 24 ± ½ hour, the specimens are removed from the water bath, excess water is wiped away and the initial comparator and weight readings are taken. After this initial reading the specimens are placed back into the saturated lime water bath at 23 ± 0.5 °C for an additional 27 days. Thus, the total curing time is 28 days, including the first day of curing. At the end of the curing period the specimens are measured for a second time in

the comparator and placed into a drying room on cooling racks with at least 25 mm of clearance on all sides of the specimen. The drying room is maintained at a 50 ± 4 % RH with continuous air flow as well as a constant 23 ± 2 °C room temperature. Measurements are then taken in the comparator at 4, 7, 14, 28 days and 8, 16, 32, and 64 weeks after the initial 28-day curing period. The length change percentage, ΔL_x, is calculated as follows:

$$\Delta L_x = \frac{CRD - Initial\ CRD}{G} * 100\% \qquad \text{Equation 2-1}$$

where CRD is the difference between the comparator reading of specimen and the reference bar, and G is the length separation between inner gage faces embedded in the concrete specimen. In addition to length change, measurements with respect to mass change of the prism over time are also taken and calculated in a similar fashion.

2.3.2 AUTOGENOUS DEFORMATION AND CHEMICAL SHRINKAGE

2.3.2.1 Definition and Mechanisms

Although drying shrinkage is a believed to be a cause for concern with respect to this reoccurring cracking phenomena, preventative measures in design and construction have assured that drying shrinkage is minimized in the construction of the precast concrete and laboratory duplicates. With the micro-cracking issue still proving to develop in mixtures cast under laboratory conditions, this study has been led to investigate additional causes for dimensional changes with regards to autogenous shrinkage,

Autogenous shrinkage, a subset of chemical shrinkage which comprises all non-thermal volume changes due to hydraulic reactions in cementitious systems (Davis 1940) (Tazawa 1999). Unlike plastic and drying shrinkage, which are entirely dependent on environmental exposure, autogenous shrinkage occurs regardless of how much water is released into the surroundings. Because autogenous shrinkage occurs out of an internal lack of water, it produces a more uniform form of bulk shrinkage on the concrete as compared with plastic and drying shrinkage. Despite the autogenous shrinkage mechanism being clearly defined for half a century the interests with its potentially harmful effects came back into light with the development and extensive use of high performance concrete (HPC). Although HPC has been a positive advent for the concrete industry through increasing concretes strengths, durability and speed of construction, it has also raised concern with respect to cracking that could only be interpreted by restrained autogenous shrinkage (Tazawa 1992) (Sellevold 1995). HPCs are typically classified as mixtures with increased binder content, incorporation of silica fume (or other pozzolans), low w/c ratios (<0.40) and use of superplasticizers (Bentz and Jensen 2004).

The lack of water in the system causes the reaction products formed during hydration of cement to occupy less space than the original reactants via dissolution precipitation process (Le Chatelier 1900; Barcelo et al. 2005; Jensen and Hansen 2001; Lura et al. 2003). This process where the hydration products have smaller absolute (non-porous) volume than the anhydrous cement and water is included in the chemical shrinkage mechanism, which is the overall reduction of solid and water volume in in the plastic state of the paste (Powers 1946; Locher 2000). Figure 4 provides a diagram of how autogenous shrinkage is developed as a part of chemical shrinkage. When water is

unavailable to fill the empty pores that are created via chemical shrinkage, self-desiccation ensues and is defined by autogenous shrinkage (Tazawa 1999; Jensen 2001). Autogenous shrinkage is shrinkage that is not due to thermal effects, external loads or restraints, loss of moisture to the environment (Lynam CG 1934).

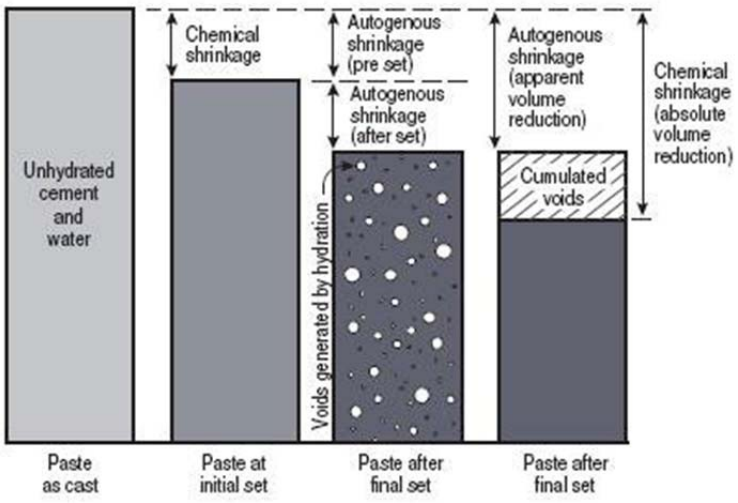

Figure 4: Autogenous shrinkage as a function of chemical shrinkage for volume change in paste. Not to scale (D'Ambrosia)

Autogenous shrinkage is extremely dependent on the w/c ratio and the shrinkage effects become even more distinct when the w/c ratio is brought below 0.35, which is well below the 0.28 – 0.33 w/cm ratios that is employed across Texas precast plants. Autogenous shrinkage can prove to be more damaging as it occurs more uniformly throughout the system apposed to drying shrinkage as it begins to take effect early on in the fresh state of the paste when the concrete has not fully developed preventative mechanical properties such as modulus of elasticity (Dela BF 2000).

Through the creation of the highly dense C-S-H gel reaction product gel pores form and occupy the space of the original hydration products (Powers and Brownyard 1946; Locher 2006). The drying out of the pores begin with the larger pore sizes. The progressive drying out of evaporable water causes capillary forces to draw water from saturated to less saturated areas. The pore size structure of concrete may be broken into two factions: capillary and gel pores. Capillary pores are significantly larger (10,000 to 10 nm), whereas gel pores with evaporable water are sized from 10 to 0.5 nm (Mindess et al. 2002). Yet it is the smaller gel pores that contain what Powers and Brownyard have defined as evaporable water and promote chemical shrinkage within cement paste due to the development of capillary pressures (1946). In order to quantify the capillary stresses that are subsequently created by this internal drying process the Kelvin equation (Equation 2-2) has been developed as a function of the pore size, relative humidity and temperature:

$$RH_K = \exp[\frac{-2\gamma M cos\theta}{\rho r RT}] \qquad \text{Equation 2-2}$$

Where γ: surface tension, M: molar weight of the fluid, θ: contact angle (0° for complete wetting), ρ: density of the fluid, r: radius of meniscus, R: ideal gas constant (8.314 J/mol*K), T: absolute temperature (K). The equation indicates that as the pore size decreases, the humidity threshold also decreases and as the pores become less saturated the humidity also decreases (Czernin 1977; Jensen and Hansen 1995). Figure 5 provides a logarithmic scale of Kelvin equation proving a pore's internal relative humidity dependence with respect to its pore size (Holt 2001).

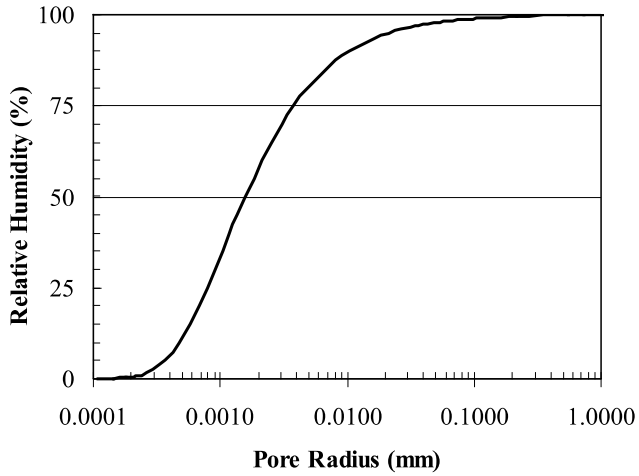

Figure 5: Pore relative humidity dependence on pore size, based on Kelvin's Equation ($T_{Constant}$=20°C) (Holt 2001)

The capillary pressure or negative pressure, σ_{cap} (Pa), that increases with decreasing pore radius is calculated via the Young Laplace equation (Equation 2-3). This capillary pressure causes the menisci to extend the tension into a compression force on the cement paste inducing what is called self-desiccation or autogenous shrinkage of the concrete.

$$\sigma_{cap} = \frac{2\gamma \cos(\theta)}{r} \qquad \text{Equation 2-3}$$

To better describe this equation, Figure 6 shows that with increasing pressure between two cement particles the pressures on the convex side of the menisci prove to be lower than the concave side (atmospheric pressure) and evaporable water (W) exits the system even prior to the bleed water (W_s) (in this instance) (Radocea 1992).

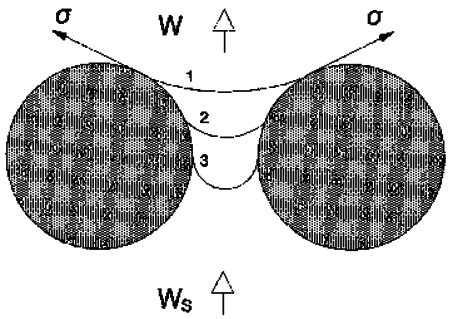

Figure 6: Stresses pulling the water meniscus lower between two cement particles due to moisture transfer and capillary pressure development. [Radocea 1992]

Strain is typically used to quantify the extent of which shrinkage occurs in the concrete and therefore Equation 2-4 (Bentz and Jensen 2004) may be considered more useful than Equation 2-3 since strain measurements can be calculated directly.

$$\varepsilon = \frac{S\sigma_{cap}}{3}\left(\frac{1}{K} - \frac{1}{K_S}\right) \qquad \text{Equation 2-4}$$

Where s: degree of saturation of the cement paste, K: bulk modulus of the paste, and K_s: is the bulk modulus of solid framework inside the cement paste. The extent of self desiccation is dependent on the stiffness and viscoelasticity of the paste surrounding the pores.

2.3.2.2 Testing

2.3.2.2.1 Chemical Shrinkage

Chemical Shrinkage commonly measured on the basis of the degree of hydration of the cementitious materials and the volume change of the paste that coincides with that

process. Although chemical shrinkage is very difficult to differentiate from autogenous shrinkage in physical testing due to its overlap, there are a number of methods that have been developed to measure the different mechanisms including: volumetric method (dilatometric), density method (pycnometric) and buoyancy method (gravimetric). All of which measure how much water enters the cement system, either by visual inspection or increasing weight through increasing water demand of the sample. The volumetric and density methods are the two most commonly used methods and closely correlate to the ASTM C1608, Standard Test Method for Chemical Shrinkage of Hydraulic Cement Paste (2012).

A photograph of the volumetric method setup is shown in Figure 7. The paste sample consisting of a specified height (5 to 10 mm) is placed in a glass vessel that is set in a 23 °C water bath to achieve isothermal conditions. The sample is permitted to have access to infinite de-aired water over the lifetime of the test. Furthermore, an oil barrier at the top of the water level in the graduated capillary tube is used to prevent evaporation and provide a better indication of the extent of water demand recorded by the visual data logging equipment.

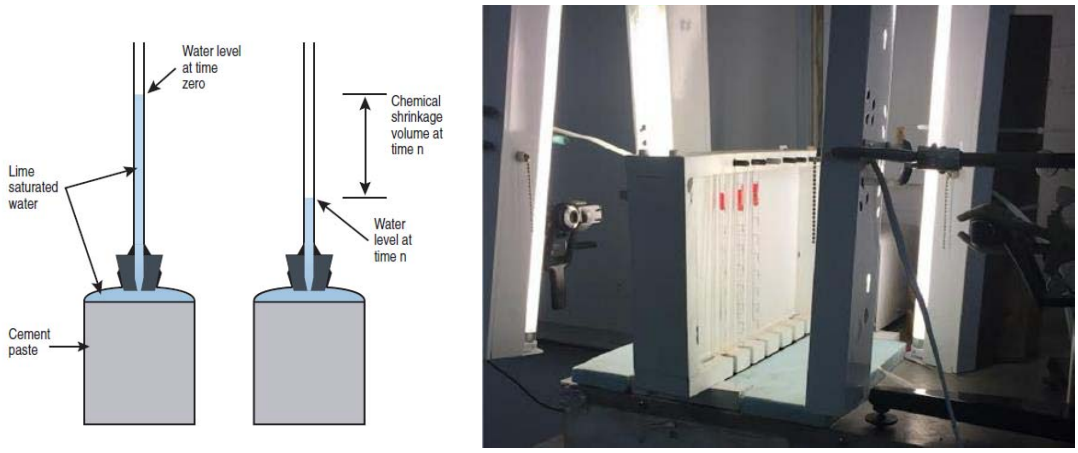

Figure 7: Diagram and automated setup of the dilatometry method used for measuring chemical shrinkage (Kosmatka 2008)

ASTM C1608 standard specifies measuring the changes in pipet level every 30 minutes to an hour for the initial 8 hours of testing, and periodically for the remaining 24 hours. The benefit of the automated system is that the entire development of the chemical shrinkage can be measured and so a period of 14 days with measurements taken every 3 minutes is employed at The University of Texas at Austin. Lastly, to calculate chemical shrinkage as a function of time (t) the following equation is used:

$$CS(t) = \frac{h_x - h_o}{M_{Paste}} \qquad \text{Equation 2-5}$$

Where *CS(t)* is the chemical shrinkage measured in mL/g cement at a particular time, ho is the height of the water in the graduated capillary tube in (ml) at 60 minutes after the introduction of water to the cement and h_x is the height at the time of interest and M_{Paste} is the mass of the sample (g).

Gravimetry, the buoyancy method, utilizes a scale that measures the samples change in water absorption over time. As the sample takes in additional pore solution the total volume of the weighed sample is decreased and the mass is subsequently increased, as per the principles of buoyancy. Figure 8 demonstrates the setup employed for isolating the paste sample and measuring the introduction of water into the sample.

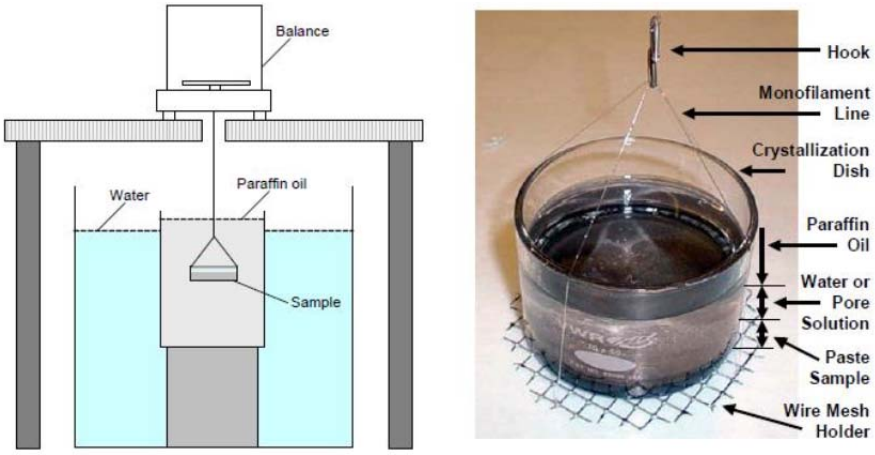

Figure 8: Diagram and photograph of the buoyancy method used for measuring chemical shrinkage (Sant et al. 2006).

Similar to the volumetric method the buoyancy method casts the paste in a glass container offering infinite de-aired water just above the sample with a layer of paraffin oil just above the water to prevent evaporation into the environment. Automated recordings from the scale are performed over the length of the test. The following equation is used to calculate the chemical shrinkage over a given length of time:

$$CS(\Delta t) = \frac{M_x - M_o}{M_{cem} * \rho_{oil}} \qquad \text{Equation 2-6}$$

Where M_x is the mass recorded taken at a particular time(g), M_o is the mass taken 30 minutes after the introduction of water (g), M_{cem} is the mass of cement for the given sample (g) and ρ_{oil} is the density of the paraffin oil (g/ml).

2.3.2.2.2 Autogenous Deformation

Autogenous deformation is defined as the bulk or visually observed volume change of the cement paste due to lowering of the internal relative humidity (Jensen and Hansen 2001). Chemical shrinkage and autogenous shrinkage have been proven to develop the same until final time of set (Tazawa 1998). Due to the nature of the chemical shrinkage testing requiring unlimited access to water to enter the system (i.e., it is considered an open system), chemical shrinkage testing cannot differentiate from the effects of autogenous shrinkage in the early material age. Yet because autogenous shrinkage does not permit the introduction of water into the pore spaces, autogenous testing subject specimens to a closed system measuring only external volume changes. Figure 9 depicts the development of autogenous shrinkage versus chemical shrinkage for cement paste. Note that the concern for collecting strain data does not typically begin until initial set of the cement is determined, only there after is structure prone to non-plastic stress and crack development.

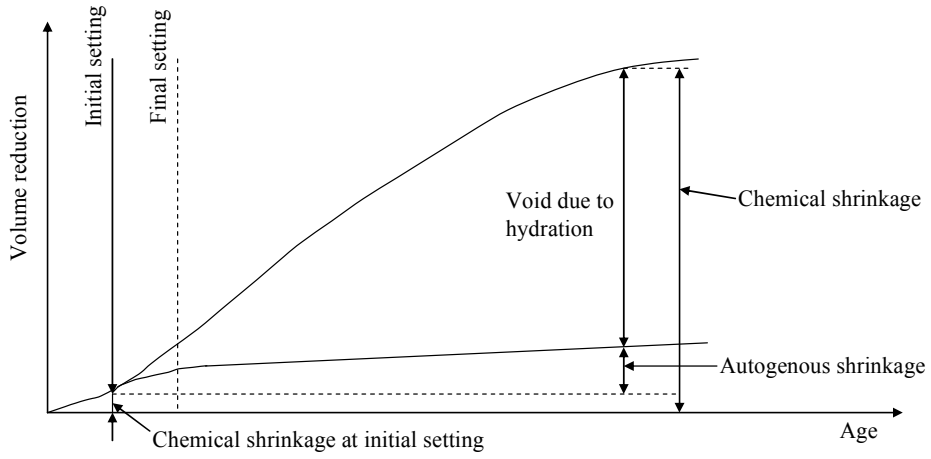

Figure 9: Autogenous shrinkage and chemical shrinkage overlap as depicted by Japan Concrete Institute (Tazawa, 1998)

Two main testing options are utilized to quantify autogenous shrinkage and the strain: volumetric strain and linear strain. The volumetric method employs a sample suspended from a scale that monitors the change in weight over time via the buoyancy principle. Cement paste (typically 100-150 g) is cast into an elastic membrane consisting of a non-latex condom. Sufficient agitation is applied to the paste held in the condom to draw out any entrapped air. The membrane is neatly tied off with a zip tie to assure that the paste is held in a completely sealed system. The weight of the paste (note that the membrane weight, zip tie, etc is not included) is recorded and then the sample is strung from a hook on the bottom side of the scale. A diagram of the setup alongside a photograph of a two sample setup that is employed at the University of Texas is shown in Figure 10.

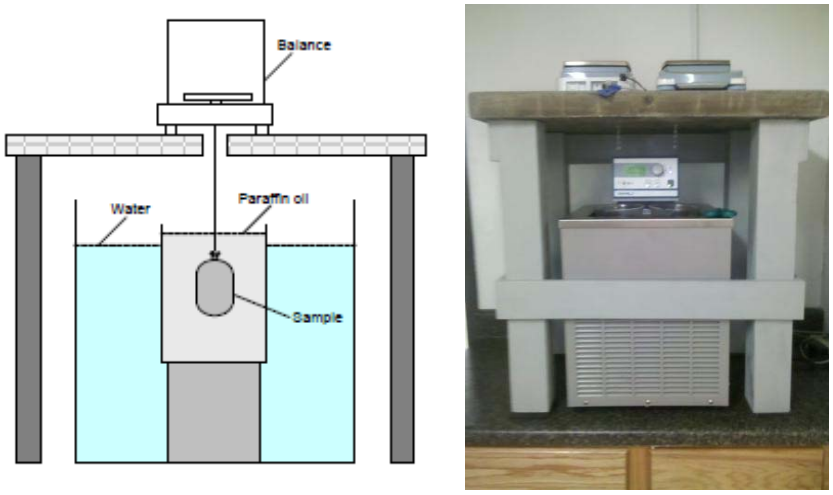

Figure 10: Diagram and photograph of the volumetric method used for measuring autogenous shrinkage (Sant et al. 2006).

The sample is suspended into a beaker filled with paraffin oil in order to further assure the paste is in a closed system and the condom does not allow any update of moisture. The increased density of the paraffin oil eliminates errors associated with absorption of moisture into the paste through the membrane (Lura and Jensen 2005). The beaker also allows for the samples to sit in the temperature controlled water bath at 23 °C without being disturbed by the vibrations the water bath's pumps create. This test setup allows for measurements to begin just minutes after the introduction of water to the cement to assure isothermal conditions and eliminate temperature deformation effects. Measurements are recorded via a data recording software that pulls the instantaneous weight provided on the scale with a measurement sensitivity of 0.01 g every 60 s. After the conclusion of the test, the paste is measured again to determine if any paraffin oil was absorbed through the membrane over the duration of the test. If the sample weight change was in excess of 0.02 g the data is discarded. The volumetric stain, ε_{vol}, for the paste is calculated as follows:

$$\varepsilon_{vol} = \frac{\Delta V_{paste}(t)}{V_{paste_o}} = \frac{W_{sub}(t) - W_{sub_o}}{\rho_{oil} * V_{paste_o}}$$ Equation 2-7

Where ΔV_{paste}(t) (ml) is the change in volume at any time t, V_{paste_o} is the volume of the paste taken 30 minutes after the water addition, $W_{sub}(t)$ (g) is the weight of the submerged paste at time t, W_{sub_o} (g) is the weight of the submerged paste taken 30 minutes after the water addition, and ρ_{oil} is the density of the paraffin oil (g/ml). The volumetric strain accounting for shrinkage in the x, y, and z direction and isotropic conditions may be converted into linear strain for comparison to other testing methods:

$$\varepsilon_{lin} = \frac{\varepsilon_{vol}}{3}$$ Equation 2-8

Although the volumetric technique is a cost effective alternative to other autogenous testing methods the technique is somewhat more laborious due to errors associated with pressures exerted by the membrane, reabsorption of bleeding water and entrapped air in the sample (Hammer 2002) (Douglas and Hover 2002) (Lura and Jensen 2005). The use of paraffin oil has also not completely removed the error associated with absorption as the oil can still present itself as additional weight on the membrane itself (Bouasker, Moutnanga, Cou`e and Khelidj 2008).

The linear method using the dilatometer was run along side the the volumetric method to extend the validity of the new corrugated tube method employed at the University of Texas. The corrugated tube test has been standardized under ASTM C1698,

Standard Test Method for Autogenous Strain of Cement Paste and Mortars (2009). The linear method permits the use of mortar or cement paste to be cast in a rigid module with minimal friction, an example of which is shown in Figure 11. The concept behind the corrugated tube was developed by Jensen and Hansen 1995, to transform the volumetric deformation into a linear length change.

Figure 11: Corrugated polyethylene autogenous test setup (Germann Instruments)

A caveat of the existing ASTM standard is the use of displacement indicators or linear variable differential transformers (LVDT) all supply a normal force on the end of the tube and therefore cannot take measurements of autogenous shrinkage of the cement at the plastic stage (Tian and Jensen 2005). Indicators widely used on hardened cement pastes such as the Mitutoyo length gage employs as much as 2.5 Newtons in order to make sufficient contact with the sample in question. Likewise, the vertical measurement method may not be used to accurately measure pure autogenous shrinkage because of the error associated with influence of gravity force on the shrinkage of the tube (Bjøtengaard and Hammer 2004).

In order to increase the measurement precision for autogenous shrinkage of cement paste at a very early age, the corrugated tube system was improved through the use of a non-contact LVDT sensor (Gao, Zhang, Luo, Wei and Yu 2013). Continuous measurement of samples paired with non-force protruding measurement indicators confirmed the most accurate and least scatter in the collected data. Measurements are taken at minute intervals for a 24-hour period immediately after the sample is placed into the testing apparatus. Strain measurements are calculated using the following equation:

$$\varepsilon_{AS} = \left(\frac{S_t}{L_o}\right) * 100\% \qquad \text{Equation 2-9}$$

Where St is the displacement of the tube at time t, L_o is the initial length of the paste. This form of test setup combats the issues associated with the current ASTM C 1698 standard, which only initiates measurements at the age of final set and daily increments then there after.

Lastly, an autogenous shrinkage testing procedure was created to simply distinguish a paste's propensity to cracking with respect to time. The test was purely visual based, where the user would inspect the paste samples to determine if cracking had occurred. The test method was heavily influenced by work performed by Lura et al. (2008). The work performed by Lura et al. called for small cylindrical paste samples cast with different seized steel rods placed in the middle acting as the potential aggregate sizes that are commonly used in HPC. The work was based upon previous work performed by Dela, who investigated the stress development around spherical ceramic aggregate (Dela 2000). As well as work from Pease, who examined stress development cracking behavior

around cylindrical aggregate (Pease, Neuwald, Weiss 2003). However, the use of stainless steel rods was preferred over the use of rock because of the mechanical properties and surface characteristics of steel rods are better defined and more reproducible than rock. Paste was cast into silicone molds with steel bars with sizes of 1.5, 3 and 6 mm each providing differential restraint for the autogenous shrinkage effects in the paste leading to crack development. Figure 12 provides a diagram of the paste sample and the potential crack development that stems from the steel bar restraint.

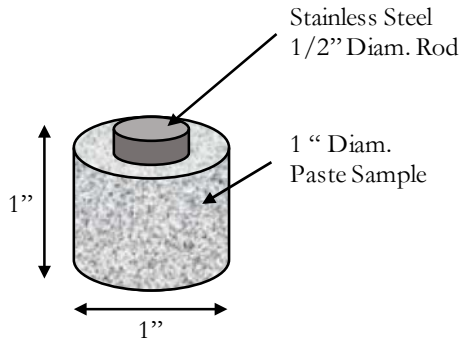

Figure 12: Diagram of paste sample sizing surrounding steel bar to encourage autogenous cracking

Small sample sizes were selected to decrease thermal gradient as well as external restraint during the setting process. Precautions were taken to assure complete isothermal conditions throughout the preparation process as well as throughout the entire testing duration. The samples were held in watertight glass containers and subsequently submerged in a water bath held at 32 ± 0.2 °C for a 1-month period. After which, the samples were subjected to gallium intrusion. The gallium was forced into the cracks of the sample to emphasize the size and location of the cracking that was the resultant of

autogenous shrinkage. Thereafter, the samples were prepared for analysis via scanning electron microscopy (SEM). The gallium served to accentuate cracks that had developed around the stainless steel bar from autogenous shrinkage, but not the cracking that was incurred during sample preparation for SEM. The study revealed that larger that steel rods embedded in the paste encouraged larger autogenous shrinkage effects and thus more substantial crack widths (Lura, Jensen and Weiss 2008).

2.3.3 PLASTIC SHRINKAGE

2.3.3.1 Definition and Mechanisms

The plastic shrinkage mechanism is one that can be easily minimized, and yet still persists in the industry as a result of negligence or lack of knowledge regarding the potential damaging effect on the durability of the concrete of plastic shrinkage. Plastic shrinkage cracking generally occurs in structures that have large surface area to volume ratio of concrete or experience excessive evaporation during the plastic stages due to environmental conditions (Al-Fadhala and Hover 2001; Almusallam et al. 1998; Cohen et al. 1990; Kwak and Ha 2006; Shaeles and Hover 1988). In instances where the concrete is exposed to poor curing conditions, low relative humidity (RH), high winds and/or high temperatures, free water is wicked up to the surface of the concrete encouraging excessive bleeding. Continual evaporation of the wicked water on the concrete's surface creates a vacuum similar to the one discussed in section 2.3.1 via the Young-Laplace equation and Figure 6 of this thesis. The negative capillary pressures build up is the main mechanism that causes plastic shrinkage cracking (Slowik et al. 2008) (Wittmann 1976). Once excessive evaporation has taken place the meniscus separating the particles

becomes too small and air is permitted to enter the paste. This process is defined as the time of air entry, and is the sole mechanism that drives the plastic cracking phenomenon (Slowik et al. 2008). Plastic shrinkage cracking will only occur in locations where this air entry has occurred provided there is sufficient restraint of the concrete structure to facilitate cracking (Holt and Leivo 2004) (Kronlof et al. 1995) (Radocea 1994).

Other parameters can serve to further promote or demote the effects of plastic shrinkage with respect to the mixture design and mixing procedures. Aggregate shape and size, SCM use and, cement content can play a role in the concrete's bleeding rate. HPC is highly susceptible to plastic shrinkage cracking due to its lower w/c ratio, and bleeding is reduced due to the dense microstructure that results from the the high cement content and increased fines (e.g. silica fume) usage. (Dao et al. 2010) (Mora-Ruacho et al 2009) (Lura et al. 2007). The Young-Laplace equation (Equation 2-3) further confirms that mixtures containing finer cement and silica fume are more susceptible to plastic shrinkage cracking (Cohen 1990).

Plastic shrinkage has also shown to perpetuate along elevated or near surface reinforcement or changes in cross section thickness of the concrete (NRMCA, 1998). This anomaly has been attributed to differential paste and aggregate settlement, and therefore plastic shrinkage is not common in low slump or properly consolidated concrete mixtures (Powers 1968) (Weyers et al. 1982) (Qi et al. 2003). Evaporation of bleed water is also a factor that can promote plastic shrinkage since the evaporation encourages a thermal dilation differential to occur between the surface of the concrete and the bulk concrete in the plastic stages. Simpkins and Kolver verified that increased cooling over the concretes surface occurs during evaporation causing a thermal gradient (Simpkins 1986) (Kolver 1995).

2.3.3.2 Testing

The most common testing practice for evaluating plastic shrinkage cracking is ASTM C1579 – Standard Test Method for Evaluating Plastic Shrinkage Cracking of Restrained Fiber Reinforced Concrete (Using a Steel Form Insert) (2013). The test method provides drying and restraint conditions that can lead to increased understanding of how concrete mixture proportioning impacts drying shrinkage cracking. Figure 13 shows a schematic of the testing rig that the concrete is tested in. Stress risers perpetuate differential settlement of the concrete and restraining bars both aid in driving the plastic shrinkage reaction.

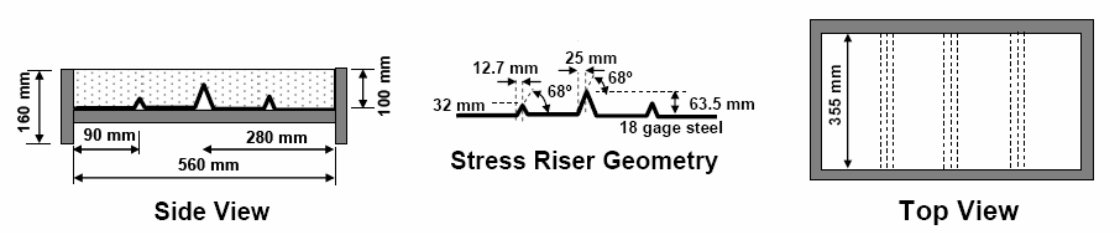

Figure 13: Diagram of Specimens used for plastic shrinkage evaluation (ASTM C 1579 – 13)

Samples are placed in a climate and humidity controlled chamber that maintains a constant temperature of 36 ± 3 °C and a RH of 30 ± 10%. A fan capable of maintaining minimum evaporation rate of the bleed water must also be a part of the system. The test is run for a period of 24 hours after the introduction of water, during which, a scale set to collect mass loss in the concrete from the moisture loss at 30 min intervals with a

minimum 5-gram resolution. Lastly, evaluation of the crack width is measured at the conclusion of the test.

2.3.4 THERMAL DEFORMATION

2.3.4.1 Definition and Mechanisms

As the cementitious elements in concrete react with the mixing water an exothermic reaction occurs and there is a spike in the heat development (Stage I – Initial Hydrolysis). After which, the induction period (Stage II) takes place where the heat of hydration is lowered and plateaued. The heat of hydration is then spiked in the acceleration period (Stage III) followed by a subsequent drop in the heat of hydration, where the atmosphere can begin to further interact with the concrete, eventually bringing the paste and/or concrete to an equilibrium with the environment (Stage IV and V Induction Period and Steady State Period). Thermal deformation and stresses are a large cause for concern in mass concrete structures, where the temperature gradient between the surface and the bulk concrete can create a substantial thermal shock causing large cracking that will run parallel to the reinforcement (NRMCA 2009). In addition, reinforcement held within the concrete or external restraints can also serve as stress and strain inducing elements that produce additional thermal stresses on the concrete. However, cracking will not occur if the thermal stresses develop do not exceed the current tensile strength state of the concrete.

Literature has shown to be in steadfast agreement with respect to the correlation of coefficient of thermal expansion (CTE) on the moisture content and the existence of time-dependent deformations (DD) related to temperature-induced redistribution of

moisture in the pore system (Sellevold and Bjøtengaard 2006). Mechanisms associated with thermal deformation of cement paste have been broken into three categories (Bazant 1970):

- Pure thermal dilation (due to thermal dilation of constituents)
- Thermal shrinkage or swelling (due mainly to a difference in latent heats and entropies between the diffusible layers and free absorbed water layers)
- Hygrothermic dilation (due to change in humidity of water vapor in the pores at a constant water content)

Pure thermal dilation is described as the effect when the accelerated temperature period (Stage III) is followed by an isothermal period, resulting in quick expansion and immediate deformation (ID). This process is then followed by a time dependent contraction period (DD), where the newly created capillary stress as a result of the higher CTE of water compared to solids in the pores is dissipated by the flow of pore solution to the environment or surrounding pores. Therefore, the DD mechanism acts negatively and represent a recovery of the ID thermal dilation (Bazant 1970). It has been shown that the permeability of the paste as well as the pore-to-pore distance play a role in the pressure releasing rate and ID may be taken as CTE or as DD (Scherer 2000) (Ai et al. 2001).

The second mechanism, thermal shrinkage or swelling, is a part of delayed dilation, caused by the latent heat contrast between the water present in small pores (lower entropy) and larger free absorbed pores (higher entropy) (Bazant 1970). The process works as follows: with the increase in temperature there is a subsequent decrease of free energy with the small pores as compared with the larger free absorbed pores due to the higher latent heat of absorption. As the water begins to flow out from the smaller

pores the deformation begins to recover in order to establish equilibrium and shrinkage occurs (Bazant 1970) (Sellevold and Bjøntegaard 2006).

The third mechanism, hygrothermic dilation, is the change in relative humidity caused by change in vapor pressure as a result of a change in temperature. The RH effects act within the ID due to the fast acting deformation. An increase in temperature leads to the expansion of water held within the pores, increasing the radii of the meniscus leading to a greater air-to-water surface area and therefore an increase in the RH (in accordance with the Kelvin equation) (Sellevold and Bjøntegaard 2006). The increase temperature also leads to a reduction of the interfacial tension of the pore water, again causing an increase in the RH (Radjy et al. 2003).

2.3.4.2 CTE Testing

The currently adopted testing regimen for looking at CTE was adapted from the AASHTO TP60 test method and developed at the University of Texas at Austin for TxDOT who now subjects all continuously reinforced concrete pavement mixtures to the CTE test specification Tex-428-A (Won 2005). The specimens used for the test are first submerged in limewater at 23 °C ± 2 °C for no less than 48 h. Sample preparation is complete once two successive weighings of the surface-dried conditions do not show an increase in weight of more than 0.5%. Place samples with support frame and LVDT attachment in water bath after taking an initial reading of the concrete sample at room temperature to the nearest 0.1 mm, designating it as length L. After setting the water bath to 10 °C ± 1 °C begin collecting displacement, temperature and time readings every minute at a constant temperature for an hour. Next the water bath temperature is increased to 50 °C ± 1 °C, again, measuring the displacement, temperature and time

readings every minute at a constant temperature for an additional hour. Return the temperature to 10 °C ± 1 °C taking the like data as before. The temperature versus displacement is plotted verifying an R-squared value greater than 0.999. Lastly the CTE value is determined as follows:

$$CTE = \frac{M}{L} + CF \qquad \text{Equation 2-9}$$

Where M is the line slope calculated (mm/°C), L is the length of the specimen (mm). CF is the correction factor related to the temperature related deformation of the support frame.

2.3.5 CRACKING ASSOCIATED WITH VOLUME CHANGE

2.3.5.1 Definition and Mechanisms

Early age cracking has been shown to be heavily dependent on the extent of volume change. However, the cracking may or may not occur depending on the level of restraint placed in or on the structure and the stress relaxation effect, which may be particularly high in early age concrete (Bentur 2003). In an instance where stresses develop in the concrete as a result of internal restraint the stresses are in fact lowered, analytically due to creep effects that may be predicted by Hooke's law. Unlike creep in the traditional sense, where structural elements under service load conditions begin to deform with time, concrete creep in the early ages of concrete can be interpreted as stress relaxation. Due to the complexities of stress relaxation, concrete creep cannot be simply interpreted by using a simple load cell in taking into account stress relaxation (Kovler

1994). Figure 14 models the cracking resistance and residual stress development plotted vs time, proving that cracking will only occur in an instance where the lines intersect and the stress exceeds the tensile capacity of the material.

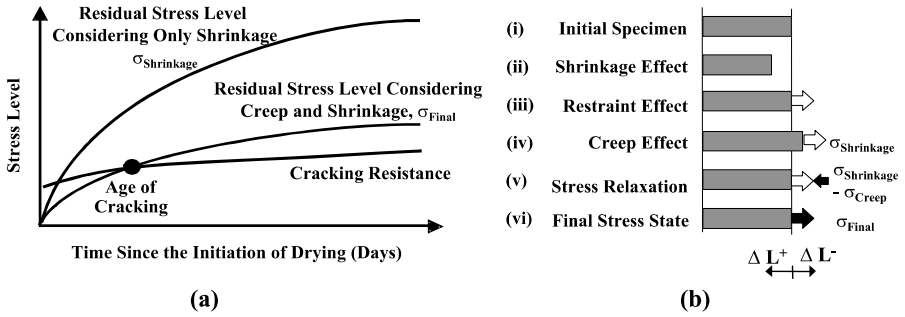

Figure 14: (a) Stress Development and influence on cracking (b) Conceptual description of relaxation effect. Taken from the Transportation Research Board E-C107 (2006

With respect for high performance concrete HPC with lower w/c ratio the main cause for concern with respect to early age cracking is a result of autogenous shrinkage and thermal deformations effect occurring simultaneously (Pease 2003). Although free shrinkage measurements can serve as an indicator of the overall shrinkage potential of a mixture cracking is complex and is not only dependent on shrinkage potential, but also on the material property development, creep relaxation, shrinkage rate and degree of restraint. (Weiss 1999; Pease 2003; Bentz 2008). In order to capture cracking potential for a concrete mixture, stress collection testing with respect to time until cracking data has been developed through the use of a series of restrained shrinkage testing apparatuses. Restrained shrinkage testing may be broken up into four categories: ring tests with a restrained core, panel tests in which the restraint is at the circumference of the panel, longitudinal tests where the restraint is provided at specimen edges and testing

where stresses are generated by the substrate, all of which are used in order to simulate performance for repair of retrofit (Bentur 2003).

2.3.5.2 Testing

The most common and researched form of restrained shrinkage testing is the restrained shrinkage test that has been standardized under ASTM C1581, Determining Age at Cracking and Induced Tensile Stress Characteristics of Mortar and Concrete under Restrained Shrinkage (2009). The test was developed in an attempt to eliminate stress concentrations associated angled restraints. Although testing that utilizes linear specimen geometry in a longitudinal type frame may be simpler to interpret the data, the laboratories that have access to the frame only have one due to the high cost of the machine and therefore lack repeatability and quality control assurance. (Weiss 1998; Altoubat 2001). Whereas, the concrete ring is economical, repeatable and simple to perform, and does not pose difficulties with respect to end restraint as with linear test methods. The concrete ring may be considered as a long prismatic specimen (Lam 2004). Therefore, for the extent of this research the restrained shrinkage ring test was selected to provide a comparative testing procedure for superplasticizers autogenous shrinkage effects.

The ring test consists of casting concrete around a restraining core (typically steel) and the concrete is permitted to shrink against it. The rings are cast in a room fixed at 50% RH and 23 °C to provide semi-adiabatic and laboratory testing conditions. All mechanisms associated shrinkage: chemical, plastic and drying impart a stress on the inner steel ring. The stresses are monitored via strain gauges that are glued on the inner surface of the steel ring. The concentric radial stresses allow for corresponding strain

readings for each of the strain gauges prior to cracking. Once a crack occurs, the strain in the closest gauge to the crack will undergo and immediate, significant decrease and the time at which this decrease occurs corresponds to the time of cracking of that particular mixture. Stresses on the ring cannot be actively controlled throughout the testing process, and therefore it is classified as a passive restrained testing technique, and time to crack may take as long as several months. Figure 15 is a typical setup of the restrained shrinkage ring testing setup.

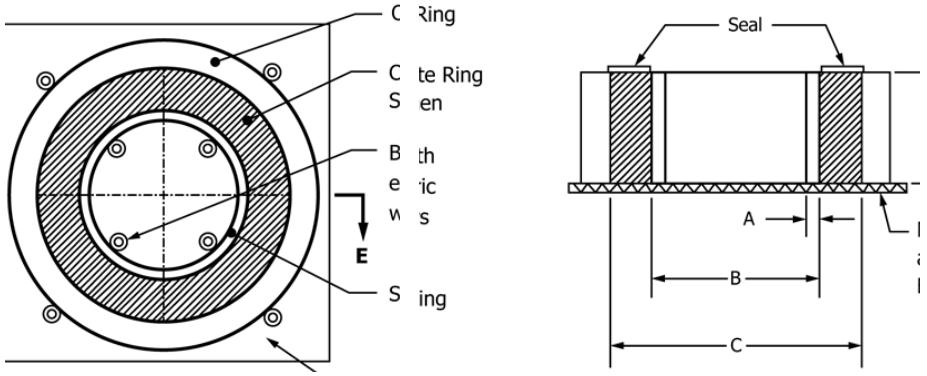

Figure 15: Typical restrained ring test setup before (left) and after (right) casting concrete (ASTM C1581)

In recent years a great deal of research has been spent on perfecting the issues and inaccuracies associated with the restrained ring test. The most promising of modifications have been from either developing a temperature profile that would assimilate to performance in the field or cooling the ring throughout the heat of hydration process to make the test completely isothermal (Weiss 2008). Recent work has also encouraged modifying the ring set-up to include an outer ring as well an inner ring. Adding the outer ring provides measurement of volumetric expansion throughout the curing process (Zou 2014), such expansion cannot be captured using a single inner ring set-up. To further

minimize temperature effects associated with expansion and contraction, the steel restraint rings are can be constructed out of invar. Invar is a steel with an extremely low coefficient of thermal expansion (Weiss 2008).

Although several different equations have been created to interpret the strain data produced from the steel ring and collected with the strain gauges, perhaps the simplest equation (Equation 2-10) converts the strain in the steel to strain seen by the concrete by idealizing the strains seen by the steel to be equal and opposite to that of the concrete cylinder (See et al. 2004):

$$S_{residual}(t) = \left(\frac{E_{st}R_{ic}h_{st}}{R_{is}h_c}\right) * \frac{|\alpha|}{2\sqrt{t}} \qquad \text{Equation 2-10}$$

where R_{is} and R_{ic} are the inner concrete radii and the outer steel ring radii, and Est is the elastic modulus of the steel. h_{st} and h_c are the heights of the steel ring and concrete ring, respectively. Alpha "α" is approximated based on the net strain versus the square toot of time after induction of the drying period as shown in Figure 16.

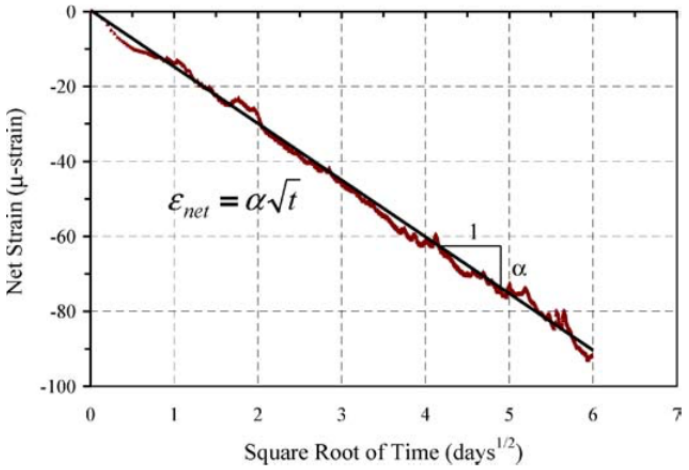

Figure 16: Net Strain versus square root of time solving for α (See et al. 2004)

2.3.6 CARBONATION SHRINKAGE AND DEPTH

2.3.6.1 Definition and Mechanisms

Carbonation decreases the pH of the concrete and depassivates the steel reinforcement. This depassivation increases the susceptibility of the reinforcement to corrosion and can reduce the service life of the concrete structure. This same carbonation mechanism plays a role in causing shrinkage on the surface layers on the concrete (Bazant 1995; Weiss 1999). Carbonation occurs as a result of a reaction between CO_2 from the ambient air attacking calcium bearing phases in the concrete and converting them into smaller volume occupying calcium carbonate phases and thereby inducing shrinkage. The reaction of the concrete and paste is shown below:

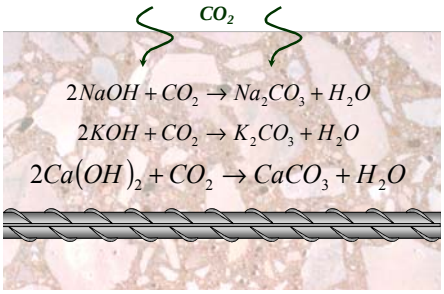

Figure 17: Chemical Reaction of CO2 Changing Calcium Bearing Phases (Taken from NRMCA Concrete Durability Course Presenter: Mike D.A Thomas)

In the presence of moisture, the reaction is exacerbated as the CO_2 forms carbonic acid. The carbonic acid reacts with calcium hydroxide $Ca(OH)_2$, which composes 25-50 wt% in the cement and forms calcium carbonate $CaCO_3$ (Thomas 1992). This reaction may be analytically measured as the carbon dioxide atom molecular weight is substantially greater than the carbon in hydrogen (Persson 1998).

A study found that issues related to carbonation shrinkage can be dismissed in HPC when w/c is at 0.28 and a silica fume content around 10% (Persson 1998). At low w/c and high silica fume all the calcium hydroxide $Ca(OH)_2$ was consumed which nearly eliminated carbonation and any shrinkage effects (Persson 1998). Yet precast plants do not typically employ the use of silica fume, but instead use 20 to 30 wt% fly ash in the mixture design. The difference in size and replacement of supplementary cementing materials in concrete directs the CO_2's ability to react with the concrete. Concrete mixtures containing fly ash as partial replacement have shown to be less resistant to carbonation as compared with ordinary Portland cements (OPC). This lesser resistance is due to the lowered effectiveness of an SCM's in excess of 30% replacement (e.g. fly ash) to consume the calcium hydroxide and instead increases the porosity of the pore structure (Khunthongkeaw 2006). The increased incorporation of SCM's also inherently lowers the

overall pH of the concrete mixture due to the lower portlandite ($Ca(OH)_2$) content more than a conventional concrete mixture (Hewlett 1998). Lower portlandite due to greater SCM replacement can lead to carbonation of other concrete reaction products (Roziere et al. 2009; Houst and Wittmann 2002).

Although carbonation shrinkage induced cracking is not a cause for concern in the bulk of the concrete, the carbonation shrinkage may be more pronounced in the surface of the concrete, influencing cracking (Persson 1998).

2.3.6.2 Testing

The most common method for identifying carbonation ingress on concrete specimens is the colorimetric method using a phenolphthalein solution that is sprayed on concrete. Carbonation is indicated based on a via change in color pigmentation. When the pH is greater than 9, the phenolphthalein will display a distinct purple pigmentation; however, if the pH is less than 9, the phenolphthalein solution will will be colorless. The European standard CEN/TS 12390-10 (2008) Determination of The Relative Carbonation Resistance of Concrete provides two means of testing for carbonation: (i) accelerated via exposure to controlled natural levels of carbonation and (ii) natural carbonation testing sheltered and unsheltered from direct rainfall. The sheltered specimens make use of Stevenson screens that prevent water from filling up pores in the concrete that may hinder the diffusion of CO2 through the concrete. The Stevenson screens allow CO_2 to enter the shelter but provide sufficient shelter preventing water from entering the housing. The laboratory testing procedure consists of castings concrete prisms or cylinders and curing the specimens at 23°C ± 3°C (73°F ± 5°F) under wet burlap and plastic for 24 hours. After demolding the concrete is either subjected to natural outdoor conditions or sheltered

conditions. The blocks are cut and sprayed with a phenolphthalein solution at select periods selected by the user. The device used to cut the prisms used at the University of Texas along with a depiction of a sprayed specimen is shown in Figure 18.

Figure 18: (Left) Device used to cut concrete carbonation specimens. (Right) Phenolphthalein spayed specimen and depth measurement front

Carbonation depth is measured at 5 points along the four sides of the recently cut square specimen (De La Rilem 1988). Results of carbonation depth measurements are averaged for each individual mixture.

CHAPTER 3: MATERIALS

3.1 INTRODUCTION

This chapter outlines the materials utilized to evaluate the micro-cracking issue throughout this project. Appendix I includes information about the source of the materials.

3.2 PORTLAND CEMENTS

Two Type III portland cements (coined "PC-III-A" and "PC-III-B") and one Type I/II portland cement (coined "PC-I-A") in accordance with ASTM C150 were used for this project (2015). The bulk of the study made use of Type III cements due to its common if not exclusive use in precast plants across the state of Texas. The Type III cements were taken from two different commercially used Texas cement plants. Table 1 provides the oxide analysis obtained for the different cement sources and types as per determined by TxDOT's cement laboratory.

Table 1: Oxide Analysis for Different Cement Sources and Types

Cement	SiO_2	$Al2O_3$	$Fe2O_3$	CaO	MgO	SO_3	Na_2O	K_2O
	mass %	mass %	mass %	mass %	mass %	mass %	mass %	mass %
PC-III-A	19.8	4.3	3.1	64.2	0.6	4.1	0.1	0.7
PC-III-B	19.8	5.1	1.9	63.5	1.1	5	0.1	0.6
PC-I-A	18.6	5.4	2.6	64.9	1.1	3.3	0.1	1

3.3 FLY ASH

One Class F fly ash in accordance with ASTM C618 was used for this project (2015). The fly ash was taken from a local Texas source. Table 2 provides the chemical composition analysis as per determined by TxDOT for the fly as used.

Table 2: Oxide Analysis for Class F Fly Ash

Fly Ash	SiO2	Al2O3	Fe2O3	CaO	MgO	SO3	Na2O	K2O
	mass %	mass %	mass %	mass %	mass %	mass %	mass %	mass %
Class F	52.07	23.07	3.95	11.65	2.06	0.48	0.403	0.74

3.4 AGGREGATES

3.4.1 COARSE AGGREGATE

Three different coarse aggregate sources were used for this project. All sources were composed of siliceous river gravel and/or limestone and were graded according to ASTM C33 grading size 57 (2016). Table 3 outlines the specific gravity and absorption capacity of the coarse aggregates.

Table 3: Physical Properties of the Coarse Aggregates

Coarse Aggregate	Mineralogy Type	Specific Gravity	Absorption Capacity (%)
CA-R	Siliceous	2.54	1.31
CA-L	Limestone	2.47	3.25
CA-RII	Siliceous	2.26	1.52

3.4.2 FINE AGGREGATE

Three different fine aggregates sources were used for this project. The majority of the mixture designs were composed of siliceous river gravel (FA-R). Several mixtures were composed of a limestone source (FA-RII), and a light weight fine aggregate (FA-LW). Table 4 outlines the specific gravity and absorption capacity of the fine aggregates.

Table 4: Physical Properties of the Fine Aggregates

Fine Aggregate	Mineralogy Type	Specific Gravity	Absorption Capacity (%)
FA-R	Siliceous	2.47	1.14
FA-RII	Siliceous	2.57	1.96
FA-LW	Manufactured	1.86	22.50

3.5 CHEMICAL ADMIXTURES

Since the focus of this study was to identify the potential harmful effects of the use of high range water reducing admixtures (HRWRA) on HPC at precast plants, only the most current and future proposed HRWRAs used in TxDOT precast concrete applications were utilized. Exclusively polycarboxylate-based high range water reducers (HR-P1, HR-P2, HR-P3, HR-P4, and HR-P5) along with stabilizing agents or viscosity modifying admixtures (VMA) (NR-1, NR-2) were selected for use from two chief distributors used at the precast plants in Texas. Table 5 contains details about the recommended dosages and specific gravity of the chemical admixtures used in this work.

Table 5: Classification of Admixtures used throughout this Study

Admixture Name	C-Polymer Type	ASTM C494 Classification	Specific gravity
HR-P1	Polycarboxylate	F	1.1
HR-P2	Polycarboxylate	F	1.1
HR-P3	Polycarboxylate	F	1.1
HR-P4	Polycarboxylate	F	1.1
HR-P5	Polycarboxylate	F	1.1
NR-1	Normal Range Water Reducer and Retarding	B & D	1.2
NR-2	Normal Range Water Reducer and Retarding	B & D	1.2
VMA-1	Viscosity Modifier	S	1.1

CHAPTER 4: LABORATORY TESTING: EVALUATION OF SUITABILITY OF ASTM C494 PROCEDURES FOR PRECAST CONCRETE MIXTURES

4.1 INTRODUCTION

In this chapter our goal is to test the following hypothesis: that if ASTM C494, Standard Specification for Admixtures in Concrete, performance requirements are valid for predicting the micro-crack development observed in precast girders, then mixtures that have observed cracking (herein called "poor performance mixtures") in the field should also fail in ASTM C494 testing (2010). Thus, in the event that the poor performance mixtures pass all or some of the tests outlined in ASTM C494, then the standard is considered inadequate or not fully adequate. Figure 19 provides a graphical representation of the devised ASTM C494 qualification process.

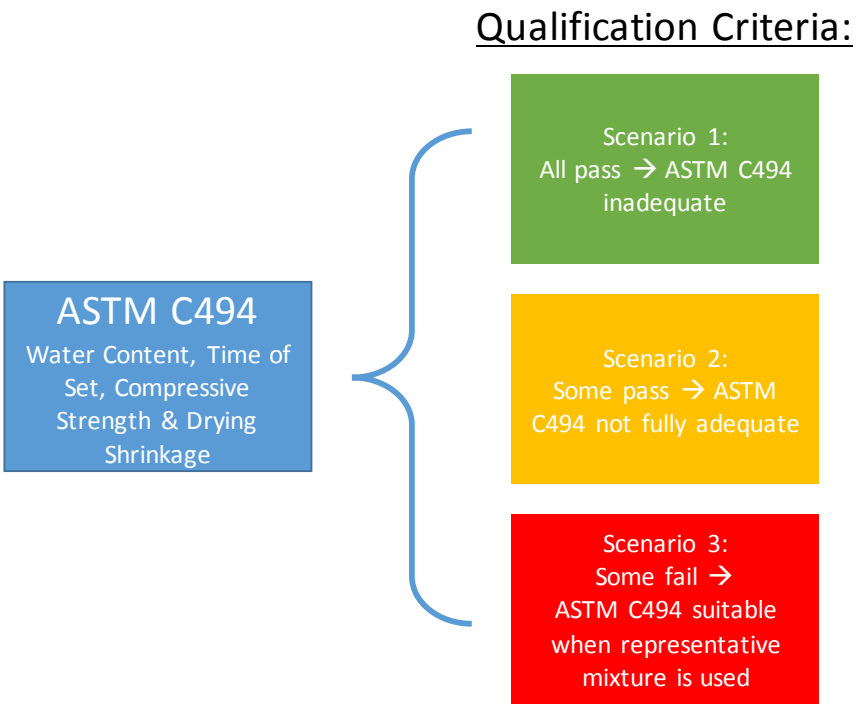

Figure 19: Testing performed and qualification criteria used to evaluate the relevancy of ASTM C494 to predict the latent cracking observed in the precast concrete barriers

ASTM C494 was initially carried out through the "specific approach" and would attempt to quantify a mixture design's cracking potential through select testing standards: water content, ASTM C403 time of set, ASTM C39 compressive strength, and ASTM C157 free shrinkage, ASTM C78 flexural strength, and ASTM C666 freeze-thaw testing. In this project, the flexural strength and freeze-thaw testing was omitted since both TxDOT and the research team at University of Texas at Austin were in agreement that testing concrete in flexural and freeze thaw for HPC would not aid the investigation efforts. Additional mixtures were carried out via the "non-specific approach," as specified in ASTM C494, which suggests specific changes in mixture proportions based

on specific mixture property alterations. Figure 20 outlines the tests employed as a part of the ASTM C494 testing, the passing limits and their respective chapter locations.

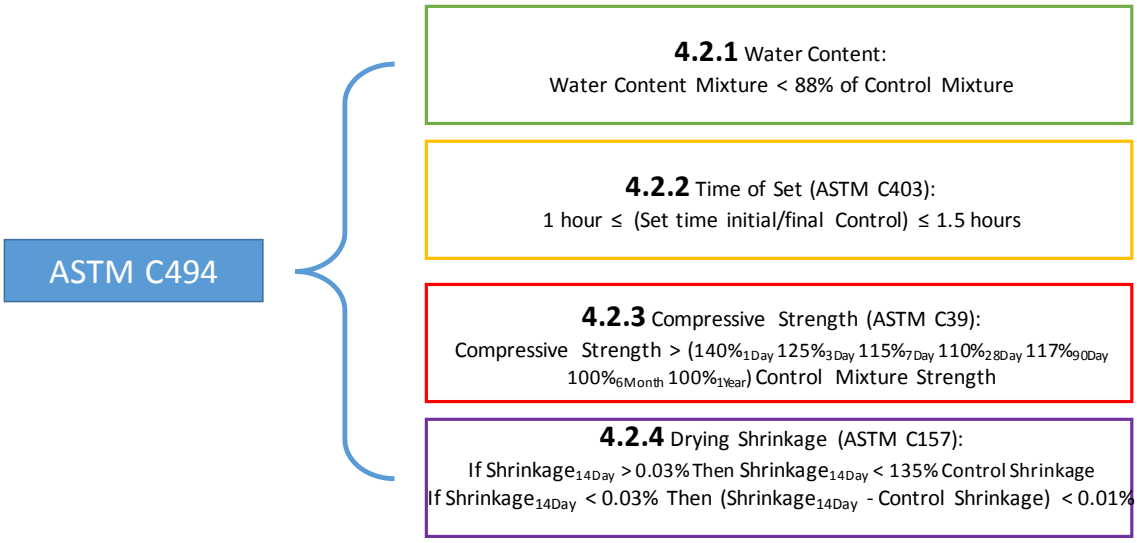

Figure 20: Tests performed for ASTM C494 and their respective limits and chapters

4.2 OVERVIEW OF ASTM C494 AND TESTING MATRIX

Each of the sections within this chapter will begin by outlining the particular laboratory testing procedure and its potential relevance with ASTM C494. All concrete mixtures for ASTM C494 testing were mixed in a rotary drum mixer in accordance with ASTM C192 mixing procedure. For assurance of quality control, each mixture was tested for air content and unit weight (ASTM C231, Standard test method for air content of freshly mixed concrete by the pressure method) and slump test (ASTM C143, standard test method for slump of hydraulic-cement concrete) (2014) (2015). In the event that the standard deviation of air content (%) or slump (in.) deviated from the goal set by precast

plants or prescribed in our matrix the was repeated. Details about the material properties and characteristics of the cement, aggregates and chemical admixtures used in these concrete mixtures were detailed in Chapter 3 (see Tables 1-5). Unless otherwise stated, the primary aggregates used throughout this study were CA-R and FA-R.

Initially, 3 mixtures that failed in the field in terms of micro-cracking (herein called "bad" performers) and 2 mixtures that have no observed cracking, herein called "good" performers, were cast and subjected to the testing prescribed by ASTM C494. Table 6 outlines the 5 mixtures selected for testing. The key included in Table 6 displays the "good" and "bad" performers. In the case of the 3 "bad" and 2 "good" performance mixtures.

Table 6: Initial testing matrix for ASTM C494. Evaluating 3 "bad performers" (Yellow) and 2 "good performers" (Blue)

w/cm	Cement Type	Cement Content (lb/yd^3)	SCM Content (lb/yd^3)	Admixtures			
				Type	(floz/100 lb cement)	Type	(floz/ 100 lb cement)
0.26		705	175		6.5		1.5
0.28		705	175		12		3
0.31	PC-III-A	663	271	HR-P1	5.5	NR-1	2.5
0.31		640	213		6		2
0.33		658	0		6.5		3

KEY:	-"Bad" Perfomer
	-"Good" Perfomer

The "bad" (yellow) and "good" (blue) nomenclature was used throughout this chapter as a means of illuminating the original testing series used for evaluating the effectiveness of ASTM C494 testing through the specific approach. An additional matrix of 22 mixtures were cast, which focused on determining the sensitivity of ASTM C494 testing limits for "tests not for a specific approach." The testing "not for a specific

approach" implemented variations in mixture proportioning, specifically mixture proportions related to precast mixtures commonly used in Texas. The study compared mixtures through the evaluation with variations in HRWR dosage and type, cement content and source, water to binder ratio and fly ash content as a means of using ASTM C494 in discerning differences in future micro-cracking potential. For completeness the entire spectrum of mixtures evaluated using ASTM C494 have been composed in a single matrix (see Table 8). Of those 28 mixtures, a set of 19 mixtures had 4 distinguishable controls.

However, because a true control mixture in reference to a mixture design requiring the usage of HRWR is not possible, controls were created by imposing either increased water contents and or smaller dosages of HRWR. The CWB control was developed in an attempt to reduce the omit/reduce the superplasticizer used in the mixture by increasing the water-to-binder ratio of one the concretes. Tables 7-8 displays the mixture designs and the correlative control mixtures that they were compared with for the ASTM C494 qualification.

Table 7: 4 Mixture proportions for the different control types used for ASTM C494 qualification

Control ID	w/cm	Cement Type	Cement Content (lb/yd^3)	SCM Content (lb/yd^3)	Admixtures			
					Type	(floz/100 lb cement)	Type	(floz/ 100 lb cement)
CSP-1	0.26	PC-III-A	705	175	HR-P1	8.25	NR-1	1.5
CWB	0.4		658	0		2		2
CSP-2	0.33		658	0		5.5		2
CLWA			658	0		5		2.5

CSP1 & 2:	Control Mixtures based on HRWR dosage
CWB:	Control Mixtures based on water to binder ratio
CLWA:	Control Mixtures based on lighweight fine aggregate replacement

Table 8: 19 Different mixtures each organized alongside the control mixtures in Table 7 in order to test with ASTM C494 qualification. Additionally, "bad performers" (Yellow) and "good performers" (Blue) have been illuminated

Control ID	w/cm	Cement Type	Cement Content (lb/yd^3)	SCM Content (lb/yd^3)	Admixtures			
					Type	(floz/100 lb cement)	Type	(floz/ 100 lb cement)
CSP-1	0.26	PC-III-A	705	175	HR-P1	5.25	NR-1	1.5
			517	129		25.75		3
			705	175	HR-P2	8.25		3
			705	175	HR-P3	10	NR-2	3
		PC-III-B	705	175	HR-P1	8.25	NR-1	3
		PC-III-A	705	233		6.5		3
	0.38		700	175	-	-	-	-
	0.45		705	175		-		-
	0.26		705	175		6.5		1.5
	0.28		705	175		12		3
CWB	0.31	PC-III-A	663	271	HR-P1	5.5	NR-1	2.5
	0.31		640	213		6		2
	0.33		658	0		6.5		3
CWB, CSP-2 & CLWA	0.26	PC-III-A	658	219	HR-P1	6.5	NR-1	3
	0.33		517	0		30.5		3
	0.33		658	0		11.88		3
	0.3		658	0		6.5		3
	0.52		658	0	-	-	-	-
	0.56		658	0		-		-

Although 28 total mixtures were cast and subjected to ASTM C494 evaluation only 19 had a proper control mixture to compare it to. Mixtures tested for qualification of HRWR agents were assigned controls based upon either like w/cm, HRWR dosage or comparison of lightweight aggregate replacement. If the similarities were not found within the base control mixtures in Table 7 than the mixture was not adequate towards ASTM C494 evaluation.

4.2.1 WATER CONTENT

4.2.1.1 PROCEDURE AND EXPERIMENTAL SETUP

The qualification for ASTM C494 with respect to HRWR Type F requires that the water content of the admixture test mixture in question not exceed 88% of the control total water content. Considering that the intent of HRWR addition in concrete mixtures is to reduce the need for water to obtain a workable mixture, exceeding the control mixtures water content is not a concern. Yet due to the fact that the controls are not a "true" control mixture designs with respect to the admixtures or mixture designs results have been tabulated purely as a means of complete fulfillment of ASTM C494 testing procedures.

4.2.1.2 RESULTS

Mixture design comparison stated the water content as "pass" for water addition less than or equal to 88% of the respective control or "fails" for water greater than 88% of the control. Table 9 provides the Pass/Fail of mixture designs with respect to their controls.

Table 9: Water content pass/fail for ASTM C494 in reference to control mixtures. Additionally, “bad performers” (Yellow) and “good performers” (Blue) have been illuminated

w/cm	Cement Type	Cement Content (lb/yd^3)	SCM Content (lb/yd^3)	Admixtures				Water Content Max			
				Type	(floz/100 lb cement)	Type	(floz/ 100 lb cement)	CSP-1	CWB	CSP-2	CLWA
0.26	PC-III-A	517	129	HR-P1	25.75	NR-1	3	Pass	-		
		658	219		6.5		3	-	Pass	Fail	Fail
		663	271		7		2.5	-			
		705	175		5.25	NR-1	1.5	Pass	-		
		705	175		8.25		1.5	-	Pass	-	-
		705	175		8.25		1.5	-			
		705	175	HR-P2	8.25		3	Pass	-		
		705	175	HR-P3	10	NR-2	3	Pass	-		
	PC-III-B	705	175		8.25		3	Pass	-		
		705	233		6.5		3	Pass	-		
0.28		705	175	HR-P1	12	NR-1	3	-	Pass	-	-
	PC-III-A	663	271		5.5		2.5	-	Pass	-	-
		640	213		6		2	-	Pass	-	-
0.31		705	175	HR-P2	5.5		2.5	-	-		
		705	175	HR-P3	7.25	NR-2	2.5	-	-		
	PC-III-B	705	175	HR-P1	6		2.5	-	-		
0.33	PC-III-A	517	0	HR-P1	30.5	NR-1	3	-	Pass	Fail	Fail
		658	0		11.88		3	-	Pass	Pass	Pass
		658	0		6.5		3	-	Pass	Fail	Fail
		658	0		5.5		2	-	-		
		658	0		5		2.5	-	-		
		663	271		5		2.5	-	-		
0.38		700	175	-	-	-	-	Fail	-		
0.4		658	165	HR-P1	2	NR-1	2	-			
		658	0		2		2	-			
0.45		705	175	-	-	-	-	Fail	-		
0.52		658	0				-	-	Fail	Fail	Fail
0.56		658	0				-	-	Fail	Fail	Fail

Table 9 indicates that typically mixtures with HRWR addition will pass with respect to their subsequent control when the mixture utilizes a w/cm ratio below 0.31. Although several mixture designs fail (especially in the higher w/cm range), the mixtures were created for comparison purposes toward superplasticizer shrinkage effects. All "bad" performing mixtures passed with respect to the "CWB" control. The only mixtures that failed were ones that had high cementitious contents (>800lbs/yd^{3-}) with respect to their controls. Because "good" and "bad" performers both primarily passed with respect to their controls, water content cannot be used as a proper means of evaluating a mixture's potential towards micro-cracking. Therefore, ASTM C494-water content is inadequate for micro-cracking prediction.

4.2.2 TIME OF SET

4.2.2.1 PROCEDURE AND EXPERIMENTAL SETUP

The qualification for ASTM C494 with respect to HRWR Type F requires that both initial and final time of set of the admixture test mixture is within a certain range of the control mixture's initial and final set time. Each mixture employed the time of set analysis through ASTM C403, Standard test method for time of setting of concrete mixtures by penetration resistance (2008). For this test, approximately 0.25-ft^3 of concrete was sieved through a No. 4 sieve with the aid of a vibrating table in order to ascertain a mortar mixture. The mortar was then set into a 6x6-in steel cylindrical tin, capped and held in a 73°C testing environment. The time of set testing equipment is shown in Figure 21.

Figure 21: Time of set equipment used throughout this project

Time of set measurements were initiated 3 hours after the introduction of cement to water. Thereafter, 15 min increments were employed to determine the length of time until the mortar achieved 500 psi for an indication of initial set or 4000 psi as an indication of final set of the concrete.

4.2.2.2 RESULTS

According to ASTM C494, the HRWR test mixture set time can not be less than 1 hour and not more than 1.5 hour in reference to the control time of initial and final set measurement. Table 10 presents the Pass/Fail of mixture designs with respect to their control for the ASTM C494 set time requirements.

Table 10: Time of set pass/fail for ASTM C494 in reference to control mixtures. Additionally, “bad performers” (Yellow) and “good performers” (Blue) have been illuminated

w/cm	Cement Type	Cement Content (lb/yd^3)	SCM Content (lb/yd^3)	Admixtures				Initial Time of Set				Final Time of Set			
				Type	(floz/100 lb cement)	Type	(floz/ 100 lb cement)	CSP-1	CWB	CSP-2	CLWA	CSP-1	CWB	CSP-2	CLWA
		517	129		25.75		3	Fail	-			Pass	-		
		658	219		6.5	NR-1	3		Fail	Fail	Fail		Fail	Fail	Fail
		663	271	HR-P1	7		2.5	-				-			
		705	175		5.25		1.5	Fail	-			Fail	-		
	PC-III-A	705	175		8.25		1.5		Pass	-	-	-	Pass	-	-
0.26		705	175		8.25	NR-1	1.5	-				-			
		705	175	HR-P2	8.25		3	Pass	-			Pass	-		
		705	175	HR-P3	10	NR-2	3	Pass	-			Pass	-		
	PC-III-B	705	175		8.25		3	Pass	-			Pass	-		
		705	233		6.5		3	Fail	-			Fail	-		
0.28		705	175	HR-P1	12	NR-1	3		Fail	-	-	-	Pass	-	-
	PC-III-A	663	271		5.5		2.5		Pass	-	-	-	Pass	-	-
		640	213		6		2		Fail	-	-	-	Fail	-	-
0.31		705	175	HR-P2	5.5		2.5	-				-			
		705	175	HR-P3	7.25	NR-2	2.5	-				-			
	PC-III-B	705	175	HR-P1	6		2.5	-				-			
		517	0		30.5		3	-	Fail	Fail	Fail	-	Fail	Fail	Fail
		658	0		11.88		3	-	Fail	Fail	Fail	-	Fail	Fail	Fail
		658	0	HR-P1	6.5	NR-1	3	-	Fail	Fail	Fail	-	Fail	Fail	Fail
0.33		658	0		5.5		2	-				-			
		658	0		5		2.5	-				-			
	PC-III-A	663	271		5		2.5	-				-			
0.38		700	175	-	-	-	-	Fail	-			Fail	-		
0.4		658	165	HR-P1	2	NR-1	2	-				-			
		658	0		2		2	-				-			
0.45		705	175	-	-	-	-	Fail	-			Fail	-		
0.52		658	0		-		-	-	Pass	Pass	Pass	-	Pass	Pass	Pass
0.56		658	0		-		-	-	Pass	Pass	Pass	-	Pass	Pass	Pass

Table 10 indicates that overall there were fewer “passes” with respect to initial set as compared to final set. Also, lower w/cm ratio mixtures (<0.31) had more variability in passing and failing as compared to higher w/cm mixtures. With regards to the “good” and “bad” performing mixtures half of the “good” (2 out of 4) performers passed and half of the “bad” (3 out of 6) performers failed. Based on the inconclusiveness of the time of set testing results, ASTM C494, time of set, is deemed inadequate for micro-cracking prediction.

4.2.3 COMPRESSIVE STRENGTH

4.2.3.1 PROCEDURE AND EXPERIMENTAL SETUP

The qualification for ASTM C494 with respect to HRWR Type F requires that compressive strength of the admixture test mixture in question exceeds a certain percentage of the compressive strength of the control for 1, 3, 7, 28, 90 day, 6 and 12 months. To evaluate the compressive strength of the concrete, 3x6-in specimens were cast and subsequently subjected to the ASTM C39, Compressive Strength of Cylindrical Concrete Cylinders (2016). 24 3x6-in concrete cylinders were cast in plastic compressive cylinder molds for each mixture. The 24 specimens were cured for a 24-hour period and stored in a temperature controlled room at 23 ± 3 °C and covered with wet burlap and plastic sheeting to prevent evaporation. In order to provide a representation of concrete cast and demolded in the precast yard 3 cylinders were stripped and measured at 18 hours after cement was added to water. After which, the specimens were demolded and set in a moist curing environment at 23 ± 3 °C up until they were to be tested in compression.

Three cylinders were tested in compression for each compression date. The average compressive stresses along with standard deviations for each concrete mixture are included in the Appendix III of this report.

4.2.3.2 RESULT

In order to assess if the mixture designs are applicable towards ASTM C494 Table 10 provides the Pass/Fail along with the strength percentage of the mixture designs with respect to their controls. The pass/fail limits for each of the dates according to ASTM C494 for type F HRWR are listed in Table 11.

Table 11: Compressive Strength pass/fail for ASTM C494 in reference to control mixtures (1-7 Day). Percentages in header row lists the ASTM C494 minimum strength ratio for that specific day. Percentage number in cells indicate the percentage that the base mixture varies from the control mixture. Values over 100% means that the strength of the base mixture exceeded the control mixture. Additionally, “bad performers” (Yellow) and “good performers” (Blue) have been illuminated

w/cm	Cement Type	Cement Content (lb/yd^3)	SCM Content (lb/yd^3)	Admixtures				1 Day - 140%				3 Day - 125%				7 Day - 115%			
				Type	(floz/100 lb cement)	Type	(floz/ 100 lb cement)	CSP-1	CWB	CSP-2	CLWA	CSP-1	CWB	CSP-2	CLWA	CSP-1	CWB	CSP-2	CLWA
0.26	PC-III-A	517	129	HR-P1	25.75	NR-1	3	62%	-			42%	-			42%	-		
		658	219		6.5		3	-	0%	0%	0%	-	23%	27%	17%	-	68%	57%	39%
		663	271		7		2.5	-				-				-			
					5.25		1.5	92%	-			58%	-			52%	-		
					8.25	NR-1	1.5	-	149%	-	-	-	130%	-	-	-	129%	-	-
		705	175		8.25		1.5	-				-				-			
				HR-P2	8.25		3	77%	-			65%	-			55%	-		
				HR-P3	10	NR-2	3	38%	-			36%	-			35%	-		
	PC-III-B				8.25		3	94%	-			63%	-			51%	-		
			233		6.5		3	18%	-			41%	-			53%	-		
0.28			175	HR-P1	12	N	3	-	111%	-	-	-	118%	-	-	-	124%	-	-
	PC-III-A	663	271		5.5		2.5	-	86%	-	-	-	87%	-	-	-	94%	-	-
		640	213		6		2	-	109%	-	-	-	93%	-	-	-	100%	-	-
0.31		705	175	HR-P2	5.5		2.5	-	-			-	-			-	-		
				HR-P3	7.25	NR-2	2.5	-	-			-	-			-	-		
	PC-III-B			HR-P1	6		2.5	-	-			-	-			-	-		
0.33	PC-III-A	517	0	HR-P1	30.5	NR-1	3	-	92%	103%	61%	-	74%	88%	57%	-	84%	79%	55%
		658			11.88		3	-	82%	92%	54%	-	76%	90%	58%	-	84%	82%	57%
					6.5		3	-	139%	155%	92%	-	117%	140%	89%	-	118%	136%	94%
					5.5		2	-				-				-			
					5		2.5	-				-				-			
		663	271		5		2.5	-				-				-			
0.38		700	175	N/A	0	N/A	0	50%	-			33%	-			34%	-		
0.4		658	165	HR-P1	2	NR-1	2	-				-				-			
			0		2		2	-				-				-			
0.45		705	175	N/A	0	N/A	0	88%	-			63%	-			62%	-		
0.52		658	0		0		0	-	83%	93%	55%	-	78%	92%	60%	-	84%	79%	55%
0.56					0		0	-	86%	96%	57%	-	78%	92%	60%	-	84%	80%	55%

Table 11 (cont.): Compressive Strength pass/fail for ASTM C494 in reference to control mixtures (28-Day through 6-Month). Percentages in header row lists the ASTM C494 minimum strength ratio for that specific day. Percentage number in cells indicate the percentage that the base mixture varies from the control mixture. Values over 100% means that the strength of the base mixture exceeded the control mixture. Additionally, "bad performers" (Yellow) and "good performers" (Blue) have been illuminated

w/cm	Cement Type	Cement Content (lb/yd^3)	SCM Content (lb/yd^3)	Admixtures				28 Day - 110%				90 Day - 117%				6 Month - 100%			
				Type	(floz/100 lb cement)	Type	(floz/ 100 lb cement)	CSP-1	CWB	CSP-2	CLWA	CSP-1	CWB	CSP-2	CLWA	CSP-1	CWB	CSP-2	CLWA
		517	129		25.75		3	36%	-			68%	-			68%	-		
		658	219		6.5	NR-1	3	-	51%	56%	44%	-	90%	95%	78%	-	99%	99%	79%
		663	271	HR-P1	7		2.5	-				-				-			
	PC-III-A				5.25		1.5	45%	-			73%	-			76%	-		
0.26					8.25	NR-1	1.5	-	148%	-	-	-	140%	-	-	-	149%	-	-
		705	175		8.25		1.5	-				-				-			
				HR-P2	8.25		3	47%	-			96%	-			100%	-		
				HR-P3	10	NR-2	3	30%	-			70%	-			73%	-		
	PC-III-B				8.25		3	44%	-			91%	-			91%	-		
			233		6.5		3	46%	-			86%	-			82%	-		
0.28			175	HR-P1	12	N	3	-	129%	-	-	-	126%	-	-	-	149%	-	-
	PC-III-A	663	271		5.5		2.5	-	108%	-	-	-	113%	-	-	-	133%	-	-
		640	213		6		2	-	107%	-	-	-	113%	-	-	-	116%	-	-
0.31		705	175	HR-P2	5.5		2.5	-	-			-	-			-	-		
				HR-P3	7.25	NR-2	2.5	-	-			-	-			-	-		
	PC-III-B			HR-P1	6		2.5	-	-			-	-			-	-		
		517			30.5		3	-	64%	70%	55%	-	133%	140%	115%	-	145%	145%	116%
					11.88		3	-	64%	70%	55%	-	132%	140%	114%	-	137%	137%	110%
0.33		658	0	HR-P1	6.5	NR-1	3	-	115%	126%	99%	-	111%	117%	96%	-	118%	117%	94%
					5.5		2	-				-				-			
					5		2.5	-				-				-			
	PC-III-A	663	271		5		2.5	-				-				-			
0.38		700	175	N/A	0	N/A	0	29%	-			60%	-			59%	-		
0.4		658	165	HR-P1	2	NR-1	2	-				-				-			
			0		2		2	-				-				-			
0.45		705	175	N/A	0	N/A	0	53%	-			90%	-			50%	-		
0.52		658	0		0		0	-	64%	70%	55%	-	131%	139%	114%	-	137%	137%	110%
0.56					0		0	-	64%	70%	55%	-	119%	125%	103%	-	122%	122%	98%

Table 11 indicates that strengths of HRWR tested mixtures primarily failed with respect to their controls especially in early ages (≤ 28 Days). The bad performing mixtures exceeded the strength of the controls for just over half of the testing dates (11 out of 18). The good performing mixtures exceeded the strength of their controls for just less than half of the testing dates (10 out of 24). The remainder of the matrix with the HRWR controls (CSP-1 and CSP-2) and the lightweight aggregate control (CLWA) produces a high number of failures especially in the early ages. Due to the variability in compressive strengths with respect to good and bad performers, ASTM C494-compressive strength is inadequate for micro-cracking prediction.

The compressive strength pass/fail and percentage have only been presented to provide proof of fulfillment if ASTM C494 testing as a part of Task 3 of this research project. The collection of compressive strength data for each mixture performed in this project is located in the Appendix III of this report.

4.2.4 DRYING SHRINKAGE

4.2.4.1 PROCEDURE AND EXPERIMENTAL SETUP

In accordance with ASTM C494 testing procedures testing for free shrinkage due to drying shrinkage was assessed. To evaluate the drying shrinkage effects on concrete the length change of concrete prisms was subjected to the ASTM C157 testing method (2008). Six concrete prisms were cast in rigid molds for each mixture. The six specimens were cured for a 24-hour period and stored in a temperature controlled room at 23 ± 3°C and covered with wet burlap and plastic sheeting to prevent evaporation. After which, the specimens were demolded and set in a moist curing environment at 23 ± 3°C for a 15-30

minute period. Initial readings were immediately taken with a comparator along with mass measurements. Of the six prisms, three specimens were stored in a climate controlled room at 50% RH and 23°C; the remaining three specimens were cured in a saturated lime solution for a 28-day period from the date of casting. Both sets of prisms had successive measurement readings taken at ages of 4, 7, 14, 28, 56, 112 and 224 days. If applicable additional measurements were taken beyond the dates required in the ASTM standard. The length change for each specimen, $\Delta L_x(\%)$ was calculated using the following equation:

$$\Delta L_x = \frac{CRD_t - CRD_{initial}}{G} * 100\% \qquad \text{Equation 2-1}$$

where CRD_t is the difference between the comparator reading of specimen and the reference bar at time "t". $CRD_{initial}$ is the difference between the comparator reading of specimen and the reference bar at t=0 (i.e., the initial reading), and G is the length separation between inner gage faces embedded in the concrete specimen (250 mm).

4.2.4.2 RESULTS

The following sections first provide the complete drying shrinkage matrix alongside the qualification for ASTM C 494 with respect to HRWR Type F. ASTM C 494 requires that if the shrinkage at 14 days (in accordance to ASTM C 157) exceeds 0.03% than the shrinkage relative to the control mixture should not exceed 135% (2008). However, if the shrinkage at 14 days is less than 0.03% than the difference between the control and tested mixture should not be less than 0.01%. Table 12 provides the Pass/Fail along with the shrinkage percentage or difference of mixture designs with respect to their

controls. The remainder of the drying shrinkage results section provides comparisons of drying shrinkage in accordance with Task 4: effect of w/cm ratio, cement source, cement type, HRWR type, HRWR dosage, cement content, fly ash addition and shrinkage reducing parameters such a light weight aggregate. All drying shrinkage curves can be found in Appendix V.

Table 12: Drying Shrinkage pass/fail for ASTM C494 in reference to control mixtures (1 Day Cure). Additionally, "bad performers" (Yellow) and "good performers" (Blue) have been illuminated

w/cm	Cement Type	270	SCM Content (lb/yd^3)	Admixtures				1 Day Cure							
				Type	(floz/100 lb cement)	Type	(floz/ 100 lb cement)	14 Day					Ultimate		
								CSP-1	CWB	CSP-2	CLWA	CSP-1	CWB	CSP-2	CLWA
0.26	PC-III-A	517	129	HR-P1	25.75	NR-1	3	74%	-			67%	-		
		658	219		6.5		3	-	106%	0.010	100%	-	137%	0.02	114%
		663	271		7		2.5	-				-			
		705	175		5.25		1.5	78%	-			81%	-		
		705	175		8.25	NR-1	1.5	-	103%	-	-	-	146%	-	-
		705	175		8.25		1.5	-				-			
		705	175	HR-P2	8.25		3	76%	-			86%	-		
		705	175	HR-P3	10	NR-2	3	84%	-			91%	-		
	PC-III-B	705	175		8.25		3	77%	-			91%	-		
		705	233		6.5		3	100%	-			105%	-		
0.28		705	175	HR-P1	12	NR-1	3	-	104%	-	-	-	143%	-	-
	PC-III-A	705	175		5.5		2.5	-	133%	-	-	-	145%	-	-
		705	175		6		2	-	141%	-	-	-	150%	-	-
0.31		705	175	HR-P2	5.5		2.5	-				-			
		705	175	HR-P3	7.25	NR-2	2.5	-				-			
	PC-III-B	705	175	HR-P1	6		2.5	-				-			
0.33	PC-III-A	517	-	HR-P1	30.5	NR-1	3	-	129%	0.016	122%	-	179%	0.031	149%
		658	-		11.88		3	-	112%	0.012	106%	-	139%	0.022	115%
		658	-		6.5		3	-	124%	0.015	117%	-	153%	0.040	200%
		658	-		5.5		2	-	124%	-	-	-	153%	-	-
		658	-		5		2.5	-				-			
		663	271		5		2.5	-				-			
0.38		700	175	N/A	0	N/A	0	76%	-			58%	-		
0.4		658	165	HR-P1	2	NR-1	2	-				-			
		658	-		2		2	-				-			
0.45		705	175	N/A	0	N/A	0	78%	-			82%	-		
0.52		658	-		0		0	-	104%	0.010	99%	-	100%	0.005	83%
0.56		658	-		0		0	-	102%	0.009	97%	-	87%	-0.004	72%

Table 12 (cont.): Drying Shrinkage pass/fail for ASTM C494 in reference to control mixtures (28 Day Cure). Additionally, "bad performers" (Yellow) and "good performers" (Blue) have been illuminated

w/cm	Cement Type	270	SCM Content (lb/yd^3)	Admixtures				28 Day Cure							
				Type	(floz/100 lb cement)	Type	(floz/ 100 lb cement)	14 Day				Ultimate			
								CSP-1	CWB	CSP-2	CLWA	CSP-1	CWB	CSP-2	CLWA
0.26	PC-III-A	517	129	HR-P1	25.75	NR-1	3	57%	-			35%	-		
		658	219		6.5		3	-	142%	0.003	69%	-	153%	0.005	88%
		663	271		7		2.5	-				-			
		705	175		5.25		1.5	60%	-			51%	-		
		705	175		8.25	NR-1	1.5	-	148%	-	-		125%	-	-
		705	175		8.25		1.5	-				-			
		705	175	HR-P2	8.25		3	193%	-			51%	-		
		705	175	HR-P3	10	NR-2	3	71%	-			85%	-		
	PC-III-B	705	175		8.25		3	60%	-			78%	-		
		705	233		6.5		3	61%	-			57%	-		
0.28		705	175	HR-P1	12	NR-1	3	-	90%	-	-	-	129%	-	-
	PC-III-A	705	175		5.5		2.5	-	111%	-	-	-	109%	-	-
		705	175		6		2	-	145%	-	-	-	0%	-	-
0.31		705	175	HR-P2	5.5		2.5	-				-			
		705	175	HR-P3	7.25	NR-2	2.5	-				-			
	PC-III-B	705	175	HR-P1	6		2.5	-				-			
0.33	PC-III-A	517	-	HR-P1	30.5	NR-1	3	-	99%	-0.004	48%	-	168%	0.007	96%
		658	-		11.88		3	-	174%	0.006	85%	-	168%	0.007	96%
		658	-		6.5		3	-	111%	-0.001	54%	-	116%	-0.001	66%
		658	-		5.5		2	-	111%	-	-	-	116%	-	-
		658	-		5		2.5	-				-			
		663	271		5		2.5	-				-			
0.38		700	175	N/A	0	N/A	0	32%	-			29%	-		
0.4		658	165	HR-P1	2	NR-1	2	-				-			
		658	-		2		2	-				-			
0.45		705	175	N/A	0	N/A	0	51%	-			62%	-		
0.52		658	-		0		0	-	119%	0.000	58%	-	88%	-0.009	50%
0.56		658	-		0		0	-	79%	-0.009	38%	-	76%	-0.015	44%

Although not mandated for pass and failure of mixtures subjected to drying shrinkage the last available date, i.e., the "ultimate" shrinkage, of each mixture was also determined. It must be noted that the same pass and fail criterion with respect to the control used at 14-day was used at the "ultimate" shrinkage date. This was done as to not stray too far away from the ASTM standard for the "ultimate" shrinkage data comparison. For bad performing mixtures, half of the mixtures (1 out of 3) subjected to a 1-day curing period failed within the 14-day period. Additionally, the bad performing mixtures with 28-day curing (2 out of 3) failed within the 14-day period. The measurements compared at ultimate for 1-day curing failed all good and bad performing mixtures. Whereas the ultimate measurements compared with the 28-day curing procedure passed all the good and bad performers. The variability in pass/fail results for drying shrinkage confirms that ASTM C494-compressive strength is inadequate for micro-cracking prediction. The drying shrinkage pass/fail and percentages have only been presented to provide proof of fulfillment of ASTM C494 testing as a part of Task 3 of this research project.

Since drying shrinkage holds a great deal of relevance to the potential shrinkage induced micro-cracking seen in the field, a more detailed investigation of mixture design effects on drying shrinkage was performed in the following sections. Although the prescribed "good" and "bad" performers are no longer being directly compared to their respective controls in the following sections, their comparisons have been illuminated and discussed where applicable. In addition, shorthand mixture identifications are used throughout this chapter, where only the variable in the mixture designs being compared is presented throughout each figure.

4.2.4.2.1 Effect of w/cm ratio

Figures 22-24 show the drying shrinkage curve for three base concrete mixtures (M1-NC, M3-NC and M4-SCC), each of which have three additional variations in w/cm ratios. NC and SCC are normally consolidated and self consolidating concrete mixture design notations. Air and lime water storage curing procedures at 1 and 28-day accordingly for drying shrinkage measurements have been overlaid on the same graph in order to provide fulfillment of ASTM C157 specimen measurement procedures as previously described in Chapter 4.2.4.1 of this report.

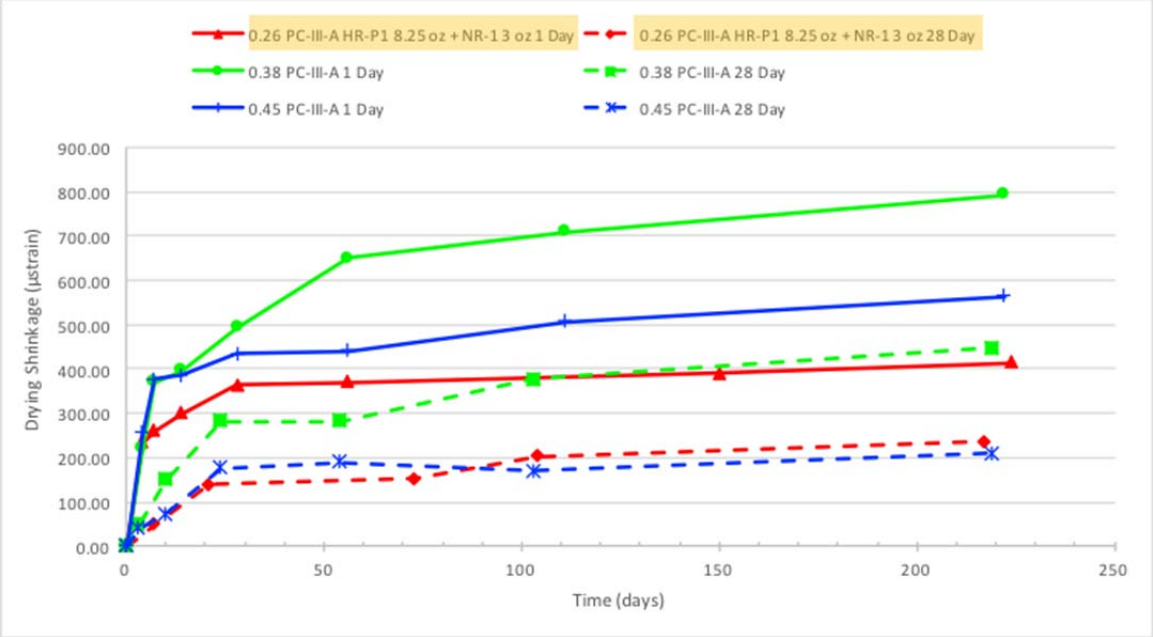

Figure 22: Drying shrinkage curve showing effect of w/cm ratio on base mixture, M1-NC (0.26 w/cm), for 1 and 28 Day Curing. For a given w/cm ratio, solid lines correspond to 1-day cure; dashed line corresponds to 28-day cure. Yellow shading denotes "bad performer" mixture from Table 6

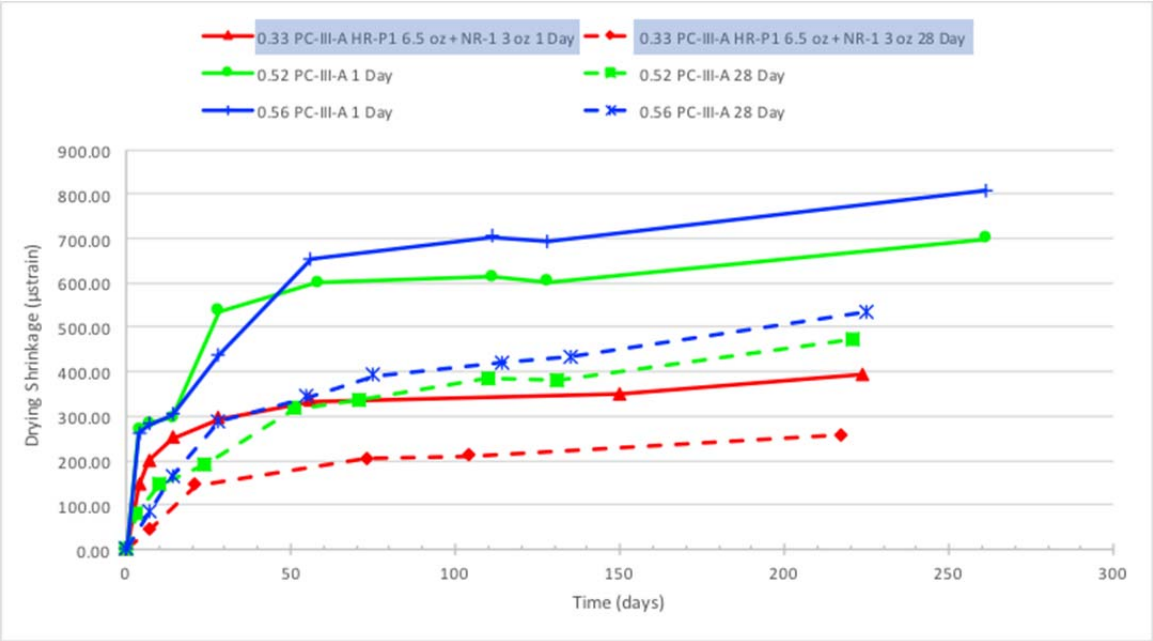

Figure 23: Drying Shrinkage Curve showing effect of w/cm ratio for base mixture M3-NC (0.33 w/cm) for 1 and 28 Day Curing. For a given w/cm ratio, solid lines correspond to 1-day cure; dashed line corresponds to 28-day cure. Blue shading denotes "good performer" mixture from Table 6

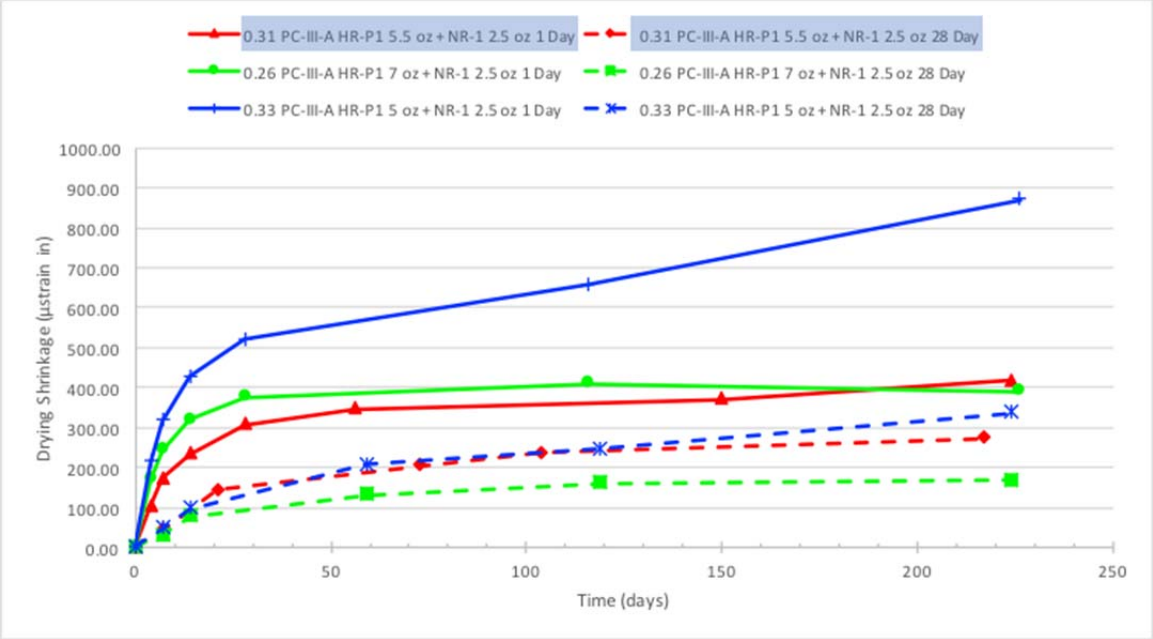

Figure 24: Drying Shrinkage Curve showing effect of w/cm ratio for base mixture M4-SCC (0.31 w/cm) for 1 and 28 Day Curing. For a given w/cm ratio, solid lines correspond to 1-day cure; dashed line corresponds to 28-day cure. Blue shading denotes "good performer" mixture from Table 6

In order to provide comparative results for these mixtures purely on the basis of w/cm ratio the cement and coarse aggregate values per cubic yard were held constant. Therefore, the true differences in the mixture designs is the water and fine aggregate content, thereby changing the paste content between each mix. Each of these mixtures and their adjacent comparative w/cm ratio mixtures do not initially confirm the established concept that with an increased w/cm ratio (cement and coarse aggregate held constant) the drying shrinkage, micro-strain, of the specimen should also be increased. However, the long term shrinkage data collected proved to be more in agreement that as the w/cm increases the drying shrinkage also increases. Concrete mixtures with lower w/cm not only develop lower shrinkage strain but also discontinue advancement shrinkage sooner by establishing a RH equilibrium with the environment at a faster rate.

With respect to good and bad performers, both showed similar degrees of shrinkage, (e.g. 400 microstrains when cured for 1 day and approximately 300 microstrain when cured for 28 days).

4.2.4.2.2 Effect of Cement Source

Figure 25 shows the drying shrinkage curve for two base concrete mixtures (M1-NC and M4-SCC), each of which, have a direct duplicate with different Type III cement sources (PC-III-A and PC-III-B) for 0.26 and 0.31 w/cm.

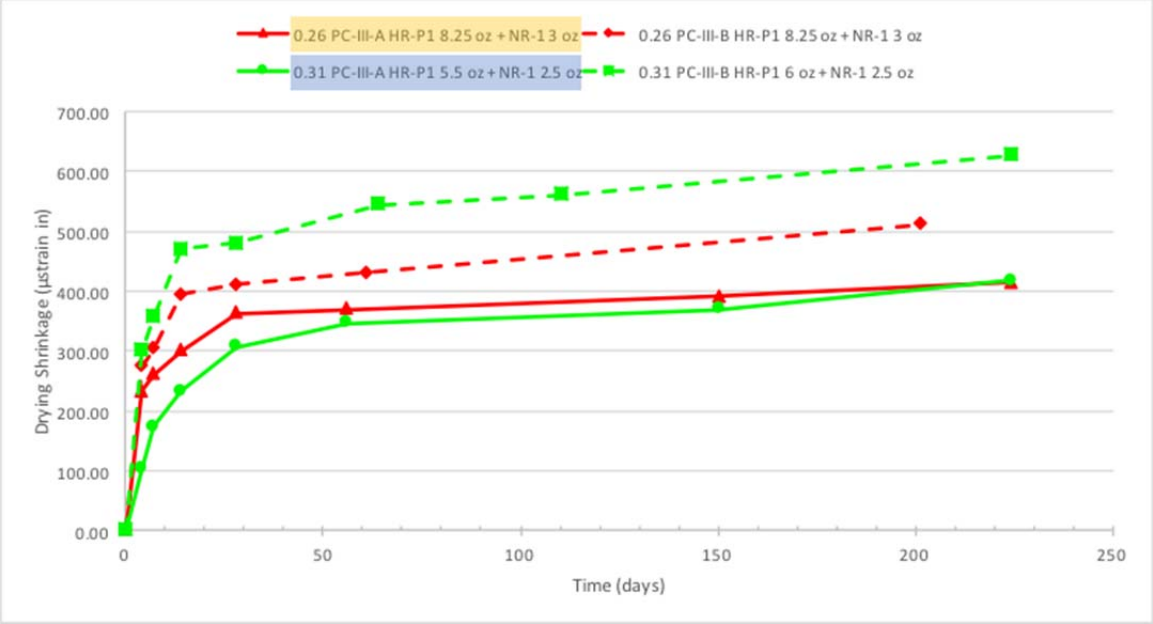

Figure 25: Drying Shrinkage Curve showing effect of Cement Source (PC-III-A and PC-III-B) for 0.26 and 0.31 w/cm ratios for base mixture M1-NC and M4-SCC respectively. Dashed line corresponds to PC-III-B cement source; solid lines correspond to PC-III-A cement source. Yellow and blue shading denotes "bad performer" and "good performer," respectively taken from Table 6

The graph shows that for both w/cm ratios the PC-III-B cement source develops more shrinkage initially as well as in the long term shrinkage compared to PC-III-A cement source. In order to provide reasoning for the shrinkage difference based on cement source the Blaine fineness of the cement was determined. As previously discussed in Chapter 3 of this report, the Blaine fineness of PC-III-A and PC-III-B were reported as 486.3 and 519.8m2/kg, respectively. Smaller cement grain size increases autogenous shrinkage effects at an earlier age (Ei-ichi et al. 1994); therefore, the increased rate of shrinkage with PC-III-B as compared with PC-III-A as seen in Figure 25 may be attributed to an increase in autogenous shrinkage occurring in conjunction with drying shrinkage. A precast temperature history profile performed and displayed in Figure 121 in the Appendix IV of this report proved that PC-III-A mixtures showed a greater delay in the initiation of the acceleration period as compared with PC-III-B.

4.2.4.2.3 Effect of Cement Type

Figure 26 shows the drying shrinkage curve for two concrete mixtures (T5-M5 and T5-M7), where both have all the same mixture design apart from cement types (PC-III-A and PC-I-A) accordingly for 0.28 w/cm.

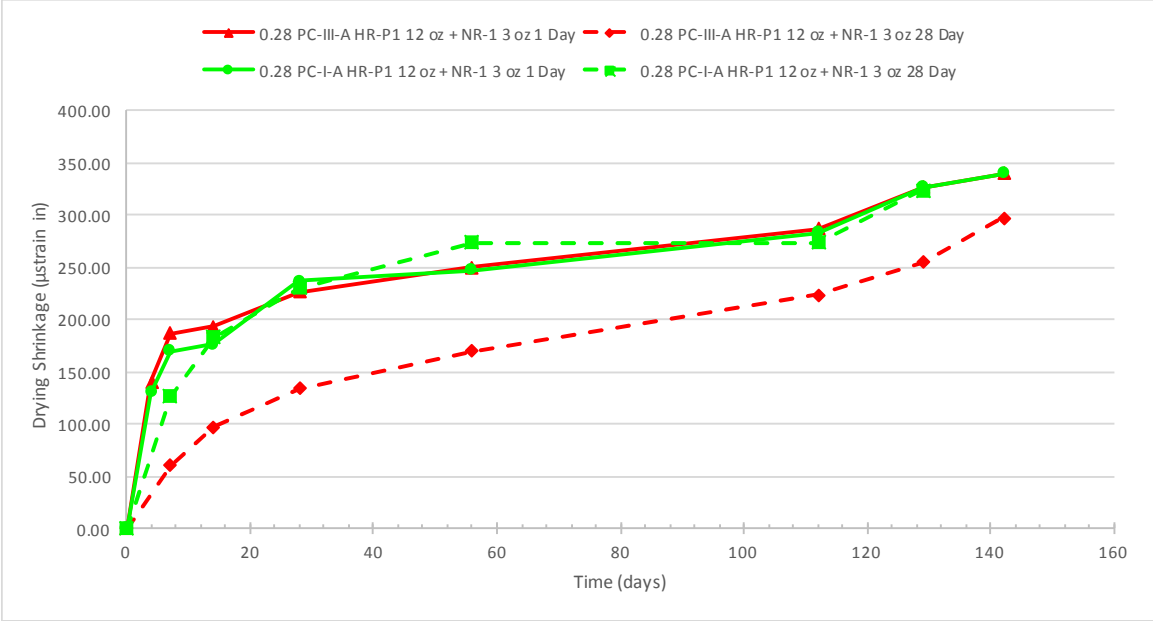

Figure 26: Drying Shrinkage Curve showing effect of Cement Type (PC-III-A and PC-I-A) and curing period for 0.28 w/cm ratios for mixtures T5-M5 and T5-M7. Green lines correspond to an ASTM C150 Type I cement; red line corresponds to an ASTM C150 Type III cement. Dashed lines correspond to 28-day cure; solid lines correspond to 1-day cure.

Figure 26 clearly indicates that there is no difference between the use of a type III vs a type I cement taken from the same source from 1-day cure. The minimal strain difference between 1-day cure and 28-day cure for type I cement lacks reasoning and has been attributed to potential measurement error.

4.2.4.2.4 Effect of HRWR Dosage

Figure 27-28 shows the drying shrinkage curve for two base concrete mixtures (M1-NC and M3-NC), each of which, have a direct duplicate with varying HRWR dosages for 0.26 and 0.33 w/cm.

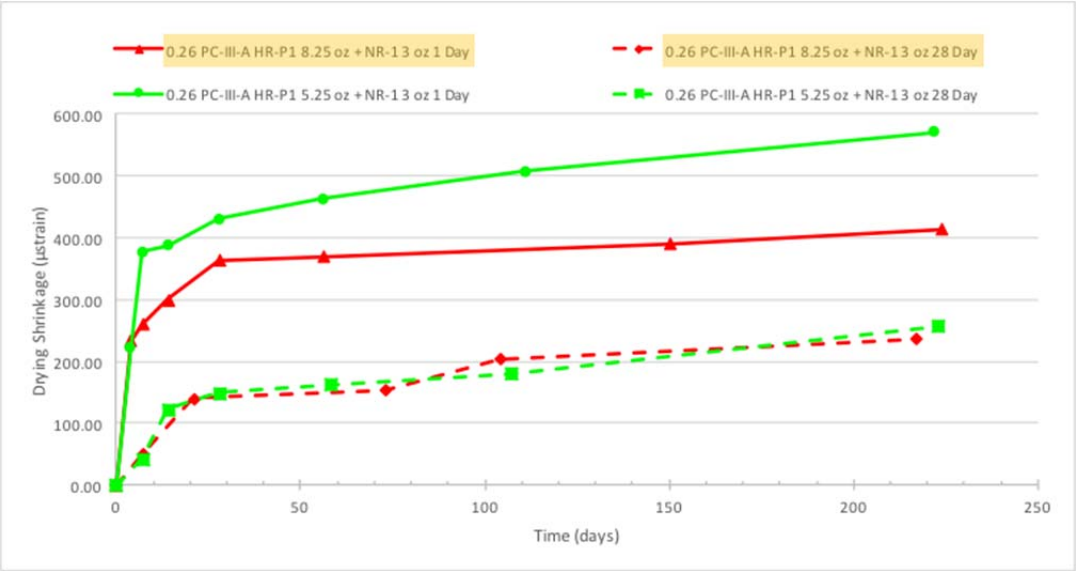

Figure 27: Drying Shrinkage Curve showing effect of HRWR Dosage for base mixture for M1-NC for 1 and 28 Day Curing. Dashed lines correspond to 28-day cure; solid lines correspond to 1-day cure. Yellow shading denotes "bad performer" mixture from Table 6

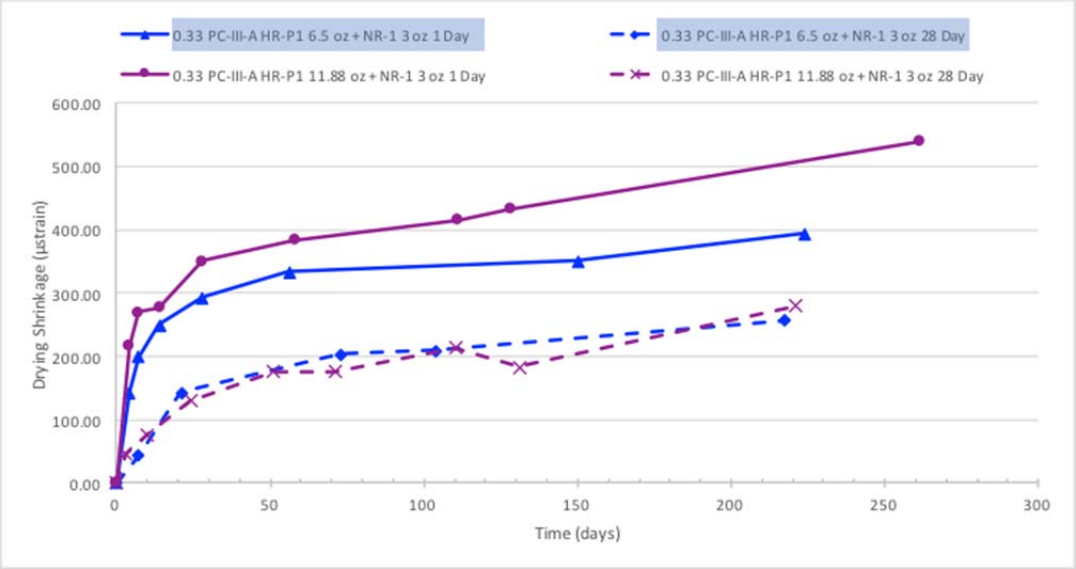

Figure 28: Drying Shrinkage Curve showing effect of HRWR Dosage for base mixture M3-NC for 1 and 28 Day Curing. Dashed lines correspond to 28-day cure; solid lines correspond to 1-day cure. Blue shading denotes "good performer" mixture from Table 6

Figure 27 models base mixture M1-NC (0.26 w/cm with a HR-P1 8.25 fl oz/100 lb cement dosage and NR-1 3 fl oz/100 lb cement) compared to 0.26 w/cm mixture with a HR-P1 5.25 fl oz/100 lb cement with NR-1 3 fl oz/100 lb cement mixture. The mixture with lower HRWR dosage proves to continue to develop extensive shrinkage beyond the base M1-NC mixture. However, Figure 28 tells a different story, as the increase in HRWR from 6.5 fl oz/100 lb cement to 11.88 fl oz/100 lb cement proves to develop shrinkage at a greater rate.

4.2.4.2.5 Effect of HRWR Type

Figure 29-30 shows the drying shrinkage curve for two base concrete mixtures (M1-NC and M4-SCC), each of which, have a direct duplicate with three different HRWR types (HR-P1, HR-P2 and HR-P3) for 0.26 and 0.31 w/cm.

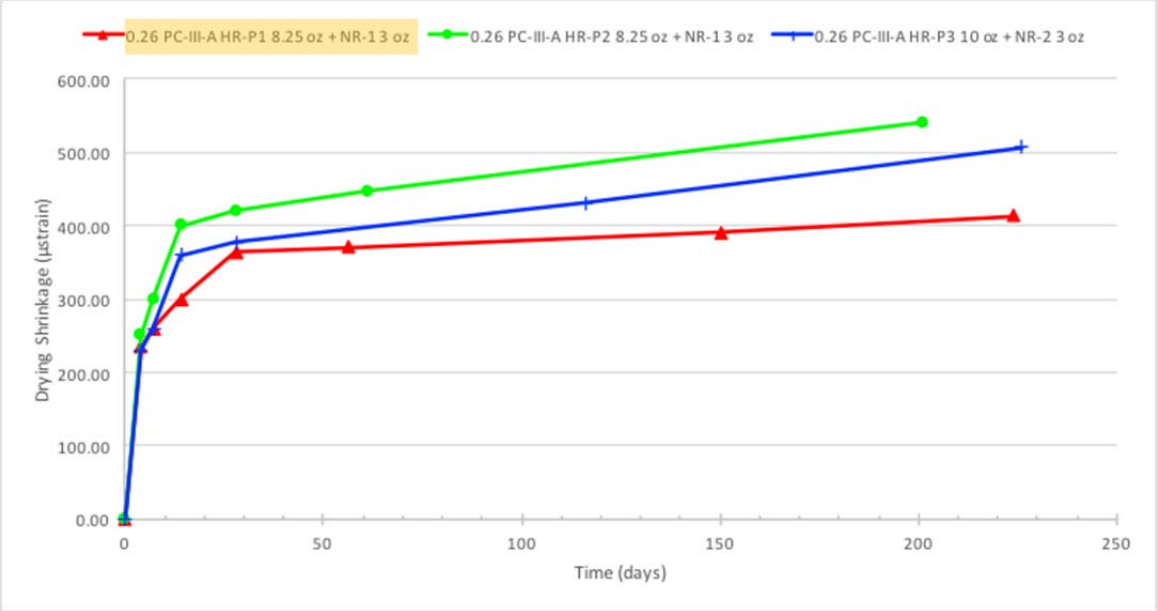

Figure 29: Drying Shrinkage Curve showing effect of HRWR type (HR-P1, HR-P2 and HR-P3) base mixture for M1-NC. Yellow shading denotes "bad performer" mixture from Table 6

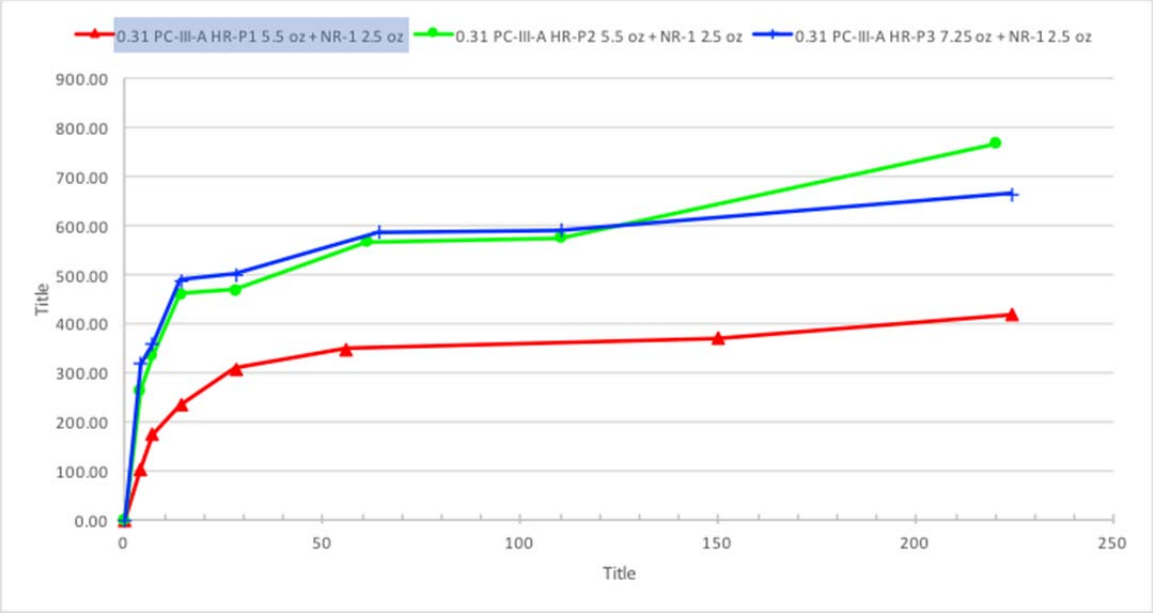

Figure 30: Drying Shrinkage Curve showing effect of HRWR type (HR-P1, HR-P2 and HR-P3) for base mixture M4-SCC. Blue shading denotes "good performer" mixture from Table 6

Three different Polycarboxylate-based HRWRs (HR-P1, HR-P2 and HR-P3) in conjunction with two different normal range water reducing and retarding (Type D) admixture (NR-1 and NR-2) were used for the comparison. The selection of the HRWR types along with their corresponding dosages was based on common admixture practices observed at precast plants, as well as targeted slumps obtained in the lab for proper consistency between different mixture designs.

For w/cm 0.26 mixtures, the comparison of drying shrinkage proved fairly similar between the three polycarboxylate (HR-P1, HR-P2 and HR-P3) mixtures, especially early ages, as shown in Figure 29. Continued development of shrinkage shows that HR-P1 shows the least amount of shrinkage followed by HR-P3 and HR-P2 with the largest amount of shrinkage. Whereas, Figure 30, w/cm 0.31 mixtures, shows that the HR-P1 developed a significantly lower rate of shrinkage as compared with the other 0.31 w/cm mixtures with HR-P2 and HR-P3. Note, that in order to establish a similar slump to the other mixtures, the mixture containing the HR-P3 HRWR agent required an additional 2.25 fl oz/100 lb (i.e., dosage was 7.25 fl oz/100 lb cement in total) as compared to the mixtures. However, similar shrinkage between HR-P2 and HR-P3 was seen (see Figure 30).

4.2.4.2.6 Effect of Cement Content

Figures 31-32 shows the drying shrinkage curve for two base concrete mixtures (M1-NC and M3-NC), each of which, have a direct duplicate with different Portland cement contents (705 lb/yd3, 517 lb/yd3, 658 lb/yd3 and 517 lb/yd3) for 0.26 and 0.33 w/cm. In order to have proper comparisons between each mixture with the w/cm ratio was held as a constant alongside the changin cement content.

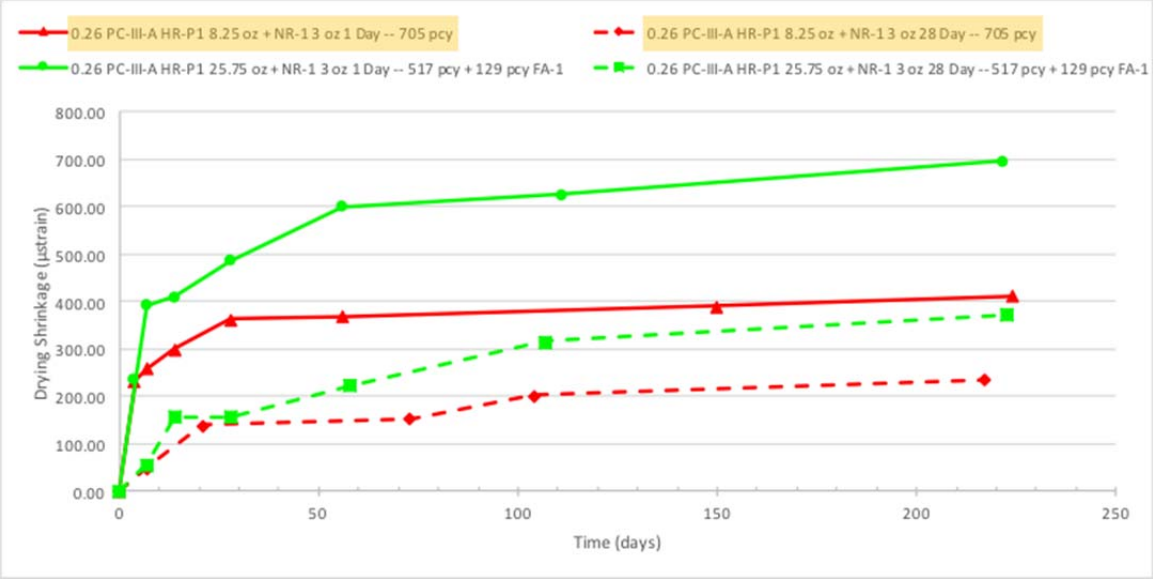

Figure 31: Drying Shrinkage Curve showing effect of Cement Content for base mixture M1-NC. Red line corresponds to mixtures with 705 lb/yd3 cement; green corresponds to 517 lb/yd^3. Dashed lines correspond to 28-day cure; solid lines correspond to 1-day cure. Yellow shading denotes "bad performer" mixture from Table 6

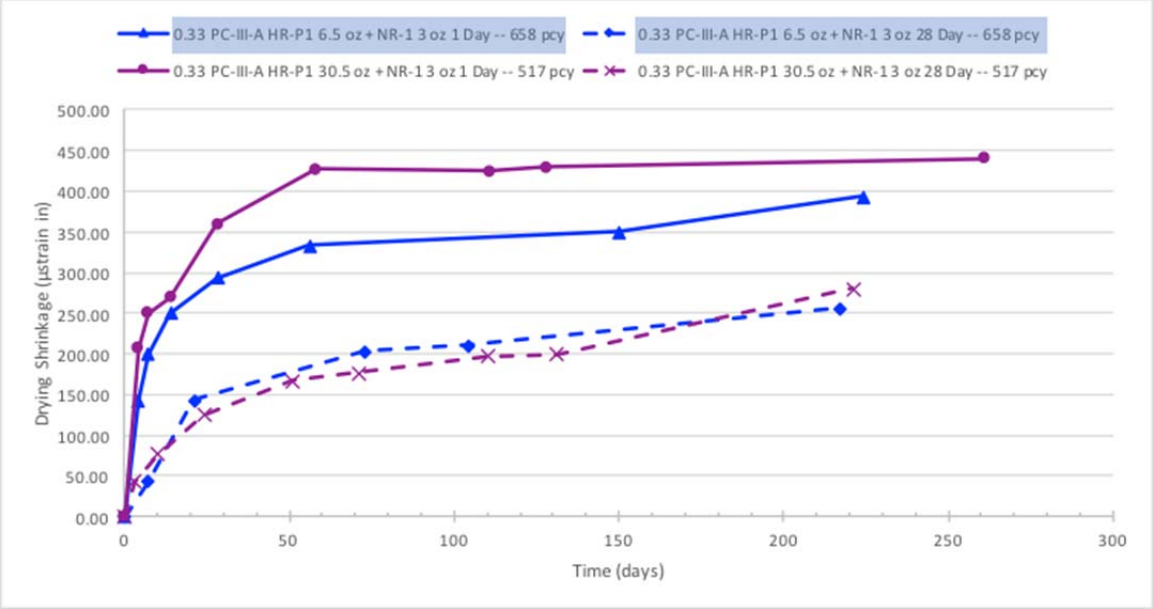

Figure 32: Drying Shrinkage Curve showing effect of Cement Content (658 lb/yd3 and 517 lb/yd3) for base mixture M3-NC. Dashed lines correspond to 28-day cure; solid lines correspond to 1-day cure. Blue shading denotes "good performer" mixture from Table 6

In order to establish similar slumps between the two cementitious contents of Figure 32, 30.5 oz was required with the 517 pcy mixture as compared with 6.5 oz for the 658 pcy mixture. Even still, the ultimate shrinkage did not appear to be effected by this substantial increase in dosage. Since drying shrinkage is majorly experienced by the paste, it is reasonable that the mixtures with greater cement content develops greater volume change. Until equilibrium is met between the concrete specimen and the testing chamber continued shrinkage measurements should reveal that the mixtures with higher paste contents develop the largest amount of shrinkage.

4.2.4.2.7 Effect of Fly Ash Addition

Figure 33-36 shows the drying shrinkage curve for five base concrete mixtures (M1-NC, M3-NC, M4-SCC, M6-CFA and M3-CWB), each of which, have a comparative duplicate with different fly ash additions (25%, 33% and 40% addition) for 0.26, 0.31, 0.33 and 0.40 w/cm.

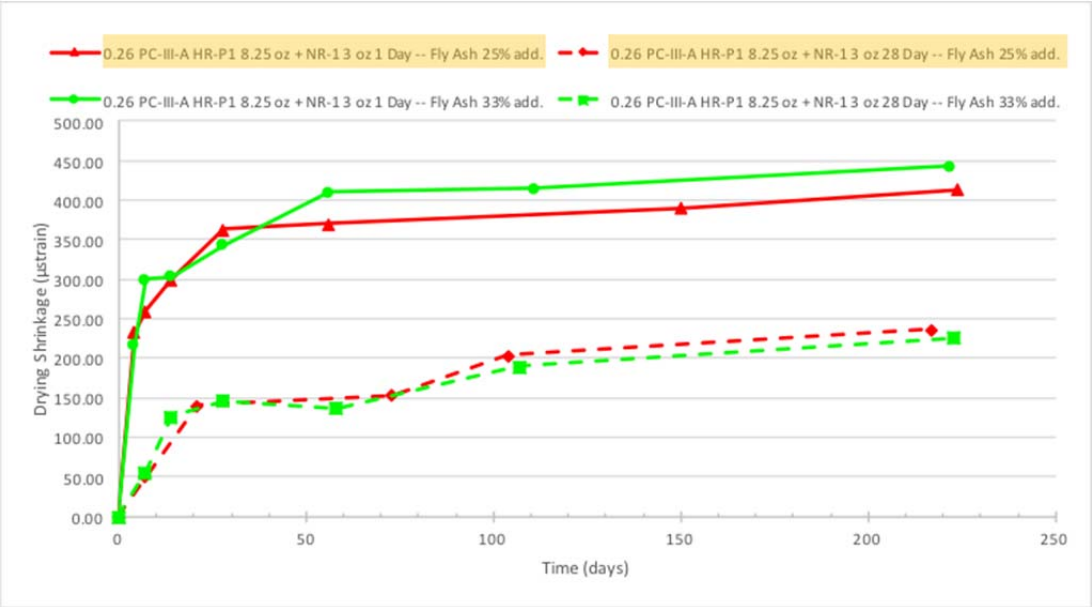

Figure 33: Drying Shrinkage Curve showing effect of Fly Ash Addition (175 lb/yd3 – 25% add. and 233 lb/yd3 – 33% add.) for base mixture M1-NC. Dashed lines correspond to 28-day cure; solid lines correspond to 1-day cure. Yellow shading denotes "bad performer" mixture from Table 6

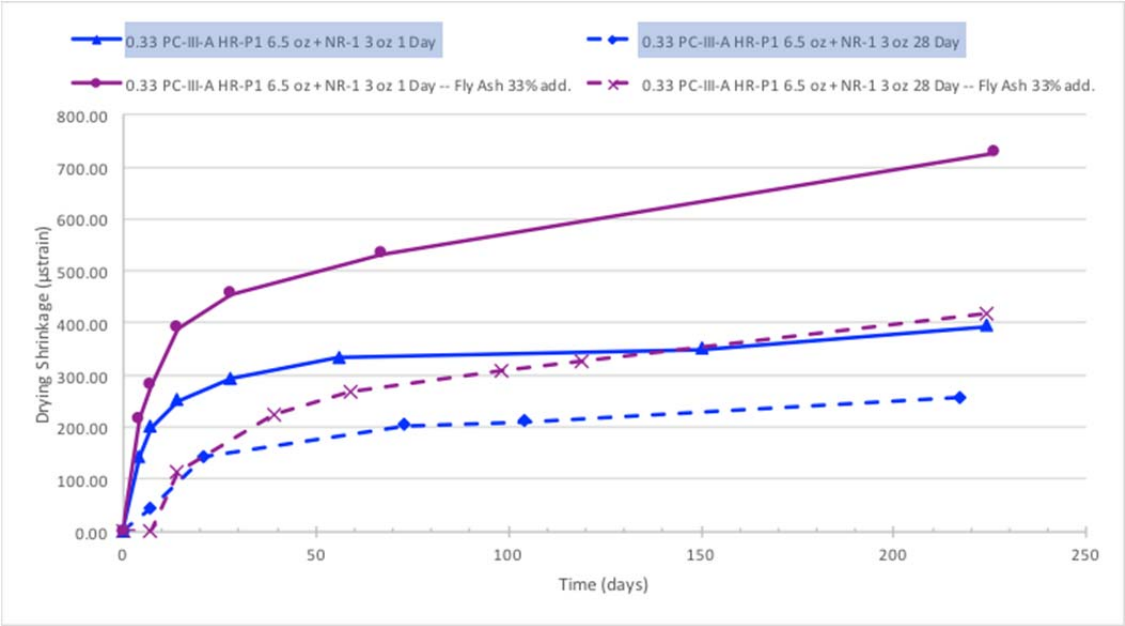

Figure 34: Drying Shrinkage Curve showing effect of Fly Ash Addition (219 lb/yd3 – 33% add) for base mixture M3-NC. Dashed lines correspond to 28-day cure; solid lines correspond to 1-day cure. Blue shading denotes "good performer" mixture from Table 6

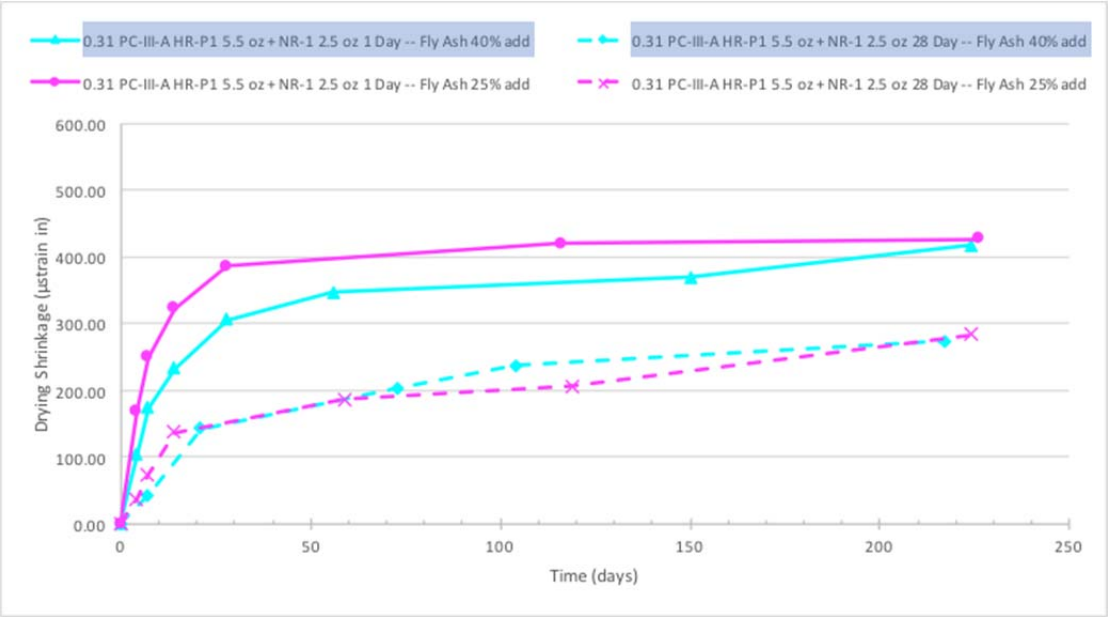

Figure 35: Drying Shrinkage Curve showing effect of Fly Ash Addition (271 lb/yd3 – 40% add and 165 lb/yd3 – 25% add) for base mixture M4-SCC. Dashed lines correspond to 28-day cure; solid lines correspond to 1-day cure. Blue shading denotes "good performer" mixture from Table 6

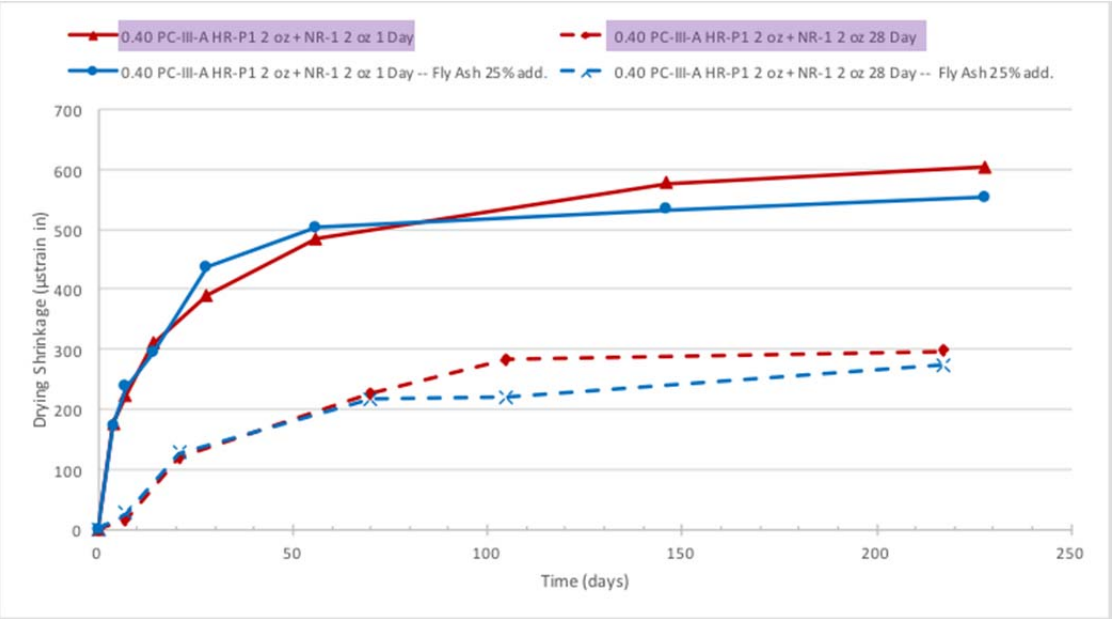

Figure 36: Drying Shrinkage Curve showing effect of Fly Ash Addition (165 lb/yd3 – 25% add) for base mixtures M6-CFA and M3-CWB. Dashed lines correspond to 28-day cure; solid lines correspond to 1-day cure. Purple shading denotes "CWB" control mixture from Table 7

As depicted in all Figures 33-36 the greater the addition of fly ash by mass of cement (25%, 33% and 40%) the more shrinkage experienced by the specimen as compared with lower cementitious contents. This phenomenon is explained by the fact that the water-to-cementitious materials ratio was held constant and therefore with the increased addition of fly ash the mixing water was also increased. The increase in drying shrinkage can be attributed to the increase in both the mixing water content and paste content. If the mixing water was to be held constant or reduced despite the fly ash addition the shrinkage of the fly ash incorporated mixtures would be substantially lower than the straight cement mixtures (Thomas 2007) (Brooks and Jiang 1999).

4.2.4.2.8 Effect of Lightweight Aggregate

Figure 37 shows the drying shrinkage curve for three concrete mixtures (M3-NC, M3-CSP and M3-CLWA) all with 0.33 w/cm ratio, but varying fine aggregate sources FA-A, FA-B and FA-LW.

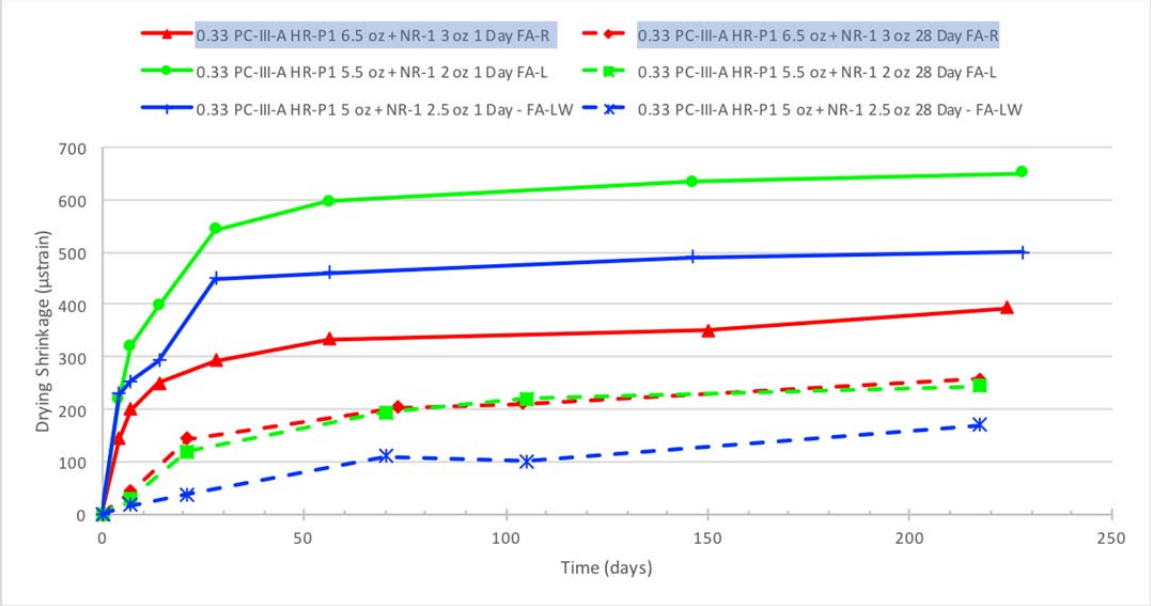

Figure 37: Drying Shrinkage Curve showing effect of Fine Aggregate Source (FA-A, FA-B and FA-LW) for mixtures M3-NC, M3-CSP and M3-CLWA (20% of the fine aggregate replacement with lightweight aggregate). Dashed lines correspond to 28-day cure; solid lines correspond to 1-day cure.

Literature has shown that the use of saturated lightweight fine aggregate can aid in internal curing of the concrete and mediate or even eliminate autogenous shrinkage effects, while maintaining the critical tensile stress well under the tensile capacity of the concrete (Cusson 2008). Yet in order to have true comparison of w/cm ratio proper care must be taken as to not provide excess water to the mixture with respect to the saturated light aggregate. Prior to mixing using the manufactured light weight aggregate the sand

was oven dried. Then 24 hours prior to mixing, the water required to get the sand in a saturated surface dried state (SSD) in addition to several pounds of mixing water was used to fully submerge and soak the sand. Despite the special attention that was provided to mixing with FA-LW the benefits of using the lightweight aggregate remain to be unseen with respect to drying shrinkage measurements.

4.2.4.3 SUMMARY AND CONCLUSIONS

Based on the results of this section the following conclusions may be drawn:

- "Good" and "Bad" Performers: For each individual comparison both the "good" and "bad" performance mixtures showed less shrinkage than the mixtures that the individual parameter was compared to. This again, reaffirms that ASTM C494 cannot properly discern between mixtures prone to cracking and not prone to cracking through the non specific approach.
- The increase in w/cm ratio where the paste is held as a constant showed to be directly related to an increase in ultimate drying shrinkage of the concrete. w/cm ratio proved to be the greatest governing factor with respect to effecting ultimate drying shrinkage measurements.
- The two cement sources PC-III-A and PC-III-B for the same mixture designs developed different drying shrinkage curves. PC-III-B in all cases developed significantly greater linear strain from drying shrinkage as compared with PC-III-A. This could be related to the coarser cement grain size of PC-III-A, which creates a less porous microstructural network structure than the PC-III-B cement. This has the effect of reducing reduces chemical and thereby autogenous shrinkage of the concrete in the initial weeks after casting (Ei-ichi et al. 1994).

- Differences in cement type PC-I-A and PC-III-A proved to have minimal effects with respect to drying shrinkage.
- No conclusions may be drawn to associated HRWR dosage and its effect on drying shrinkage. Increase and or decrease in dosages for the same mixture design and admixtures did no correlate to an increase or decrease in drying shrinkage.
- Changes in HRWR type for two separate mixture designs concluded that HR-P3 incurred the most amount of drying shrinkage followed by HR-P2 and HR-P1 developed the least linear shrinkage.
- It has been well established in literature that higher paste content results in greater drying shrinkage. It is believed that the ultimate drying shrinkage for the mixtures compared in this report will inevitably confirm that higher paste content results in higher linear drying shrinkage stain.
- The incorporation of fly ash addition as compared to straight cement mixtures resulted in increased drying shrinkage. This can be attributed to the increase in paste content that was a result of holding the water-to-cementitious ratios constant.
- No conclusion can be drawn from the incorporation of FA-LW with respect to drying shrinkage. Continued measurements may reveal more latent effect of the ultimate reduction in drying shrinkage as compared with the other two aggregate sources. At 224 days the mixture with the siliceous aggregate FA-A has experienced the least amount of shrinkage for 1-day cure.

4.3 SUITABILITY OF ASTM C494: RESULTS AND CONCLUSIONS

Currently, The Standard Specification for Chemical Admixtures in Concrete, ASTM C494, attempts to evaluate admixtures based on limited testing procedures, non of which, are able to properly quantify the extent of the latent cracking effect as seen in the field as a result of excessive shrinkage. Therefore, the tests revealed that the hypothesis of implementing a specific and non specific approach with ASTM C494 is not capable of discerning "good" and "bad" performers. Below is a bulleted representation of the results of each individual test performed towards the hypothesis:

- *Water Content:* Both the "good" and "bad" performers passed with respect to the CWB control mixture. Therefore, water content evaluation cannot be used to predetermine a mixture designs cracking potential.
- *Time of Set:* Both the "good" and "bad" performers passed and failed for half of their respective mixtures. Therefore, time of set should not be used as a discernable means of evaluating a mixture designs cracking potential.
- *Compressive Strength:* Both of the "good" and "bad" performers passed or failed approximately half of the set compression limits and according dates for ASTM C494. Therefore, compressive strength should not be used as a discernable means of evaluating a mixture designs cracking potential.
- *Drying Shrinkage:* Both of the "good" and "bad" performers passed or failed half of limits set in ASTM C494 and at the last available measurement date (6-months). Therefore, drying shrinkage should not be used as a discernable means of evaluating a mixture designs cracking potential.

CHAPTER 5: PARAMETRIC STUDY: DEVELOPING A COMPLEMENTARY TESTING MATRIX TO ASTM C494

5.1 INTRODUCTION

Based on the preconceived notion that ASTM C494 testing procedures would likely be inadequate towards testing HRWR's potential towards inciting micro-cracking in concrete mixtures, a complementary testing matrix to ASTM C494 was developed. This matrix consisted of a parametric study based on concrete mixtures and paste mixtures to the restrained shrinkage and autogenous shrinkage behavior of the mixtures (see Figure 38).

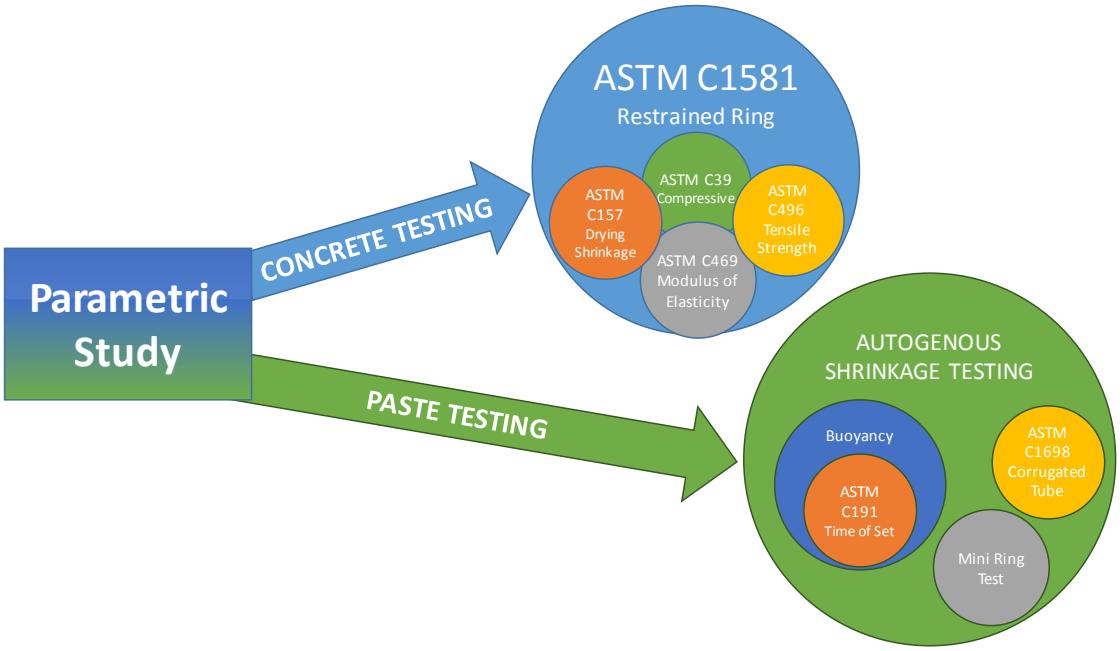

Figure 38: Parametric study testing breakdown between concrete and paste analysis

The following sections are divided into Concrete Testing (5.2) and Paste Testing (5.3). Both concrete and paste analysis testing required completely new integration and development of instrumentation. Detailed information has been provided regarding the newly developed testing setups to ensure that if applicable equipment can be replicated and or improved upon in the future.

Due to the disconnect between concrete and paste results with respect to autogenous testing the results of each were tabulated separately.

5.2 PARAMETRIC STUDY: CONCRETE TESTING

This chapter will describe the laboratory parametric study that was developed to investigate HRWR Type F prevalence towards increased latent micro cracking in concrete. The testing involved evaluating select concrete mixtures with HRWR in order to study their effect with respect causing cracking in the restrained shrinkage ring test, ASTM C1581. The mixtures employed were selected based on actual precast plant mixtures that had proven to develop latent micro cracking in the field. Table 13 presents the mixtures selected for concrete evaluation in the restrained ring test.

Table 13: Concrete mixtures subjected to the restrained ring test parametric study

Mix ID	w/cm	Cement Type	Cement Content (lb/yd^3)	SCM Content (lb/yd^3)	Aggregate Source		Admixtures			
					FA	CA	Type	(floz/100 lb cement)	Type	(floz/ 100 lb cement)
Mix 7	0.26	PC-III-A	705	175	FA-R	CA-R	HR-P2	8.25	NR-1	3
Mix 6			705	175	FA-R	CA-R	HR-P3	10	NR-2	2
Mix 4		PC-III-B	705	175	FA-R	CA-R	HR-P1	8.25	NR-1	3
Mix 3	0.28	PC-I-A	705	-	FA-R	CA-R	HR-P1	12	NR-1	3
Mix 1		PC-III-A	705	-	FA-R	CA-R	HR-P1	12		3
Mix 5	0.3	PC-III-A	564	188	FA-RII	CA-RII	HR-P3	8.25	NR-2	2
Mix 8	0.31	PC-III-A	663	271	FA-R	CA-R	HR-P4	7.25	NR-2	2.5
Mix 2	0.33	PC-III-A	658	-	FA-R	CA-R	HR-P2	12	NR-1	3

5.2.1 RESTRAINED SHRINKAGE RINGS

5.2.1.1 PROCEDURE AND EXPERIMENTAL SETUP

As described in Chapter 2, the testing program employed for measuring stress development in concrete due to restrained shrinkage is the restrained shrinkage ring test as per ASTM C 1581. The restrained shrinkage ring test was implemented along with drying shrinkage prims with like surface area to volume ratio as well with 3x6-in cylinders that were subjected to the same drying and temperature conditions. These complementary samples were cast with the rings to procure compressive, tensile and modulus of elasticity properties at 1, 3, 7 and 28 days after casting. This section will discuss how the measured mechanical properties coincide as well as how these properties may be used to predict the results derived from the restrained ring setup.

The setup that was implemented at the University of Texas at Austin was created to fulfill the requirements outlined in ASTM C1581 as well to as implement cost-effective nuances as per current literature and developments in the test. The core of the setup is built around a mild, 0.5 ± 0.05-in thick, steel ring. The outer diameter of the ring was 13.0 ± 0.12-in. The inner and outer circumferences of the rings were machined to a specification of at least 63 micro-inches. An outer ring constructed of HPVC pipe was placed around the steel ring. The diameter of the HPVC ring was 16.0 ± 0.12-in and the height of the HPVC ring was 6.0 ± 0.25-in. The HPVC ring was cut or "slit" longitudinally in order to allow the user to de-mold the concrete ring at final set. The slit was re-aligned through a stainless steel vise as pictured alongside the CAD drawing in Figure 39.

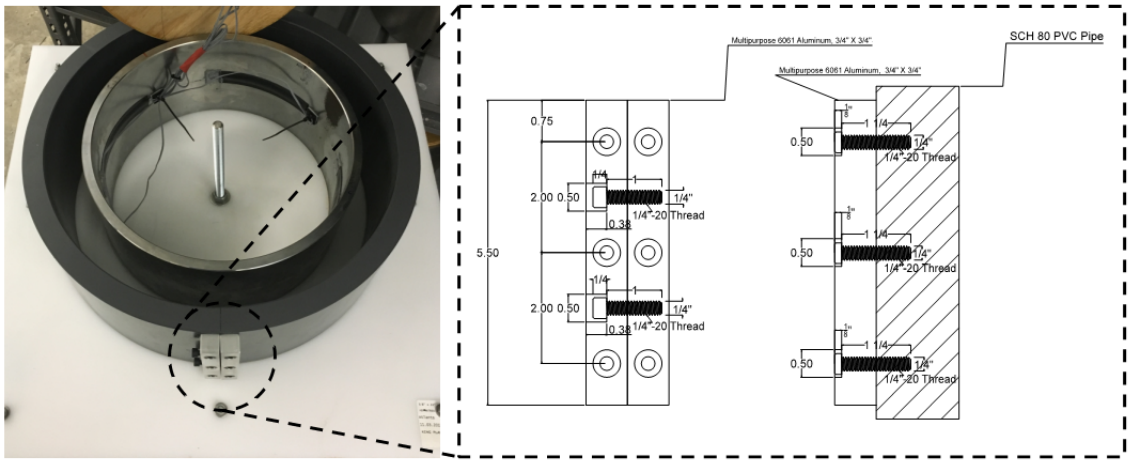

Figure 39: Stainless steel vise and CAD drawing used to align the 6-in longitudinal slit in the outer HPVC 16-in pipe

Both the steel ring and the outer HPVC rings were set on a 3/8-in thick, 24x24-in dimensions, rigid HDPE polyethylene plastic sheet The plastic was selected for its low friction, non-absorptive and economical cost properties. The plastic bases were routed or grooved in order to accept both the inner steel ring and the outer HPVC 16-in inner diameter pipe. The grooved edges created a tight seal between the rings and the plastic substrate as well as assured that the rings were set perfectly centered within one another. The bases have 3 locations to secure and lock down the outer HPVC ring into place as and the inner ring is locked into place through the use of a centralized piece of ½" stainless steel all-thread. Both mechanisms for securing the inner and outer rings during casting are pictured in Figure 40.

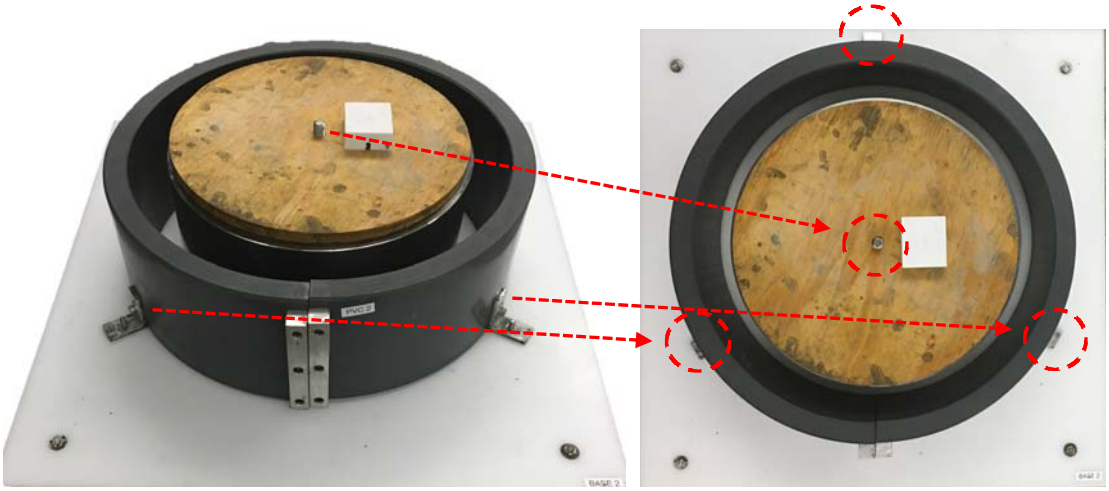

Figure 40: Locking locations for securing the inner and outer rings to the restrained shrinkage ring bases denoted in red

The strain monitoring aspect of the restrained shrinkage rings is composed of 4 two-wire strain gauges (FLA-6-11-1L). The gages are set at the midpoint of the ring and at a quarter circumferential distance from one another. The gages are set using Loctite (496 Instant Adhesive) epoxy and have been carefully oriented to measure solely lateral deformation. The gages are each covered by viscoelastic membrane (Dow 700) to assure that they are not disturbed during the casting process and/or encounter future corrosion issues. The gage wire is carefully tapered around the ring and the bound up and set into a terminal that is seated on a wood casing. The wire terminal accepts the +/- from each of the strain gages and strategically organizes the wire within the box denoting the gage location on each of the rings. Figure 41-42 provides a photo of the gages that are set in each of the restrained rings as well as a diagram of the input terminal with each of the gages H (+) and L (-). These figures also show the location of the strain gage relative to one another. Note that Figure 41 denotes the location of where the collection of strain

gage wires have been set through. At this location the strain gage wire leads are accepted on the other side into the input terminal as shown in Figure 42.

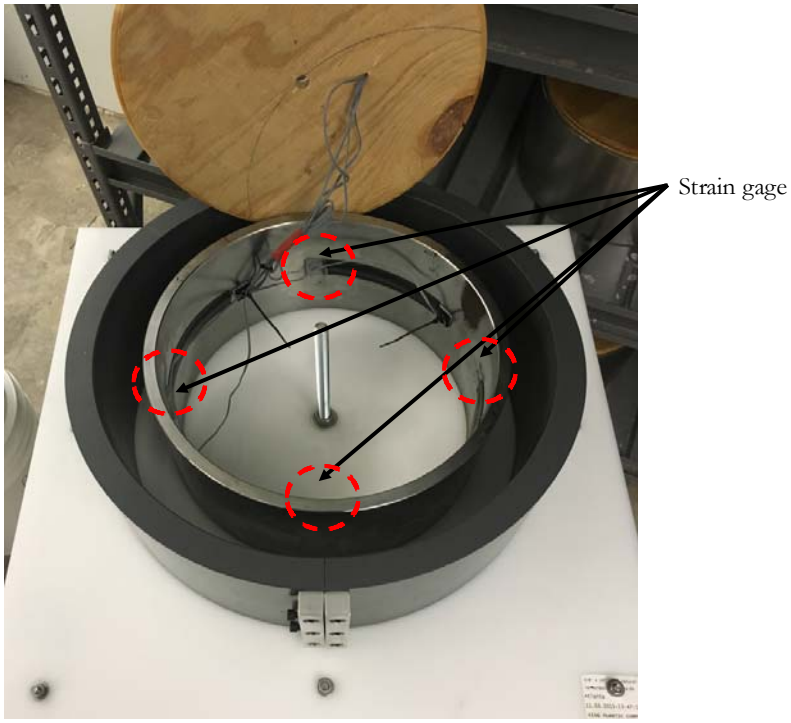

Figure 41: Strain gage locations on restrained shrinkage ring

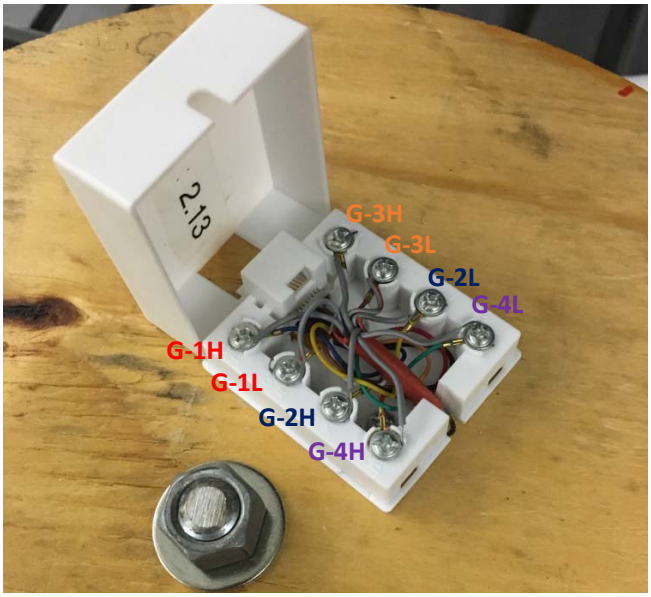

Figure 42: Terminal diagram for restrained shrinkage ring strain gages

From the terminal input an Ethernet cable with wires that are individually insulated to reduce interference is used. The Ethernet cable was selected based on the gage wire similarity to the strain gages as well as its economic properties and individually insulated cabling. The Ethernet cables are set just above each of the rings dropping down just over the top of the terminal inputs as pictured in Figure 42. From the rings the Ethernet cables are run to the data acquisition system (DAQ). Figure 43 denotes the setup implemented at the University of Texas at Austin for collecting strain data on the restrained shrinkage rings.

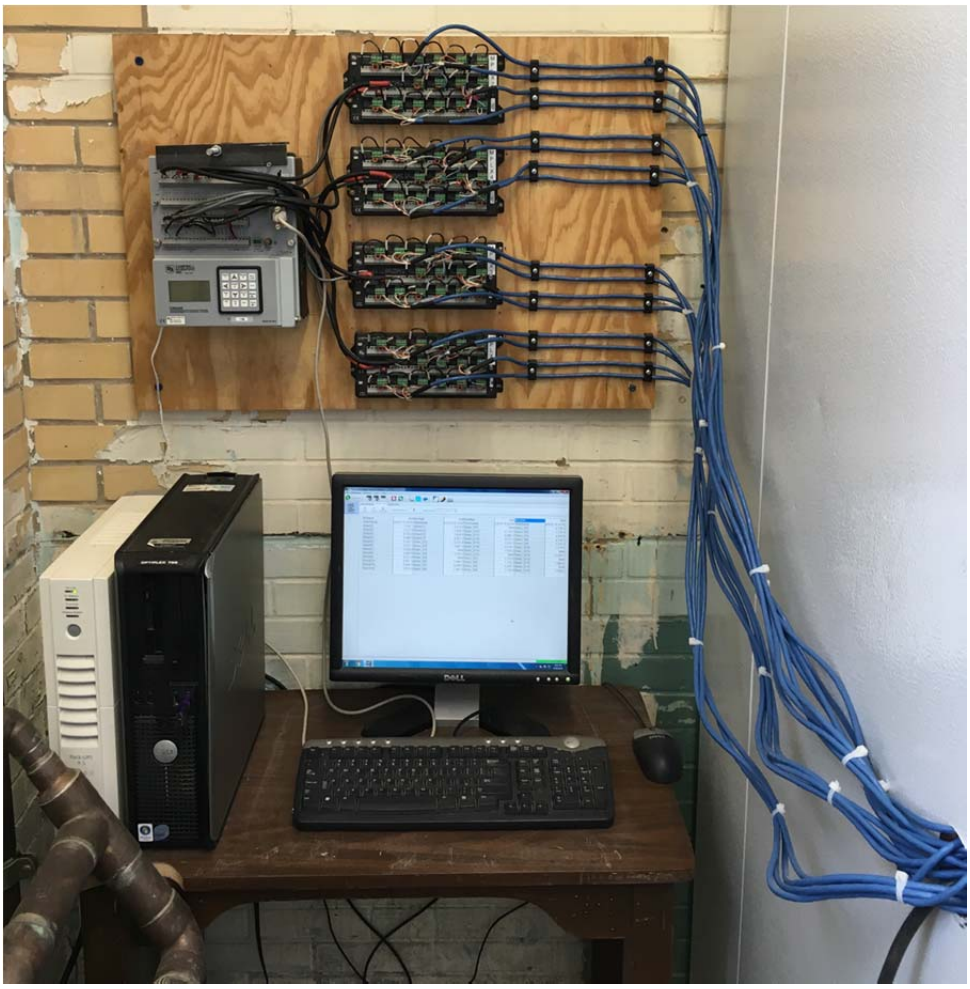

Figure 43: DAQ setup employed at the University of Texas for Collecting restrained shrinkage ring strain data

The central component of the restrained shrinkage ring DAQ is a Campbell Scientific CR 5000. Extending from the CR 5000 is a set of 4 multiplexers (AM 16/32). Each of the multiplexers have the capacity to collect data from 16 strain gages and therefore the capacity to measure 4 restrained rings setups. From the multiplexers, calibrated terminal input modules (TIM) (4SWB120's) have been used in order to collect the data from each of the strain gages. The TIM each act as the three other quadrants of a

Wheatstone bridge. Each of the strain gages are directly connected to a TIM. A diagram of the DAQ and how it is interconnected with the restrained shrinkage ring is shown in Figure 44.

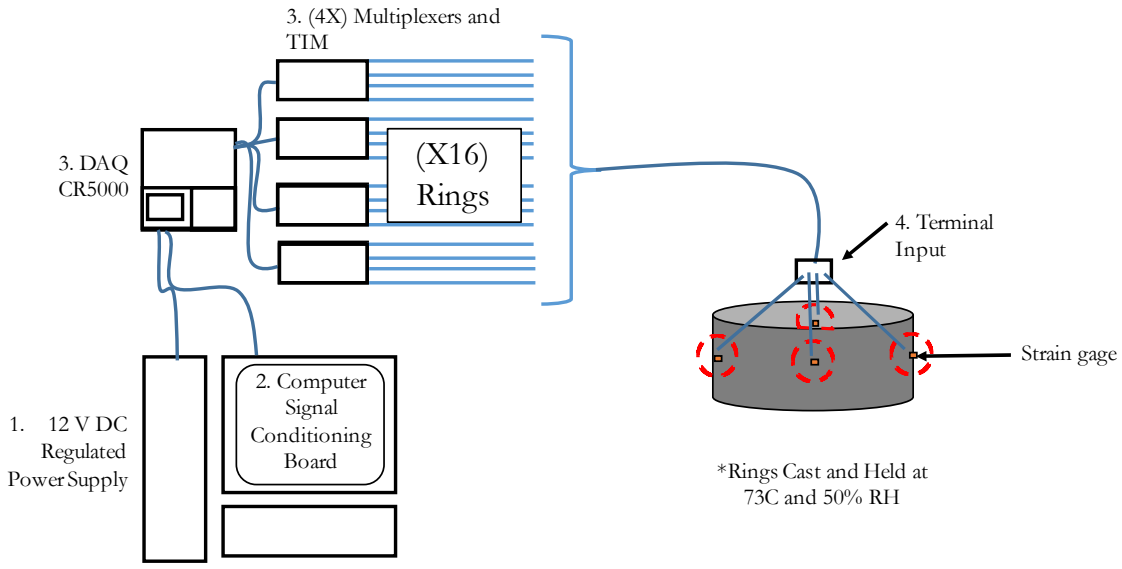

Figure 44: Diagram of the restrained shrinkage ring setup

The DAQ was programed in Campbell Scientific CR Basic program via PC400. The program calls to excited the strain gages every minute and collect data on each of the gages at 5 min intervals. The excitations were supplied with a second of interim delay between each subsequent reading to not provide interference between adjacent gages. The shortcut programing code implemented for this projects has been outlined in Appendix V, Figure 148 of this report.

The casting procedure of the restrained shrinkage rings followed the process outlined in ASTM C1581. The concrete was cast and set in thermally controlled rooms at

23 ± 3°C. Prior to casting the ring molds were sufficiently oiled and individually set on a vibrating table. Each ring was cast in two lifts, where each lift was subjecting to rodding for a 75 count as well as 30 sec of vibrating on a vibrating table to eliminate entrapped air and reduce “bugholes” on the concrete’s surface. Assuring that the surface has limited imperfections is key to determine the true time of cracking. In the event that large entrapped air voids propagate along the surface, the concrete ring will have a smaller cross sectional area to combat the tensile stresses and can cause the ring to crack and fail prematurely. Three rings were cast for each mixture. Figure 45 provides a photo of the ring on the vibration table.

Figure 45: Casting restrained shrinkage ring on vibrating table

Since the rings were cast in the testing environment, the rings went directly from the vibrating table and into position on the drying racks. Once the rings were set into position, the Ethernet cables were connected to the terminal input and wet burlap was applied as well as plastic sheets to insulate the wet burlap over the exposed concrete

surface. The outer HPVC ring was released and removed at the time of final set. Final set was determined by ASTM C403, measuring penetration resistance of mortar specimens obtained from the concrete by sieving through a number 4 sieve. The strain was taken as zero from the point at which the rings were demolded and re-positioned onto the drying racks. The rings were sealed with HVAC tape on the tops and bottoms of the rings to facilitate solely circumferential drying shrinkage effects. Figure 46 models a 4 mixtures (3 rings each) being monitored in the testing environment (23°C and 50% RH).

Figure 46: Restrained shrinkage rings (4 mixtures), Monitored in the testing room

As discussed in Chapter 2 of this report, the stress rate in the steel rings was calculated using Equation 2-10. The average of all 4 strain gages was plotted with respect to the square root of time. An example for Mixture 8 is shown in Figure 46. The alpha, α, in Equation 2-10 is obtained using a best fit linear line for the strain development measured from the strain gages on the steel from the shrinking concrete. The strain is plotted over the square root of time after demolding the specimens.

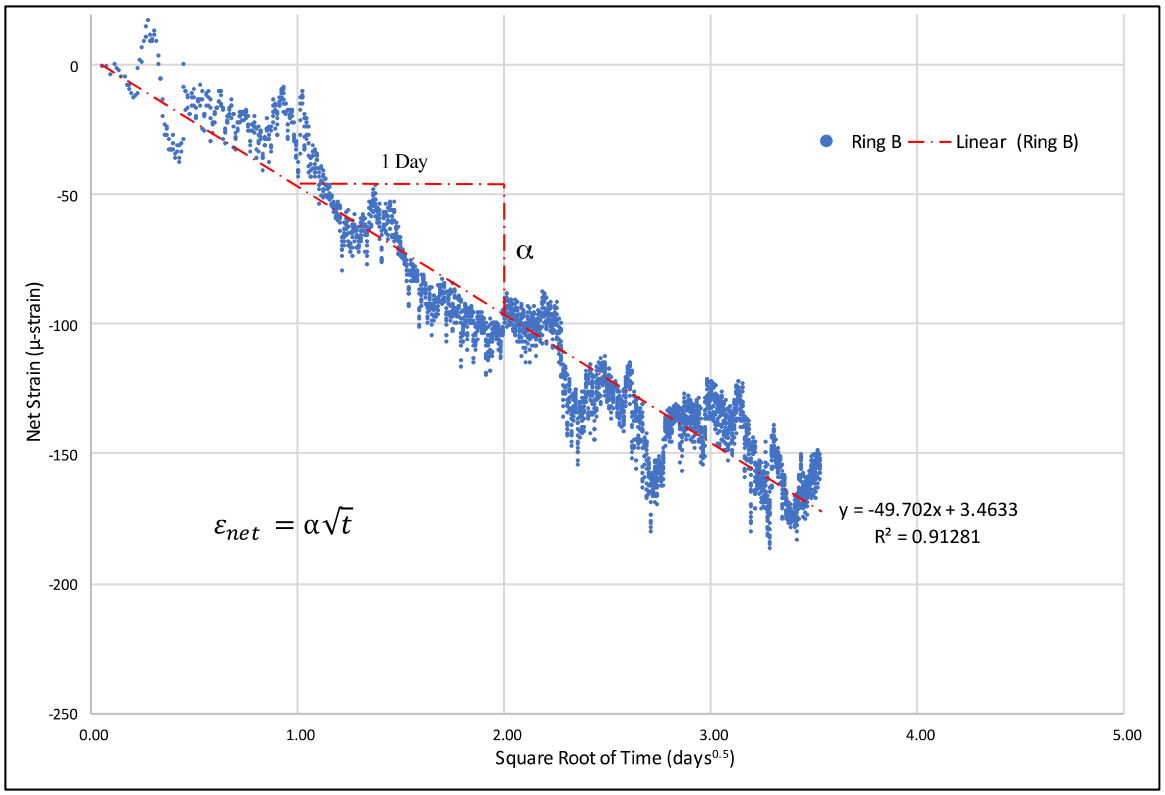

Figure 47: Net strain versus the square root of time (days) after demolding (Mixture 8)

Furthermore, based on work performed by See et al. (2004), complementary cylinders held in the same curing conditions as the restrained shrinkage rings were cast

for evaluation of mechanical properties with respect to strength and modulus as well as prisms for drying shrinkage. These complementary specimens were evaluated at 1, 3, 7, 14, and 28 days after casting. Assuming that the steel ring provides the degree of restraint, R_m, as a function of concrete's modulus, E_c, can be determined using Equation 4-1 (See et al. 2004):

$$R_m \cong 1.0\text{-}7.4*10^{-3}E_c \qquad \text{Equation 4-1}$$

5.2.1.2 RESULT AND DISCUSSION

The following sections have composed several methods for comparisons on restrained autogenous shrinkage with ASTM C1581. In order to provide development of the concrete's mechanical properties cylinders and drying shrinkage specimens were cast in conjunction with the restrained shrinkage rings. Table 14 shows the mechanical properties at 1, 3, 7 and 28 days relative to the stress rate and net time to cracking observed in the restrained ring test.

Table 14: Net time-to-cracking and stress rate for all ring mixture

RSF Mixture ID	Age (days)	Compressive Strength (psi)	Splitting Tensile Strength (psi)	Modulus of Elasticity (ksi)	Net Time to Cracking (days)	Stress Rate Cracking Psi/Day
Mix 1	1	5591	790	2478	25	20.5
	3	8127	790	3108		
	7	8698	1059	3498		
	28	9594	979	2720		
Mix 2	1	3606	501	1885	26	11.7
	3	5953	655	2655		
	7	6728	584	2934		
	28	8017	1009	2650		
Mix 3	1	1292	275	873	5	99.5
	3	5037	706	2513		
	7	5980	840	2467		
	28	6790	774	2576		
Mix 4	1	6096	578	2059	5	105.4
	3	9583	928	2628		
	7	10529	947	2877		
	28	11614	1101	2865		
Mix 5	1	3566	576	2200	TBD	TBD
	3	5016	838	2543		
	7	5395	809	2905		
	28	-	-	-		
Mix 6	1	7597	860	1901	22	37.9
	3	9921	1125	3041		
	7	11028	1090	2907		
	28	-	-	-		
Mix 7	1	1915	857	1421	14	47.6
	3	9375	986	2946		
	7	11066	929	2977		
	28	-	-	-		
Mix 8	1	7110	839	2675	TBD	TBD
	3	5016	838	2867		
	7	10801	1012	2869		
	28	-	-	-		

Table 14 shows that the greater the stress rate (psi/day) the sooner the cracking of the concrete ring occurs. Time of cracking and mechanical properties with respect to tensile strength modulus and compression strength for all completed (cracked) mixtures

was further analyzed in Figure 48-50. The plots were constructed to approximate the mechanical properties at the mixture's cracking point through linear interpretation.

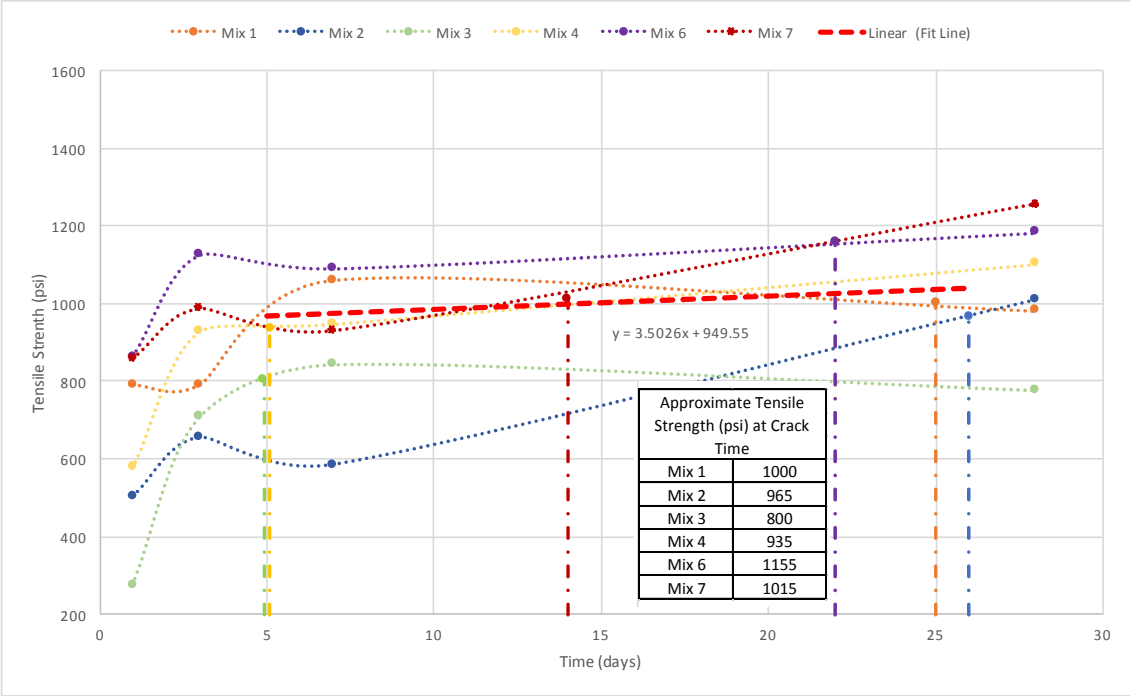

Figure 48: Tensile strength (psi) approximately determined through curve fit at time of cracking

Although tensile strength does not show significant development or rate of change between 1 and 28 day measurements the correlation between the date of cracking and the best fit linear interpretation of the approximated tensile strength (psi) data points at cracking is just over 100 psi (105 psi). Eliminating mixture 3 which is a Type I cement mixture (used for comparison purposes) the standard deviation is reduced to 75 psi. The plotted tensile strength development and best fit interpretation of tensile strength (psi) at cracking shows a very strong correlation to a value of approximately 950 psi (945.55 psi)

given mixture 3 is omitted for its inherently weaker mechanical performance. Based on the data tabulated in Figure 48 there is a strong correlation between the concrete's tensile strength development and cracking date.

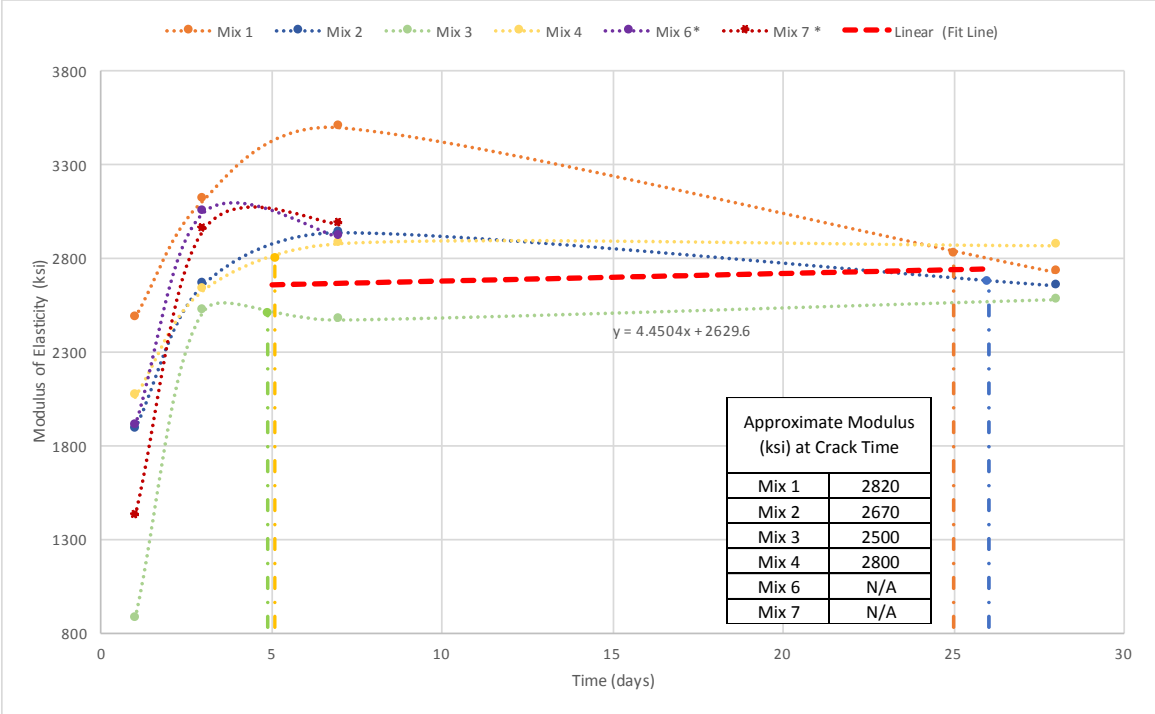

Figure 49: Modulus of Elasticity (ksi) approximately determined through curve fit at time of cracking. Best fit line (Linear) outlined in red.

The plotted modulus of elasticity development and best fit interpretation of modulus (ksi) at cracking shows a very strong correlation to a value of approximately 2600 ksi (2629.6 ksi). Unfortunately, results have been based upon 4 mixtures, but the standard deviation between approximate modulus at cracking is less than 130 ksi (128 ksi). Again, eliminating mixture 3 which is a Type I cement mixture the standard deviation is reduced to 65 ksi. Based on the data tabulated in Figure 49 there is a very strong correlation between the concrete's modulus of elasticity and cracking date.

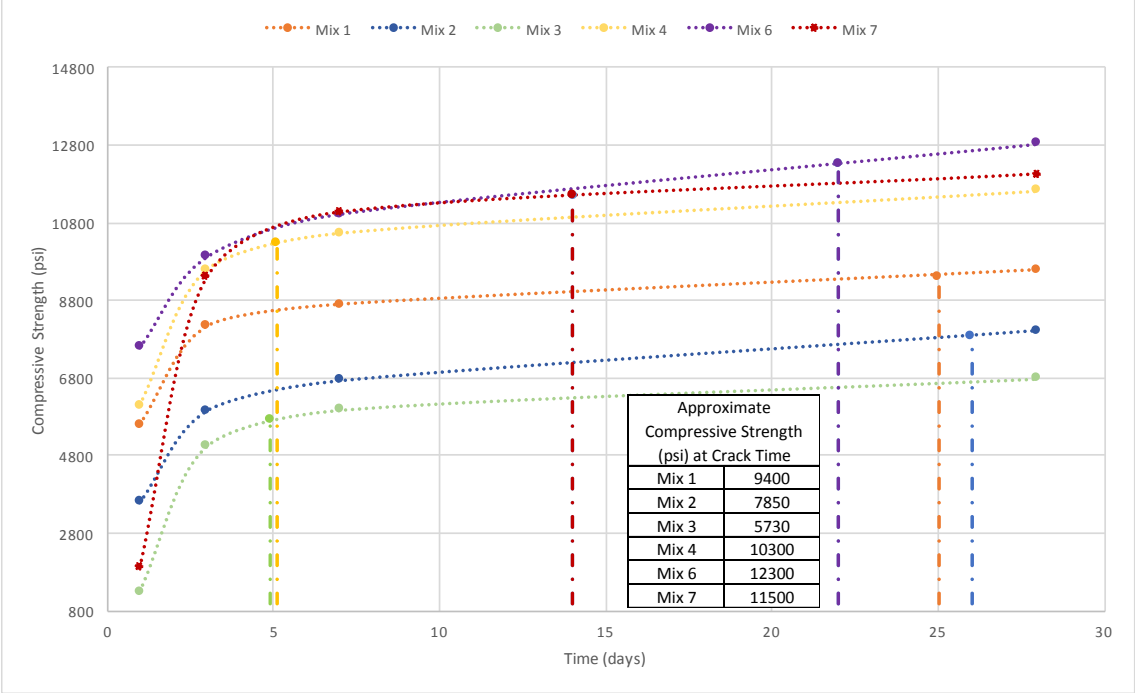

Figure 50: Compressive strength (psi) approximately determined through curve fit at time of cracking

Although tensile strength and modulus proved more consistent values, where the concrete ring. Compression data for the concrete rings produced a standard deviation between the 6 mixtures of over 2000 psi (2214 psi). Even omitting mixture 3 data the standard deviation of compressive strength at approximate time of cracking was over 1500 psi. Due to this disconnect a more detailed investigation was performed to determine cracking performance with respect to previous literature.

Based on See's work, a data set was mapped correlating drying shrinkage and modulus of concrete providing a user with the 4 quadrants for potential cracking (high,

moderate-high, moderate-low and low). These quadrants have been mapped and 7-day drying shrinkage vs. 7-day drying shrinkage values have been plotted in Figure 51.

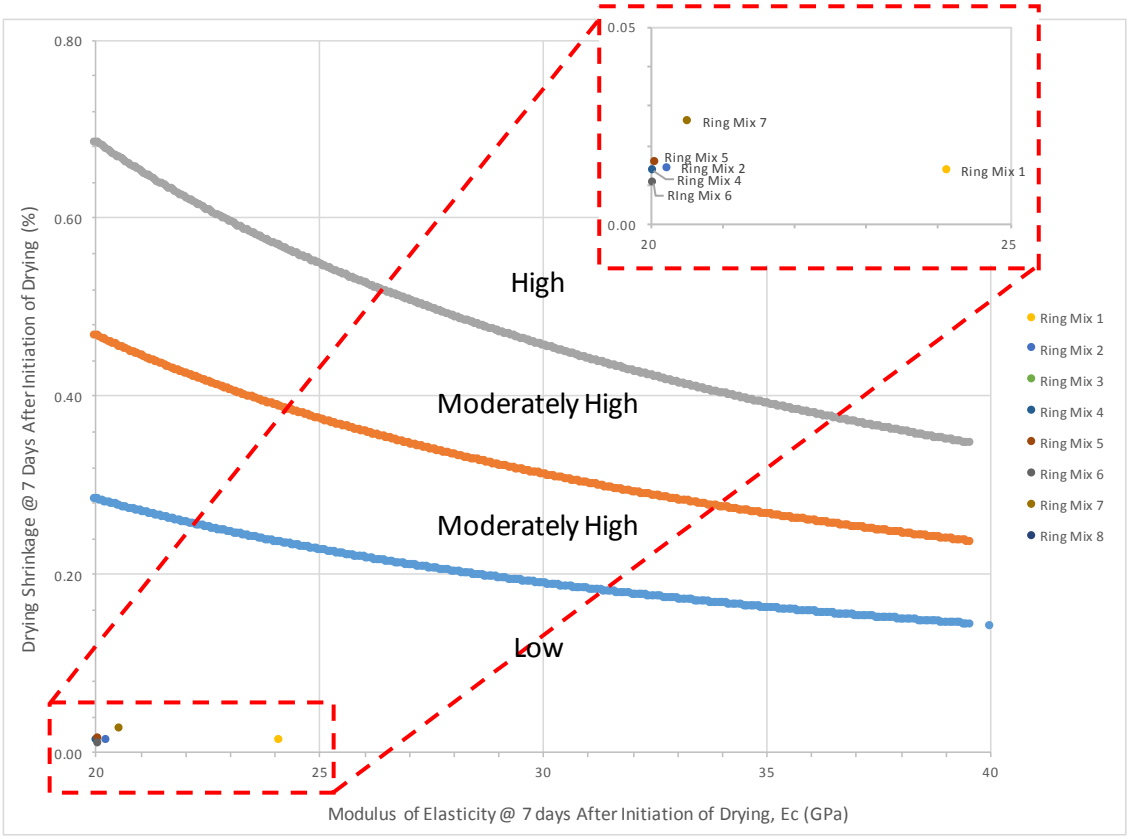

Figure 51: Cracking potential envelopes outlining the potential for each of the 8 mixture designs cast

Figure 51 shows that in reference to See's work the cracking potential of the mixture designs performed in this project have very minimal cracking potential. This can be attributed to the fact that 6 out of the 8 mixtures employed in this study are lower or as low in terms of cracking potential as the work previously performed on HPC in See's investigation (2004). Figure 52 displays the average temporal evolution of strain data for

each mixture (note, it's based on the average of 3 rings). Individual mixture design ring strain shrinkage results may be found in Appendix VII.

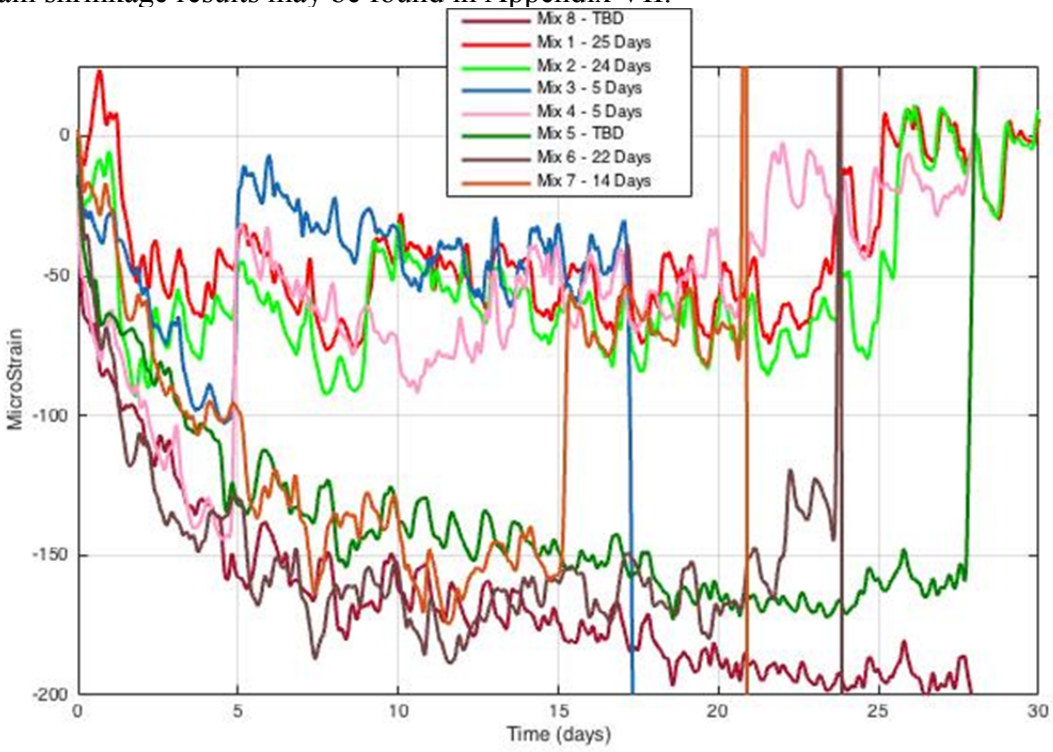

Figure 52: Net MicroStrain development over time (days) for all ring mixtures along with date of cracking

5.2.1.2.1 Effect of Cement Type

Figure 53 outlines the stress development seen by the restrained shrinkage test analyzing the effect of changing the cement type with Mixture 1 – PC-III-A and Mixture 3 – PC-I-A. Figure 54 provides the mechanical property development of the two mixtures with compressive strength, tensile strength and elastic modulus at 1, 3, 7 and 28 days. All

mechanical properties apart from net strain observed from the strain gages were procured through cylinder testing.

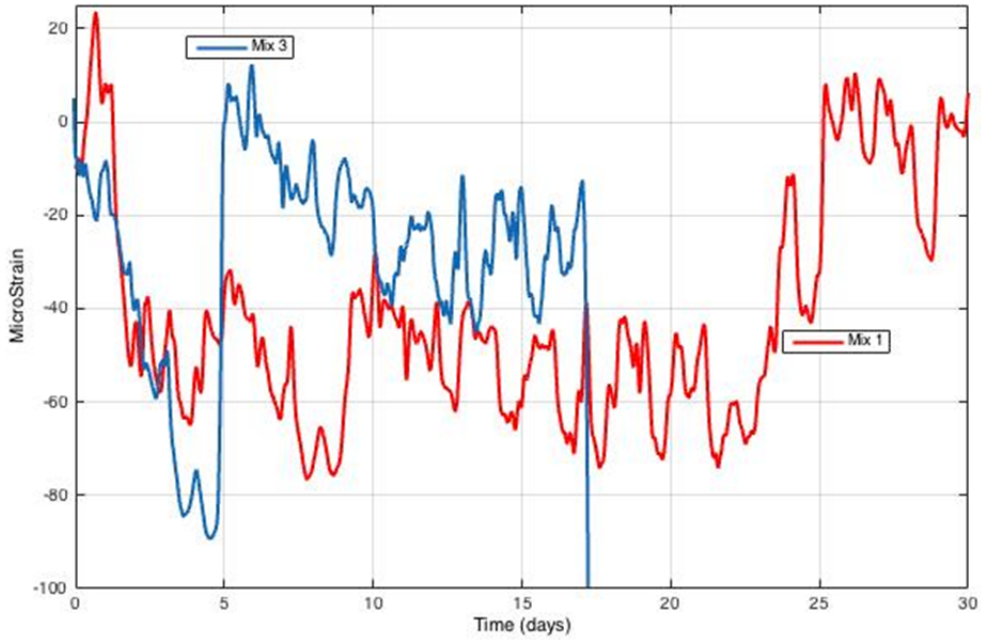

Figure 53: Restrained Shrinkage ring data with respect to time: Effect of cement type- Mixture 1 – PC-III-A and Mixture 3 – PC-I-A

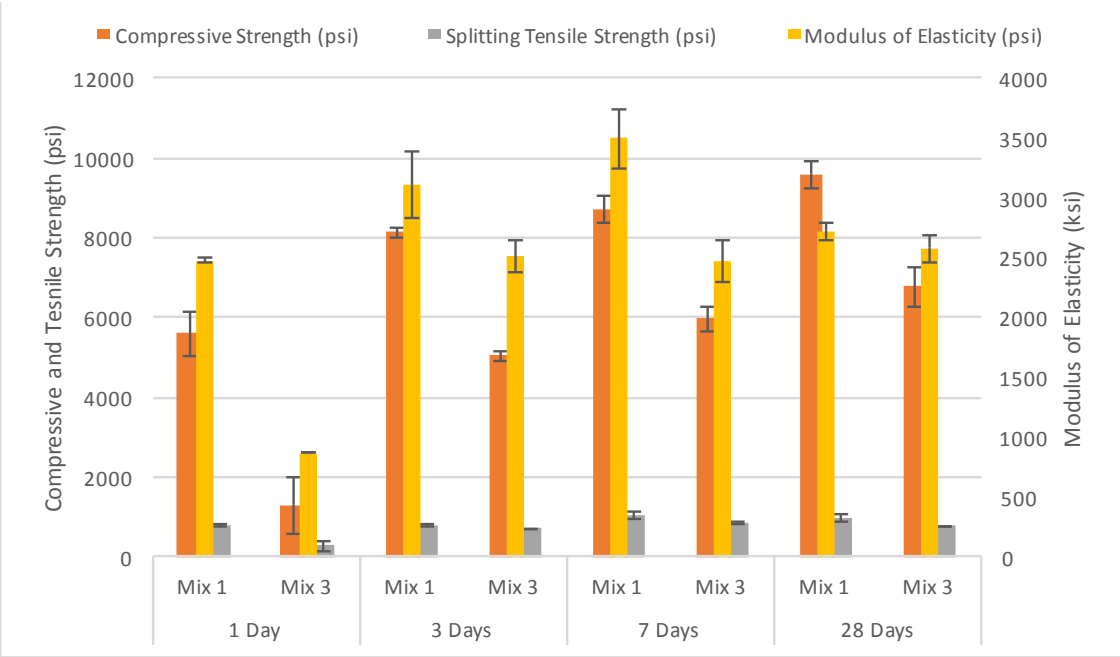

Figure 54: Compressive strength, splitting tensile and modulus of elasticity for Mixture 1 and Mixture 3

Based on the data plotted in Figures 53 and 54 the cement type (Mixture 1 – Type III and Mixture 3 – Type I) plays a considerable role in the strain rate and cracking date of the rings. The concrete containing the Type III developing strain 5 times faster than the concrete containing the Type I cement. The early cracking date of the Type I cement in comparison to Type III may be attributed to the significantly higher rate of strength and modulus development shown in Figure 54.

5.2.1.2.2 Effect of w/cm ratio

Figure 55 shows the stress development that occurred in the restrained shrinkage test based on analyzing mixtures according to their w/cm ratio. Mixture 1 has a w/cm of 0.28; whereas Mixture 2 has a w/cm of 0.33. Figure 56 provides mechanical property

development of the two mixtures with compression strength, tensile strength and elastic modulus at 1, 3, 7 and 28 days.

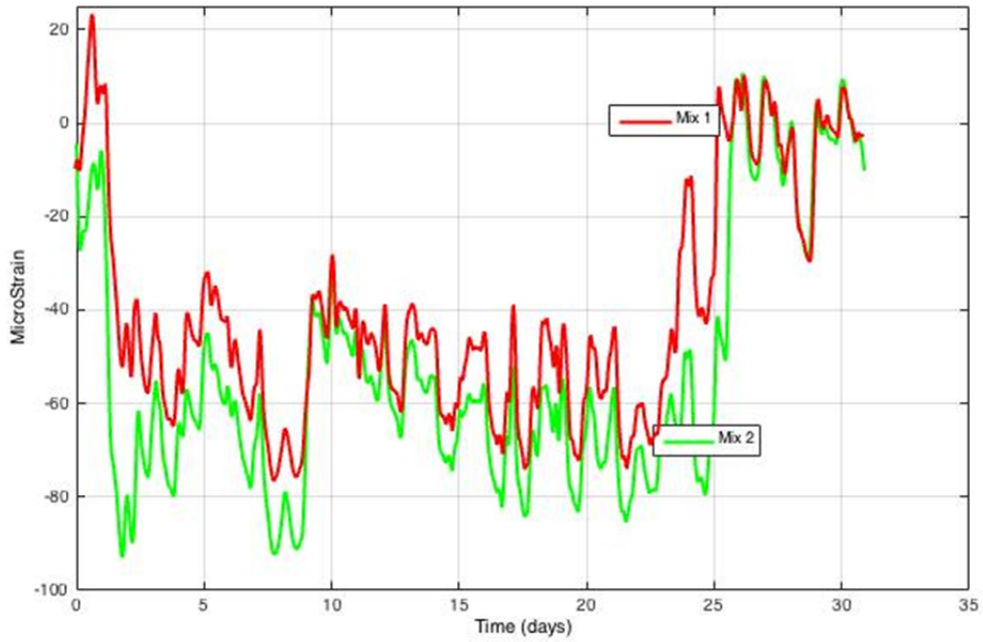

Figure 55: Restrained Shrinkage ring data with respect to time modeling effect of w/cm for Mixture 1 – 0.28 w/cm and Mixture 2 – 0.33

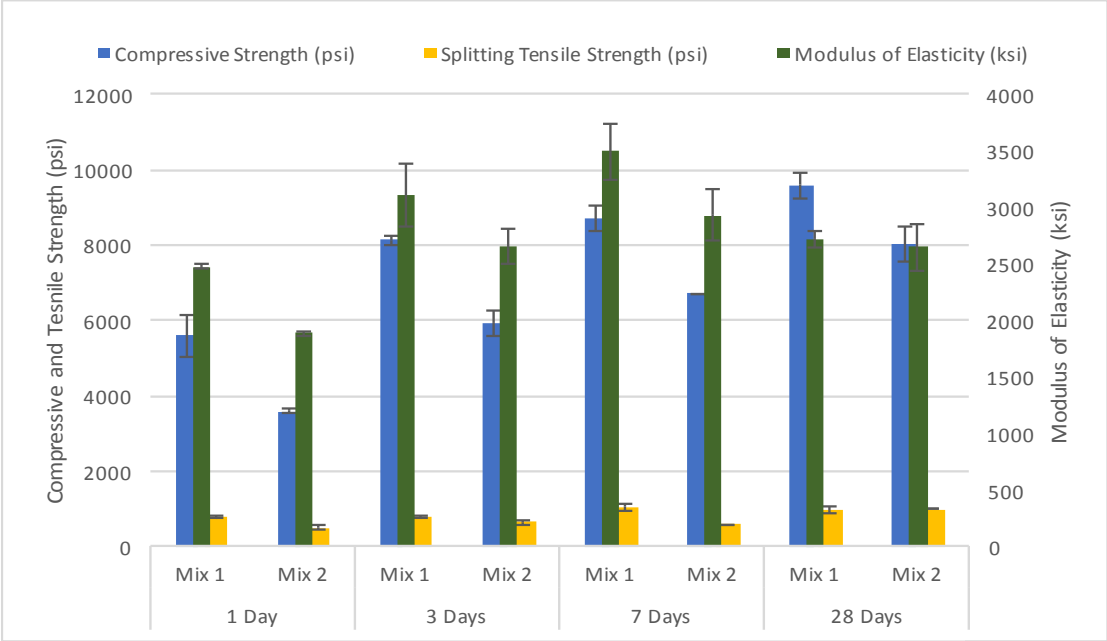

Figure 56: Compressive strength, splitting tensile and modulus of elasticity for Mixture 1 and Mixture 2

Based on the data plotted in Figures 55 the w/cm content (Mixture 1 – 0.28 and Mixture 2 – 0.33) did not play a decisive role in the strain seen by the steel ring and the crack date. Although Mixture 1 had greater compressive strength (≅ 2000 psi more) than Mixture 2 the splitting tensile and modulus of the two mixtures were no more that 25% of one another.

5.2.1.2.3 Effect of HRWR Type

Figure 57 outlines the stress development seen by the restrained shrinkage test analyzing the effect of changing the HRWR type with Mixture 4 – HR-P1 and Mixture 5 - HR-P3 and Mixture 7 – HR-P2. Note that Mixture 7 utilizes a different cement source PC-III-B, but was inserted here to provide an additional mixture comparison. Figure 58

provides mechanical property development of the three mixtures with compressive strength, tensile strength and elastic modulus at 1, 3, 7 and 28 days.

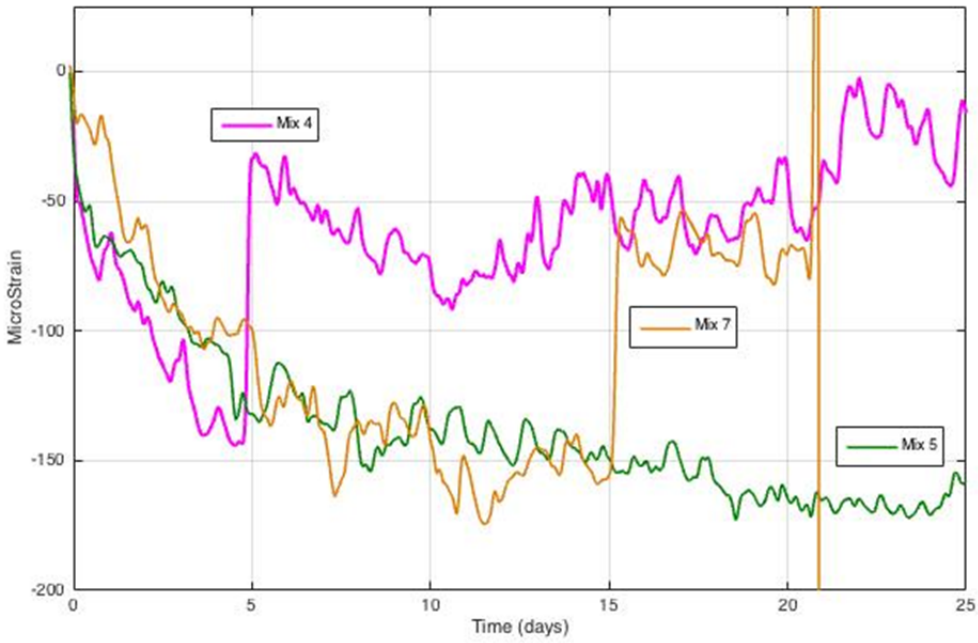

Figure 57: Restrained Shrinkage ring data with respect to time modeling effect of the HRWR type with Mixture 4 – HR-P1 and Mixture 5 – HR-P3 and *Mixture 7 – HR-P2

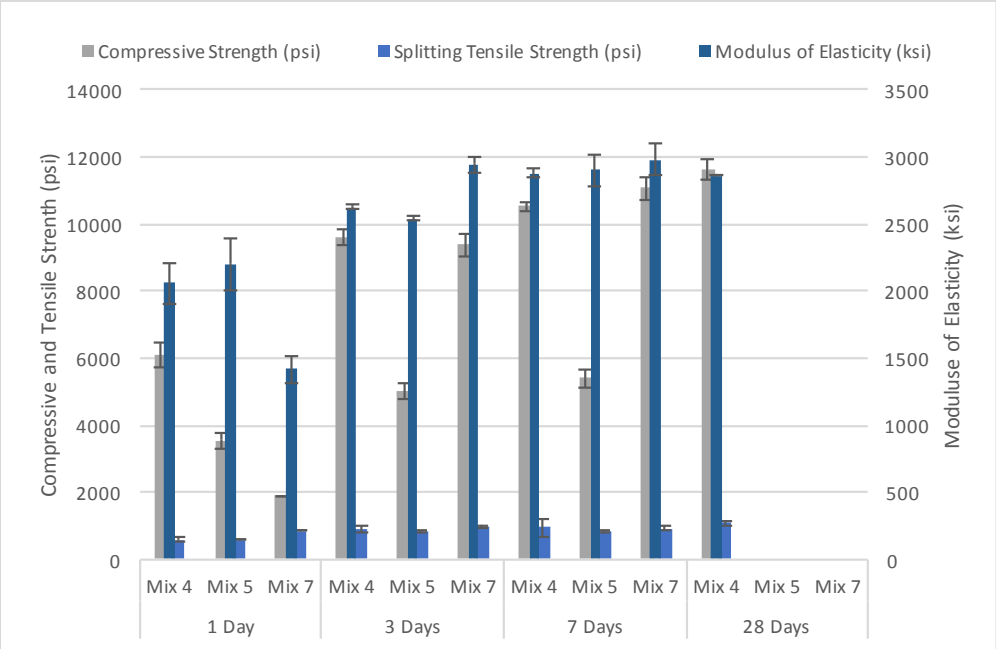

Figure 58: Compressive strength, splitting tensile and modulus of elasticity for Mixture 4, Mixture 5 and Mixture 7

Based on the the data plotted in Figures 57 and 58 the w/cm content (Mixture 4 – HR-P1 and Mixture 5 – HR-P3 and *Mixture 7 – HR-P2) did played a considerably decisive role in the the crack date of the concrete rings. Dates of cracking was HR-P1 mixture at 5 days followed by HR-P2 at 15 days followed by HR-P3 at a date TBD but in excess of 25 days. Figure 56 shows that the low compressive strength of mixture 5 and the slower development of compressive strength for mixture 7 may indicate that slower development of compressive strength with each of the different HRWR's effects the cracking date.

5.2.2 PARAMETRIC STUDY: CONTRETE: RESULTS AND CONCLUSIONS

The mixtures selected for the restrained ring test all were selected based upon their usage in precast plants in Texas. The mixtures are all classified as HPC mixture designs and therefore had a very low likelihood of cracking due to high early strength development as denoted in Figure 47. However, comparing between the different HPC mixtures the following may be concluded:

- Type III cement as compared to type I cement is much more effective in developing strength and increasing the length of time at which cracking occurs in the restrained ring test.
- Differences in w/cm ratio did not effect the rate or time of cracking in the restrained ring test.
- Type of HRWR plays a pivotal role with respect to the rate at which strength is developed as well as the time to cracking. However, referring to previous data (Figures 29 and 30), HRWR type HR-P1 showed the least amount of drying shrinkage with respect to HR-P2 and HR-P3, yet Mixture 4 containing HR-P1 showed the earliest date to cracking (5 days). This shows that although drying shrinkage and restrained ring testing expose the concrete to like conditions the shrinkage performance is not analogous to one another. Therefore, drying shrinkage for precast mixtures may not be a good indicator of cracking performance with respect to autogenous shrinkage ring testing. More work is required to verify this conclusion.

A more complete matrix should be composed to continue creating comparisons between precast plant HPC mixture designs showing both good and bad performance. It should also be noted that Mixture 1 and 2 should be performed again due to learning curve that is associated with the DAQ and strain gage equipment that was sorted out with the mixtures that followed (3-8).

5.3 PARAMETRIC STUDY: PASTE TESTING

The parametric study also looked into testing paste mixtures with varying HRWR dosage and w/cm ratio in several autogenous testing apparatuses: buoyancy test, corrugated tube test and mini ring rest. Table 15 presents the paste mixtures that were evaluated throughout the paste study.

Table 15: Pastes mixtures subjected to the autogenous parametric study

w/cm	Cement Type	Admixtures	
		Type	(floz/100 lb cement)
0.31	PC-III-A	HR-P1	6.5
			8.25
			12
		HR-P2	6.5
			8.25
			12
		HR-P3	6.5
			8.25
			12

A single w/cm ratio of 0.31 was selected because it represents the average of the w/cm ratios employed at Texas precast plants. Likewise, one source of cement was selected PC-III-A as a means of reducing the matrix to provide comparison purely based on HRWR type, dosage and their effects on paste autogenous shrinkage testing. The matrix will continue to develop with time but for the sake of completing this report it was necessary to limit and report results at one w/cm ratio and a single cement source. Figure 59 outlines how the following chapters have been segmented and cross referenced with one another.

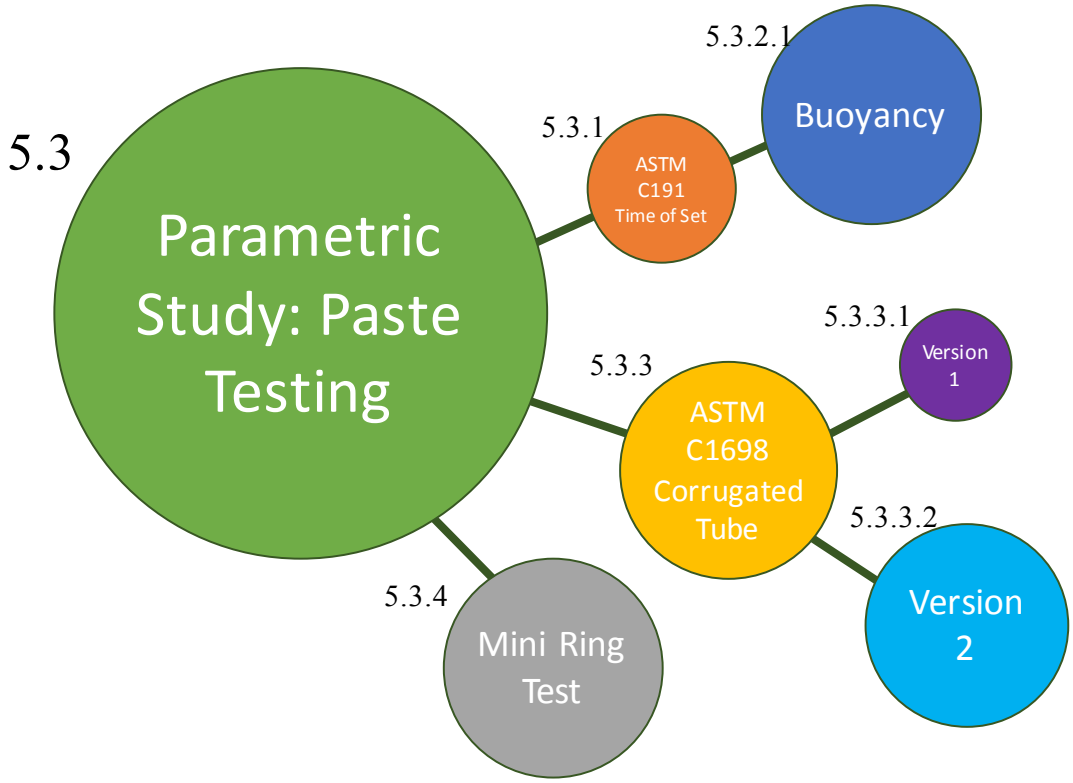

Figure 59: Parametric study testing breakdown with chapter section designation for paste analysis

5.3.1 TIME OF SET

5.3.1.1 PROCEDURE AND EXPERIMENTAL SETUP

In order to collect the initial and final set times for the paste samples listed in Table 13, the Vicat needle test, ASTM C191, Time of Setting of Hydraulic Cement by Vicat Needle was utilized. The paste was mixed in a Hobart mixer in accordance with ASTM C305. Depending on the slump of the paste produced, two unique procedures were followed. A slump of approximately zero permitted the user to fill the Vicat conical mold by following the procedure listed in ASTM C191. The user would collect the paste into a spherical ball with gloves tossing from one hand to the other for six times. The paste sample is then set into the larger radius of the Vicat mold and the paste and mold is then moved to be seated on the larger radii mold end. For a paste mixture with a slump greater than zero (typical for most samples) the mixture was poured into the conical Vicat mold while the larger end was set securely onto a weigh boat.

In order to mimic the isothermal conditions associated with all of the autogenous shrinkage testing performed throughout this research the time of set sample was set on a cold plate. The cold plate circulated 23 °C from the base of the Vicat paste sample. The Vicat needle setup was also housed in an insulated box to further stabilize temperature as well as limit drying shrinkage from ambient air flow. At least 2 samples from separate mixing dates were used to verify consistent initial and final set time results. The Vicat needle apparatus works by the release of a rod with a needle that uses gravity to impress the needle into the paste sample. The depth of the needle is collected and recorded based on a metric reading attached to the Vicat apparatus. Each sample required an initial

reading 30 min after the addition of cement and water followed by readings at 10 min intervals until a penetration reading of 25 mm or less was achieved. The Vicat setup employed for all paste samples is shown and annotated in Figure 60.

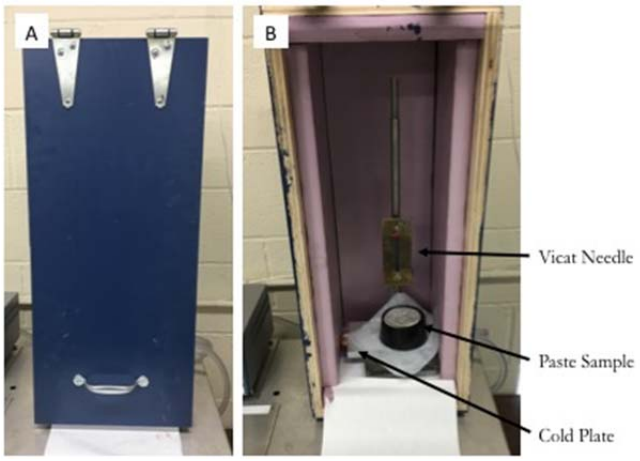

Figure 60: Vicat Needle Test, ASTM C191. Housed in an isothermal box (A) Closed. (B) Open for testing purposes.

5.3.1.2 TESTING MATRIX AND RESULTS

Several different mixture designs were carried out in this project with varying chemical admixtures and dosages. Due to the importance of determining the final set time for the autogenous shrinkage tests, the results of this section have been utilized into all subsequent autogenous shrinkage paste testing chapters. Time of set testing was carried out with two separate samples cast at separate times due to the limitation of only having one sample Vicat setup. Results of time of set were averaged and/or repeated if times differed more than 15 minutes. Table 16 shows the mixture proportions alongside

averaged initial and final setting times of the two samples. Figure 61 presents the values in bar graph form.

Table 16: Mixture proportions and averaged time of set through ASTM C191

w/cm	Cement Type	Admixtures		Time of Set (hr)	
		Type	(floz/100 lb cement)	Initial	Final
0.31	PC-III-A	HR-P1	6.5	5.03	5.80
			8.25	4.82	5.67
			12	5.60	7.45
		HR-P2	6.5	5.40	6.88
			8.25	4.58	7.83
			12	5.60	7.65
		HR-P3	6.5	3.18	4.67
			8.25	3.20	5.75
			12	4.02	5.63

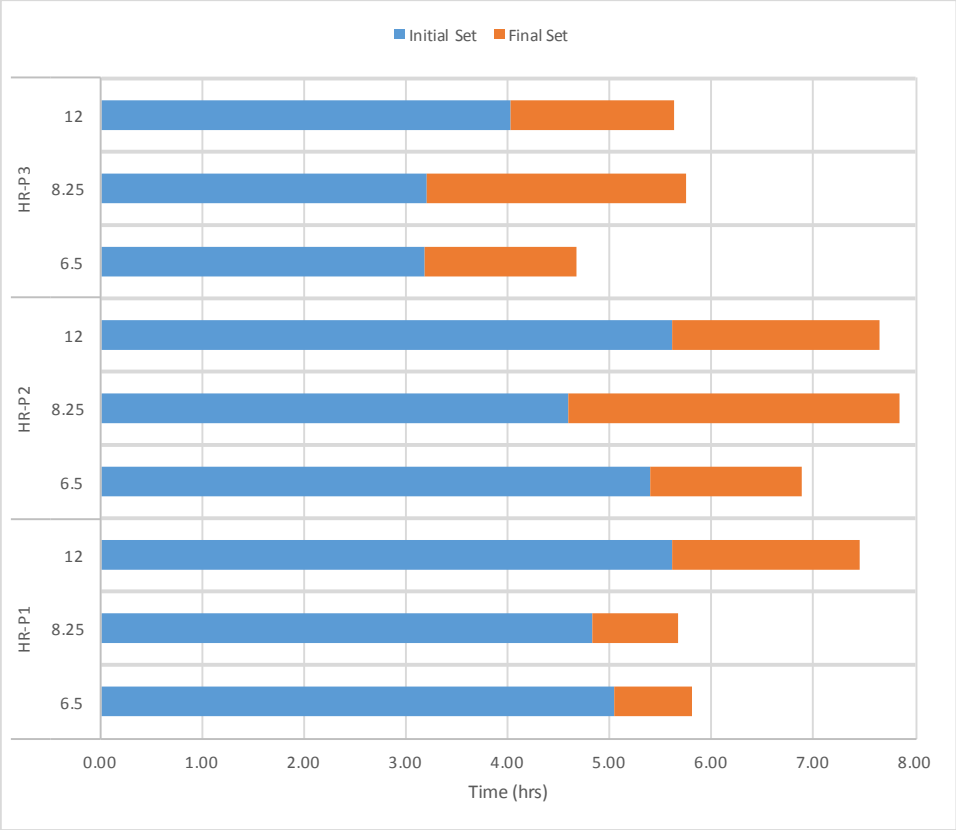

Figure 61: Averaged setting times plotted for each paste mixtures

As seen in Figure 60, typically, an increase from HRWR dosage from 6.5 fl oz/100lb cement delays the final set for nearly all HRWR types. HR-P3 retarded the setting times the least, and HR-P2 retarded the setting times the most.

5.3.2 AUTOGENOUS DEFORMATION

5.3.2.1 BOUYANCY PROCEDURE AND EXPERIMENT AND EXPERIMENTAL TEST SETUP

In order to measure the autogenous deformation of paste samples via buoyancy method the volumetric deformation of paste was determined using the test setup described in Chapter 2. The setup employed is shown in Figure 62.

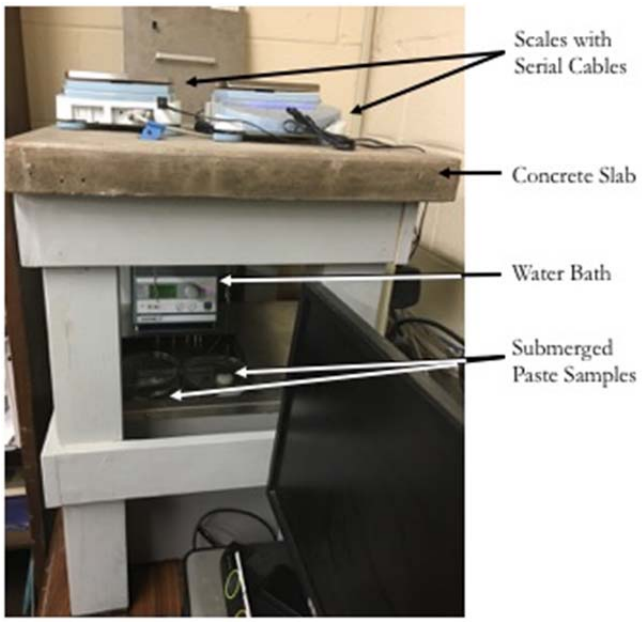

Figure 62: Autogenous Shrinkage Test Setup via Volumetric/Buoyancy Method

The setup employed at the University of Texas uses two scales that sit on a concrete slab suspended over a water bath. The setup permits the measurement of two samples at a time. The scales measure to an accuracy of 0.01 grams and are directly connected to computers via serial cables to two separate computers for continuous measurements at 1 minute intervals. The samples suspended from the scales are

unlubricated polyurethane condoms (Trojan Supra). The condoms were were filled with 100 g to 150 g of paste. The paste was mixed in accordance with ASTM C305. The paste was set into the condoms and sufficient vibration was applied. The condom was twisted and zipped-tied to ensure completely sealed conditions. A pre-tied fishing line and i-hock were attached to the zip-tie in order to allow the paste sample to be quickly immersed into a paraffin oil bath. Measurements commenced immediately upon immersion.

In order to verify initial weight of specimen against the final normal weights of the paste sample the cut off tail end of condom, and zip-tie were collected and recorded. The test was run for a three-day period. At the completion of the test, the paraffin oil was wiped off of the surface of the condom, and the sample was measured. In order to ensure the quality of the test, the final weight and initial weight should not exceed a 2% increase. Otherwise, this can indicate that excessive paraffin oil was absorbed into the membrane.

5.3.2.2 TESTING MATRIX

Several different mixture designs were carried out in this project with varying chemical admixtures and dosages. Testing was carried out using three separate samples all at 23 °C for a 3-day testing period. Autogenous shrinkage (linear strain, με) was tabulated as a positive value after final set was met (according to time of set results determined in chapter 4.3.2), and 72 hours after the introduction of cement to water. Results of the buoyancy method averaged the three samples cast per mixture design and have been outlined in Table 17.

Table 17: Autogenous Shrinkage according to mixture designs at 72 hours after introduction of cement to water.

w/cm	Cement Type	Admixtures		Final Set Time (hr)	Linear Strain ($\mu\varepsilon$)
		Type	(floz/100 lb cement)		
0.31	PC-III-A	HR-P1	6.5	5.03	611.20
			8.25	4.82	1614.60
			12	5.60	432.90
		HR-P2	6.5	5.40	422.17
			8.25	4.58	597.97
			12	5.60	651.53
		HR-P3	6.5	3.18	395.47
			8.25	3.20	151.84
			12	4.02	10.10

5.3.2.3 RESULTS

The following sections have composed several comparisons on autogenous shrinkage of the cement pastes samples listed in Table 15. Individual mixture design autogenous shrinkage results may be found in Appendix VII of this report.

5.3.2.3.1 Effect of HRWR Dosage

Figures 63-65 look to analyze the effect of increasing the HRWR dosage for each individual HRWR type. Positive strain was taken after final set as per determined in Table 15 of this report.

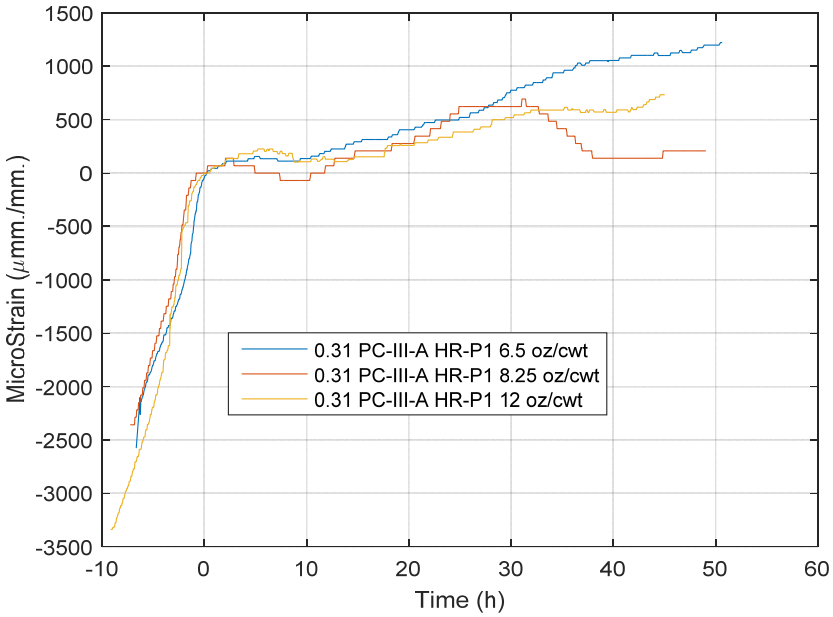

Figure 63: Buoyancy Shrinkage 0.31 PC-III-A for HR-P1 at 6.5, 8.25 and 12 fl oz/100lb cement

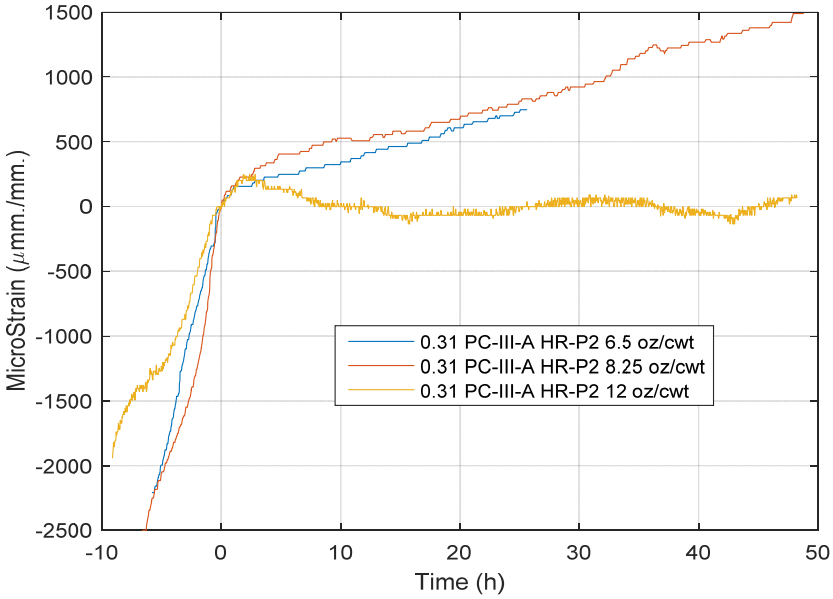

Figure 64: Buoyancy Shrinkage 0.31 PC-III-A for HR-P2 at 6.5, 8.25 and 12 fl oz/100lb cement

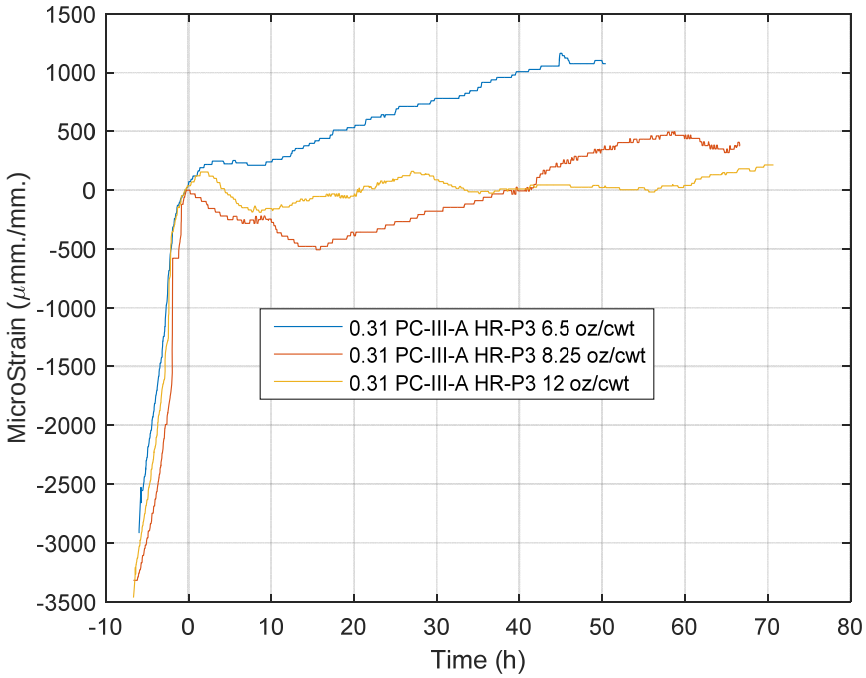

Figure 65: Buoyancy Shrinkage 0.31 PC-III-A for HR-P3 at 6.5, 8.25 and 12 fl oz/100lb cement

As shown in all cases the largest amount of shrinkage strain was observed in the pastes containing the lowest HRWR agent dosage (6.5 oz) except in the case of HRWR HR-P2, where 6.5 and 8.25 oz dosages show similar trends (see Figure 64). The higher dosage mixtures again show the increased retardation previously discussed in Chapter 5.3.1 of this report. Retardation may be seen by the slower strain development with respect to time prior to reaching final set. The increase in HRWR dosages showed that by delaying final set time the autogenous autogenous shrinkage that followed was then delayed.

5.3.2.3.2 Effect of HRWR Type

Figures 66-68 presents plots that compare the different HRWR types (HR-P1, HR-P2 and HR-P3) at a series of fixed dosage amount. Again, positive strain was taken after final set as per determined in Table 16 of this report.

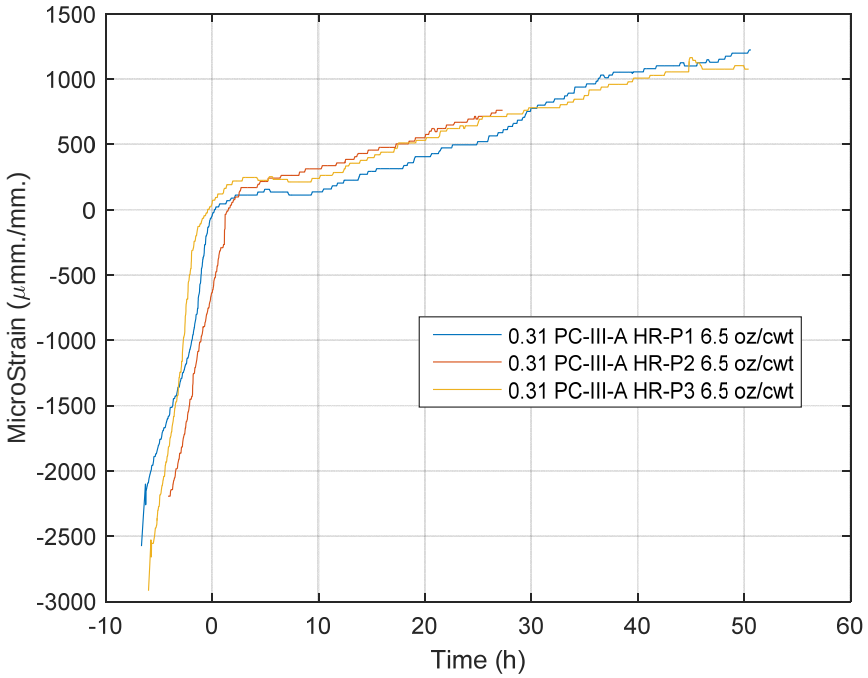

Figure 66: Buoyancy Shrinkage 0.31 PC-III-A for HR-P1, HR-P2 and HR-P3 at fixed 6.5 fl oz/100lb cement

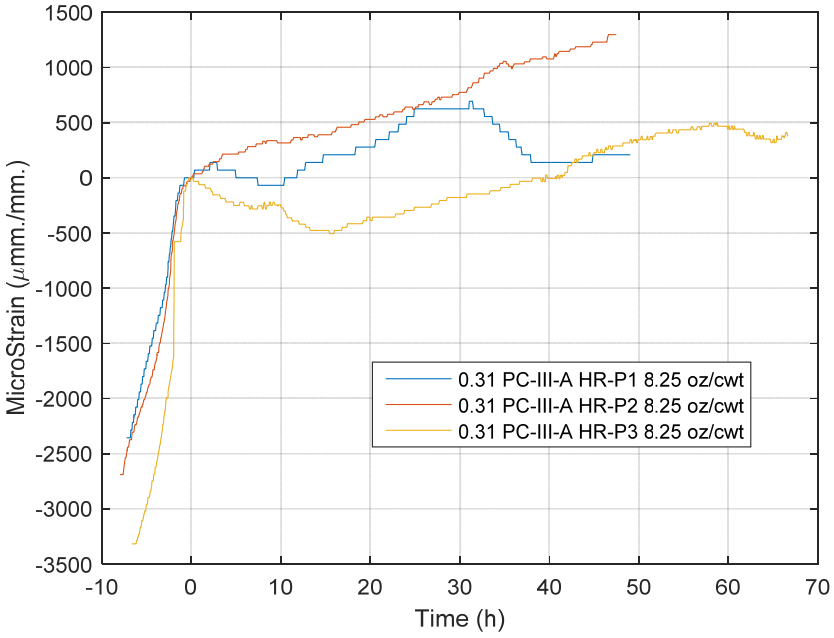

Figure 67: Buoyancy Shrinkage 0.31 PC-III-A for HR-P1, HR-P2 and HR-P3 at fixed 8.25 fl oz/100lb cement

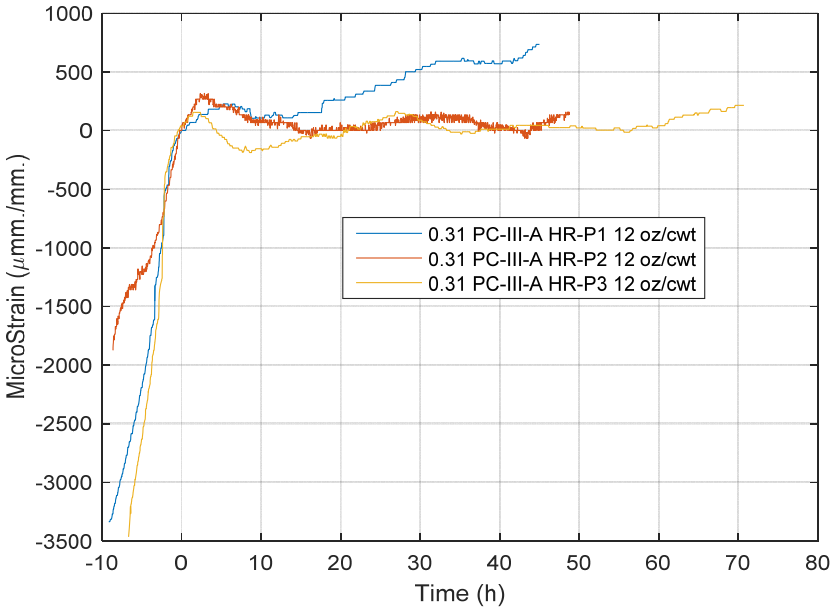

Figure 68: Buoyancy Shrinkage 0.31 PC-III-A for HR-P1, HR-P2 and HR-P3 at fixed 12 fl oz/100lb cement

Figure 66 proves to show that a fixed dosage of 6.5 oz produces the least amount of variance in shrinkage strain.

5.3.2.4 SUMMARY AND CONCLUSIONS

Based on the results of this section the following conclusions may be drawn:

- Increase in HRWR dosage proved to decrease the autogenous shrinkage after reaching final set. This was aided by the increase time till final set associated with increased HRWR dosage mixtures.
- Due to the high variability in collected strain through the volumetric method it was difficult to draw further conclusions from the data. Therefore, work towards collecting information on autogenous shrinkage was shifted entirely towards the corrugated tube test methodology.

5.3.3 CORRUGATED TUBE PROCEDURE AND EXPERIMENTAL TEST SETUP

In order to measure autogenous shrinkage through the corrugated tube test two separate versions of the test were employed. Version one duplicated the use of the corrugated measurement apparatus outlined in ASTM C1698. Figure 69 shows the CAD drawings that were developed to have the setup machined and Figure 70 shows the annotated photo of the setup employed. Version two corrugated testing apparatus was developed in order to allow procurement of results immediately after casting and in a completely isothermal environment. Figure 71 shows the CAD drawings that were

developed to have the setup machined and Figure 72 shows the annotated photo of the setup employed.

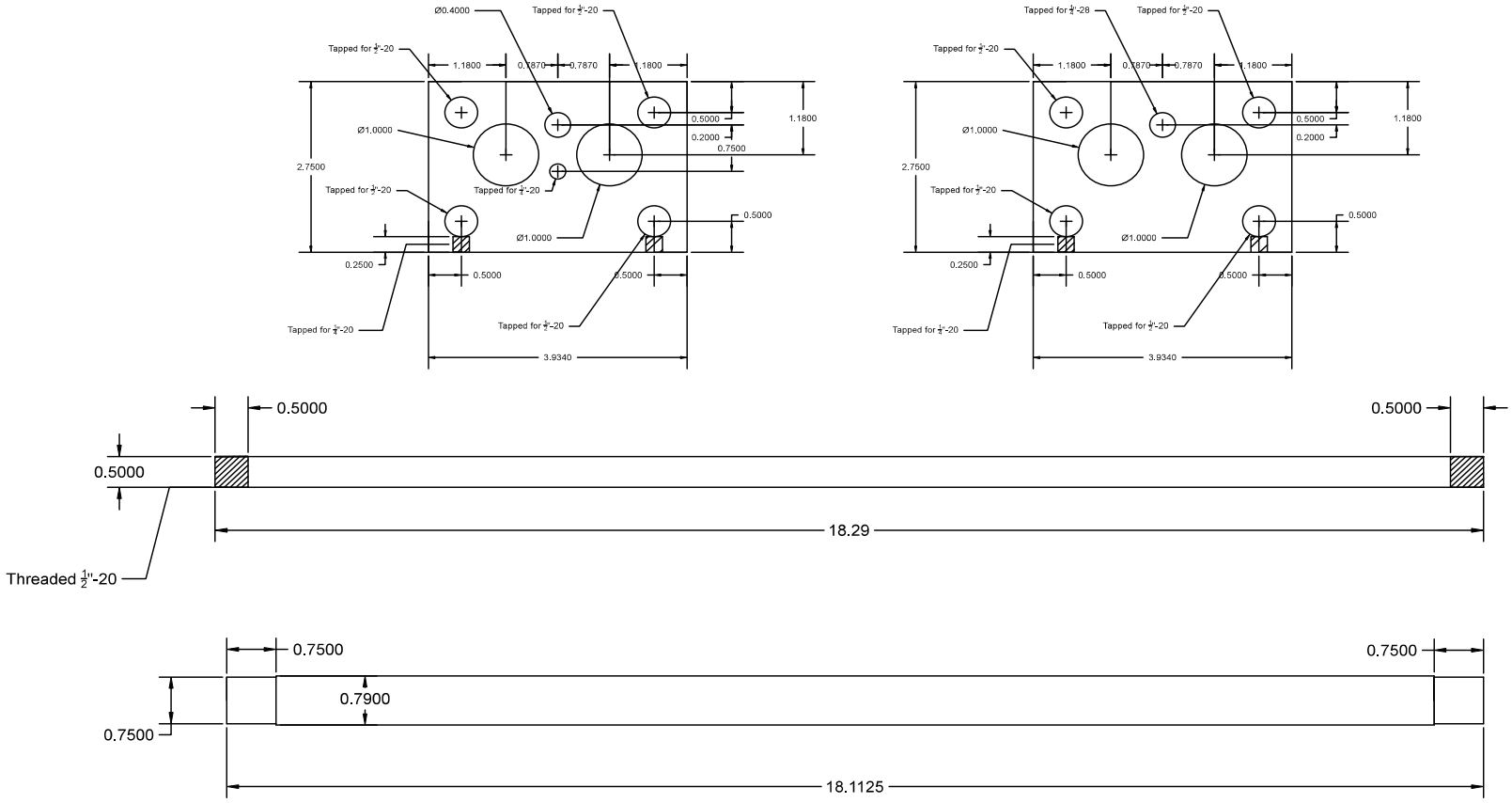

Figure 69: CAD drawing of corrugated tube test rig (version 1)

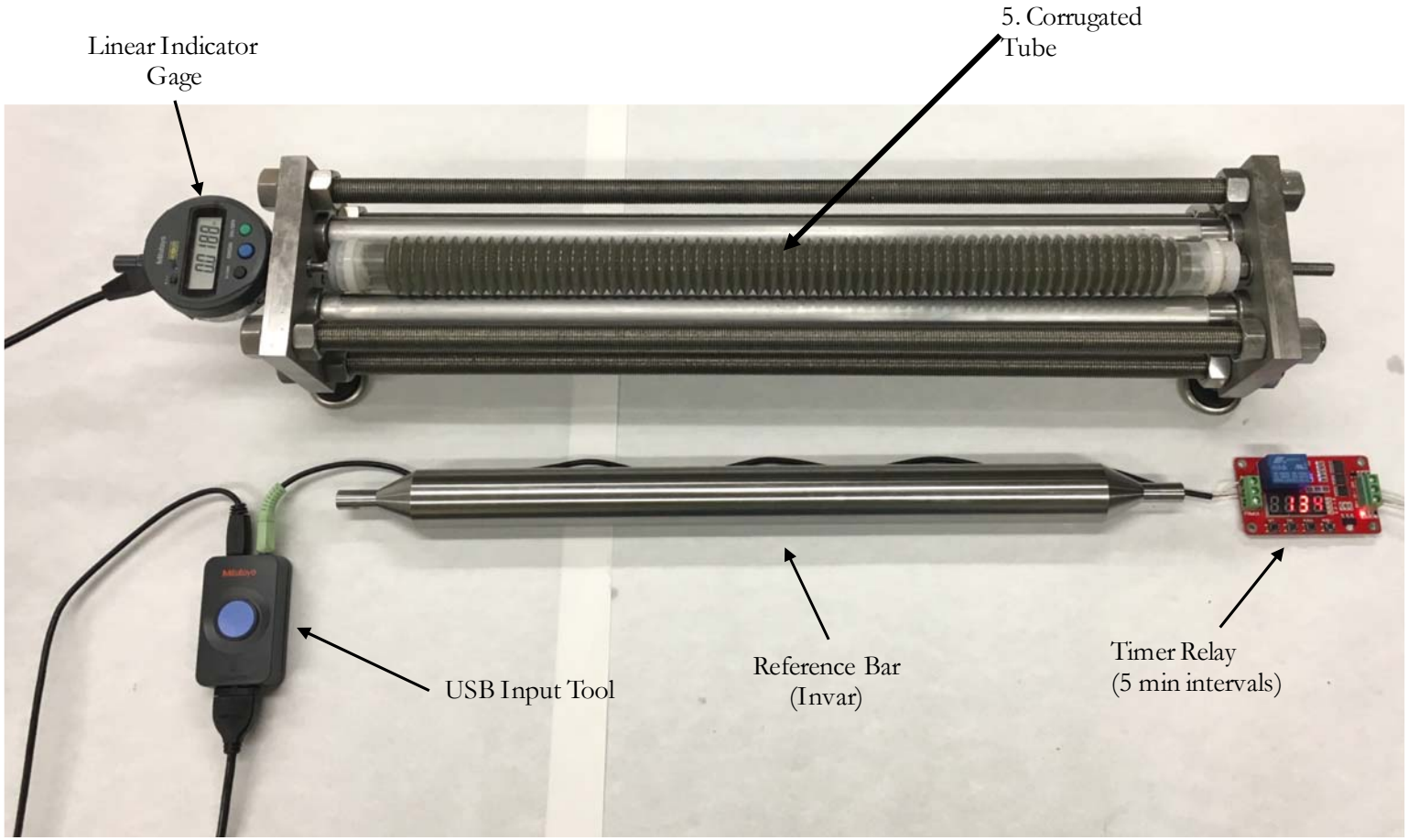

Figure 70: Test setup for the corrugated tube test (Version 1) Employed at The University of Texas at Austin

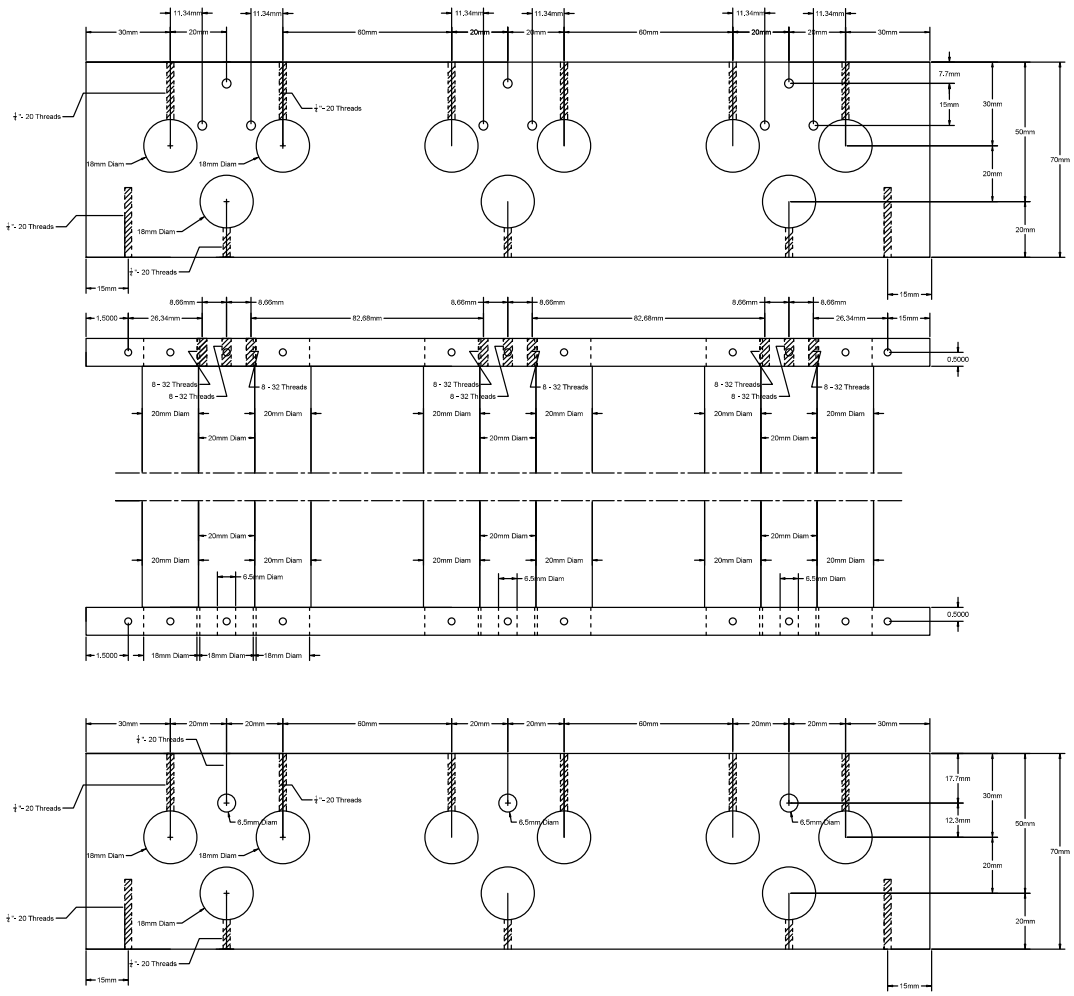

Figure 71: CAD drawing of corrugated tube test rig (Version 2)

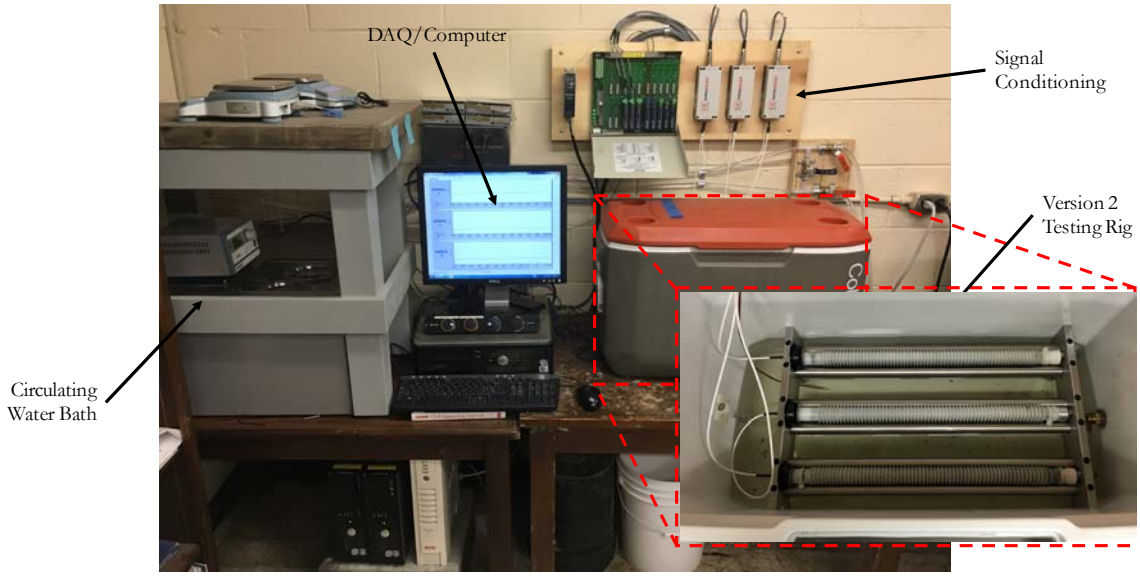

Figure 72: Test setup for the corrugated tube test (version 2) developed at The University of Texas at Austin. Note: Testing Rig is inside cooler during testing.

5.3.3.1 CORRUGATED TUBE SETUP VERSION 1:

Version 1 testing apparatus that closely conforms to the design specified in ASTM C1698. As shown in Figure 70 the Version 1 apparatus is composed to two 3/8-in end plates that have been fixed together by 4 separate 24-in long ½-in all thread. The entire apparatus was machined out of stainless steel in order to provide corrosion resistant and minimize any vibrations that may occur in the surrounding testing environment. The specimen is seated on two ¾-in stainless steel rods. The rods are chamfered at each end and are set in 4 low profile rod bearing rollers. Holes centered on each end plate are used to make contact with the end caps of the corrugated tube specimen. One end utilizes a

length indicator gage (Mitutoyo 543-793B) that places a minimal compressive force (> 1.5N) in order to take continuous measurements with a resolution of 0.0000 in. Prior to placing the specimen into the testing apparatus the indicator gage is zeroed through the use of a ¾-in machined invar reference bar. The reference bar is made of an invar steel which possesses a low coefficient of thermal expansion (1.2 ppm/°C), and is used prior to setting all specimens into the testing apparatus. The indicator gage is connected to a computer through a Mitutoyo USB input tool (264-012-10). Readings are collected through the use of a timed relay switch (Songle PLC Cycle Relay), which triggers the USB input tool to collect data onto an excel spreadsheet at a 5-minute interval for a 24 hr period.

The specimen procurement process for corrugated tube test Version 1 begins by mixing the paste samples in accordance with ASTM C305 and recording the time at which the cement was added to the water. After fulfilling ASTM C305 the paste is poured and subsequently vibrated on a small vibrating table (Southwest Science – BV1000) whilst the corrugated tube is filled (see Figure 73).

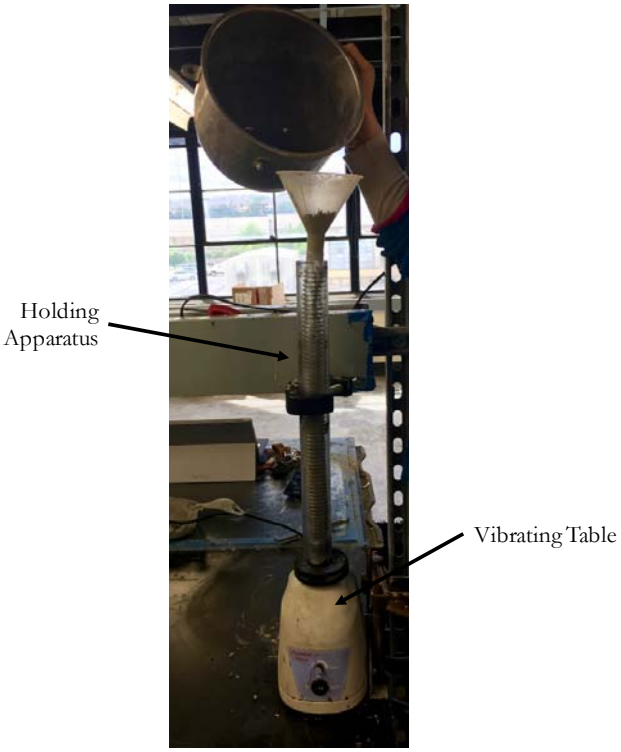

Figure 73: Corrugated tube being filled and vibrated

Sufficient vibration is added to remove as many entrapped air bubbles in the tube as possible. Once the tube is completely filled the ends are capped and sealed with plastic polyurethane caps. To assure no moisture loss zip ties are used to further secure the caps at either end of the tube. To assure that the specimens are not lengthened during transport from the mixing room to the testing room the tubes are carried in PVC pipes that have the approximate desired initial length of the specimens. The corrugated tube is then gently placed into the testing rig (Version 1). During the initial 30-minute period from the addition of cement to water the corrugated tube is rotated every 2 minutes to reduce bleeding and create a more uniform specimen paste sample. More recently an automated

turning apparatus (US Stoneware – C205015) has been used to rotate the samples at 10 revolutions per minute up until initial set as shown in Figure 74.

Figure 74: Automated turning apparatus for reducing bleeding on corrugated tube sample

Once the samples achieved final set, the length indicator is permitted to make contact with the end caps, and length measurements with respect to the reference invar begin. For the first 24 hours the samples are left in the testing apparatus and readings are collected on an excel spreadsheet at 5 minute intervals. It was observed that the Mitutoyo indicator gage was not supplying sufficient force to keep both of the corrugated tube ends in continuous contact with the opposite end of the testing rig. Instead the corrugated tube was shrinking away from both end plates of the testing rig. In order to combat this issue, one of the end caps used for the initial 24 hr testing period was machined out of stainless steel. This machined end cap is referred to as the “dead-end,” to facilitate shrinkage

solely away from the measurement end. Figure 75 presents a stainless steel end cap that was designed with respect to the standard polyurethane end caps typically employed in the corrugated tube test method.

Figure 75: Stainless steel end caps used for the version 1 setup to facilitate shrinkage solely from measurement end

At the conclusion of the initial 24 hr measurement period the specimens are measured at finite intervals of 1, 3, 7, 14, and 28 days from initial set. Due to the high cost of the corrugated tube test ($12 per sample), version 1 test setup is only employed on two samples from two separate mixtures.

5.3.3.2 CORRUGATED TUBE SETUPVERSION 2:

Version 2 testing apparatus was influenced by the early development of the corrugated tube test where the samples were originally submerged in a paraffin oil bath

and kept at a constant temperature to remove the temperature expansion effects (Jensen and Hansen 1995). Testing apparatus Version 2 was also influenced by the concept of using non-contact LVDTs in order to minimize length change noise as well as to avoid the small load that is imparted onto the sample by the linear gage tips (Gao et al. 2014). As shown in Figure 70, the Version 2 apparatus was designed in a similar fashion to Version 1 set-up, except Version 2 permits the measurement of 3 samples simultaneously. Figure 76 provides a diagram outlining how the hardware for the Version 2 setup at the University of Texas at Austin was interconnected.

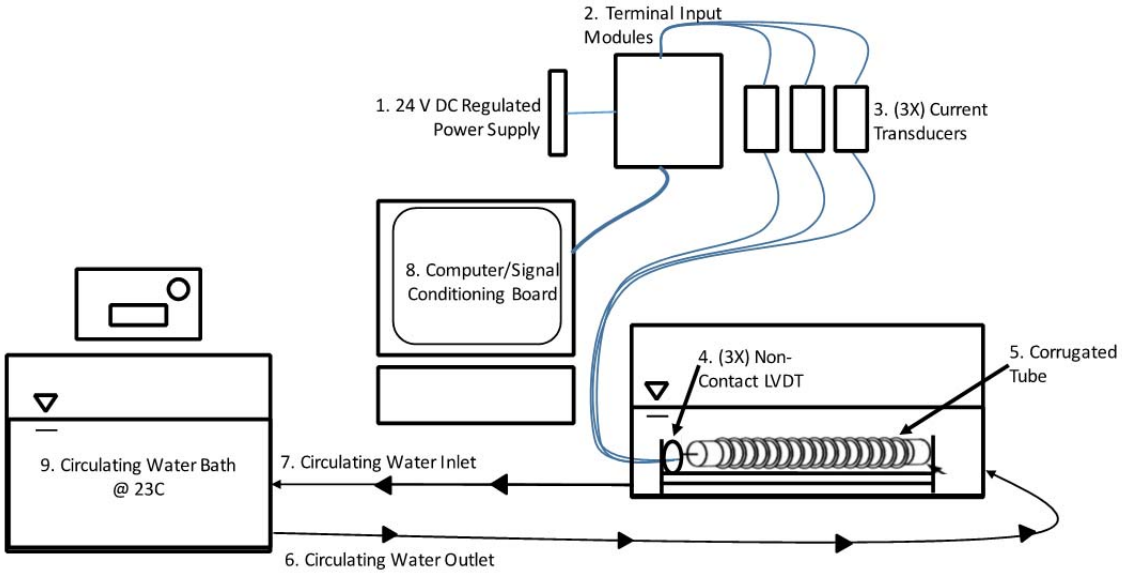

Figure 76: Diagram of the non-contact LVDT setup

The corrugated tube testing apparatus is comprised of 3/8 in stainless steel end plates that are set apart by 9 stainless steel rods which have been chamfered and secured into the end plates by set screws. One of the end plates has been tapped to accept all thread that is used to secure one end of the corrugated tube. Similar to the stainless steel

end caps used in Version 1, the caps were made to create a “dead end”; facilitating shrinkage solely from the non-contact LVDT.

The end plate with the non-contact LVDTs (Micro Epsilon eddyNCDT 3010 sensor U15) was not fixed and is referred to as the “live-end.” The non-contact LVDTs were selected based on their lower cost relative to a direct contact and waterproof LVDT, as well as for their ability to maintain accuracy, resolution and range consistent with ASTM C1698. The non-contact LVDTs provide a 15 mm range or measureable distance, alongside a 0.75 μm resolution which meets well within the prescribed standard of ASTM C1698. The sensor is adjacently connected to a transducer that is powered by a direct current regulated power supply of 24 volts and 3 amps (National Instruments PS-15). The sensor outputs an eddy current that sends and receives current to and from a ferromagnetic disk (stainless steel 1-in diameter and 0.01-in thick). Each stainless steel disk was glued to the polyurethane cap before it was set into test apparatus. The disk was also placed at an initial 2 mm separation distance from the non-contact LVDT sensor. Figure 77 focuses on the non-contact LVDT sensor in line with the stainless steel disk.

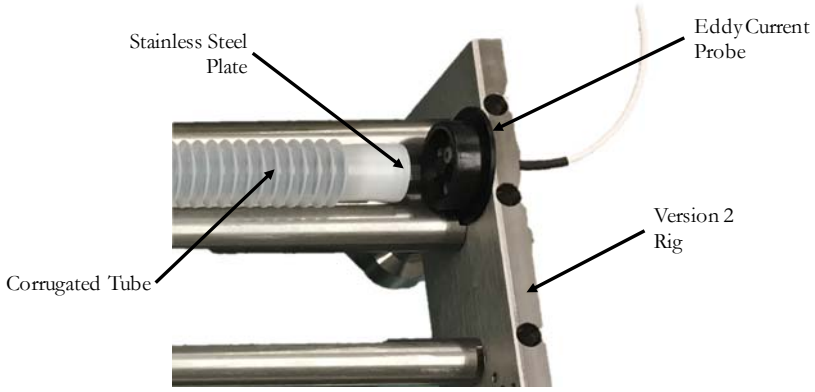

Figure 77: Excerpt of Version 2 corrugated tube set-up showing the non-contact LVDT eddy current sensor and adjacent steel plate in situ

The eddyNCDT 3010 transducer was calibrated to accept changes in current received as the targeted ferromagnetic disk moves linearly closer and further away. The calibration curve as shown in Figure 78 was used in order to directly correlate a voltage reading (1 mV) as a change in 1 mm distance.

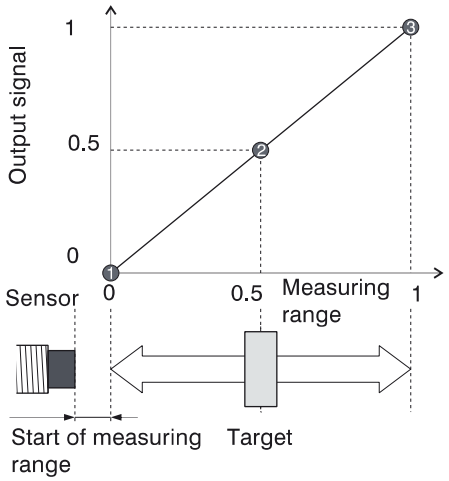

Figure 78: Typical LVDT calibration curve

The procurement of the length change in the corrugated tube was performed through the use of a LABview program developed at the University of Texas at Austin. LABview software and National Instruments hardware was used because of the versatility for future testing purposes (e.g. controlling water bath to provide heat ramping effects as seen in the field). The software program was created to compile changes in distance as a function of time for all three samples. The program also monitors temperature of the circulating water bath (VWR 1186D) as well as the separate water bath/cooler that the specimens are housed in. Figure 79 provides a screenshot of the LABview program at the conclusion of the three-day testing period.

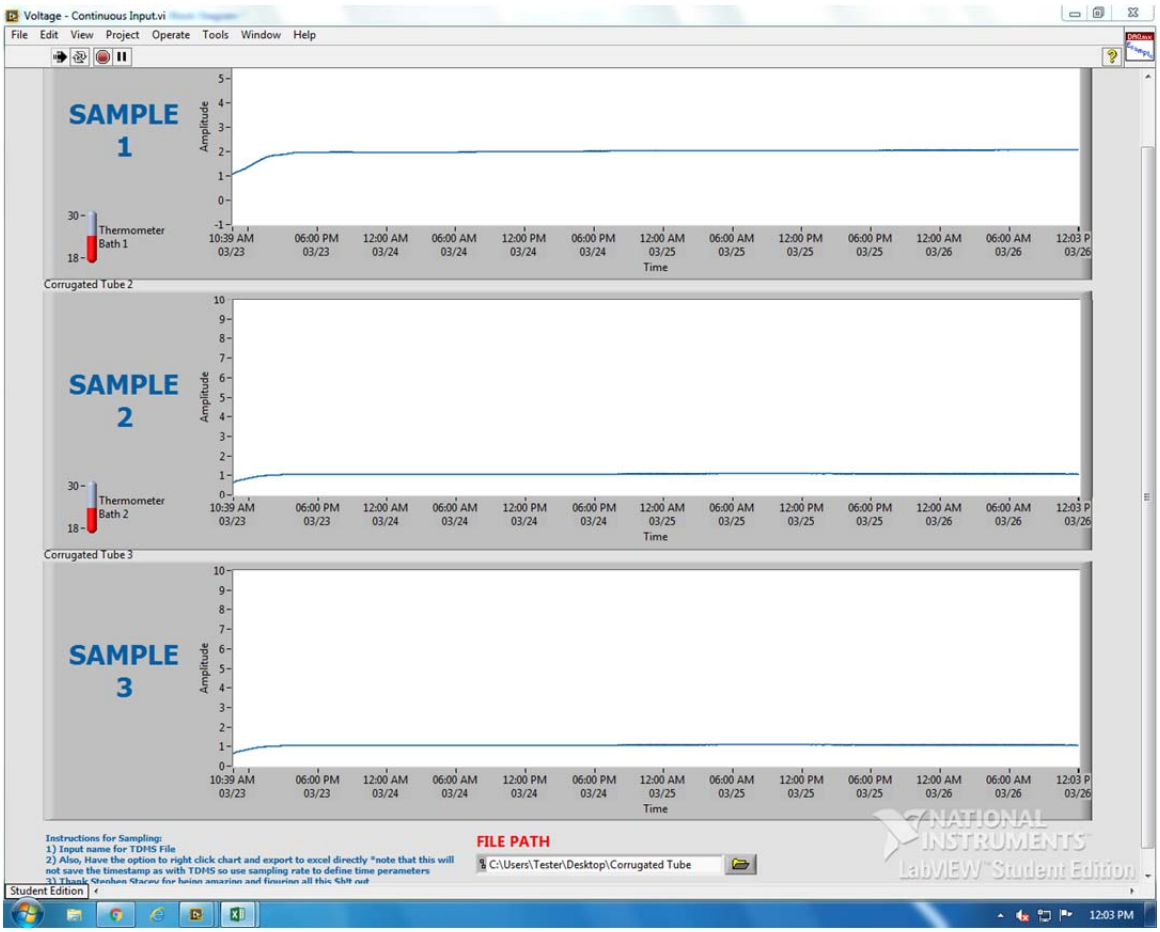

Figure 79: LABview program screen of three samples voltage readings with respect to time

The computer not only runs the LABview software but houses the data acquisition system (DAQ) (National Instruments DAQmx PCI-6220). The DAQ board has a resolution capacity of 16 Bits, well within the tolerance provided by the non-contact sensors and ASTM C 1698. The signal DAQ is connected to a signal conditioning board (National Instruments SC-2345). The signal conditioning board allows the user to have several unique input channels. Figure 80 shows the signal conditioning board housing the 4 separate signal conditioning input modules.

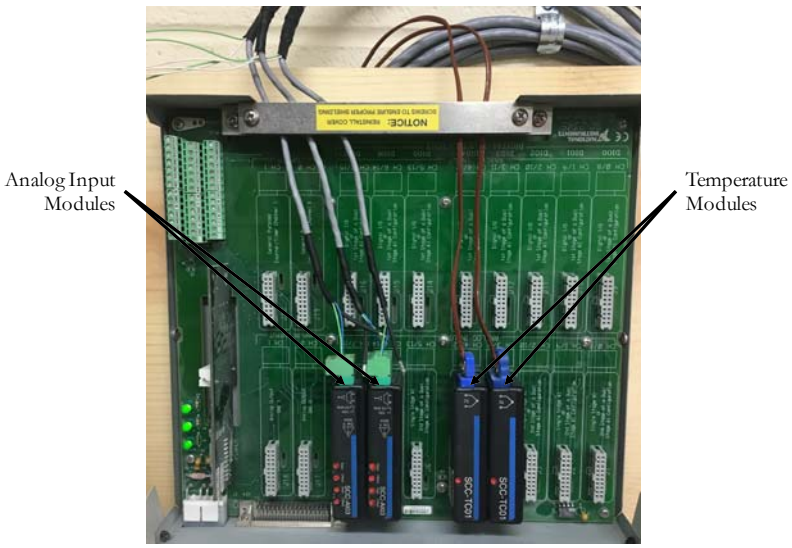

Figure 80: Signal conditioning input modules set in the signal conditioning input board

Two of the signal conditioning input modules have analog voltage reading (National Instruments SCC-AI03). The analog voltage modules have a voltage range of ±10 V input and output, which is directly interpreted by the DAQ as function of length change as seen by the LVDT sensor. Each of the analog voltage modules have the capacity to interpret voltage readings from 2 unique voltage outputs, in this instance, voltage interpreted from the non-contact LVDT sensors. The other two input modules are thermocouple input modules (National Instruments SCC-TI01). The thermocouples are set up to monitor the temperatures of the circulating water bath as well as the temperature of the circulating paraffin oil in the corrugated tube water bath (cooler).

Mixture and casting of paste in the corrugated tube test Version 2 setup performed in the same fashion as Version 1 setup described earlier in this chapter. Additional care is taken to ensure that the caps on either end of the corrugated tube provide a water tight seal. At least 1 zip tie is used to seal the corrugated tube end caps. Assuring that the caps are completely sealed allows Version 2 setup to submerge the corrugated tube samples in

a paraffin oil water bath, which enables the testing to be conducted in isothermal conditions. The paraffin oil bath also aids in reducing friction by providing lubrication between the tube and testing apparatus.

Version 2 of the corrugated tube test was run for a three-day testing period. After which, the samples were removed from the test setup, cleaned of surface oils and measured in Version 1 corrugated tube setup. The measurement would then follow the same program outlined in Version 1 testing apparatus, and measurements were collected at 3, 7, 14, and 28 days. Version 2 testing setup was limited to a three-day period in order to complete more of the testing matrix. Results have also proven that a majority of autogenous shrinkage occurs in the initial 24-hour period. Yet due to the high cost and effort that is associated with each corrugated tube sample cost it was decided that measurements would continue for 28-day period.

5.3.3.3 RESULTS

The following sections presents the results for autogenous shrinkage testing of the cement pastes samples listed in Table 15. Individual mixture design autogenous shrinkage results may be found in Appendix VIII. Due to the high precision associated with the corrugated tube test (version 2), the time-zero was taken as the time at the beginning of swelling. Swelling may be viewed as a small bump in the micro-strain with respect to time plot (see Figure 80). Although practically it would make sense to take the zero point at when tensile stresses begin to develop (ie., post-swelling) the bulk of literature boasts taking zero point prior to swelling. The swelling may be viewed as a small bump in terms of micro-strain with respect to time as shown in Figure 81. The swelling is due to the reabsorption of bleed water in the sealed system (Bjøntegaard

2003). It has been shown that the reabsorption of bleeding reduces the shrinkage of the paste and therefore has an effect on the total shrinkage (Hammer 1999). For this reason, the samples were all compared considering the zero point just as swelling began.

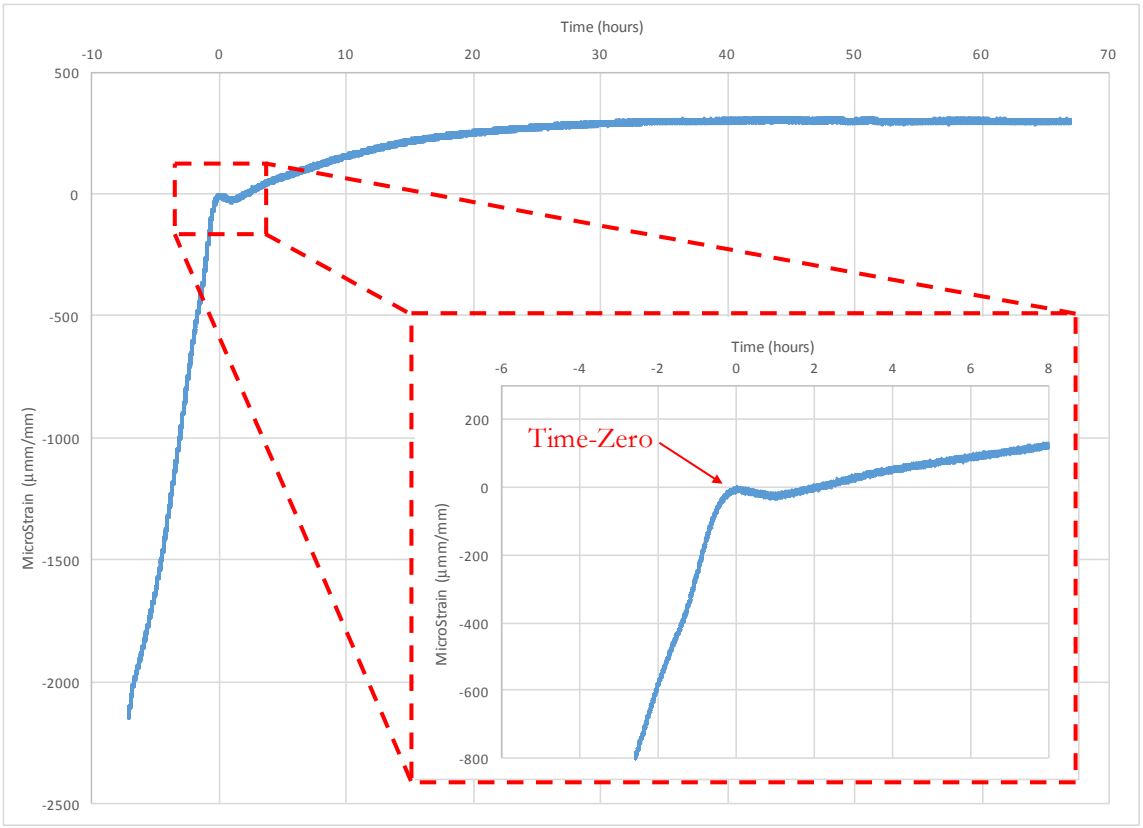

Figure 81: Swelling viewed as a bump in the microstrain vs time plot. Zero point taken at top of said bump

Yet work is still being performed in our lab in order to determine at which point the stain measurements should be zeroed or started to calculate crack inducing autogenous strain. This point coincides with final set, where the autogenous shrinkage curve develops a sizable bend or when chemical shrinkage begins to delineate from autogenous strain. In order provide the user with an isothermal initial and final set

measurements the Vicat test was set in an isothermal box. The conical mold used to hold the paste of interest was set upon a cold plate which supplied the seated paste with 23 °C cooling. The commencement for starting the cracking potential strain readings of the test was based off of the set-time determined using this set-up. Results of the corrugated tube Version 2 averaged the three samples cast per mixture design and have been outlined in Table 18.

Table 18: Autogenous shrinkage of paste mixtures determined using the Version 2 set-up. Linear strain measurements reported in the table is based on the strain measurements determined 60 hours after final set

w/cm	Cement Type	Admixtures		Final Set Time (hr)	Linear Strain ($\mu\varepsilon$)
		Type	(floz/100 lb cement)		
0.31	PC-III-A	HR-P1	6.5	5.03	431.39
			8.25	4.82	344.68
			12	5.60	348.57
		HR-P2	6.5	5.40	327.80
			8.25	4.58	285.87
			12	5.60	349.85
		HR-P3	6.5	3.18	369.11
			8.25	3.20	315.27
			12	4.02	172.56

5.3.3.4.1 Effect of HRWR Dosage

Figures 82-84 shows the effect of increasing the HRWR dosage for each individual HRWR type. Positive strain was taken after final set as explained in Figure 81.

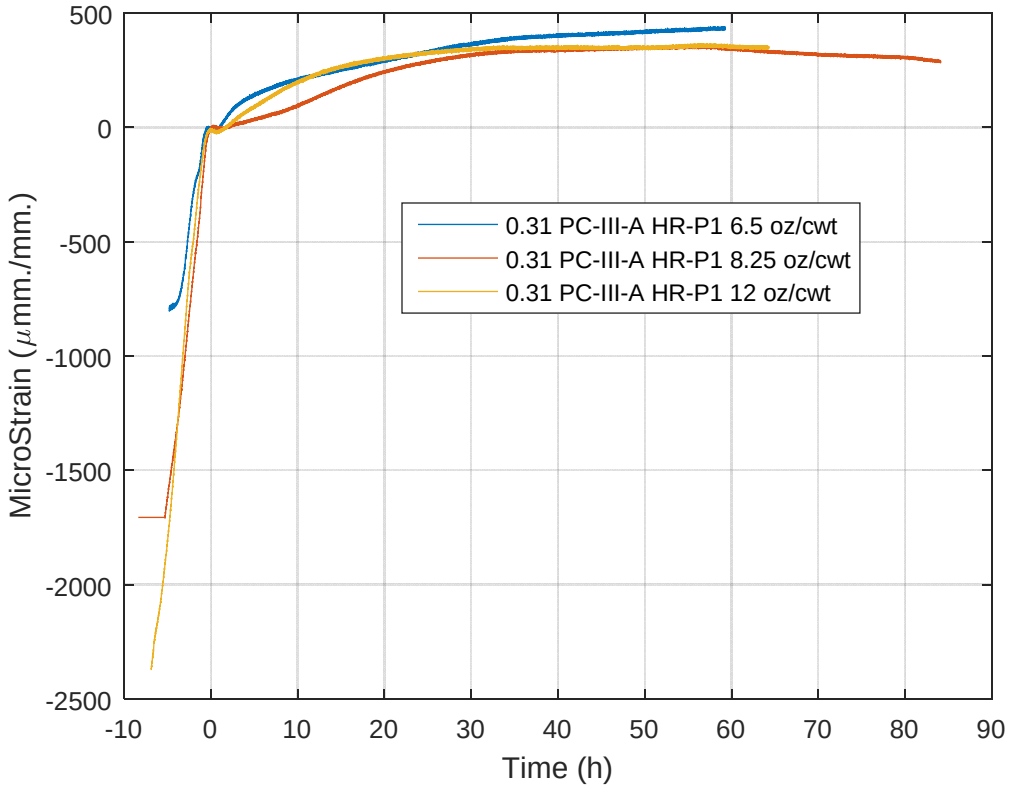

Figure 82: Corrugated Tube Shrinkage 0.31 PC-III-A for HR-P1 at 6.5, 8.25 and 12 fl oz/100lb cement

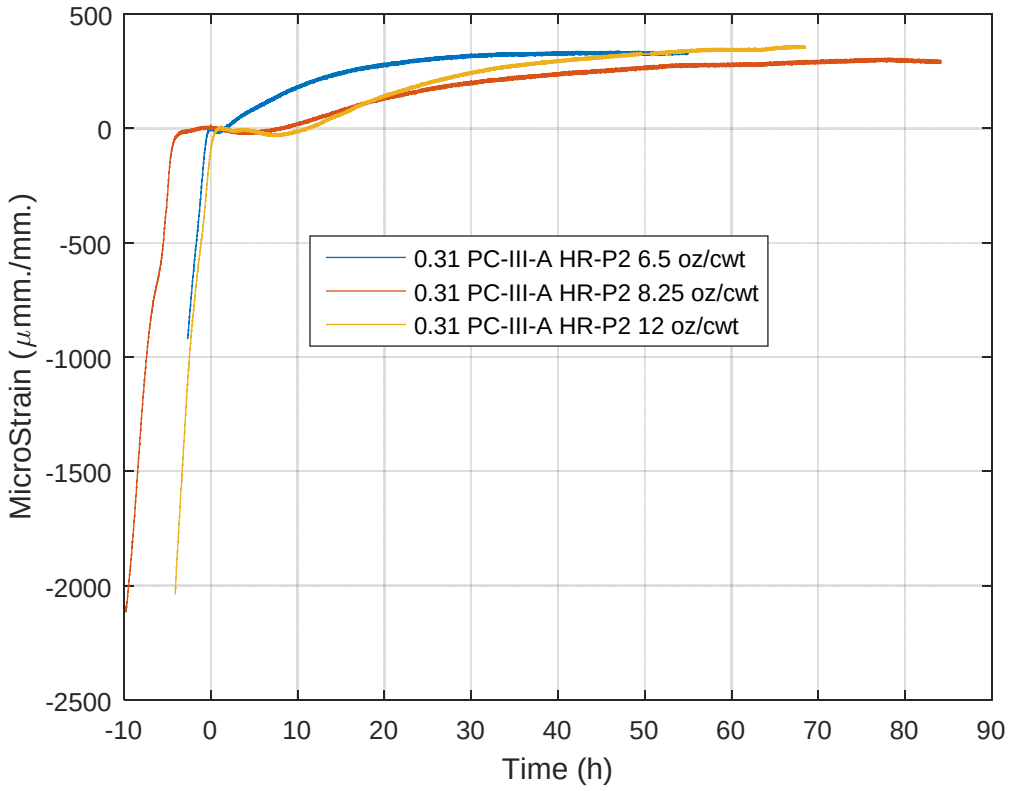

Figure 83: Corrugated Tube Shrinkage 0.31 PC-III-A for HR-P2 at 6.5, 8.25 and 12 fl oz/100lb cement

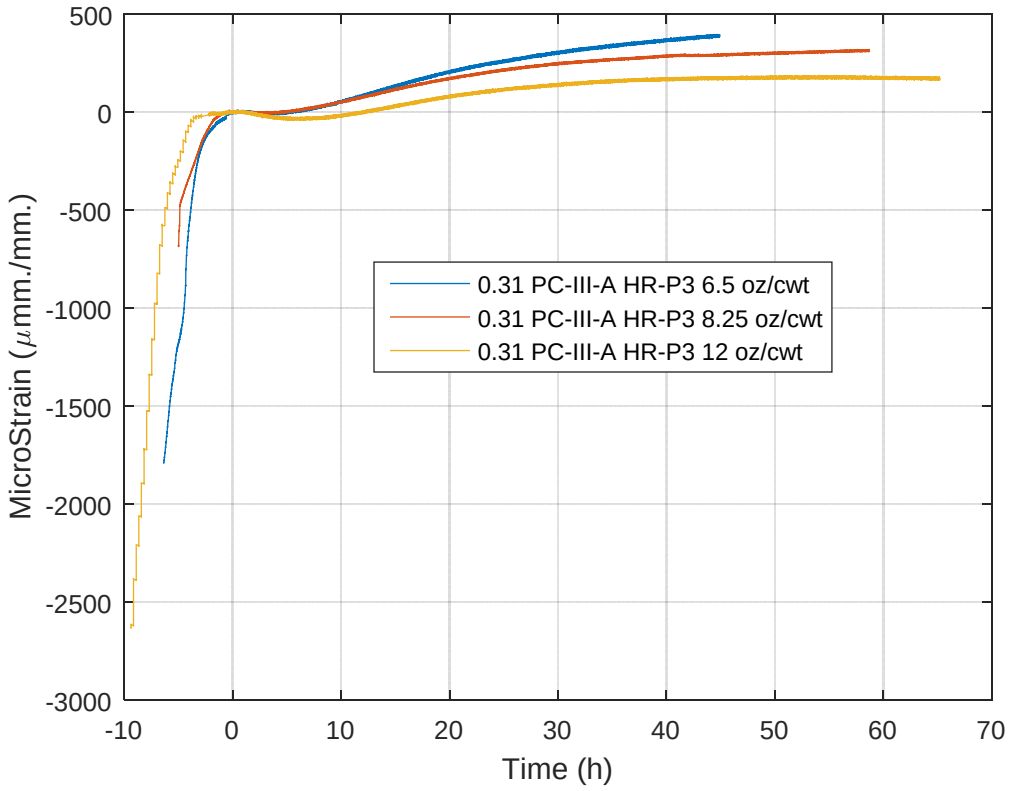

Figure 84: Corrugated Tube Shrinkage 0.31 PC-III-A for HR-P3 at 6.5, 8.25 and 12 fl oz/100lb cement

The largest amount of shrinkage strain was observed in the the paste containing the greatest admixture dosage, except in the case of HRWR HR-P2, where 6.5 and 12 oz dosages displayed similar behavior. For HRWRs HR-P2 and HR-P3, increasing the admixture dosage increased retardation as denoted in Table 18. This could be attributed to the additional liquid content that is imparted into the paste mix through the increased HRWR dosage. By the very definition of autogenous shrinkage, increasing the w/cm or water content will effectively decrease autogenous shrinkage effects (Zhang 2003).

5.3.3.4.2 Effect of HRWR Type

Figures 85-87 compares different HRWR types (HR-P1, HR-P2 and HR-P3). Again, positive strain was taken after final set as explained in Figure 81.

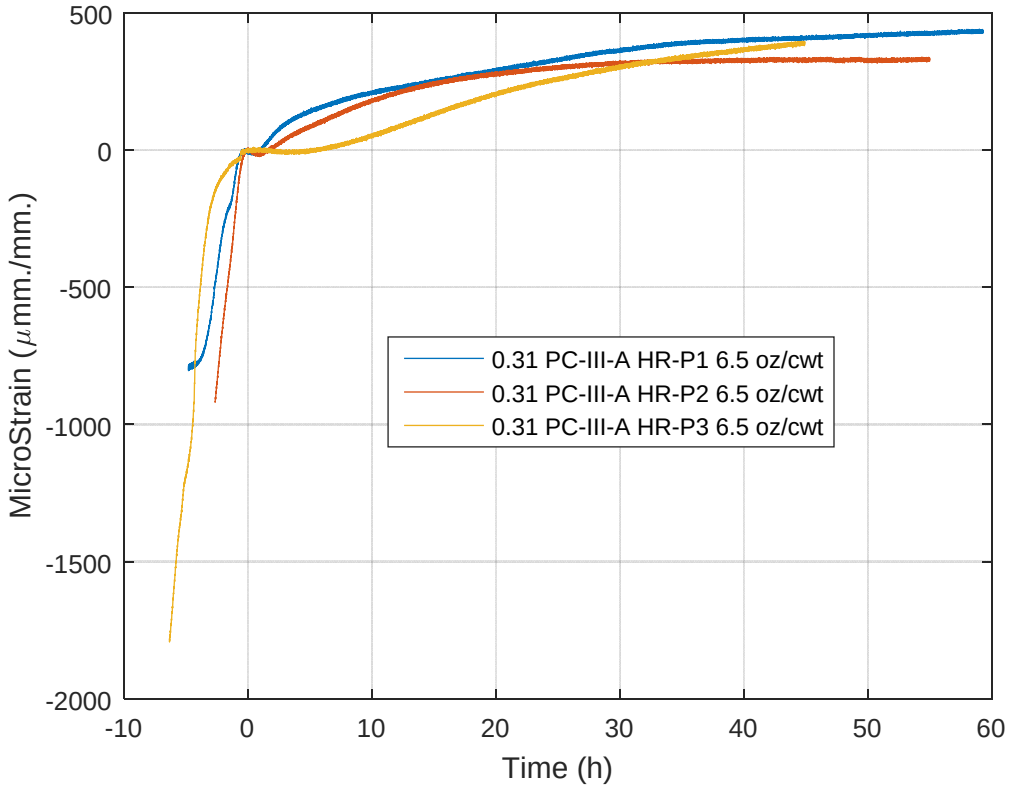

Figure 85: Corrugated Tube Shrinkage 0.31 PC-III-A for HR-P1, HR-P2 and HR-P3 at fixed 6.5 fl oz/100lb cement

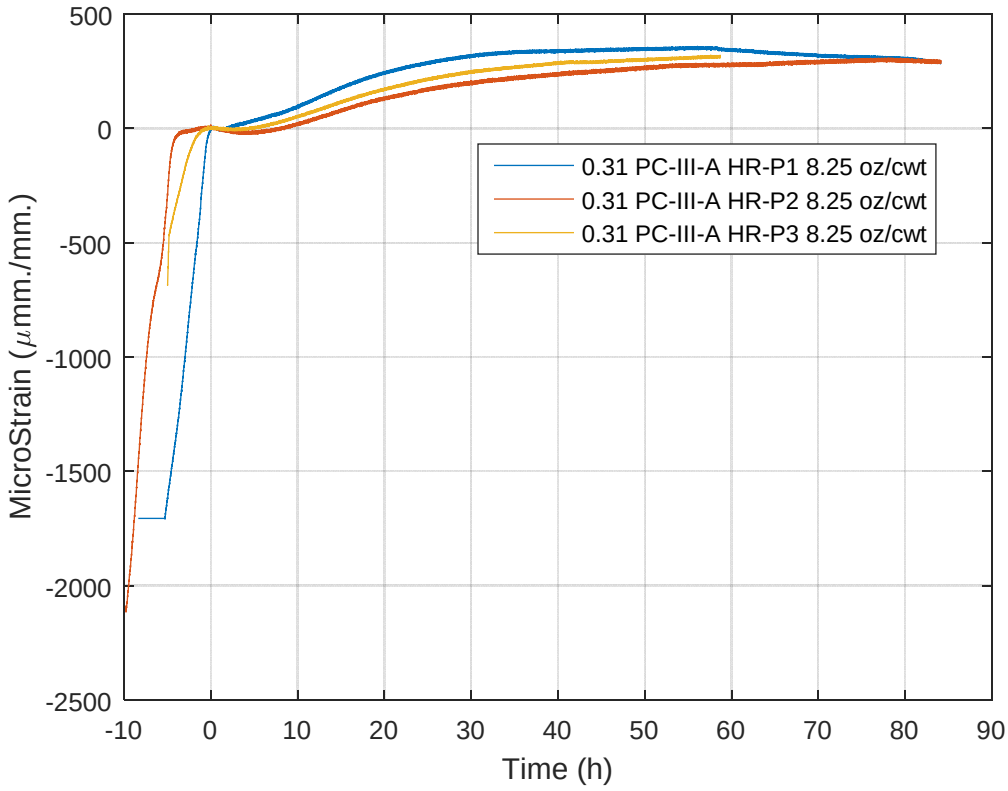

Figure 86: Corrugated Tube Shrinkage 0.31 PC-III-A for HR-P1, HR-P2 and HR-P3 at fixed 8.25 fl oz/100lb cement

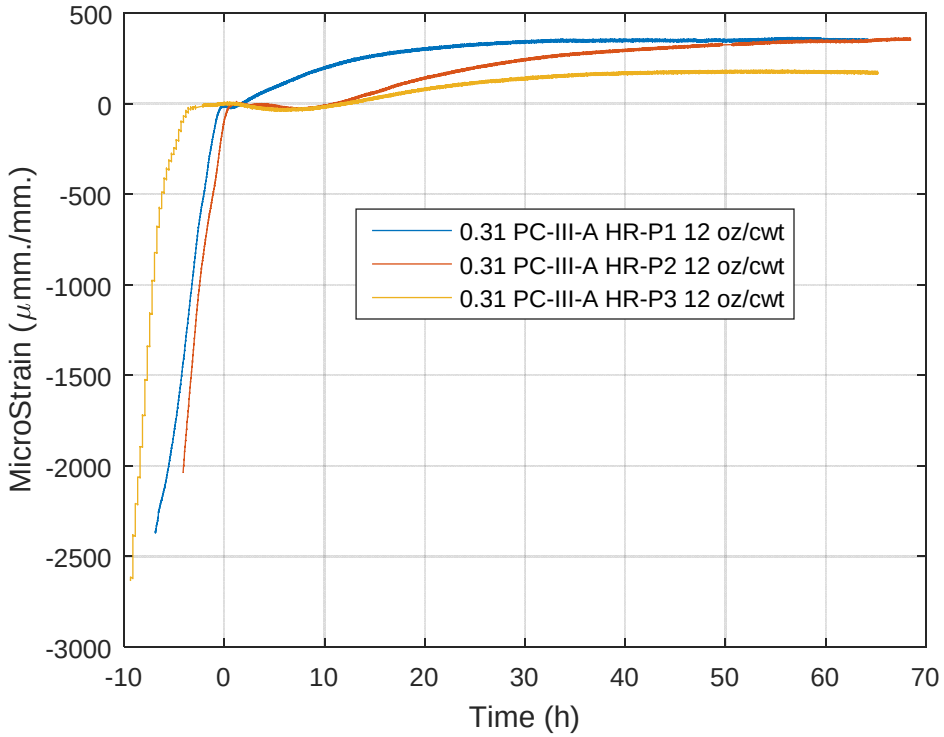

Figure 87: Corrugated Tube Shrinkage 0.31 PC-III-A for HR-P1, HR-P2 and HR-P3 at fixed 12 fl oz/100lb cement

As seen in Figures 85-87, HR-P1 showed the least variability in development of early strain after final set between each of the dosages. In all cases, pastes prepared with the HR-P1 admixture proved to incur the most amount of linear strain during the first 24 hours. HR-P2 and HR-P3 showed the inverse effect of HR-P1, as the longer development of strain (< 2 hours) after final set resulted in lower total strain at the conclusion of the testing period.

5.3.3.5 SUMMARY AND CONCLUSIONS

Based on the results of this section the following conclusions have be made:

- Pastes prepared at the higher HRWR dosage displayed increased autogenous strain than those prepared at the lower HRWR dosages
- Pastes prepared with HR-P1 showed the greatest rate of autogenous shrinkage and shortest reabsorption of bleed water (swelling). Additionally, pastes containing the HR-P1 HRWR had greater amounts of autogenous shrinkage compared to HR-P2 and HR-P3.

5.3.4 MINI RING TEST

5.3.4.1 PROCEDURE AND EXPERIMENTAL SETUP

In order to determine the cracking potential due to autogenous deformation of paste samples, the mini ring test was developed as described in Chapter 2. The setup employed is shown in Figure 88.

Figure 88: Mini restrained ring test

The samples for were prepared in 1-in diameter plastic vials that was modified by placing a 5/8-in. diameter stainless steel rod through its center. A 1-in outer diameter and 5/8-in inner diameter black rubber tube was inserted into a plastic mold to support and center the rod. Paste was prepared in accordance with ASTM C305. The paste was set into the outer ring of the mold and sufficient vibration was applied until the paste had a smooth radial surface, free of entrapped air. The paste was filled just below the top of the stainless steel rod to create a 1-in tall specimen size. After casting, the samples were sealed and placed in a water bath at 23 °C. The samples were left in the water bath and monitored on a daily basis to determine if cracking had occurred. The test is configured under the same principle as the restrained shrinkage ring test, except that the mixtures are only compared under the basis of time to cracking observed. Figure 89 provides an example of cracking of a paste sample.

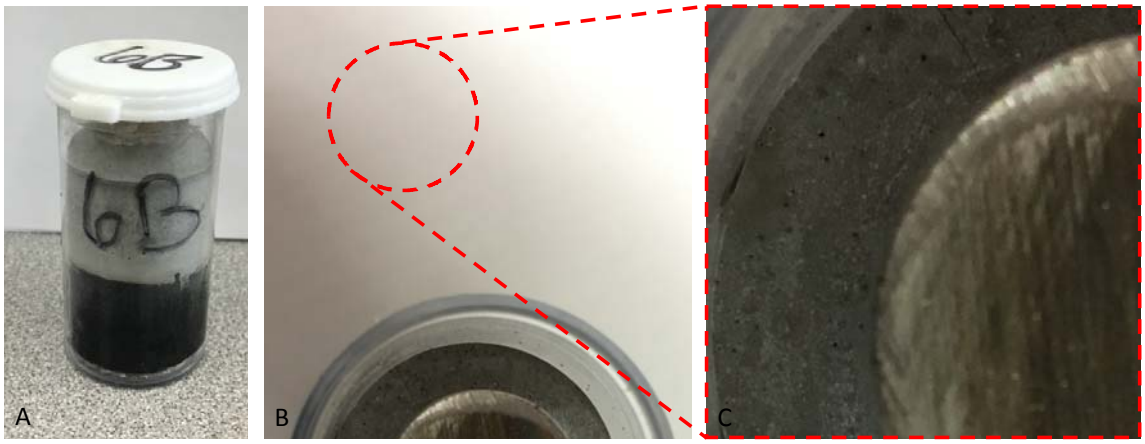

Figure 89: Crack development in mini-ring restrained test (a) 3 Month old paste sample in sample in mini-ring vial (b) red circle illuminating location of crack (c) Close-up of autogenous formed shrinkage crack

5.3.4.2 RESULTS

The concept of the mini restrained ring test was to create a quick and simple paste test that targets autogenous shrinkage, quantifying it as a function of time to cracking. Unfortunately, the testing period proved longer than expected and no monitored samples developed cracking even over a 2-month long period. Figure 88 denotes a sample where the water bath was turned off for an unknown length of time and therefore was not isolated to continuous isothermal conditions to single out autogenous shrinkage. Therefore, the sample results were dismissed, but the resulting crack provides a good good example of an autogenous shrinkage induced crack through the paste. Continued testing and visual observations will determine the validity of this testing program.

CHAPTER 6: FIELD WORK

6.1 INTRODUCTION

In this section, analysis of the data obtained from field sites (precast plants and exposure sites) is presented. A range of exposure blocks and mini-girders were cast and placed at the University of Texas at Austin exposure site for future testing and analysis. In addition to the monitored mixtures cast and placed at UT the TxDOT Cedar Park exposure site was monitored on a bi-annual basis providing visual examinations of concrete blocks that had been cast between August 2010 and October 2012.

6.2 TxDOT EXPOSURE SITE VISIT

In order to better quantify the potential cause and effects behind the micro-cracking observed in the field, three visits to the TxDOT exposure site were made. The blocks selected for visual inspection were chosen based on materials used in the concrete, mixture designs, admixtures, specimen casting date, age of specimen, as well as previous experience and knowledge with respect to the cracking issue.

6.2.1 BLOCK EXAMINATION

The TxDOT Concrete Block Exposure Site located in Cedar Park Campus is composed of more than 1500 exposure blocks that have been cast in order to observe a number of natural concrete deterioration phenomena's. Yet in order to properly target the micro-cracking that is of interest for this project, a total of 67 exposure blocks were

selected for long term visual inspection. Table 19 summarizes the selection criterion for the exposure blocks that were inspected at the Cedar Park TxDOT Site. Blocks were selected based on having at least one of the following material properties from each of the category (cement type, admixture type, coarse and fine aggregate source and w/c ratio).

Table 19: Selection Criterion for Crack Investigation of Cedar Park TxDOT Site

Cement Type	Admixture	Coarse Aggregate	Fine Aggregates	W/C Ratio
PC-A-III, PC-B-III, PC-C-III and PC-III-D	HR-P1, HR-P2, HR-P3 and HR-P4	CA-R, CA-L and CA-RIII	FA-R, FA-L and FA-RIII	0.25-0.40

In order to quantify the extent of the micro-cracking issue blocks were assigned a "crack rating" based upon the state of the visible micro-cracking on the surface; 1 showing little to no micro-cracking and 5 showing the worst micro-cracking. Table 2 displays the compilation of all the blocks that were assigned a crack rating from our site investigation in order from no visible cracking (0) to worst case cracking (4.5). Figures 90-94 provides photo evidence of the cracking that was viewed at the Cedar Park Site with crack ratings ranging from 0 to 4.5.

Figure 90: Example Crack Rating = 0

Figure 91: Example Crack Rating = 1

Figure 92: Example Crack Rating = 2

Figure 93: Example Crack Rating = 3

Figure 94: Example Crack Rating = 4.5

In hopes of determining whether there were any trends in the severity of cracks seen amongst the blocks, the blocks were grouped into four categories based on its casting date, w/c ratio, cementitious content and cement source. Figures 95-99 have been plotted to determine if there were any correlations with respect to cast date, water-cement, cement content, and cement source with the micro-cracking data collected in March of 2015.

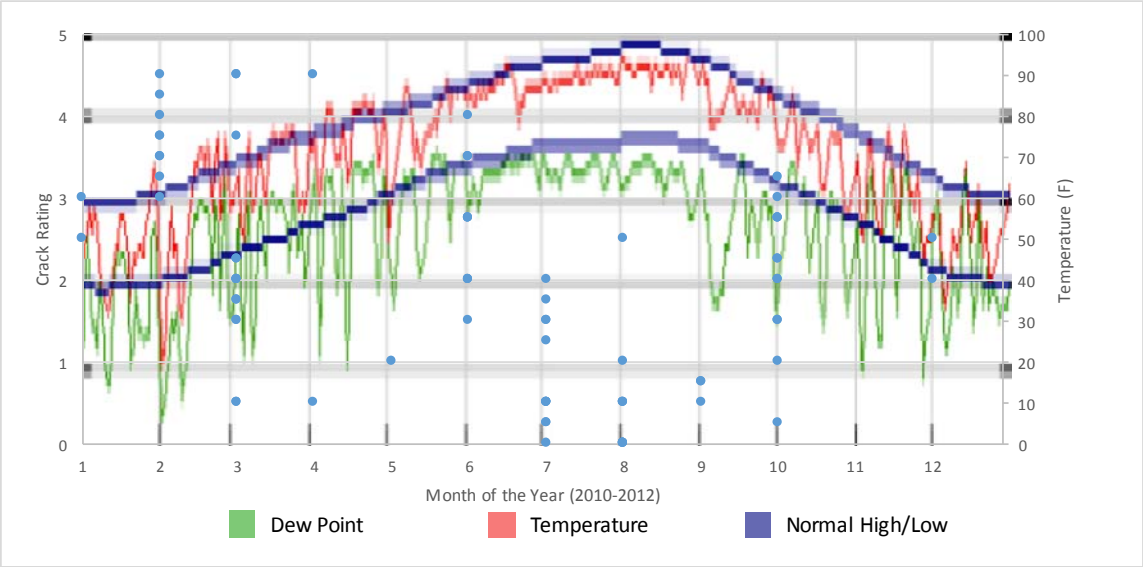

Figure 95: Exposure Block Crack Ratings with respect to month of casting. Data represents 67 distinct blocks. Dew point is a representation of RH. The "normal high/low" are averages for historical recorded temperatures. Data taken from wunderground.com (2016)

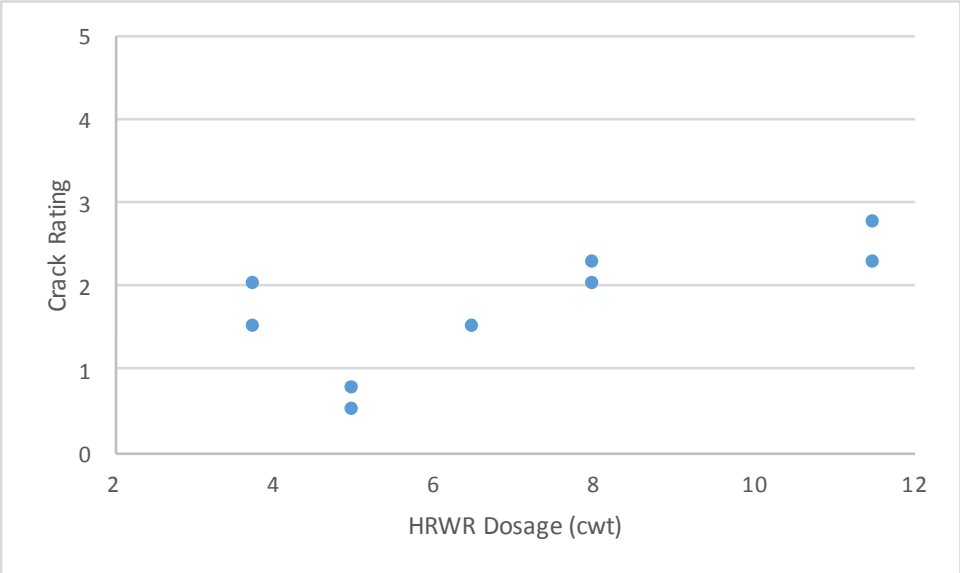

Figure 96: Exposure Block Crack Ratings according to variation in HR-P1 Dosage with all other properties held constant. Data represents on 9 distinct blocks.

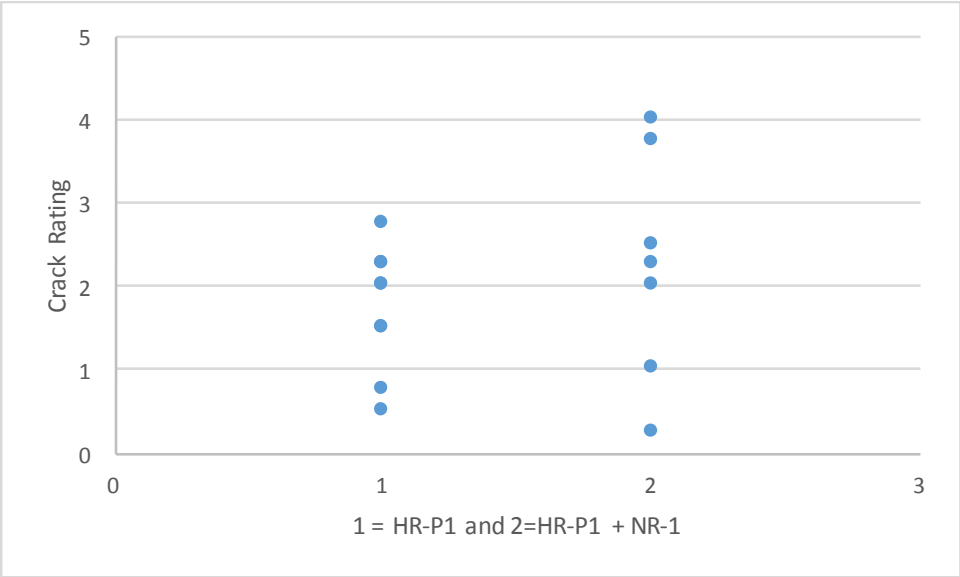

Figure 97: Exposure Block Crack Ratings according to variation in HR-P1 and HR-P1+NR-1 with all other properties held constant. Data represents on 16 distinct blocks.

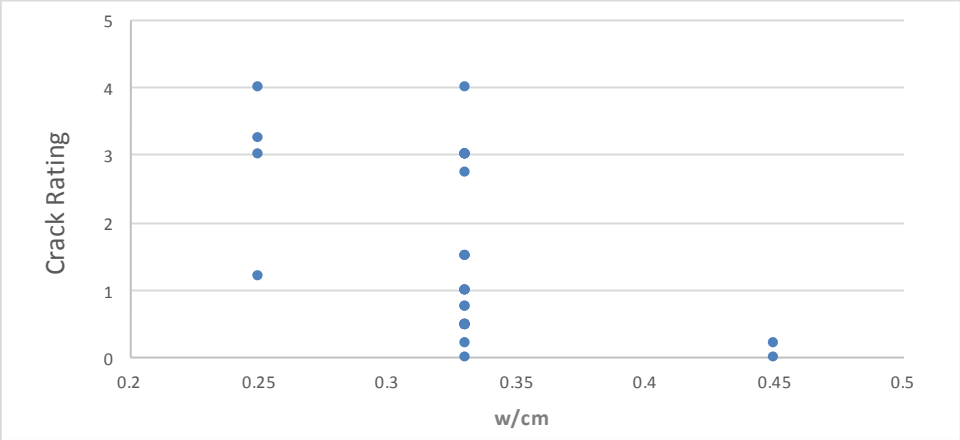

Figure 98: Exposure Block Crack Ratings according to a given water-to-cement ratio for a fixed cement content of 658 lb/yd3 Data represents on 38 distinct blocks.

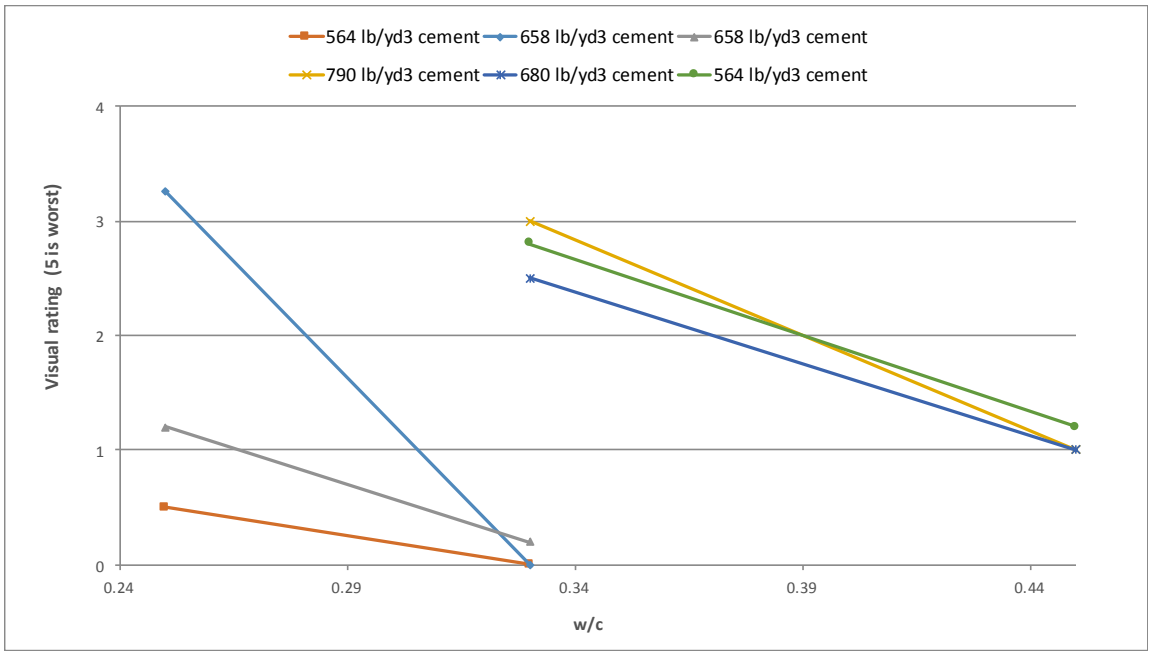

Figure 99: Exposure Block Crack Ratings according to a given cementitious content lb/yd3 Data represents on 12 distinct blocks.

Based on Figures 95 through 99 alongside the observations made on the TxDOT site regarding the severity of cracking alongside the different faces of the blocks, the following trends are proposed:

- *Effect of Casting Date:* The original thought was that the exposure conditions in early stages may have played a role in the increased development of the micro-cracking issue. While no definitive relationship can be made from Figure 95 between casting date vs. crack rating when only the month of casting is considered, overall it appears as if concrete cast during the colder periods of the year (December, January, and February—months 12, 1, 2, respectively) had higher crack ratings than blocks casts during the warmer months of June (month

6), July (month 7) and August (month 8). Further analysis should be conducted to evaluate the temperature on the date the concrete was cast since temperature can fluctuate greatly from month to month depending on the year. Additionally, it should be noted that despite the period between the first block and last block cast for this series being just short of three years, the extent of cracking for short and long term of exposure seems not to be a major governing factor. The first four sets of blocks cast in December of 2010 and January 2011 have a 1.5 through 3.0 crack rating for an average of 2.4 and the last eight blocks cast in October of 2012 have crack ratings of 1.25 through 2.75 for an average of 2.1.

- *Effect of HRWR Dosage:* Figure 96 confirms that the extent of the micro-cracking issue proves to be independent of solely the HRWR dosage. Note that this comparison using the fixed variables of the following: PC-III-A – pcy 658, 0.33 w/c, HR-P1 and CA-A and CA-AII. It is important to rule out the dosage of HRWR as a potential adverse effect on micro-cracking, however the majority of the exposure blocks cast at the Cedar Park Site did not disclose the dosages used since this was not controlled[1].

- *Effect of HRWR vs. HRWR+NR*: As shown in Figure 97 no conclusion can be drawn between the use of solely HRWR HR-P1 and HRWR HR-P1 + NR-1. However, due to the size of precast girders the laboratory research utilized the combination effect to mimic the designs currently used in the field. Since the

[1] From communication with TxDOT employees we were informed that the HRWR dosage was not recorded since the HRWR was added (sometimes incrementally during mixing) until the desired slump was achieved.

addition of normal range water reducing retarding admixtures proved non influential with respect to micro-cracking inclusion of retarders was not considered to be a key factor governing the micro-cracking issue.

- *Effect of HRWR type*: Comparing 4 different HRWR's HR-P1, HR-P2, HR-P3 and HR-P4 with and without NR-1 with all other mixture variables constant did not provide enough data to confirm different the admixture effect on cracking behavior of field specimens. In order to solely address HRWR type as a source of cracking performance only 16 out of the 67 blocks had the the same cement source, aggregate source, w/c ratio and cement content. Since the majority of the blocks (11 out of 16) contained HR-P1, there is not enough data available to evaluate the effect of HRWR composition. Therefore, HRWR type may not be eliminated as a potential variable effecting the extent for the remainder of this analysis.

- *Effect of Aggregate Source:* Aggregate source does not appear to have a strong correlation with worsening of cracking that has been seen in the field. In order to solely address aggregate source as a component of cracking performance only 24 out of the 67 blocks had the the same cement source, HRWR type, w/c ratio and cement content. Since the majority of the blocks (19 out of 24) employed the same aggregate, there is not enough data available to evaluate the effect of aggregate source. Therefore, aggregate source may not be eliminated as a potential variable effecting the extent for the remainder of this analysis. It must be noted however, a block with lightweight aggregate, Block 244 from Cedar Park

Exposure Site, had the highest crack rating (4.5) of all the blocks observed in this study. Previous research has confirmed that internal curing via soaked lightweight aggregate reduces and in some cases eliminates autogenous shrinkage effect. Block 244 suggests that the extent of micro-cracking is a not solely related to autogenous shrinkage, but that it is due to a culmination of multiple volumetric changing mechanisms.

- *Effect of Cement Source:* Cement source does not appear to have a strong correlation with worsening of cracking that has been seen in the field. In order to solely address cement source as a component of cracking performance only 17 out of the 67 blocks had the the same HRWR type, aggregate source, w/c ratio and cement content. Since the majority of the blocks (13 out of 17) employed the same cement source, there is not enough data available to evaluate the effect of cement source. A larger sample size must be taken in order to draw a proper conclusion of this variable. Therefore, cement source may not be eliminated as a potential variable effecting the extent for the remainder of this analysis.

- *Effect of w/c ratio:* In order to address the concern of drying shrinkage cracking on the exposure blocks w/c ratio vs. crack rating was investigated as seen in Figure 98. For a fixed cement content of a range of w/c ratios were expressed. It appears that there is a correlation between lower w/c and crack rating. Unfortunately, there is not a large enough sample size to discernibly confirm that higher w/c ratios result in decreased cracking potential.

- *Effect of Cement Content:* Though the data collected and plotted in Figure 98 it can be confirmed that lower cementitious contents results in a lower cracking potential.

- *Effect of Drying Orientation:* Visual inspection of the exposure blocks through multiple visits confirmed that the East and West faces of the blocks showed the worst cracking relative to the North and South faces. Therefore, consistent East facing block faces were used for cracking evaluation throughout the field investigations. This suggests that the severity of wetting and drying cycles over the lifetime of the concrete block or temperature effects is impacting the micro-cracking issue, specifically micro-cracking is exacerbated when the wetting and drying occurs quickly and/or blocks faces are subjected to higher temperature variations.

6.3 PRECAST PLANT SITE VISIT

Since the micro-cracking issue was initially discovered on girders that had been sitting in the precast yard awaiting use in the field, investigating full-scale girders at the precast plants were part of this project. These girders were rejected for use in the field due to micro-cracking. Two separate precast plants were selected to investigate the micro-cracking issue based upon production size, and differences in materials and admixtures employed at each of the plants. The visits to the plants were purely visual inspection. The severity and integrity of the cracking was measured against the following: casting dates, primary location of cracking, and size and spread of cracking.

Based upon the two separate precast plant visits the following was documented and proposed:

- *Casting Dates:* Girders that had been exposed to the environment the longest displayed some of the worst cracking. However, the mixture designs were not collected on any of the girders and a majority of the girders with like micro-cracking issues had been demolished by the precast plants. Therefore, although it is well known the delayed micro-cracking issue worsens with time no conclusion can be formally made between the different girders that were investigated at the precast plants due to lack of girders from different casting periods.

- *Location of Cracking:* Several different structural elements were investigated during the precast plant site visits, but in order to provide a more definitive comparison between the two separate precast plants (PP-A and PP-B) the focus was limited to AASHTO Type IV girders. Although the bulk of micro-cracking shows to be widespread across the girders, certain girders showed a denser allocation of cracking on different faces of the girders. Girders inspected at Precast Plant A displayed micro-cracking focused on the girder's flange, whereas girders located at Precast Plant B was concentrated on the girder's web. Figure 99 designates the cracking locations based on general observations at both plants and specific observations at the individual plants.

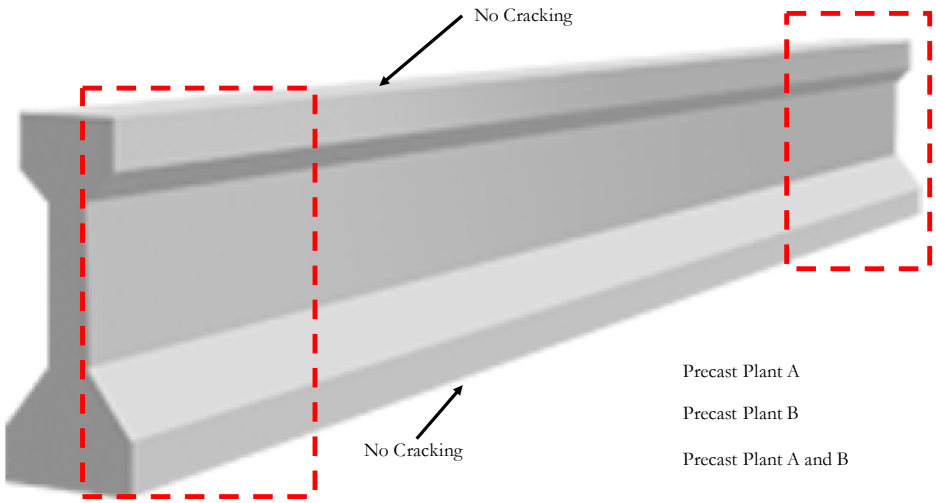

Figure 100: Concentration of map cracking pattern. Note no visible cracking on top or bottom of girders

Micro-cracking, whether on the flange or the web, propagated onto the angular flange segments of the girders. The cracking was more pronounced on the far ends of the girders and the density of the cracking lessened towards the middle segment of the girder. Cracking was either faint or not visible of either girder end faces and or top segment of the girder. With every girder regardless of the cracking intensity or location, the bottom face of the girders showed no micro-cracking. The bottom casting face anomaly also proves true in laboratory blocks that have placed on a permeable gravel foundation. Figures 101 and 102 provide photographs from both PP-A and PP-B showing the differences in micro-cracking allocation on the girder faces.

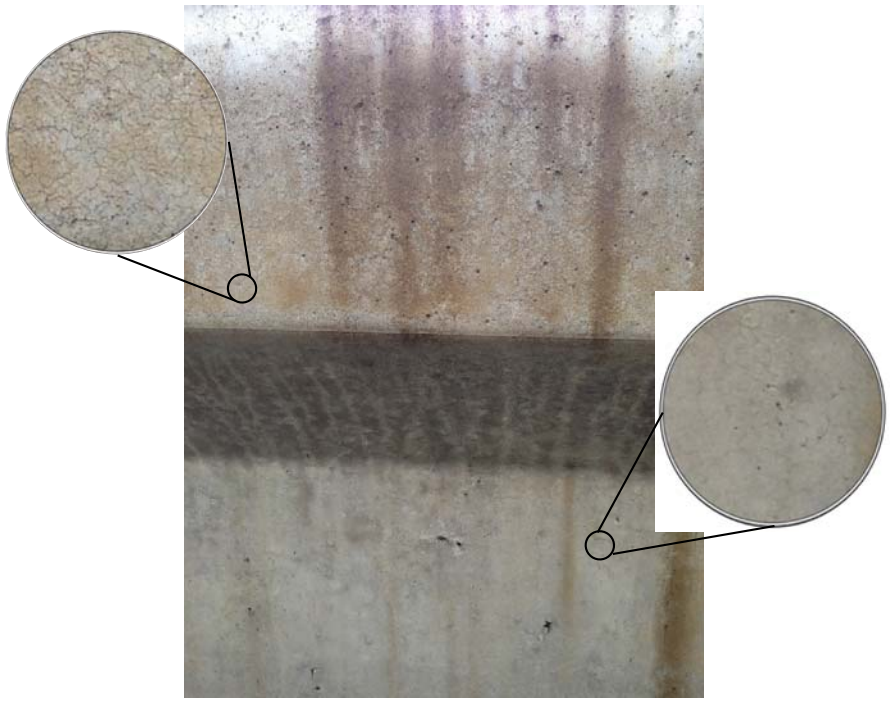

Figure 101: Girder located at PP-A: Concentration of Micro-cracking on Upper and Lower Flange

Figure 102: Girder located at PP-B: Concentration of Micro-cracking Focused on Girder Web

- Size and Spread of Cracking: Although the density and spread of the micro-cracking phenomenon increases with time, the size of the cracks do not appear to increase in width. Although the scope of this project did not investigate the propagation of crack width with time, visual inspection suggests that the cracks increase in density, but not width. The support for limited crack width enlargement with time is attributed to the structural cracks that typically develop on the girders ends. The structural cracks form as a result of the massive force release of the pre-stressed strand. The diagonal cracks as seen in Figure 103 have

not widened, however the micro-cracking has developed around the structural cracks and the micro-cracks also begin to form away from the structural cracks.

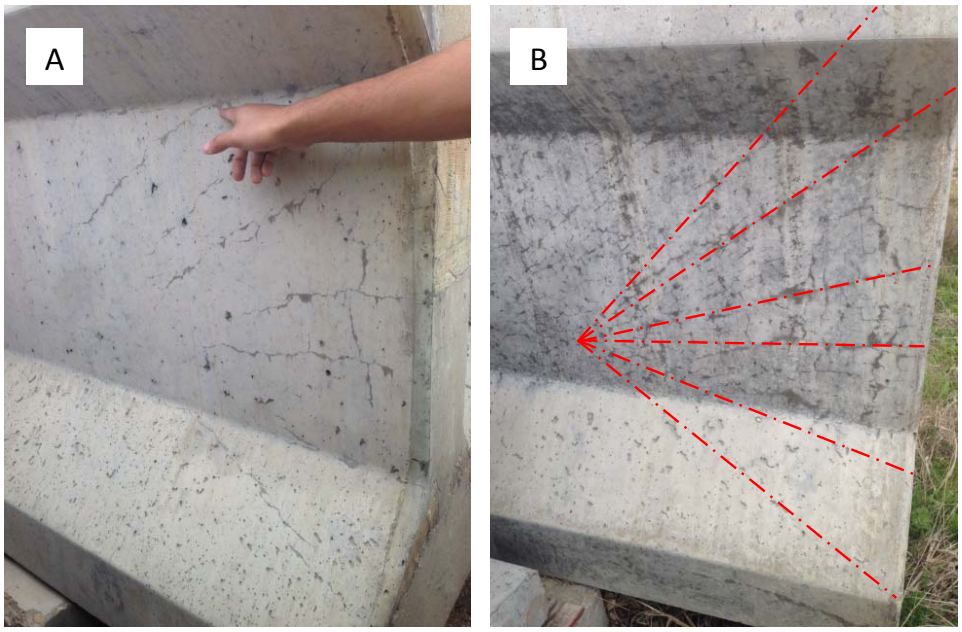

Figure 103: (A) Photo of girder located at PP-B with fingers pointing to diagonal release strand cracks. (B) Photo of a separate girder located at PP-B showing that the micro-cracks stem away from the release strand cracks and form in new space between release strand cracks

This reaffirms that this is a material based issue, otherwise the micro-cracking would just propagate the widening of the structural release strand cracks (least path of resistance) without starting new cracks. Figure 104 also shows that the micro cracks develop away and outside of the diagonal release strand cracks, which may possibly be attributed to the moisture that more readily remains in the release strand cracks after a rain. This again, refers back to the wetting and drying cycles that seems to be exacerbating the micro-cracking issue.

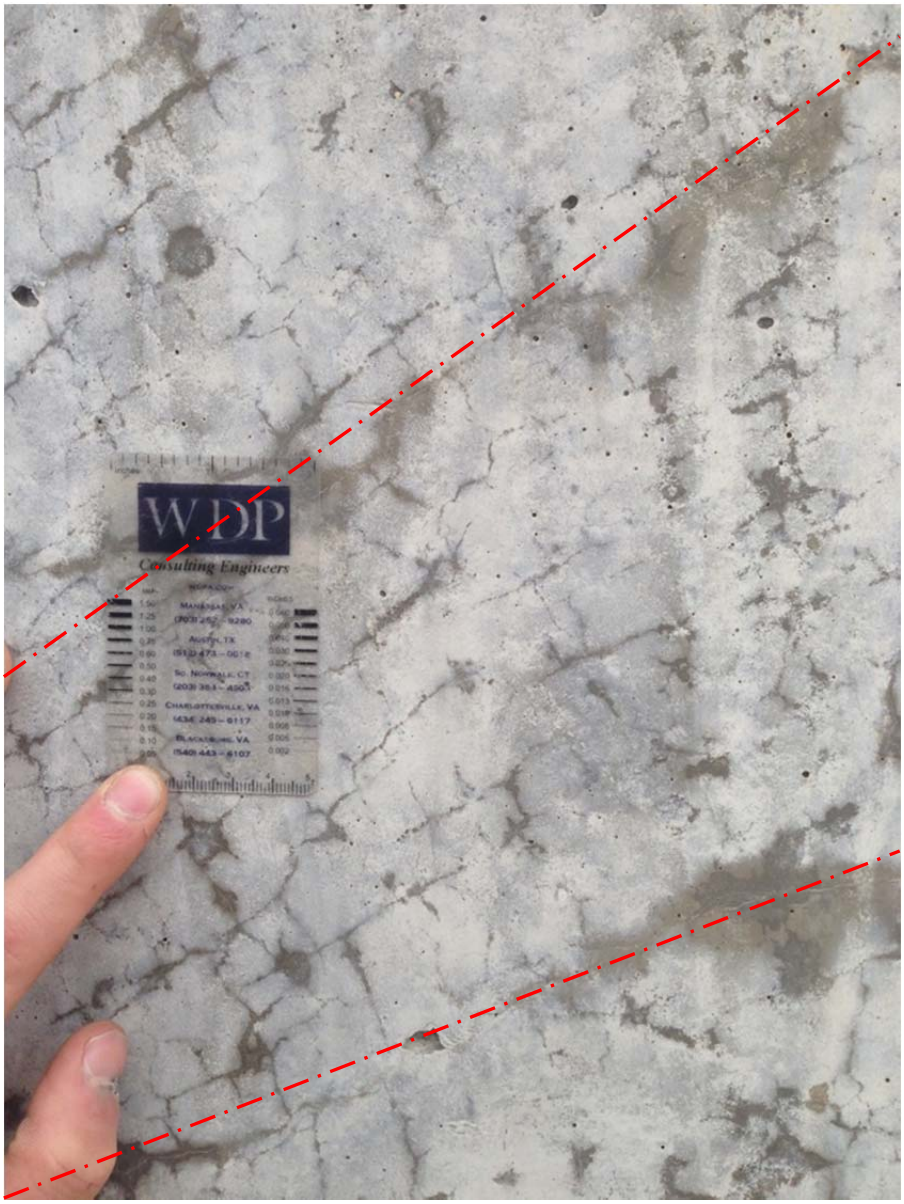

Figure 104: Close up image of Figure 102-B. This figure emphasizes the micro-cracking development separate from the outlined (dashed red) release strand cracks

6.4 UT AUSTIN EXPOSURE SITE

An additional set of exposure blocks “mini-girders” and carbonation specimens were cast and stored at the exposure site at the Construction Materials Research Group to allow for more frequent observation of the specimens than what can be achieved from

periodic visits to the precast site and TxDOT Cedar Park Exposure Site. The blocks were cast in order to provide a realistic natural environmental exposure condition cracking as compared with the laboratory testing results from autogenous free shrinkage, stress development under passive restraint, and drying shrinkage. The exposure blocks and girders were also assigned crack ratings, which will allow for further comparison of mixture design parameters and mechanical properties with cracking performance. Figure 105 provides a picture of the exposure blocks that have been cast since 2013 as a part of the girder micro-cracking investigation. To date 61 exposure blocks and 14 mini-girders have been cast.

Figure 105: UT Austin Visual and Measurement Exposure Site

6.3.1 VARIATION IN EXPOSURE SPECIMENS

6.3.1.1 Standard 3.4-ft^3 Blocks

The exposure blocks were cast in 18x18x18-in. prismatic plywood forms. Thus the volume of the blocks was 3.4 ft^3. The plywood surface that makes contact with the concrete is coated with a generous layer of polyurethane form oil to aid in the demolding process and mimic the procedures followed at the precast plants.

6.3.1.2 3.4-ft3 Block with Expansion/Shrinkage Demics

As previously mentioned in Chapter 1, the micro-cracking was originally believed to be due to ASR or DEF. ASR and DEF blocks use stainless steel tapped hex bolts that have been inset 2.5-in into the bulk of the concrete and extend out 1-in for comparator measurements. Yet when the exposure blocks showed no bulk expansion that would incite cracking TxDOT began to cast the standard 3.4 ft^3 blocks purely for visual observation (2010) and ceased measuring strains. In order to better target and quantify the extent of the micro-cracking, select concrete mixtures were cast in exposure blocks that were instrumented with the hex bolts. The bolts were set at distances 2-in and 1-in depths; in addition, demic points (to allow for surface deformation measurements) were adhered on the North, South, East and West surfaces of the exposure blocks. The demic points were adhered to the concrete surface with approximately a ¼-in diameter dab of (Devcon 11765) epoxy. Figure 106 provides a diagram of the orientation and varying depths for the measurement locations of the measureable exposure blocks. The key distance outlined in Figure 106, is 4-in separation distance between like set depth bolts or demics.

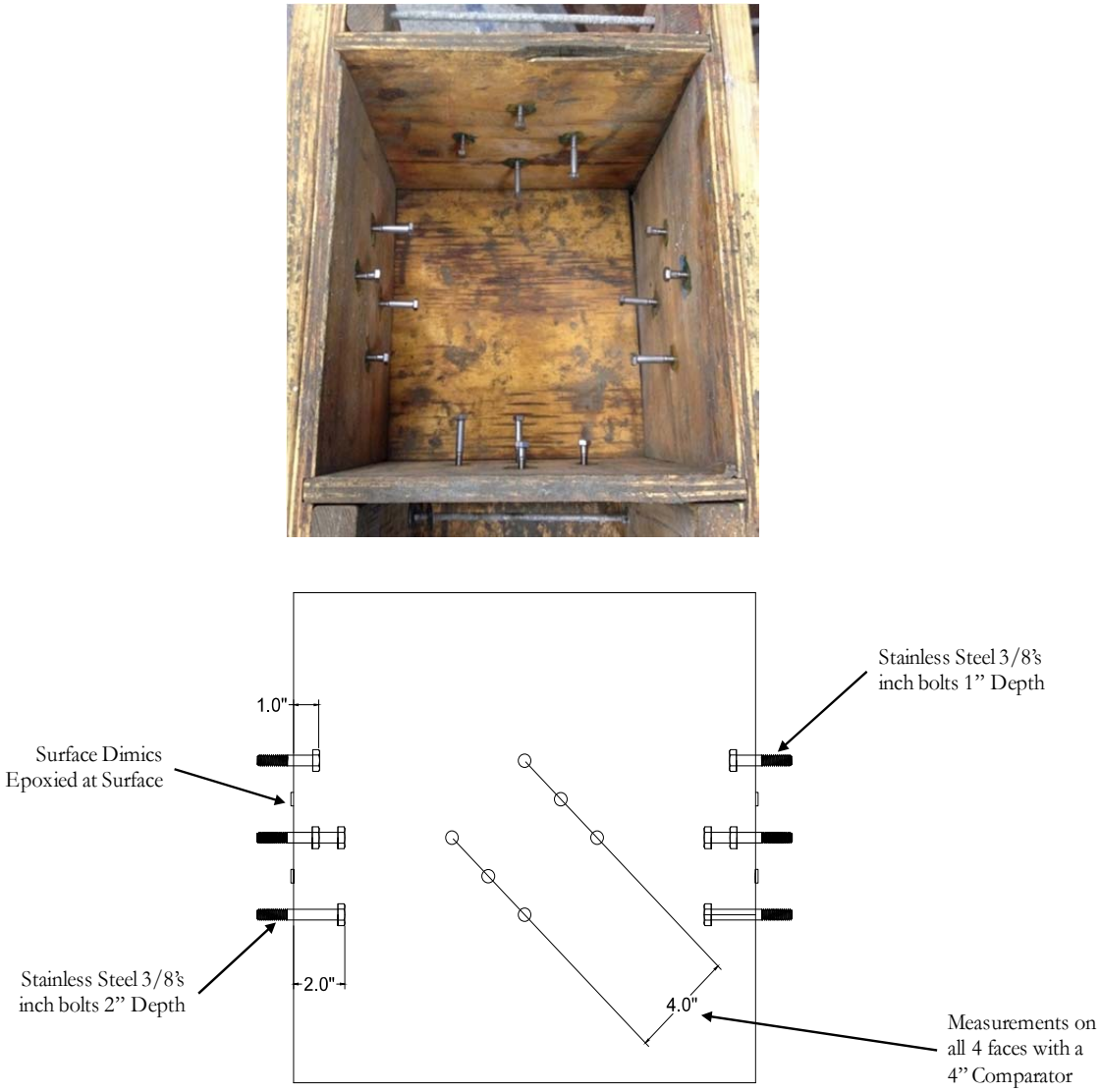

Figure 106: (Top) Wood mold used for casting measurable exposure blocks with bolts in place (Bottom) CAD drawing of various depths that bolts and surface demics were placed for future expansion/shrinkage measurements. Only the 4 in. diagonally annotated distance figured is measured with the comparator.

6.3.1.3 “MINI” GIRDERS:

In addition to the standard 3.4-ft^3 exposure blocks, AASHTO Type IV girders scaled down to approximately 1/3 from the size cast in the field were cast for this project (see Figure 107). The mini girders composed 6.4-ft^3 of concrete were cast in order to investigate the effect of volume of concrete to surface area ratio (2.3 in.) that correlates to the true sizing in the field. The extent of the latent cracking will be closely monitored on the girders in order to see cracking location and density occurs more quickly as with the precast plants. The exposure site for the mini girders is shown in Figure 108.

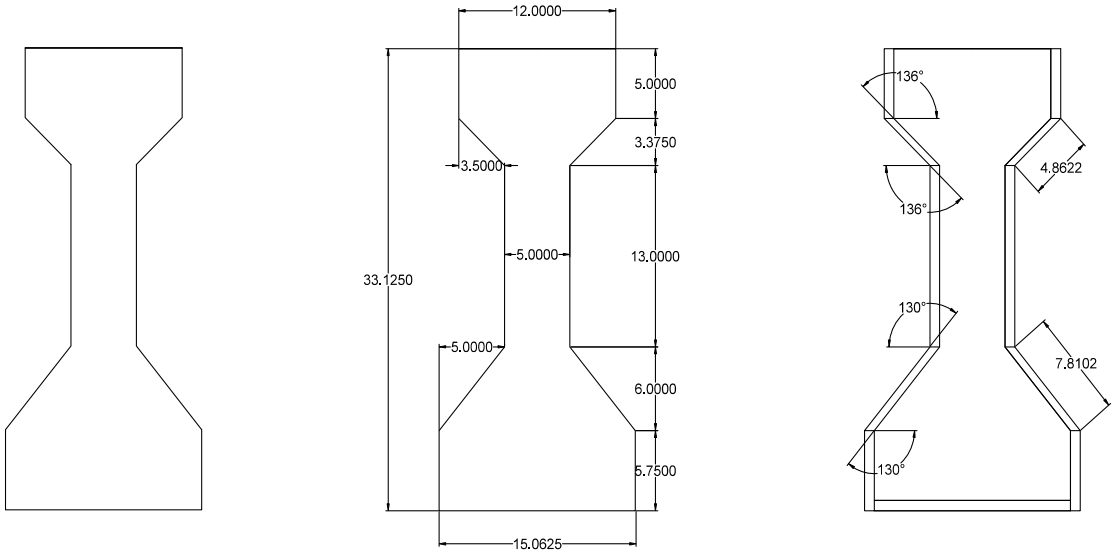

Figure 107: CAD drawing Sizing of Mini-Girders in (Inches)

Figure 108: Mini Girder Exposure Site. Photo Taken Facing East.

6.3.1.4 CARBONATION SPECIMENS:

Natural and sheltered carbonation prisms as outlined in Chapter 2 of this report were exposed to the ambient temperatures and CO_2 concentration as provided by the environment at the Construction Materials Research Laboratory located at the University of Texas at Austin's Pickle Research Campus. The 4x4x16 in. specimens were cast from the concrete mixtures used in the blocks and mini-girders. The prisms were cast in order to develop a comparative matrix in the hopes of quantifying crack intensity and depth of carbonation. Mixed and cast alongside the exposure blocks and mini girders, the prisms were subsequently demolded and stored on a pervious rock bed or sheltered in a Stevenson screen. The prismatic specimens were stored standing up on one end. Figure

109 is a photo of the carbonation field site where prisms were either sheltered or exposed to the natural elements.

Figure 109: Carbonation exposure site at UT Austin with shelter (Stevenson Screen)

6.3.2 PROCEDURE

The concrete was mixed in accordance with ASTM C192 in a 6 ft^3 drum mixer in a temperature regulated room (23 ± 3 °C). Following mixing, the concrete was directly poured into the molds for the exposure blocks, mini girders and carbonation specimens. Once initial set was reached, the specimens were covered with soaked burlap and plastic sheets to facilitate moist curing conditions as seen in the field. At an age of 18 hours the concrete molds were stripped to mimic the precast plant demolding timeline. To avoid

thermal shock, the blocks and girders would remain in the temperature controlled room for an additional time to limit the thermal gradient. Forms in the field are stripped readily once the desired strength is achieved.

6.3.3 MIXTURE DESIGNS

Table 20 shows the mixtures that were prepared for outdoor exposure specimens as well as the laboratory concrete testing that coincide with those mixture designs. The location and mixture designs for the blocks located at the University of Texas exposure site is located in the appendix of this report.

Table 20: Outdoor Exposure Specimen Mixture Designs and with corresponding testing

w/cm	Cement Type	Cement Content (lb/yd^3)	SCM Content (lb/yd^3)	Aggregate Source		Admixtures				DS	RSR	Carbon-ation	Girder	Expose. Block
				FA	CA	Type	(floz/100 lb cement)	Type	(floz/ 100 lb cement)					
0.24	PC-III-A	705	-	FA-R	CA-R	HR-P2	15	NR-1	3	X	-	X	X	X X
0.26	PC-III-A	564	141	FA-R	CA-R	HR-P2	6.5	NR-1	3	X		X	X	X
		705	175	FA-R	CA-R	HR-P1	6.5		1.5	X	-	-	-	X
		705	175	FA-R	CA-R	HR-P2	8.25		3	X	X	-	-	-
		705	175	FA-R	CA-R	HR-P3	10	NR-2	2	X	X	-	-	-
		705	175	FA-R	CA-R	HR-P1	12	NR-1	3	X	-	-	-	X
	PC-III-B	705	271	FA-R	CA-R	HR-P1	8.25		3	X	X	-	-	-
0.28	PC-III-A	705	-	FA-R	CA-R	HR-P1	12	NR-1	3	X		X	X	-
		705	-	FA-R	CA-R	HR-P2			3	X		X	X	X
		705	-	FA-R	CA-L	HR-P1	12.5		3	X		X	X	X
		705	-	FA-R	CA-L	HR-P2	12		3	X		X	X	X
		705	-	FA-R	CA-R	HR-P3	12	NR-2	3	X		X	X	X
		705	-	FA-R	CA-L	HR-P3	12		3	X		X	X	X
		705	-	FA-R	CA-L	HR-P4	12		3	X		X	X	X
	PC-III-B	705	-	FA-R	CA-L	HR-P1	12	NR-1	3	X		X	X	-
	PC-III-A	564	188	FA-R	CA-R	HR-P2	12		3	X	X	-	-	-
	PC-I-A	705	-	FA-R	CA-R	HR-P3	12		3	X	X	-	-	-
	PC-III-A	705	175	FA-R	CA-R	HR-P1	12		3	X	-	-	-	X
0.3	PC-III-A	564	188	FA-RII	CA-RII	HR-P3	8	NR-2	2	X	X	-	-	-
		564	188	FA-RII	CA-RII	HR-P3	8		2	-	-	X	X	X X
		564	188	FA-RII	CA-RII	HR-P4	8		0.5	X	X	X	X	X

*DS: Drying Shrinkage, RSR: Restrained Shrinkage Ring

Table 20 (cont.): Outdoor Exposure Specimen Mixture Designs and with corresponding testing

w/cm	Cement Type	Cement Content (lb/yd^3)	SCM Content (lb/yd^3)	Aggregate Source		Admixtures				DS	RSR	Carbon-ation	Girder	Expose. Block
				FA	CA	Type	(floz/100 lb cement)	Type	(floz/ 100 lb cement)					
0.31	PC-III-A	640	213	FA-R	CA-R	HR-P1	6	NR-1	2	X	-	-	-	X
		663	271	FA-R	CA-R	HR-P4	5.5	NR-2	0.5	-	-	X	X	X X
		663	271	FA-R	CA-R	HR-P2	5.5	NR-2	2.5	X	X	X	X	X
		663	271	FA-R	CA-R	HR-P2	5.5		2.5	X	X	-	-	X
		663	271	FA-LW	CA-R	HR-P3	7.25	NR-2	2.5	X	X	-	-	-
	PC-III-B	663	271	FA-R	CA-R	HR-P1	6	NR-1	2.5	X	X	-	-	-
0.33	PC-III-A	658	-	FA-R	CA-R	HR-P1	12	NR-1	3	X	X	-	-	-
		658	-	FA-R	CA-R	HR-P1	6.5	NR-1	3	X	-	-	-	X
		658	175	FA-R	CA-R	HR-P2	5.5		2	X	-	-	-	X
		658	-	FA-LW	CA-R	HR-P3	5		2.5	X	-	-	-	X
0.4	PC-III-A	658	-	FA-R	CA-R	HR-P4	2	NR-1	2	X	-	-	-	X
		658	165	FA-R	CA-R	HR-P5	2		2	X	-	-	-	X

*DS: Drying Shrinkage, RSR: Restrained Shrinkage Ring

6.3.4 RESULTS

The results from the blocks, mini girders and carbonation specimens are limited since micro-cracking has yet to develop substantially on the exposure specimens that have been cast since August 2014. Despite the appearance of faint micro-cracking on the exposure blocks there is no correlation between early development of faint cracking and substantial development of cracking as seen in girders and blocks cast several years ago at the TxDOT facility.

6.3.4.1 EXPOSURE BLOCK RESULTS

Table 21 provides crack rating for all blocks cast as a part of this research project as determined in April of 2016. The table provides up to date crack rating for all exposure blocks.

Table 21: Blocks Cast at UT Austin Exposure Site for TxDOT 0-6813. Precast plant mixtures performed at the precast plants and the lab replicates performed in the lab have been illuminated.

w/cm	Cement Type	Cement Content (lb/yd^3)	SCM Content (lb/yd^3)	Aggregate Source		Admixtures				Exposure Block		
				FA	CA	Type	(floz/100 lb cement)	Type	(floz/ 100 lb cement)	Cast Date	Age (Months)	Crack Rating
0.24	PC-III-A	705	-	FA-R	CA-R	HR-P2	15	NR-1	3	2/24/15	13	0.25
0.26	PC-III-A	564	141	FA-R	CA-R	HR-P2	6.5	NR-1	3	6/9/15	10	0.75
		705	175	FA-R	CA-R	HR-P3	10	NR-2	3	9/20/15	7	0.0
	PC-III-B	705	271	FA-R	CA-R	HR-P1	8.25	NR-1	3	9/20/15	7	0.0
0.28	PC-I-A	705	-	FA-R	CA-R	HR-P2	12	NR-1	3	9/20/15	7	0.0
	PC-III-A	705	-	FA-R	CA-R	HR-P2	12		3	2/27/15	13	0.0
		705	-	FA-R	CA-L	HR-P1	12.5		3	1/26/15	14	0.0
		705	-	FA-R	CA-R	HR-P1	12		3	9/20/15	7	0.0
		705	-	FA-R	CA-L	HR-P2	12		3	1/27/15	14	0.0
		705	-	FA-R	CA-R	HR-P3	12	NR-2	3	2/27/15	13	0.0
		705	-	FA-R	CA-L	HR-P3	12		3	3/20/15	13	0.0
		705	-	FA-R	CA-L	HR-P4	12		3	2/19/15	13	0.0
	PC-III-B	705	-	FA-R	CA-L	HR-P1	12	NR-1	3	5/26/15	11	0.25
		564	188	FA-RII	CA-RII	HR-P3	8		2	3/12/15	13	1 and 1.25
0.3	PC-III-A	564	188	FA-RII	CA-RII	HR-P3	8	NR-2	0.5	5/26/15	11	0.0
		564	188	FA-RII	CA-RII	HR-P3	8		2	9/20/15	7	0.0
		663	271	FA-R	CA-R	HR-P4	5.5		0.5	3/5/15	13	0.25
0.31	PC-III-A	663	271	FA-R	CA-R	HR-P2	5.5	NR-1	2.5	6/9/15	10	0.0
		663	271	FA-R	CA-R	HR-P2	7.25		2.5	9/20/15	7	0.0
		663	271	FA-R	CA-R	HR-P3	7.25	NR-2	2.5	9/20/15	7	0.0
	PC-III-B	663	271	FA-R	CA-R	HR-P1	7.25	NR-1	2.5	9/20/15	7	0.0
0.33	PC-I-A	658	-	FA-R	CA-R	HR-P1	12	NR-1	3	9/20/15	7	0.0

PP-B Plant Mix

PP-A Plant Mix

PP-B Lab Mix

PP-A Lab Mix

Results in Table 21 show that only the lab mixes showing signs of cracking are 10, 11 and 13 months old and have 0.28, 0.26 and 0.24 w/cm ratios, accordingly. Two out of the three blocks employ HR-P1 with a sizable dosage difference of 15 to 6.5 oz. Each block contains different cementitious makeup one with straight cement (PC-III-A) one with PC-III-A + 20% fly ash replacement and one with another source of straight cement (PC-III-B). Each of these mixes have very low crack rating (0.25 – 0.75). Seeing as other blocks that have similar cement content, HRWR dosage and types have not shown cracking it is too early to begin drawing conclusion about mixture components and the latent micro-cracking observed.

The mixtures cast at the precast plants (PP-A and PP-B) are both showing signs of micro-cracking. PP-B has two blocks sitting in the exposure site, hence the two unique crack ratings (1 and 1.25). Despite just a 2-3 month difference between precast plant field cast mixtures and lab cast mixtures there is zero signs of micro-cracking on the lab mixture blocks. More time is needed to monitor differences in lab and field cast exposure blocks. Blocks will continue to be monitored for cracking as it develops as a part of the ongoing research program.

6.3.4.2 EXPOSURE BLOCK EXPANSION/CONTRACTION RESULTS

Figure 110 displays a picture of the gages and demics points on an actual hardened exposure block specimen. Table 22 designates the mixture designs and date cast of the ten exposure blocks that have been cast with gage pins in the hopes of measuring the natural expansion and shrinkage of the concrete specimens and providing a quantifiable crack rating with said length change results.

Figure 110: Exposure Block with Expansion/Shrinkage Measurement Locations

Table 22: Pinned exposure block matrix at UT Austin exposure site

w/cm	Cement Type	Cement Content (lb/yd^3)	SCM Content (lb/yd^3)	Aggregate Source		Admixtures				Exposure Block	Crack Rating
				FA	CA	Type	(floz/100 lb cement)	Type	(floz/ 100 lb cement)		
0.26	PC-III-A	705	175	FA-R	CA-R	HR-P2	8.25	NR-1	3	6/9/15	0
		705	175	FA-R	CA-R	HR-P3	10	NR-2	2	6/1/15	0
	PC-III-B	705	175	FA-R	CA-R	HR-P1	8.25	NR-1	3	6/1/15	0
0.28	PC-I-A	705	-	FA-R	CA-R	HR-P1	12	NR-1	3	1/26/15	0
	PC-III-A	705	-	FA-R	CA-R	HR-P1	12		3	1/27/15	0
0.3	PC-III-A	564	188	FA-C	CA-C	HR-P3	8.25	NR-2	2	3/12/15	0
0.31	PC-III-A	663	271	FA-R	CA-R	HR-P1	7.25	NR-1	2.5	6/1/15	0
		663	271	FA-R	CA-R	HR-P4	7.25		2.5	3/5/15	0
		663	271	FA-R	CA-R	HR-P2	7.25	NR-2	2.5	6/1/15	0
0.33	PC-III-A	658	-	FA-R	CA-R	HR-P2	12	NR-1	3	6/5/15	0

Since no visible cracks have developed on any of the measureable exposure blocks we are not able to associate any of the expansion or shrinkage data taken thus far. As cracking develops in the future with the blocks measurements will be compared to draw comparisons with one another.

6.3.4.3 MINI GIRDER RESULTS

Table 23 outlines the mixture design and casting date of the 14 mini girders that have been cast. Relative to the same mixtures cast and plotted in Table 21 the mini girders show slightly more micro-cracking development. This may be attributed to the volume to surface area of effect or just the larger area to view and develop the cracking phenomenon. Figure 111 depicts mixture PP-B, which is the worst performing mixture with respect to cracking performance with a crack rating of 2.0.

Table 23: Mini Girder Matrix at UT Austin Exposure Site. Precast plant mixtures performed at the precast plants and the lab replicates performed in the lab have been illuminated.

w/cm	Cement Type	Cement Content (lb/yd^3)	SCM Content (lb/yd^3)	Aggregate Source		Admixtures				Exposure Block		
				FA	CA	Type	(floz/100 lb cement)	Type	(floz/ 100 lb cement)	Cast Date	Age (Months)	Crack Rating
0.24	PC-III-A	705	-	FA-R	CA-R	HR-P2	15	NR-1	3	2/24/15	13	0.5
0.26	PC-III-A	564	141	FA-R	CA-R	HR-P2	6.5	NR-1	3	6/9/15	10	0
0.28	PC-III-A	705	-	FA-R	CA-R	HR-P1	12	NR-1	3	10/1/14	16	0
		705	-	FA-R	CA-R	HR-P2			3	2/27/15	13	0
		705	-	FA-R	CA-L	HR-P1	12.5		3	1/26/15	14	0
		705	-	FA-R	CA-L	HR-P2	12		3	1/27/15	14	0
		705	-	FA-R	CA-R	HR-P3	12	NR-2	3	2/27/15	13	0
		705	-	FA-R	CA-L	HR-P3	12		3	3/20/15	12	0
		705	-	FA-R	CA-L	HR-P4	12		3	2/19/15	13	0
	PC-III-B	705	-	FA-R	CA-L	HR-P1	12	NR-1	3	5/26/15	11	0
0.3	PC-III-A	564	188	FA-RII	CA-RII	HR-P3	8	NR-2	2	3/12/15	13	2
		564	188	FA-RII	CA-RII	HR-P4	8		0.5	5/26/15	11	0.75
0.31	PC-III-A	663	271	FA-R	CA-R	HR-P4	5.5	NR-1	0.5	3/5/15	13	0.75
		663	271	FA-R	CA-R	HR-P2	5.5		2.5	6/9/15	10	0.25

PP-B Plant Mix

PP-A Plant Mix

PP-B Lab Mix

PP-A Lab Mix

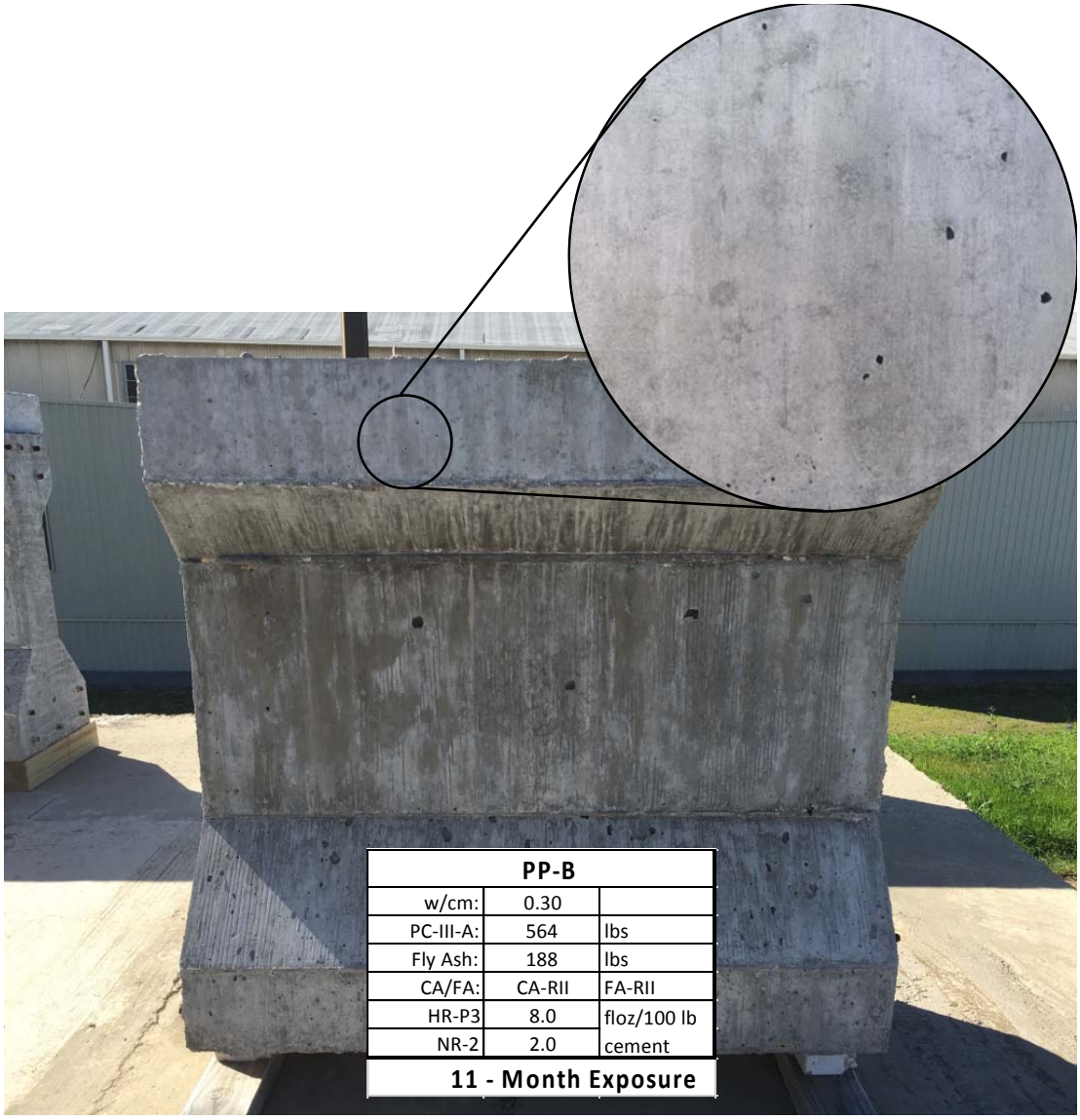

Figure 111: Precast Plant B (PP-B) Mini Girder with a crack rating of 2

6.4.4.4 CARBONATION SPECIMEN RESULTS

Table 24 provides the extent of the carbonation ingress, which was measured perpendicularly to the 4x4-in prism surfaceses. Recordings for sheltered (IN) and unsheltered (OUT) are independently presented.

Table 24: Carbonation Matrix at UT Austin Exposure Site with Carbonation Depth Per Time of Exposure and In (Sheltered), Out (Unsheltered)

w/cm	Mix ID	Cement Type	Cement Content (lb/yd^3)	SCM Content (lb/yd^3)	Aggregate Source		Admixtures				Time Since Cast (Months)	Carbonation Depth (mm	
					FA	CA	Type	(floz/100 lb cement)	Type	(floz/ 100 lb cement)		IN	OUT
0.24	G-8	PC-III-A	705	-	FA-R	CA-R	HR-P2	15	NR-1	3	12	0.65	0.35
0.26	PP-A Lab NC	PC-III-A	564	141	FA-R	CA-R	HR-P2	6.5	NR-1	3	8	0	0
0.28	G-2	PC-III-A	705	-	FA-R	CA-R	HR-P2	12	NR-1	3	12	0.10	0.05
	G-5		705	-	FA-R	CA-R	HR-P3	12	NR-2	3	12	0.10	0.075
	G-6		705	-	FA-R	CA-L	HR-P3	12		3	13	0.03	0
	G-7		705	-	FA-R	CA-L	HR-P4	12		3	12	0.10	0.075
	G-13	PC-III-B	705	-	FA-R	CA-L	HR-P1	12	NR-1	3	15	0	0
0.3	PP-B	PC-III-A	564	188	FA-RII	CA-RII	HR-P3	8	NR-2	2	13	0.08	0
	PP-B Lab		564	188	FA-RII	CA-RII	HR-P3	8		0.5	10	0.325	0
0.31	PP-A	PC-III-A	663	271	FA-R	CA-R	HR-P5	5.5	NR-1	0.5	12	0.1	0
	PP-A SCC		663	271	FA-R	CA-R	HR-P2	5.5		2.5	10	0.5	0

As expected, the extremely low w/cm ratio (and therefore low permeability) of the mixtures resulted in shallow carbonation depths for all samples. In order to address the concern that the cracking may be the resultant of carbonation induced shrinkage the concrete displaying the largest depth of carbonation ingress (G-8) was pulled to determine if the micro-cracking was visible on any of the surfaces. Figure 112 shows the depth of carbonation for (G-8) prisms exposed to "in" (inside Stevenson screens) and "out" natural outdoor exposure.

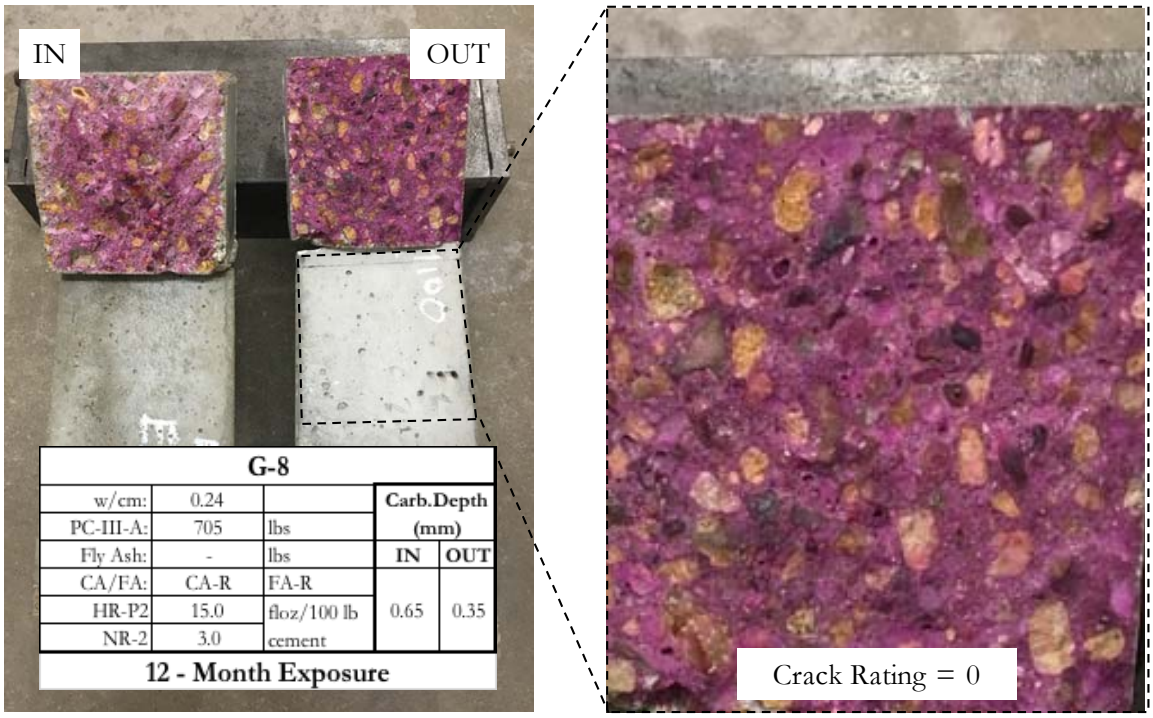

Figure 112: Carbonation depth for mixture G-8. (Left) Comparison of carbonation depth of specimens stored in sheltered conditions and unsheltered. "IN" specimens showed greater carbonation depth with zero visible surface cracking. (Right) Close-up of surface for the unsheltered specimen. No cracks visible on surface (crack rating =0).

The carbonation specimens were used as visual tools in order to learn more about the micro-cracking mechanism. Figure 112 suggests that carbonation depth and surface cracking are independent of one another. In all cases, even if a specimen showed development of the surface micro-cracking for the outdoor specimen, no visible cracks

proved to develop on the indoor specimens. The following Figures 113-117 were selected based on either visible cracking, the fact that they were cast at precast plants, and/or cast as replicates of precast plant mixtures.

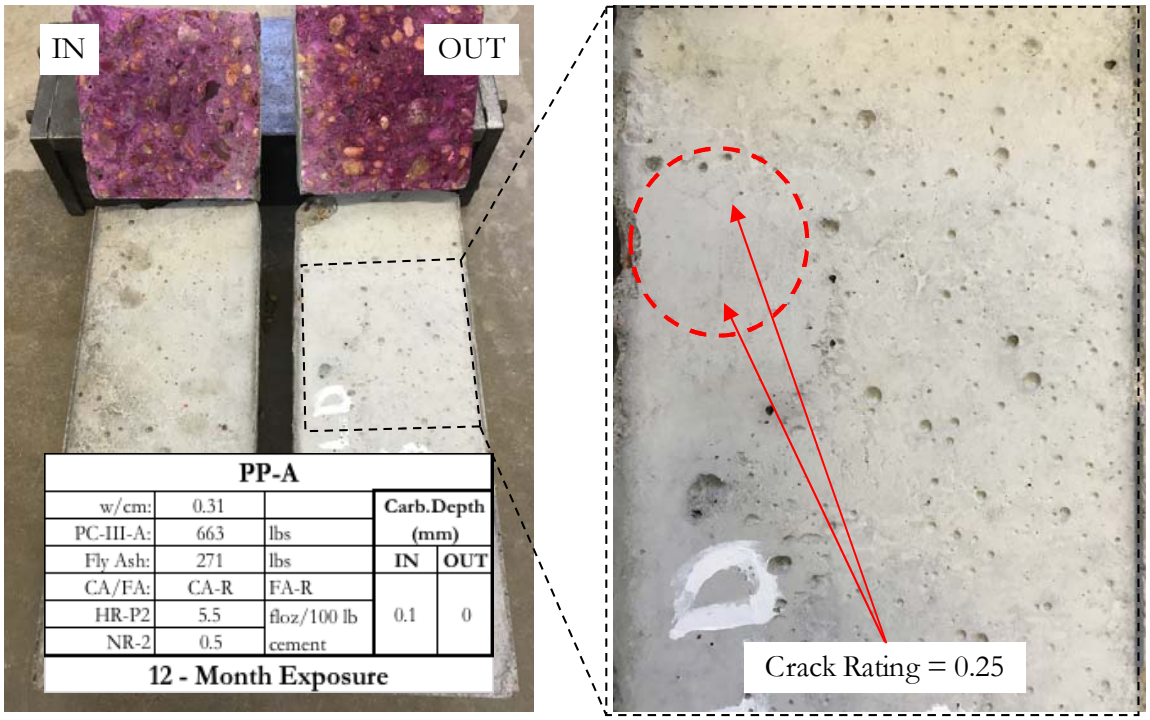

Figure 113: Carbonation depth for mixture PP-A. Showing very minimal cracking = 0.25

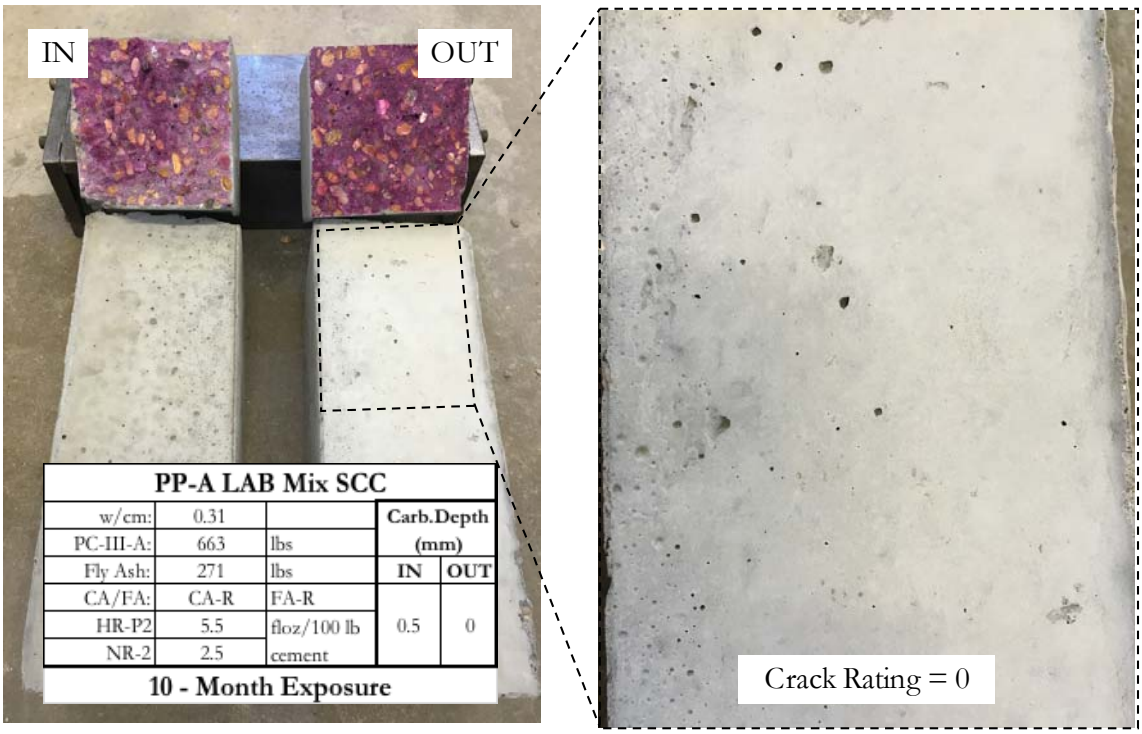

Figure 114: Carbonation depth for mixture PP-A Lab Mixture SCC. Showing no cracking = 0.0

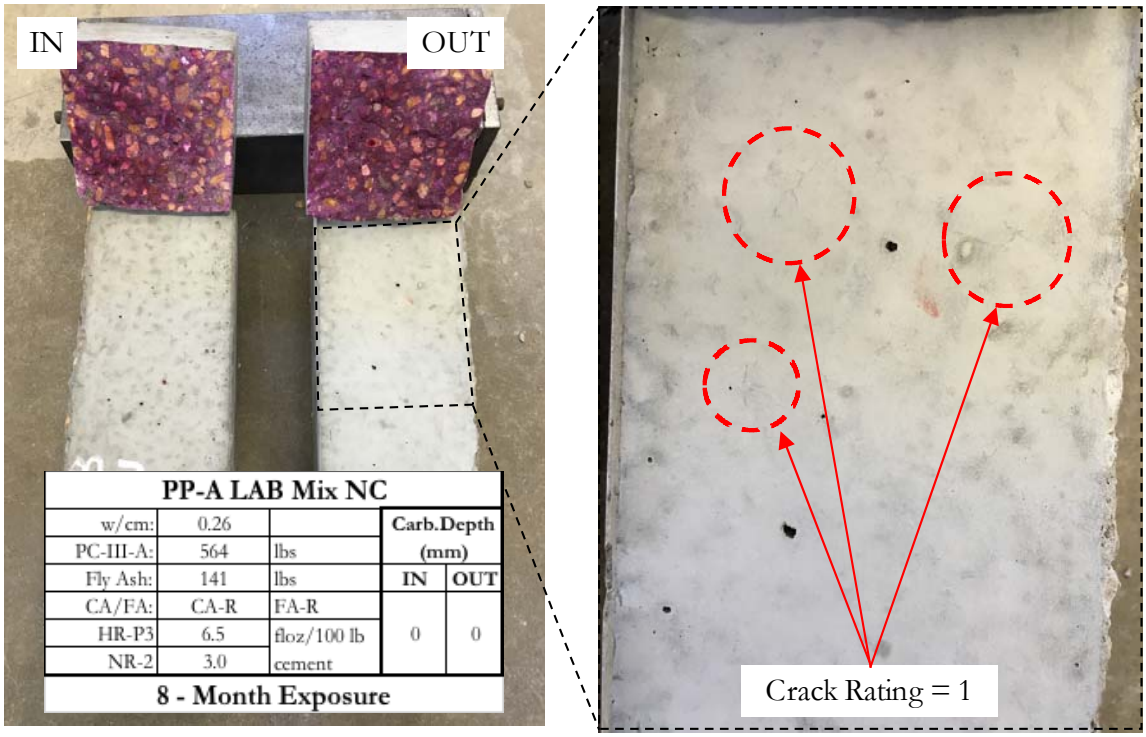

Figure 115: Carbonation depth for mixture PP-A Lab Mixture NC. Showing very minimal cracking = 1.0

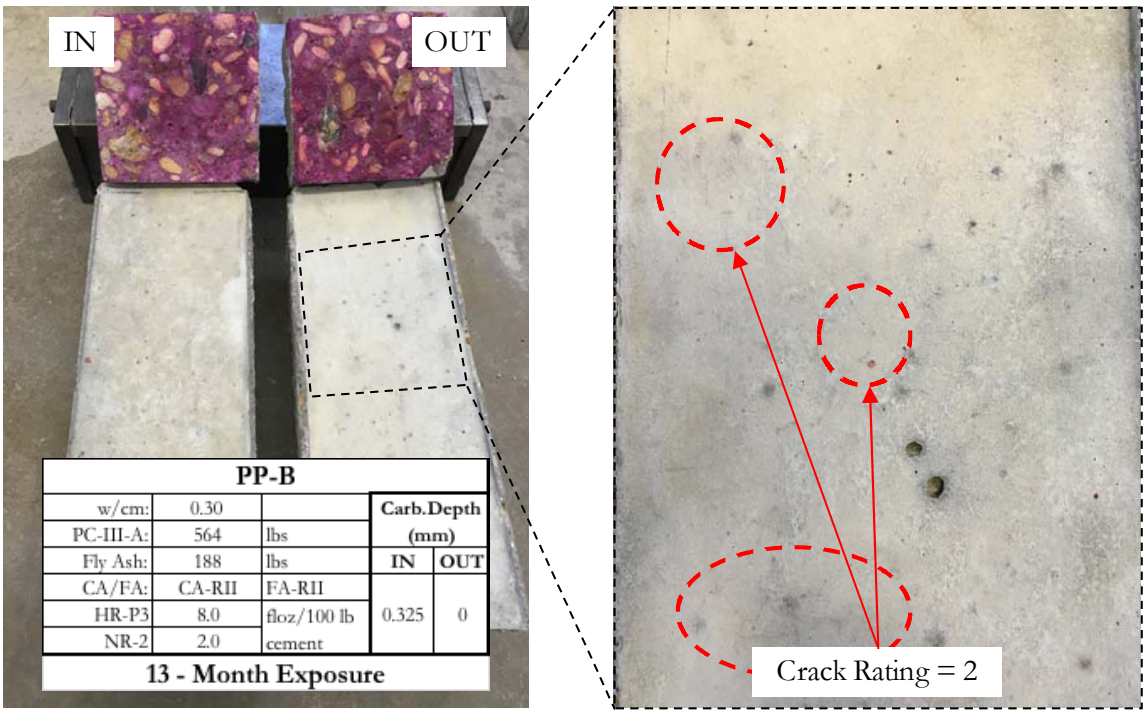

Figure 116: Carbonation depth for mixture PP-B. Showing very minimal cracking = 2.0

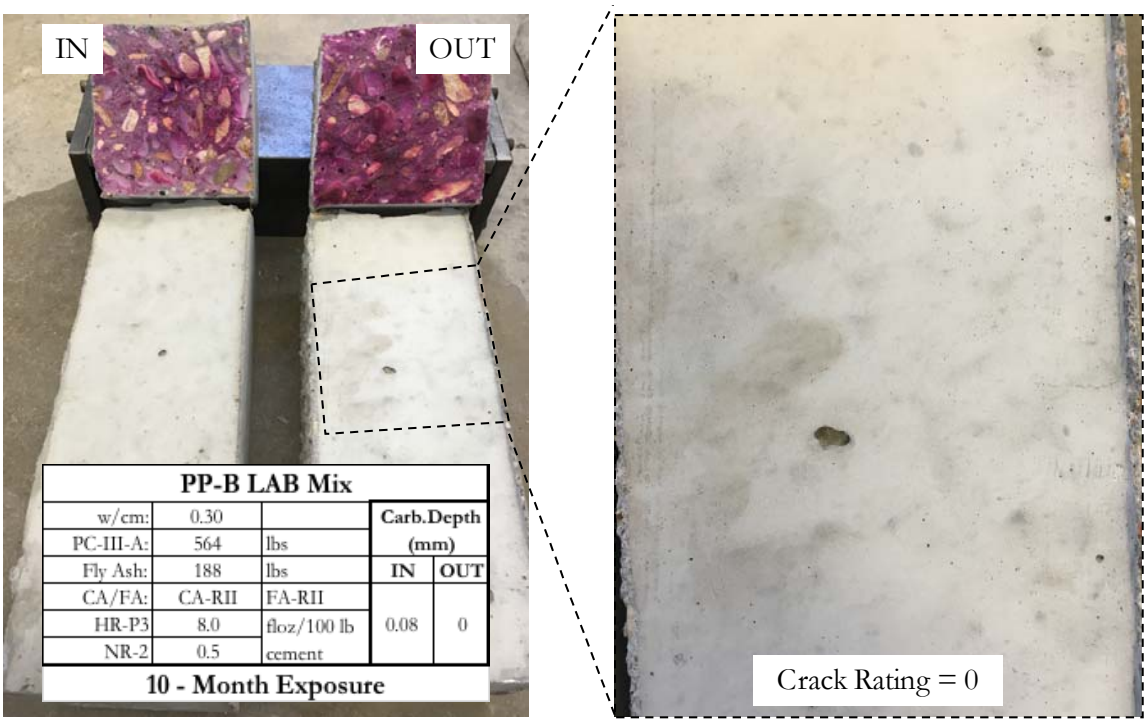

Figure 117: Carbonation depth for mixture PP-B Lab Mixture. Showing no cracking = 0.0

Based on the results of the carbonation depth ingress and the micro-cracking observed on the carbonation specimens, we believe that carbonation is not a primary mechanism with respect to micro-cracking. The carbonation prisms also reveal that the wetting and drying cycles that the outdoor carbonation specimens experienced clearly exacerbates and provokes the micro-cracking development on the surface of the concrete.

CHAPTER 7: CONCLUSION

This thesis has produced a sizable experimental matrix towards the evaluation of the suitability of using ASTM C494 to indicate a mixture propensity to micro-cracks of the nature that is seen in precast concrete girders throughout the state of Texas. In addition, a parametric analysis aimed at determining key factors and mechanisms driving the micro-cracking development seen on precast elements was conducted. ASTM C494 was evaluated by determining the pass and fail rate of select ASTM C494 parameters (water content, time of set, compressive strength and drying shrinkage) of both "good" and "bad" performance mixture designs with respect to micro-cracking observed in the field. Because a true ASTM C494 control mixture is not attainable without the use of HRWR for the precast concrete mixtures designs evaluated in this work, several control mixtures were created. The control mixtures were created to the effect of water to binder content, HRWR dosage and lightweight aggregate on the micro-cracking behavior and the aforementioned ASTM C494 testing parameters.

In addition to the evaluation of ASTM C494 for qualifying HRWR admixtures to eliminate the micro-cracking issue seen in precast applications, an exposure site was developed to monitor the natural development of micro-cracking. Mixtures were selected based on current high performance mixture designs employed at precast plants throughout the state of Texas. Natural exposure was investigated on visual exposure blocks as well as measurable exposure blocks, mini girders and carbonation specimens.

An additional testing matrix was developed with the goal of evaluating precast plant mixtures shrinkage behaviors with the hope of determining whether there was a particular shrinkage mechanism driving micro-crack formation. The testing performed in the parametric study employed autogenous shrinkage measurements on paste mixtures and concrete mixture evaluation through restrained shrinkage ring test to determine both autogenous and drying shrinkage effects. Autogenous paste testing included volumetric

(buoyancy) method, corrugated tube and mini ring test. The autogenous shrinkage evaluation through use of the corrugated tube method is currently being performed to determine the most accurate and repeatable sample preparation procedure for this test.

Based on the results of the work performed throughout this project the following conclusions may be extracted according to their respective subsections:

1) Evaluation of ASTM C494 with HRWR for predicting latent micro cracking effects:

- The testing that was performed towards fulfillment of ASTM C494 testing procedures with respect to HRWR agents (Type F) does not provide a proper means of creating a base mixture to compare the admixture agent against. Yet even with the creation of a supplement control mixture a correlation between poor performance in the field and failing in ASTM C494 testing was not apparent.

2) Parametric Study Results:

- The parametric study for concrete has revealed that different HRWR product types adversely effects the date of cracking of the concrete restrained shrinkage rings. Mechanical testing of concrete cylinders exposed to same environmental conditions as the rings proves to show a strong correlation between crack date of rings and splitting and modulus testing results. More data is required to settle on steadfast numbers, however future work may be able to determine a mixtures cracking propensity based on mechanical property developments of the mixture. The ring testing is still in the early stages and has only completed a matrix of 8 mixtures. Therefore, it is suggested that additional mixtures be cast that are known poor performers in the field as well as offer different uses of materials, HRWR's and dosages.

- Cement paste analysis with respect to autogenous shrinkage showed that increasing the HRWR dosage retards the final set of the mixture. The delay in set time causes delayed reabsorption of bleed water. The swelling incurred by the paste during reabsorption decrease the ultimate autogenous shrinkage of the paste compared to a paste mixture with a lower HRWR dosage. Correlating this paste study back to field performance, the use of higher admixtures dosages used in the field may be a factor in delaying or minimizing micro-cracking associated with autogenous shrinkage

3) Natural Exposure Results:

- Although the time of year (season) when concrete is cast shows to have negligible effect with respect to increasing or decreasing cracking performance, surface exposure to the natural elements proves to be the key to exacerbating the surface micro-cracking observed.
- Specimens with measurable pin and demic locations at different depths has the potential to provide better indication of the permissible depth of the micro-cracking as well as create a better quantifiable interpretation of the cracking. More time is needed to correlate the micro-cracking to shrinkage/expansion results collected thus far.
- Carbonation shrinkage does not seem to be a driving factor inducing the micro-cracks.

4) Future Work:

- Because the mechanism causing the micro-cracking is a function of volume change, additional measurements in the long term of the drying shrinkage specimens is suggested. Long term evaluation with respect to control proves to

fail additional mixtures that would otherwise pass in the 14-day measurement timeline prescribed in ASTM C494

- Volumetric change of specimens exposed to outdoor weather conditions in Texas appears to be the best current-day approach to capturing the latent micro-cracking as a function of volume change. More work should be performed in the area of measuring outdoor specimen's volume change with respect to time and weather monitoring.
- Further investigation of paste to formwork interaction is suggested. Variables such as temperature and humidity during casting. Bleeding effects associated with mixture design, that may be influencing the micro-cracking at paste to formwork surface.
- Developing an additional exposure site that subjects concrete specimens of like volume to surface area as the girders to daily wetting and drying cycling as a means of potentially expediting the micro-cracking.

APPENDICES

Appendix I: Materials Identification

Table 25: Cement nomenclature, distributor and Oxide Analysis

Cement	Distributor	SiO2	Al2O3	Fe2O3	CaO	MgO	SO3	Na2O	K2O
		mass %	mass %	mass %	mass %	mass %	mass %	mass %	mass %
PC-III-A	Alamo III	19.8	4.3	3.1	64.2	0.6	4.1	0.1	0.7
PC-III-B	Capitol III	19.8	5.1	1.9	63.5	1.1	5	0.1	0.6
PC-I-A	Alamo I	18.6	5.4	2.6	64.9	1.1	3.3	0.1	1

Table 26: Fly Ash nomenclature, distributor and Oxide Analysis

Fly Ash	Distributor	SiO2	Al2O3	Fe2O3	CaO	MgO	SO3	Na2O	K2O
		mass %	mass %	mass %	mass %	mass %	mass %	mass %	mass %
Class F	Rockdale	52.07	23.07	3.95	11.65	2.06	0.48	0.403	0.74

Table 27: Coarse Aggregate nomenclature, source and properties

Coarse Aggregate	Source	Mineralogy Type	Specific Gravity	Absorption Capacity
CA-R	Eagle Lake	Siliceous	2.54	1.31
CA-L	Marble Falls	Limestone	2.47	3.25
CA-RII	Trinity	Siliceous	2.26	1.52

Table 28: Fine Aggregate nomenclature, source and properties

Fine Aggregate	Source	Mineralogy Type	Specific Gravity	Absorption Capacity
FA-R	Eagle Lake	Siliceous	2.47	1.14
FA-RII	Trinity	Siliceous	2.57	1.96
FA-LW	Manufactured	Manufactured	1.86	22.50

Table 29: Admixture nomenclature, source, classification and properties

Admixture Name	Product Name	C-Polymer Type	ASTM C494 Classification	Specific gravity
HR-P1	Sika 2100	Polycarboxylate	F	1.1
HR-P2	Sika 4100	Polycarboxylate	F	1.1
HR-P3	BASF 7700	Polycarboxylate	F	1.1
HR-P4	BASF Z60	Polycarboxylate	F	1.1
HR-P5	Sika 2110	Polycarboxylate	F	1.1
NR-1	Plastiment	Normal Range Water Reducer and	B & D	1.2
NR-2	Glenium	Normal Range Water Reducer and	B & D	1.2
VMA-1	Sika 4R	Viscocity Modifier	S	1.1

Appendix II: Mixture Identification According to Task

Table 30: Task 3 Mixture ID's and Mixture Designs

/cm	Cement Type	Cement Content (lb/yd^3)	Admixtures				Other Mixture Parameters
			Type	(floz/100 lb cement)	Type	(floz/ 100 lb cement)	
.26	PC-III-A	700	HR-P1	6.5	NR-1	1.5	-
				8.25		1.5	-
.28	PC-III-A		HR-P1	12	NR-1	3	-
.31	PC-III-A	663	HR-P1	5.5	NR-1	2.5	-
		640		6		2	-
.33	PC-III-A	658	HR-P1	6.5	NR-1	3	-
				5.5		2	-
				5		2.5	### FA-LW
0.4	PC-III-A		HR-P1	2	NR-1	2	-
				2		2	Fly Ash 25% add.

Table 31: Task 4 Mixture ID's and Mixture Designs

Mixture ID		Alteration of Task 3 Mix	w/cm	Cement Type	Admixtures				Other Mixture Parameters
					Type	(floz/100 lb cement)	Type	(floz/ 100 lb cement)	
1.5	M1-NC	Fly Ash Content	0.26	PC-III-A	HR-P1	6.5	NR-1	3	Fly Ash 33% add.
1.2		Cement Content				25.75		3	517 lb/yd^3 PC-III-A & Fly Ash 25% add.
1.1		HRWR Dosage				5.25	NR-1	3	Fly Ash 25% add.
1.6		HRWR Type			HR-P2	8.25	NR-1	3	
1.7					HR-P3	10		3	
1.8		Cement Type		PC-III-B	HR-P1	8.25	NR-1	3	
1.3		w/binder	0.38	PC-III-A	-	-	-	-	
1.4		w/binder	0.45		-	-	-	-	
2.4	M3-NC	Fly Ash Content	0.26	PC-III-A	HR-P1	6.5	NR-1	3	Fly Ash 33% add.
2.2		Cement Content	0.33			30.5		3	517 lb/yd^3 PC-III-A
2.1		HRWR Dosage				11.88		3	-
2.3		w/binder	0.52			-	-	-	-
2.4		w/binder	0.56			-	-	-	-
3.1	M4-SCC	w/binder	0.26	PC-III-A	HR-P1	7	NR-1	2.5	Fly Ash 40% add.
3.3		Fly Ash Content	0.31			5.5		2.5	Fly Ash 25% add.
3.4		HRWR Type			HR-P2	5.5		2.5	
3.5					HR-P3	7.25		2.5	
3.6		Cement Type		PC-III-B	HR-P1	6		2.5	
3.2		w/binder	0.33	PC-III-A		5		2.5	

Table 32: Task 5 Mixture ID's and Mixture Designs

Mixture ID	w/cm	Cement Type	Admixtures				Other Mixture Parameters
			Type	(floz/100 lb cement)	Type	(floz/ 100 lb cement)	
G-8	0.24	PC-III-A	HR-P2	15	NR-1	3	-
G-10	0.26	PC-III-A	HR-P2	6.5	NR-1	3	SCC - Fly Ash 20% add.
M1-NC-14			HR-P2	8.25	NR-1		Fly Ash 25% add.
M1-NC-15			HR-P3	10	NR-2	2	
M1-NC-16		PC-III-B	HR-P1	8.25	NR-1	3	Fly Ash 38% add.
G-1	0.28	PC-III-A	HR-P1	12	NR-1	3	-
G-2			HR-P2				-
G-3			HR-P1	12.5			CA-L
G-4			HR-P2	12			
G-5			HR-P3		NR-2		-
G-6			HR-P3				CA-L
G-7			HR-P4				
G-13		PC-III-B	HR-P1		NR-1		
M2-NC-1		PC-III-A					-
T5-3		PC-I-A					-
T5-4	0.3	PC-III-A	HR-P3	8	NR-2	2	564 lb/yd^3 PC-III-A & Fly Ash 33% add.
G-2-Plant			HR-P3	8	NR-2	2	CA-R-II & Fly ash 25% add.
G-11-Lab						0.5	
G-1-Plant	0.31	PC-III-A	HR-P4	5.5	NR-1	0.5	Fly Ash 29% add.
G-9-Lab			HR-P2			2.5	
M4-SCC-17			HR-P2	5.5	NR-1	2.5	663 lb/yd^3 PC-III-A & Fly Ash 40%
M4-SCC-18			HR-P3	7.25	NR-2		
M4-SCC-19		PC-III-B	HR-P1	6	NR-1		663 lb/yd^3 PC-III-B & Fly Ash 40% add.
M3-NC-6	0.33	PC-III-A	HR-P1	12	NR-1	3	658 lb.yd^3 PC-III-A

Appendix III: Compressive Strength Data

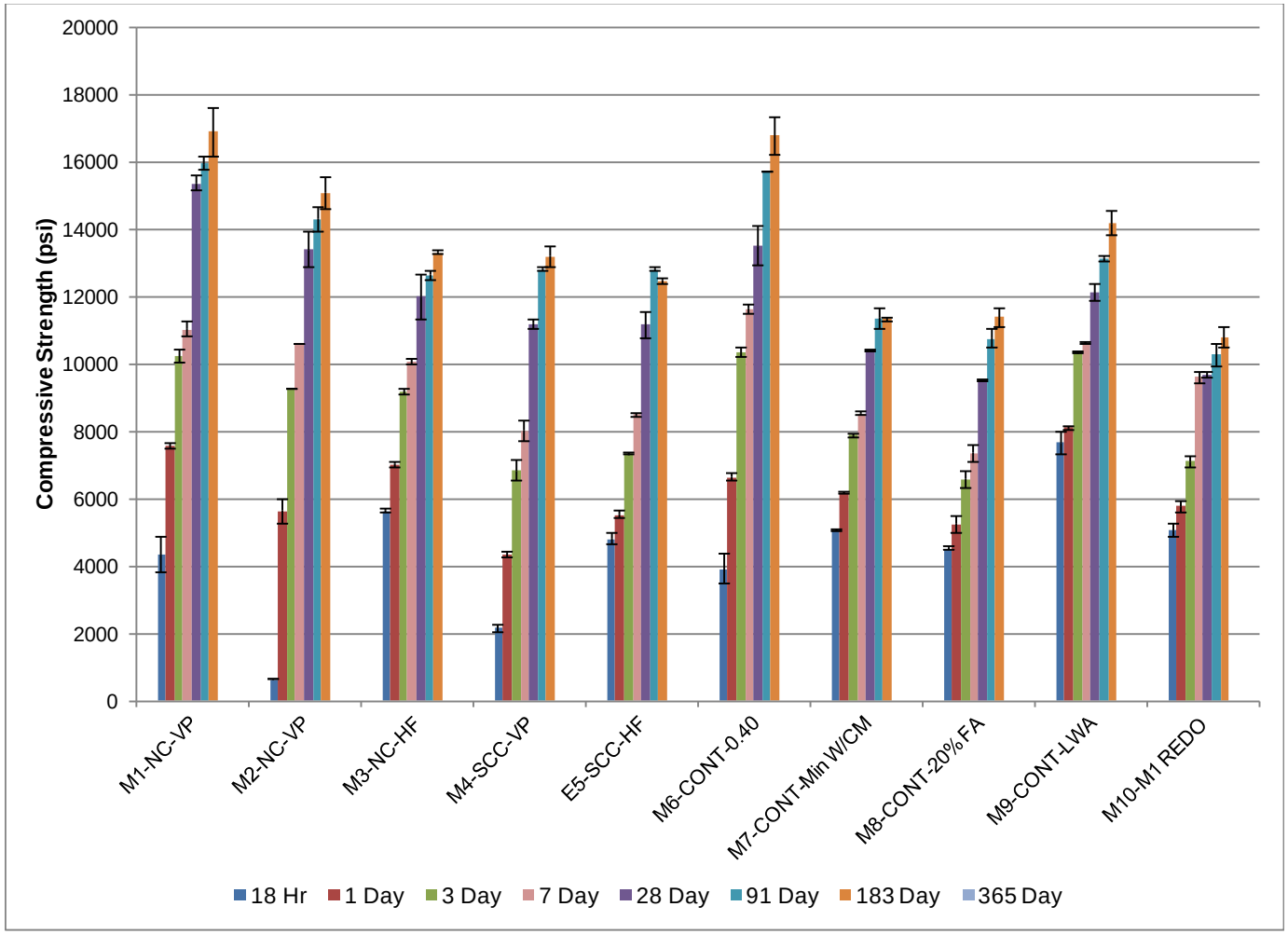

Figure 118: Compressive Strength Results Task 3

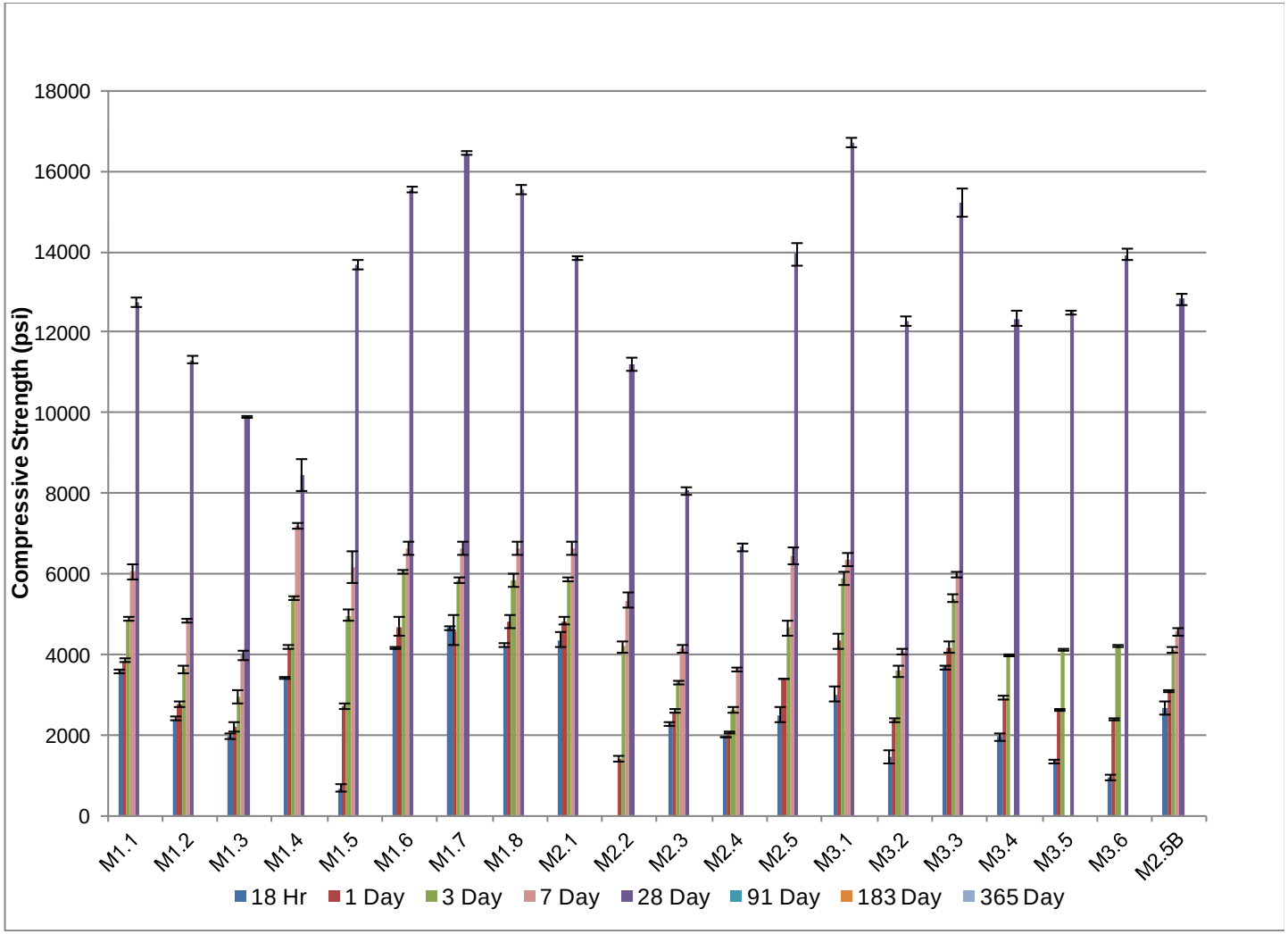

Figure 119: Compressive Strength Results Task 4

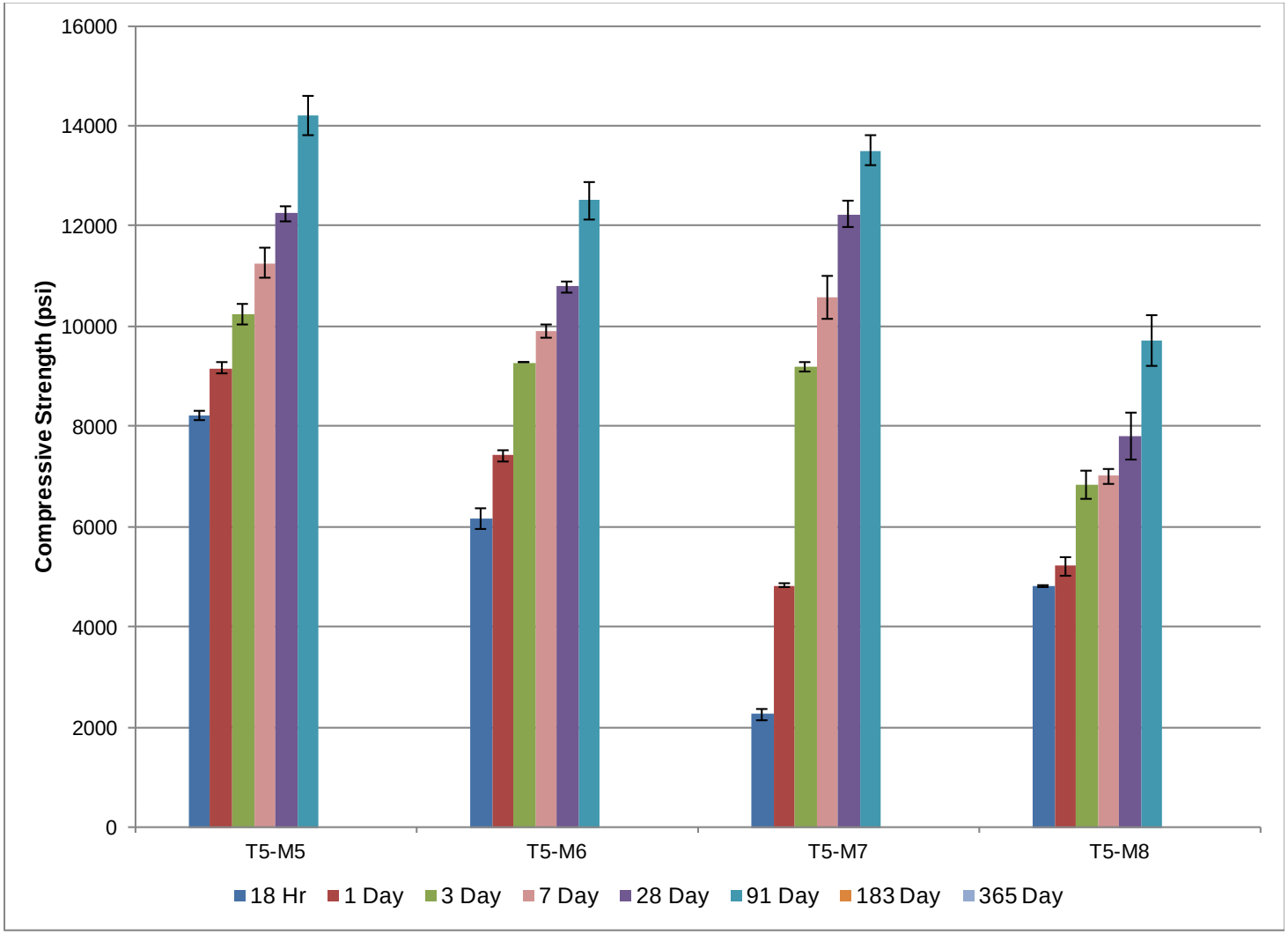

Figure 120: Compressive Strength Results Task 5

Appendix IV: Additional Cited Sources

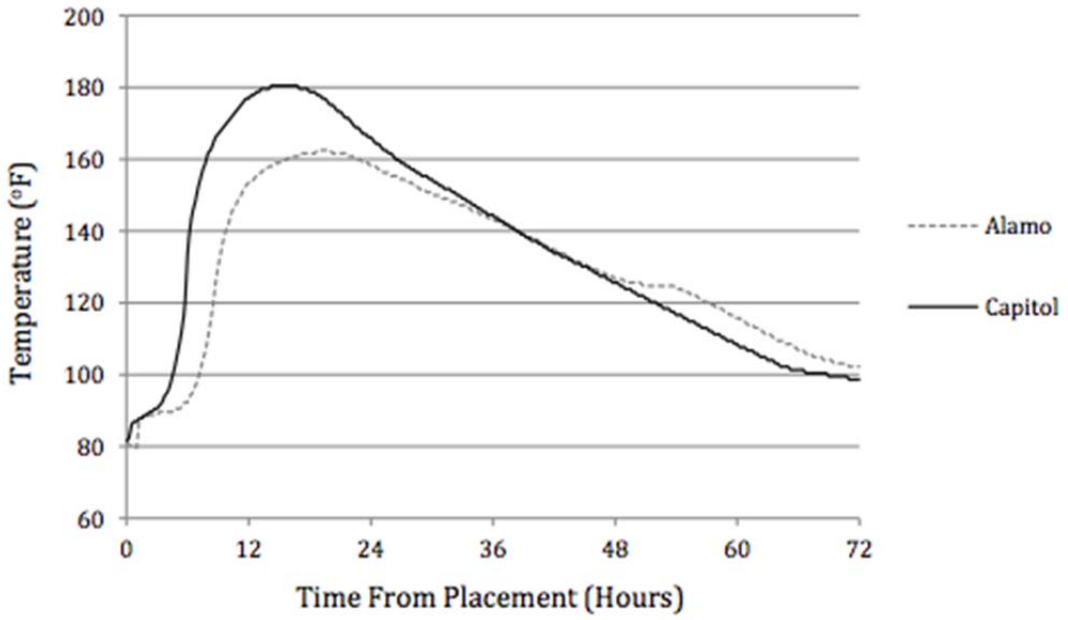

Figure 121: Time vs Temperature curve for precast concrete elements containing Alamo III and Capitol III cement taken from Implementation of Concrete Works Software in Texas Highway Construction (Meeks 2012).

Appendix V: Drying Shrinkage Curves

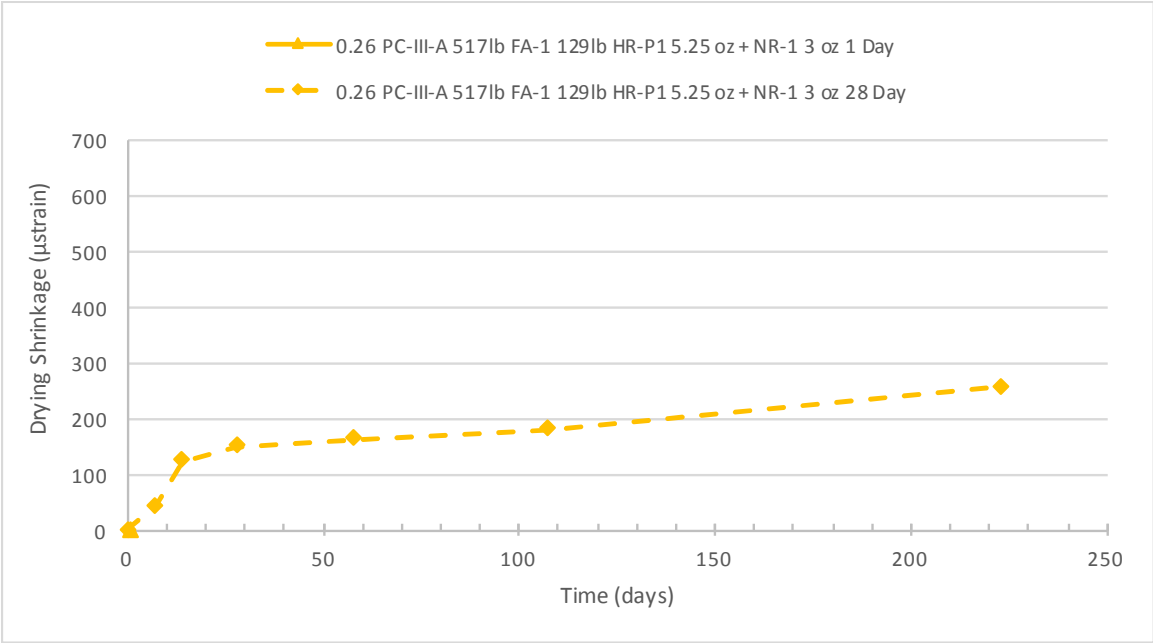

Figure 122: Drying Shrinkage 0.26 PC-III-A 517lb + FA-1 129lb HR-P1 5.25 oz + NR-1 3 oz

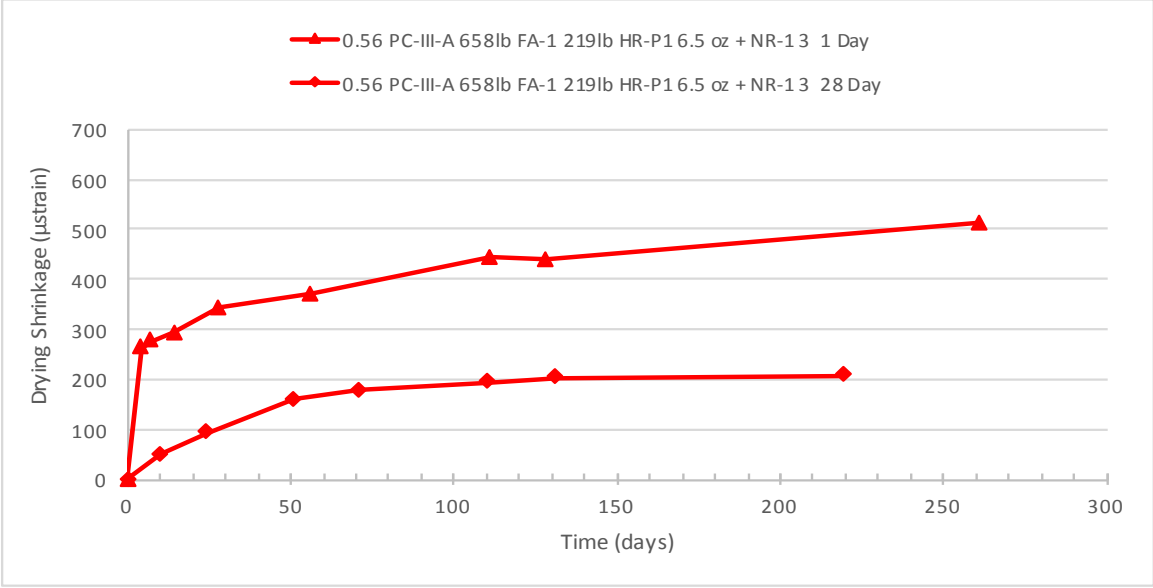

Figure 123: Drying Shrinkage 0.56 PC-III-A 658lb FA-1 219lb HR-P1 6.5 oz + NR-1 3 oz TRIAL A

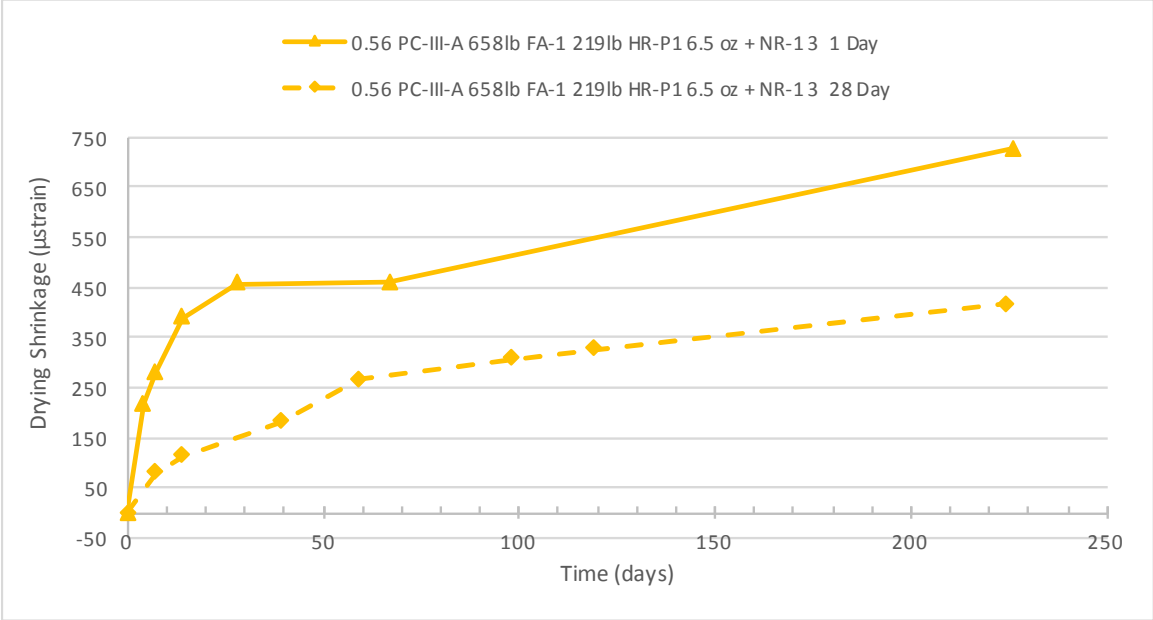

Figure 124: Drying Shrinkage 0.56 PC-III-A 658lb FA-1 219lb HR-P1 6.5 oz + NR-1 3 oz TRIAL B

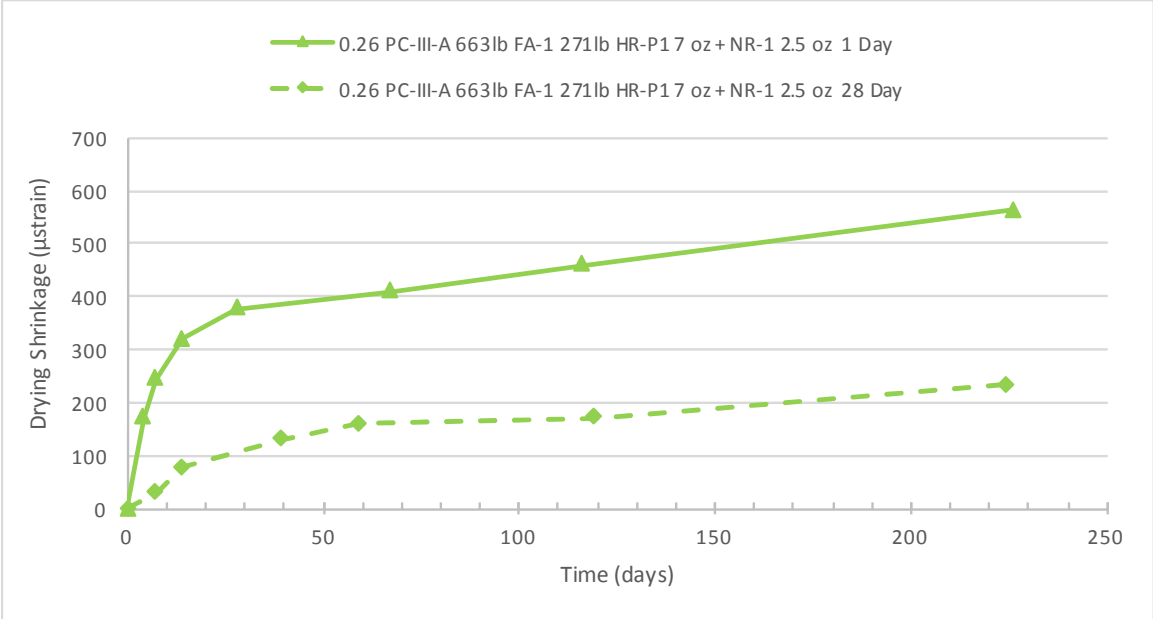

Figure 125: Drying Shrinkage 0.26 PC-III-A 663lb FA-1 271lb HR-P1 7 oz + NR-1 2.5 oz

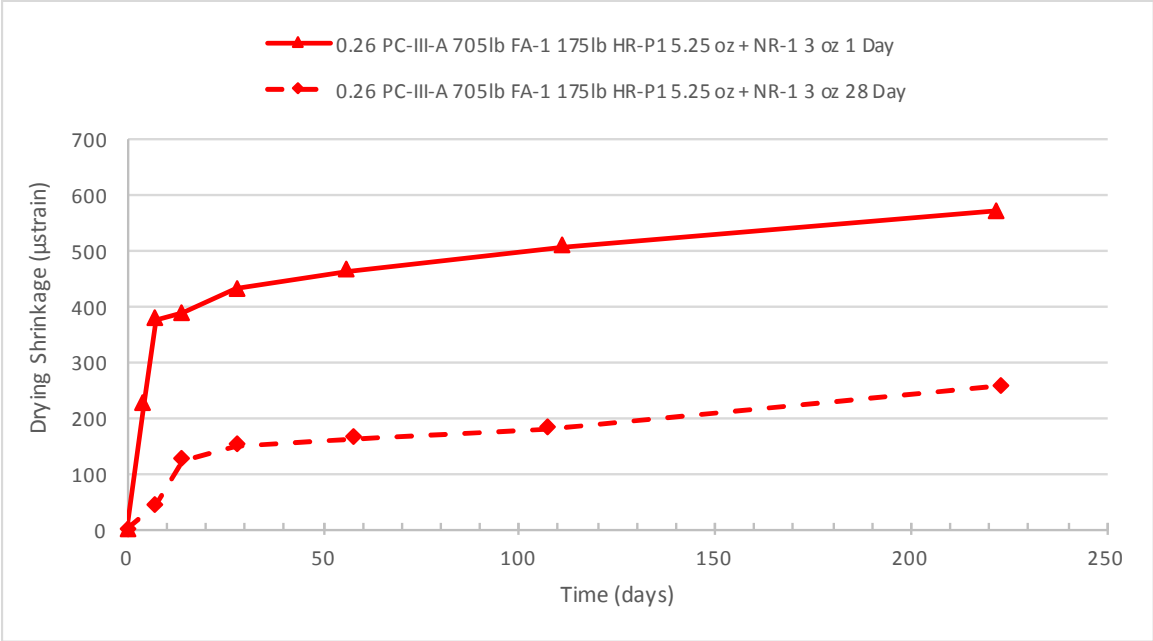

Figure 126: Drying Shrinkage 0.26 PC-III-A 705lb FA-1 175lb HR-P1 5.25 oz + NR-1 3 oz

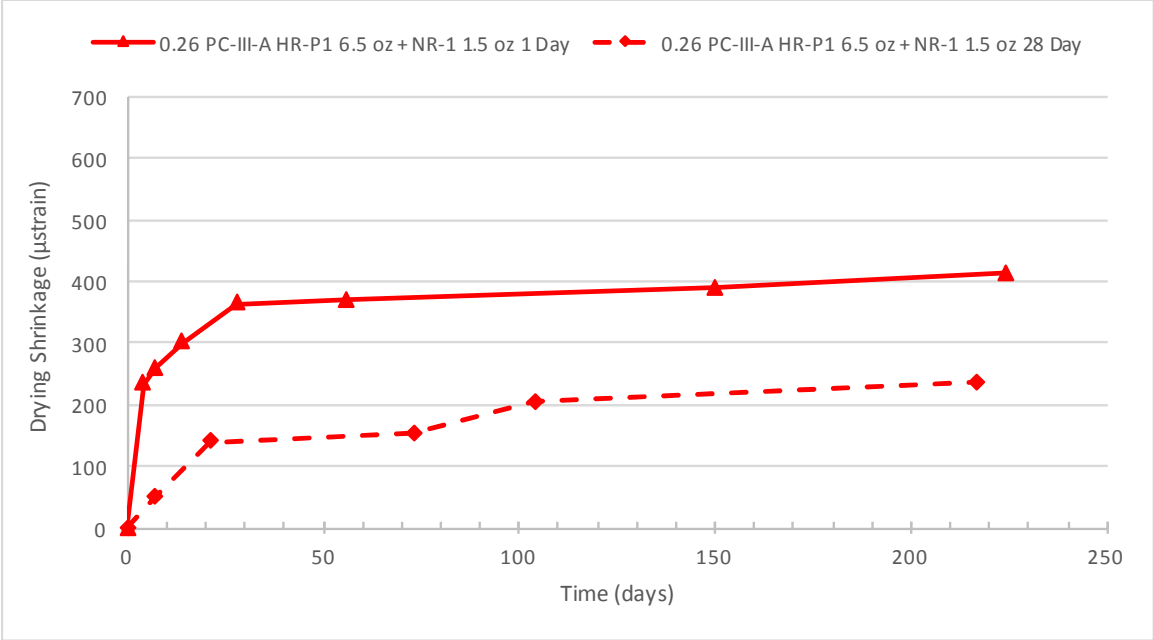

Figure 127: Drying Shrinkage 0.26 PC-III-A 705lb FA-1 175lb HR-P1 6.5 oz + NR-1 1.5 oz

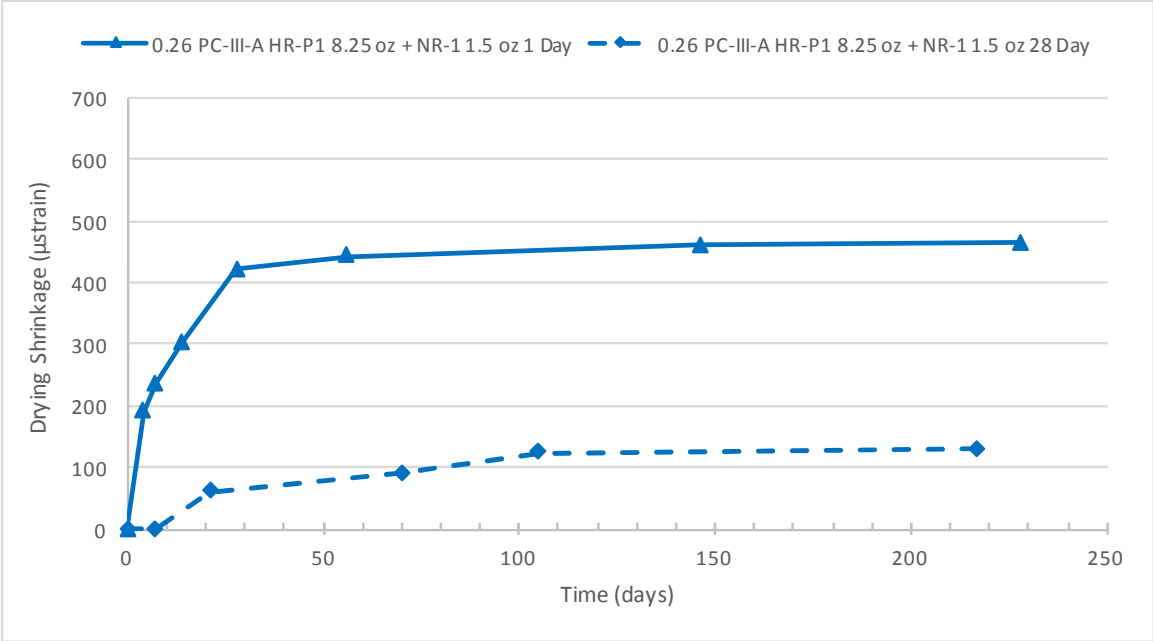

Figure 128: Drying Shrinkage 0.26 PC-III-A 705lb FA-1 175lb HR-P1 8.25 oz + NR-1 1.5 oz

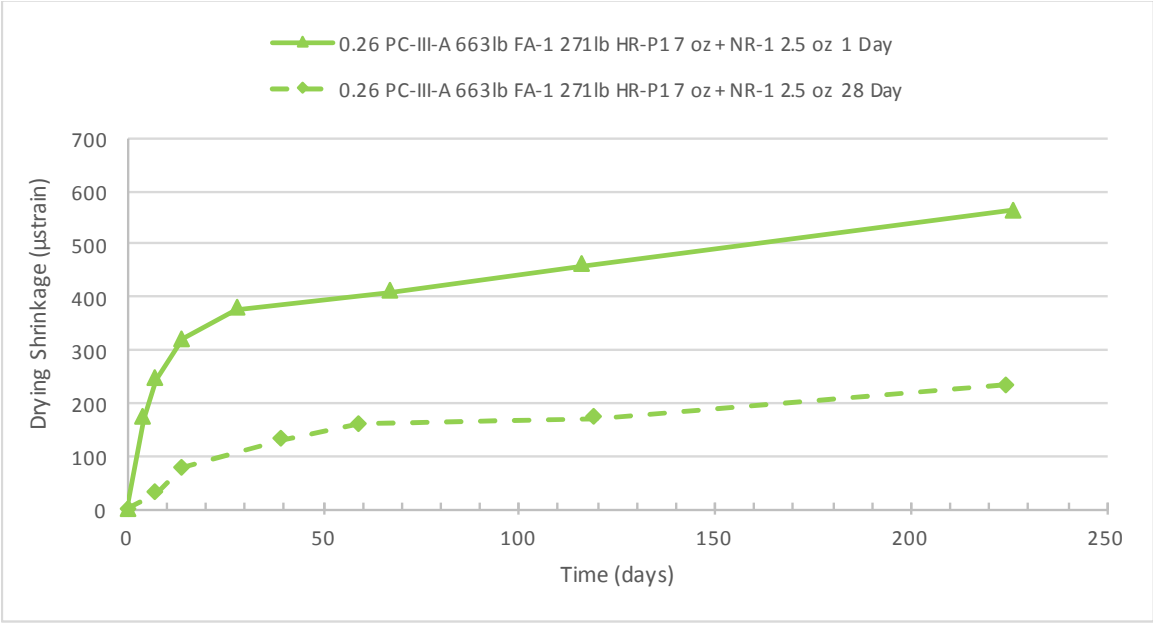

Figure 129: Drying Shrinkage 0.26 PC-III-A 663lb FA-1 271lb HR-P1 7 oz + NR-1 2.5 oz

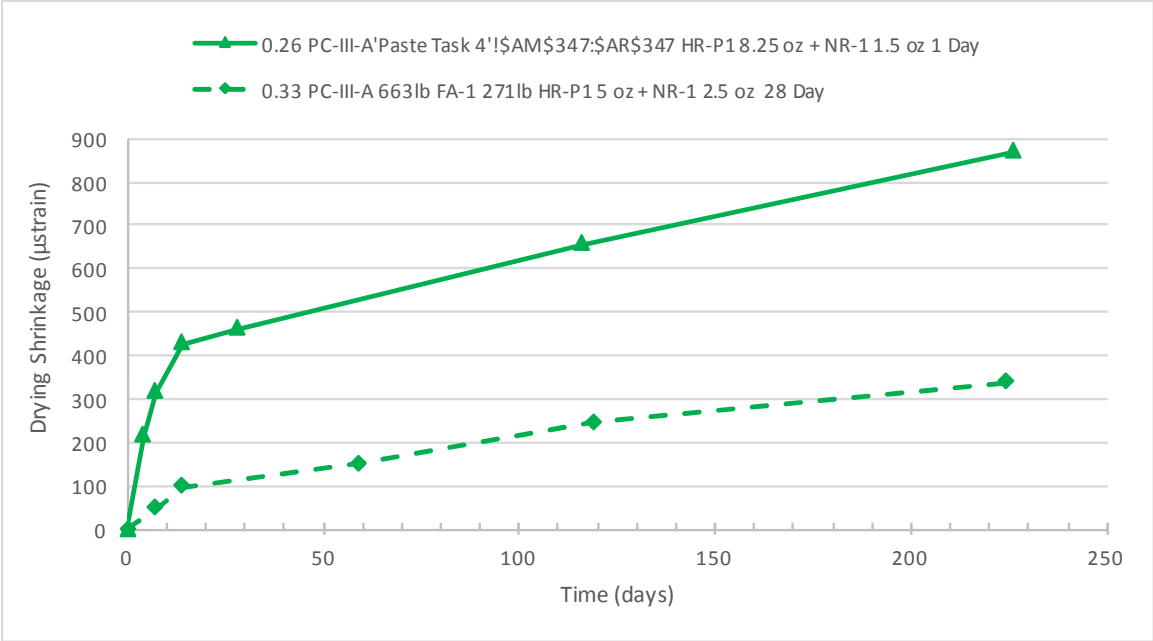

Figure 130: Drying Shrinkage 0.33 PC-III-A 663lb FA-1 271lb HR-P1 5 oz + NR-1 2.5 oz

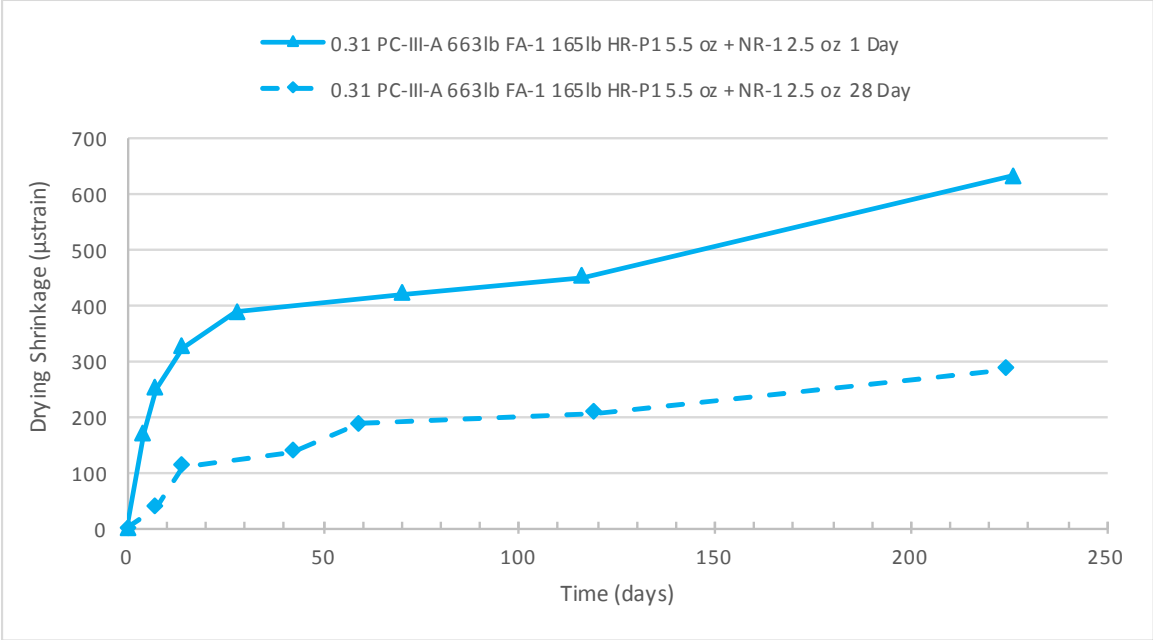

Figure 131: Drying Shrinkage 0.31 PC-III-A 663lb FA-1 165lb HR-P1 5.5 oz + NR-1 2.5 oz

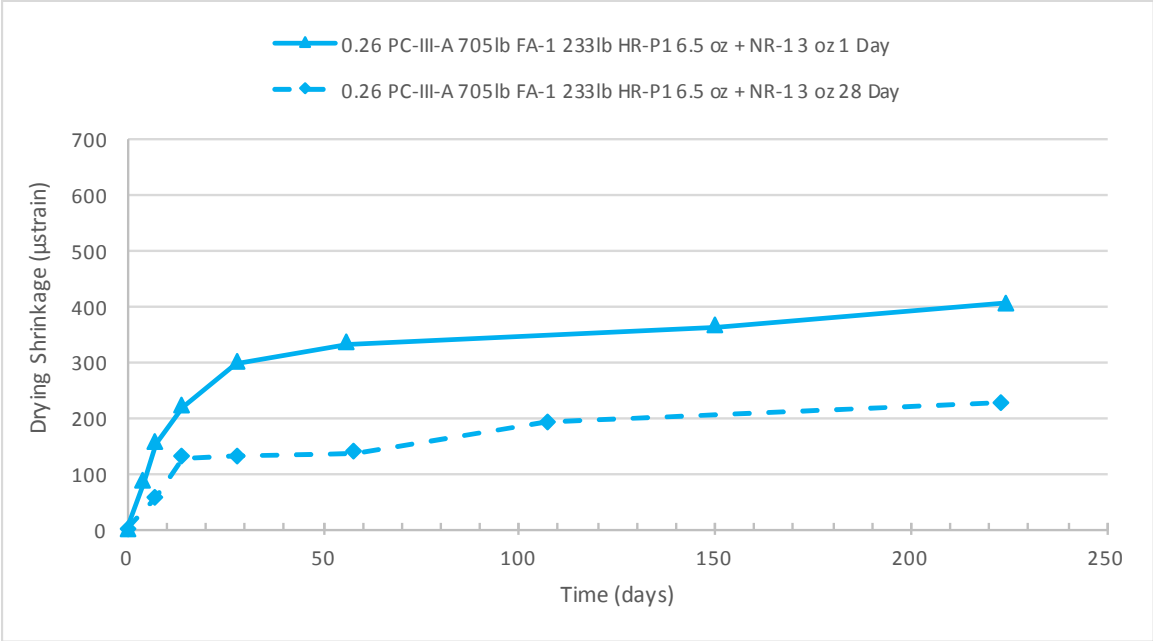

Figure 132: Drying Shrinkage 0.26 PC-III-A 705lb FA-1 233lb HR-P1 6.5 oz + NR-1 3 oz

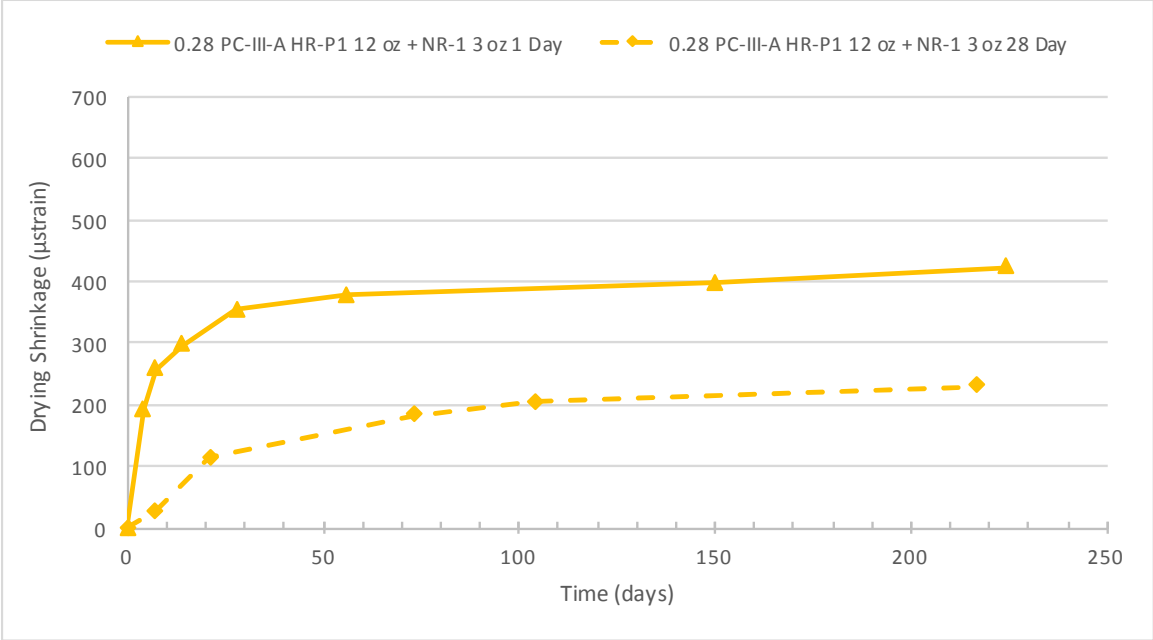

Figure 133: Drying Shrinkage 0.28 PC-III-A 705lb FA-1 175lb HR-P1 12 oz + NR-1 3 oz

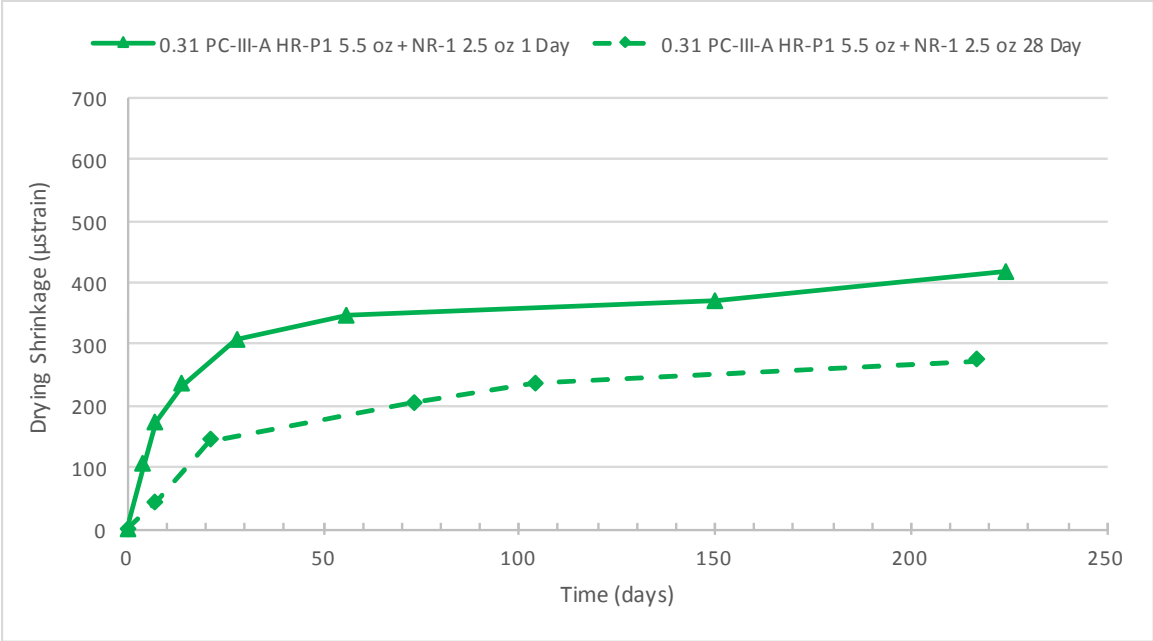

Figure 134: Drying Shrinkage 0.31 PC-III-A 663lb FA-1 271lb HR-P1 5.5 oz + NR-1 2.5 oz

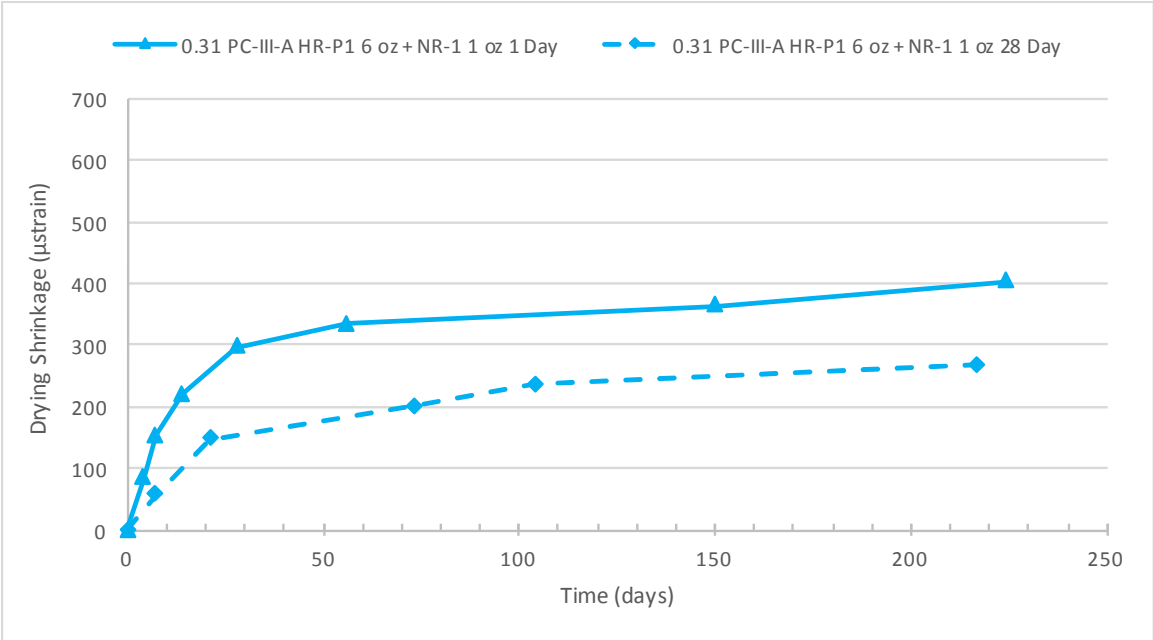

Figure 135: Drying Shrinkage 0.31 PC-III-A 640lb FA-1 213lb HR-P1 6 oz + NR-1 2 oz

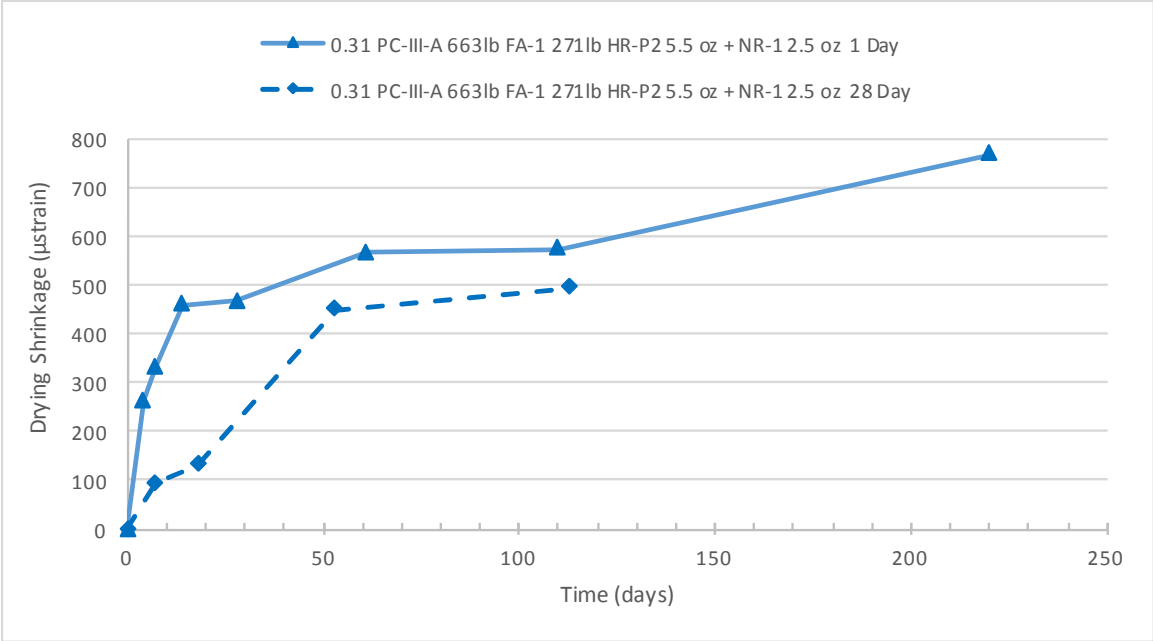

Figure 136: Drying Shrinkage 0.31 PC-III-A 663lb FA-1 271lb HR-P2 5.5 oz + NR-1 2.5 oz

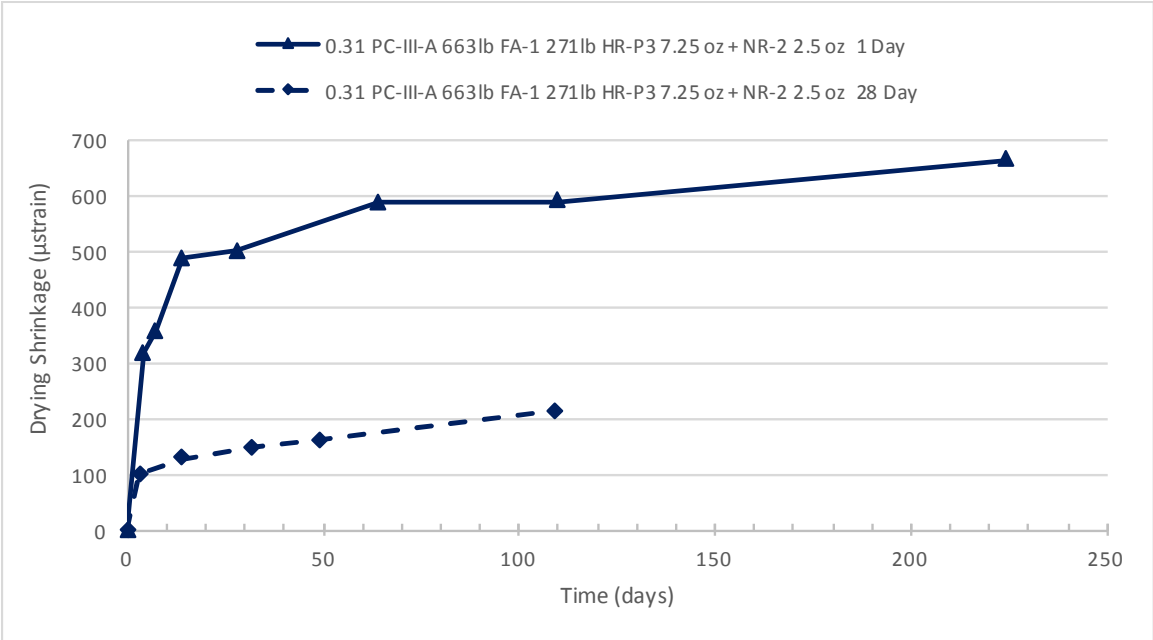

Figure 137: Drying Shrinkage 0.31 PC-III-A 663lb FA-1 271lb HR-P3 7.25 oz + NR-2 2.5 oz

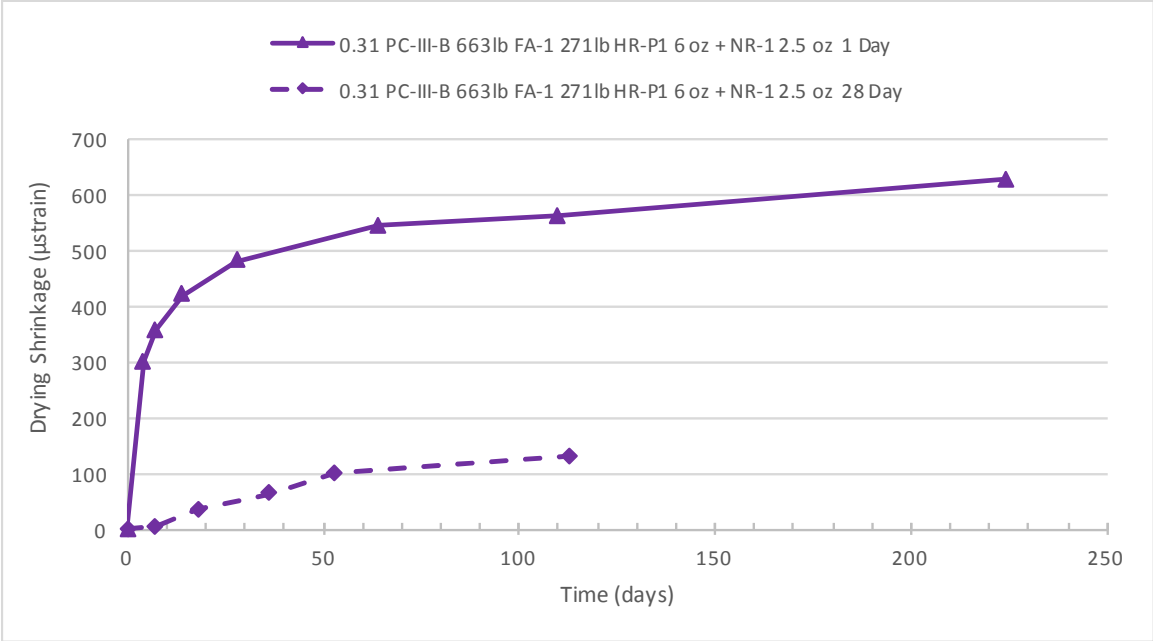

Figure 138: Drying Shrinkage 0.31 PC-III-B 663lb FA-1 271lb HR-P1 6 oz + NR-1 2.5 oz

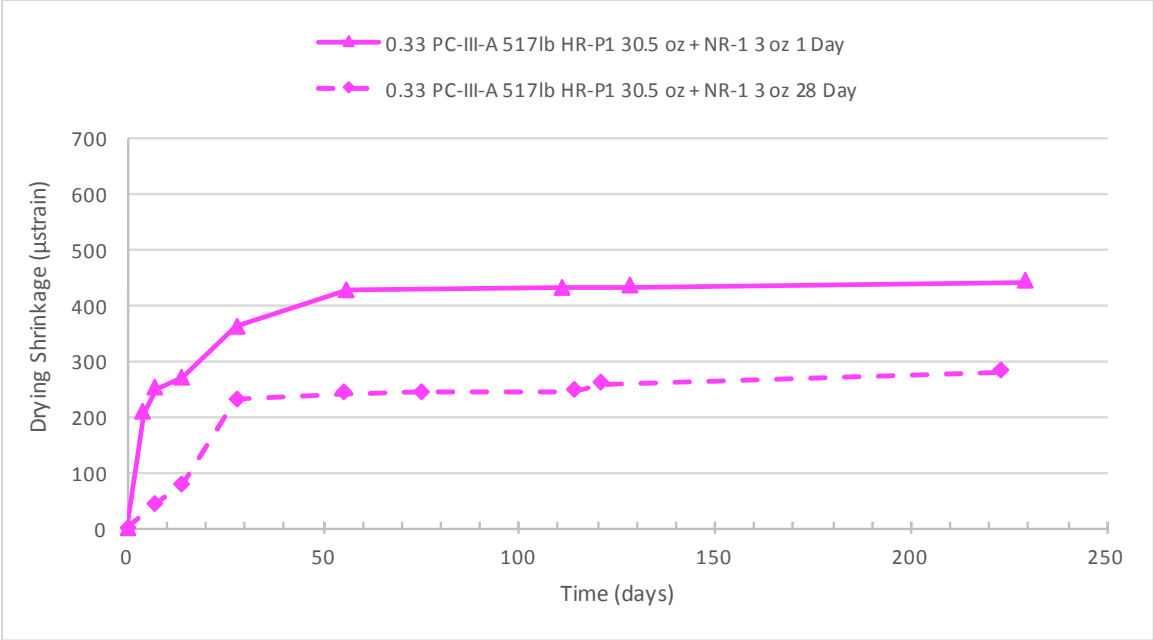

Figure 139: Drying Shrinkage 0.33 PC-III-A 517lb HR-P1 30.5 oz + NR-1 3 oz

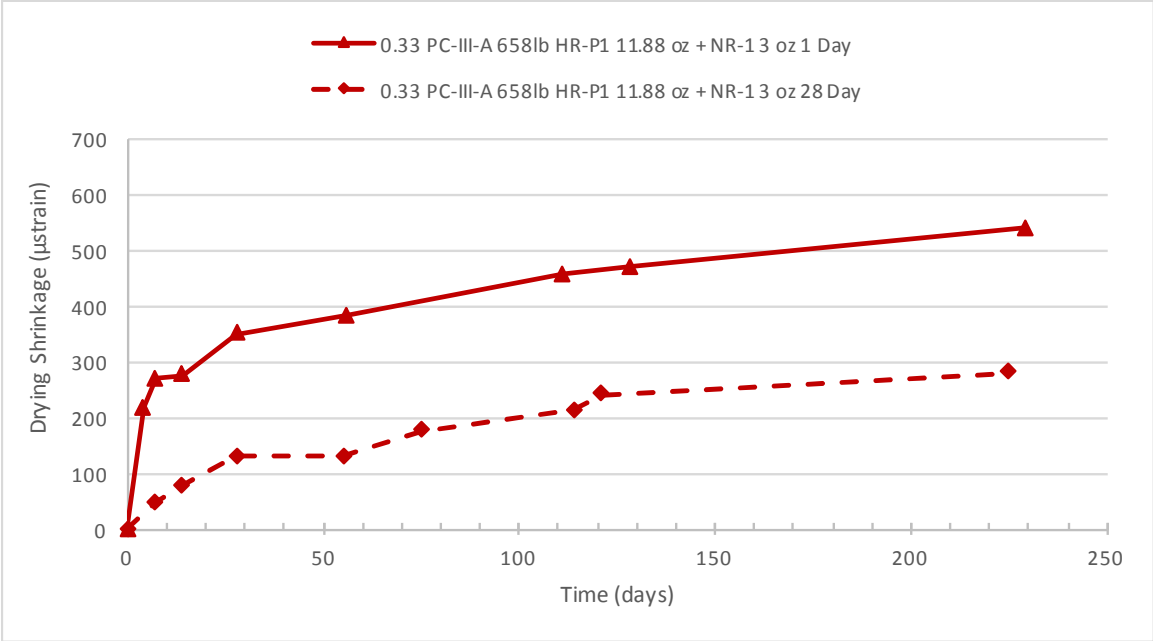

Figure 140: Drying Shrinkage 0.33 PC-III-A 658lb HR-P1 11.88 oz + NR-1 3 oz

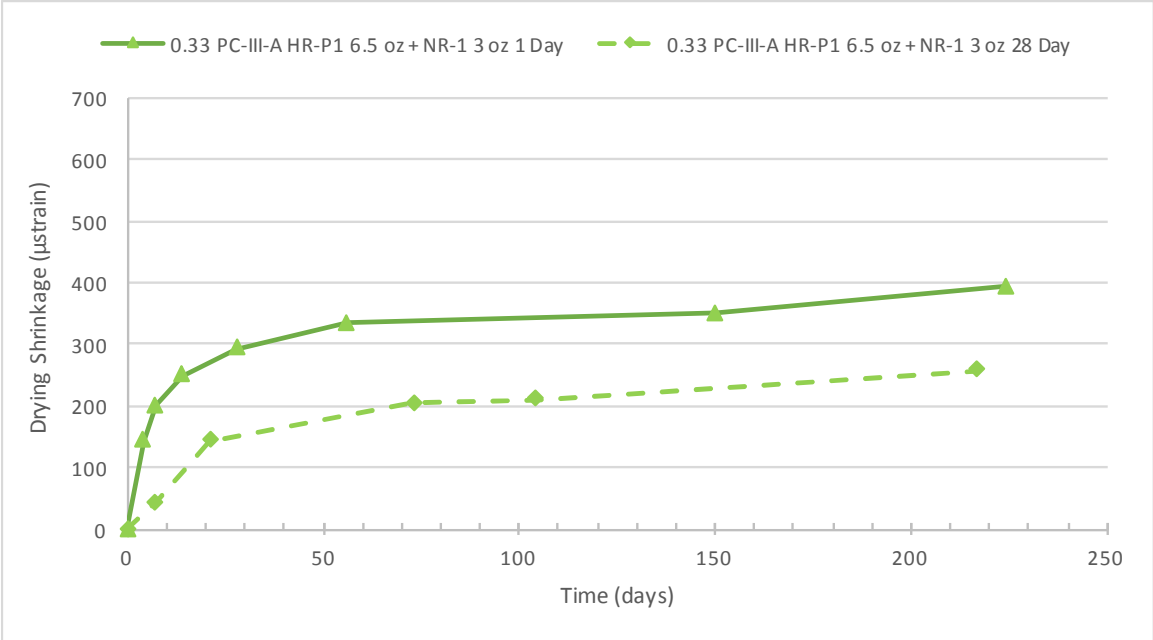

Figure 141: Drying Shrinkage 0.33 PC-III-A 658lb HR-P1 6.5 oz + NR-1 3 oz

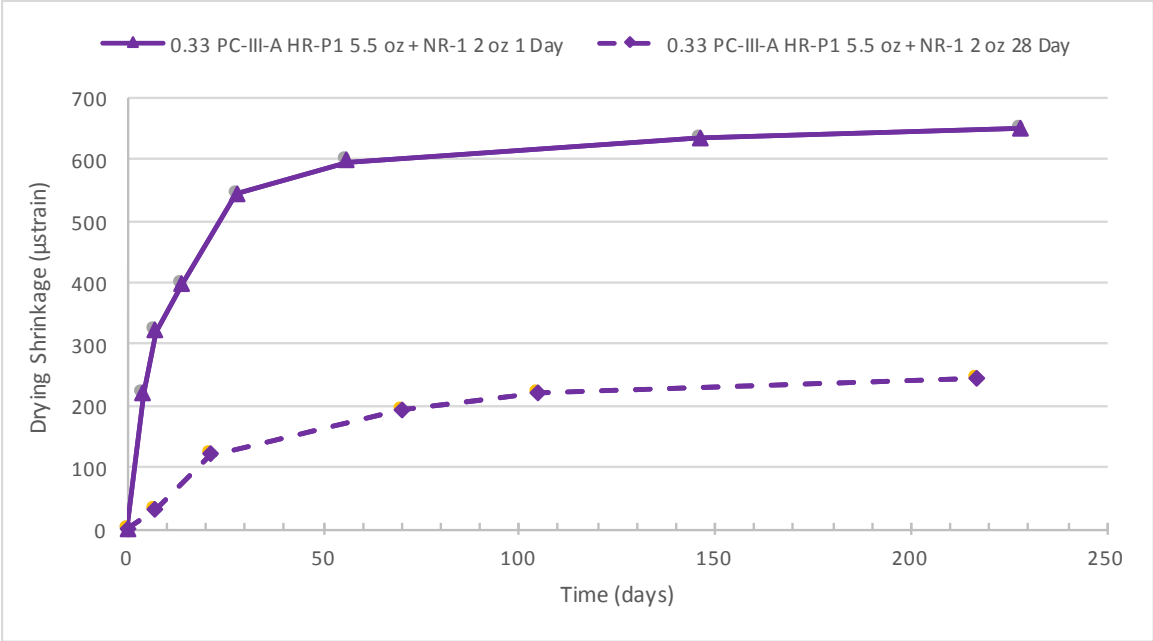

Figure 142: Drying Shrinkage 0.33 PC-III-A 658lb HR-P1 5.5 + NR-1 2 oz

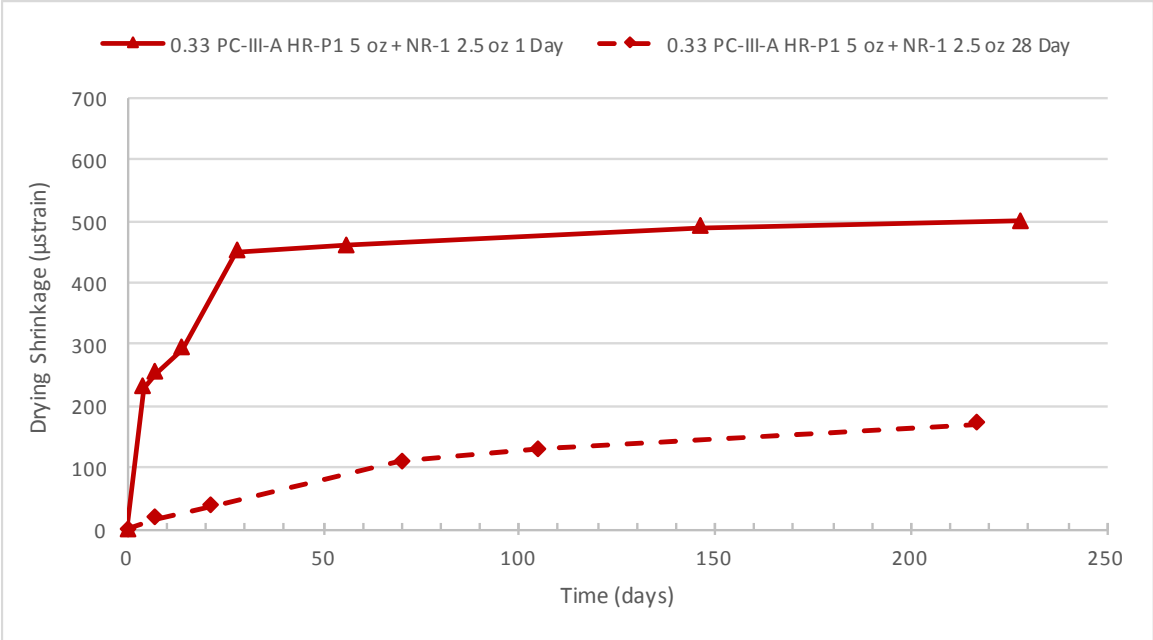

Figure 143: Drying Shrinkage 0.33 PC-III-A 658lb HR-P1 5 + NR-1 2.5 oz w/ FA-LW

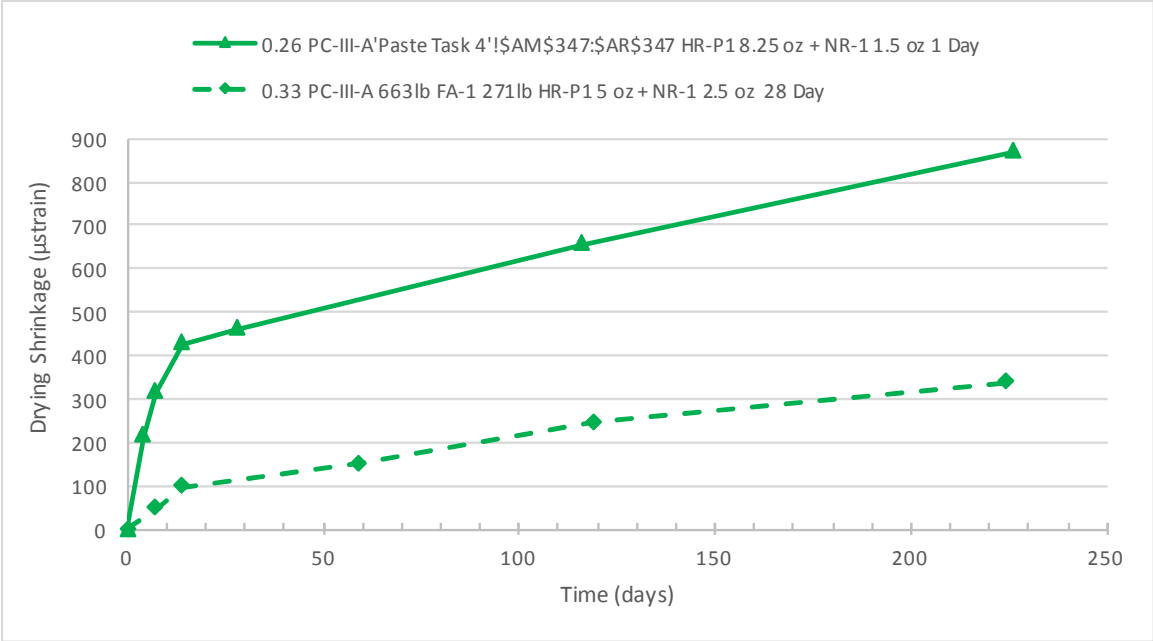

Figure 144: Drying Shrinkage 0.33 PC-III-A 663lb FA-1 271lb HR-P1 5 oz + NR-1 2.5 oz

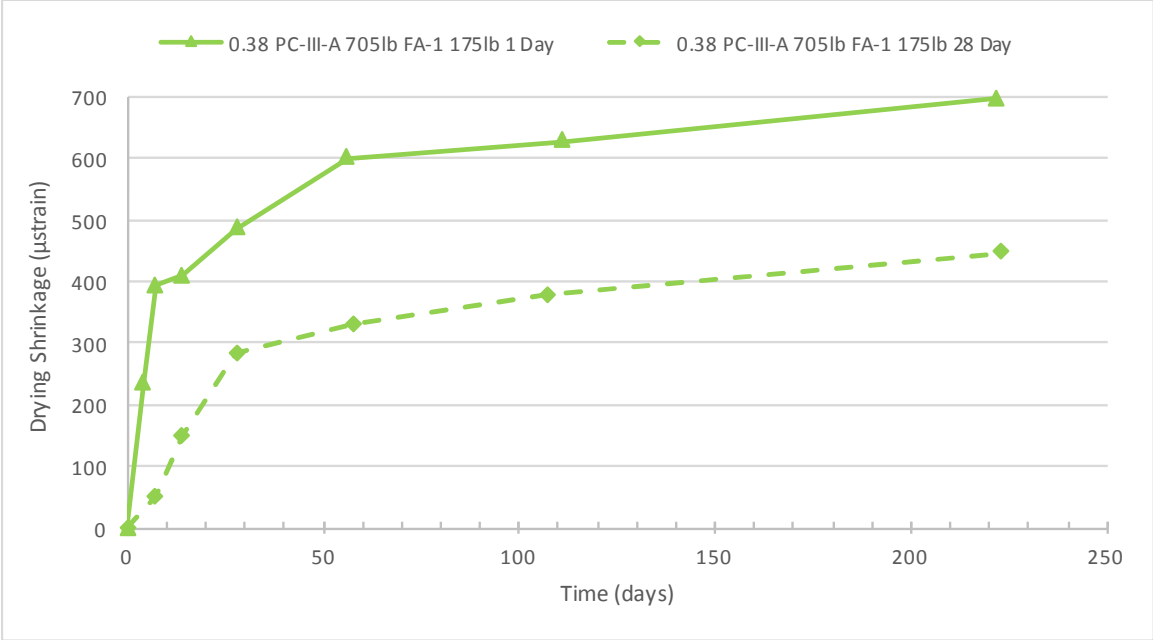

Figure 145: Drying Shrinkage 0.38 PC-III-A 705lb FA-1 175lb

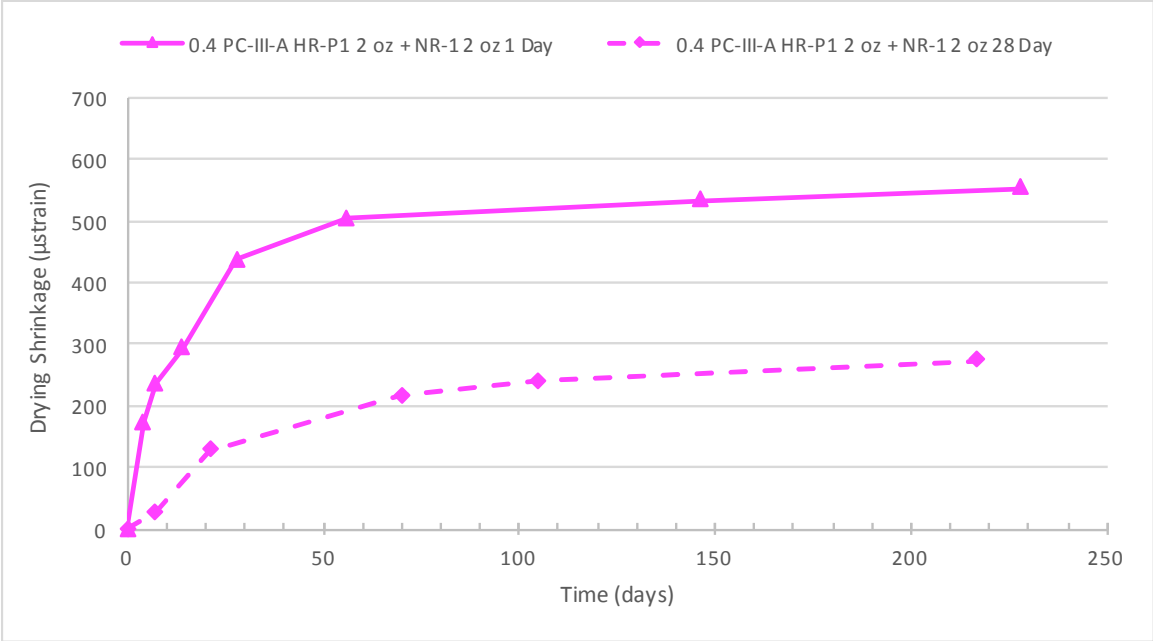

Figure 146: Drying Shrinkage 0.4 PC-III-A 658lb FA-1 165lb HR-P1 2 oz + NR-1 2 oz

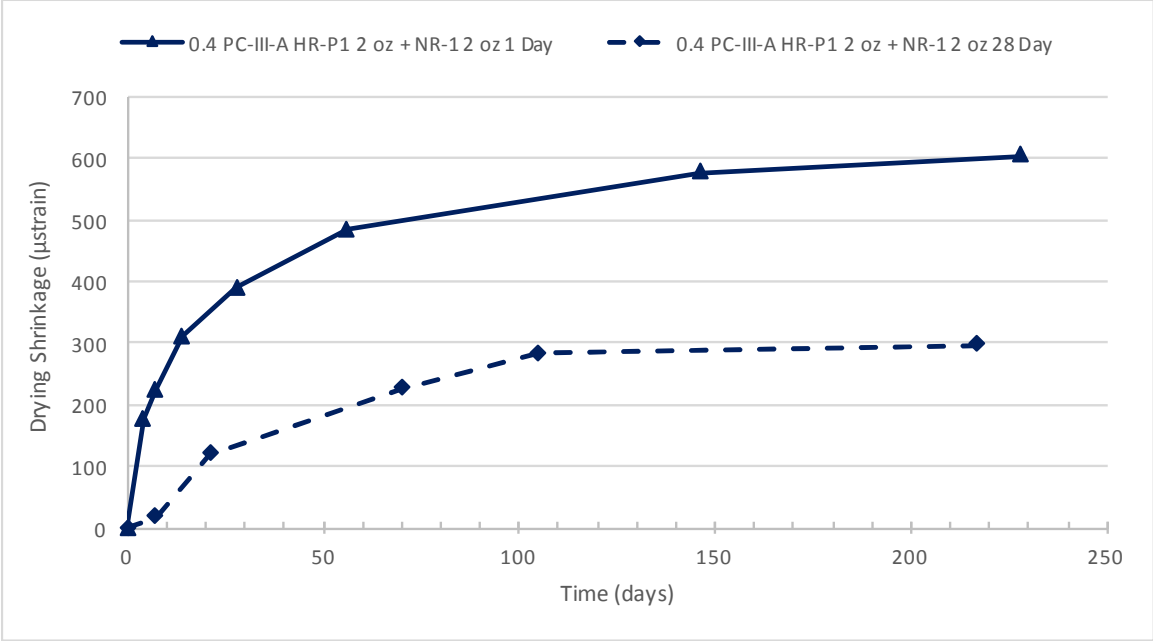

Figure 147: Drying Shrinkage 0.4 PC-III-A 658lb HR-P1 2 oz + NR-1 2 oz

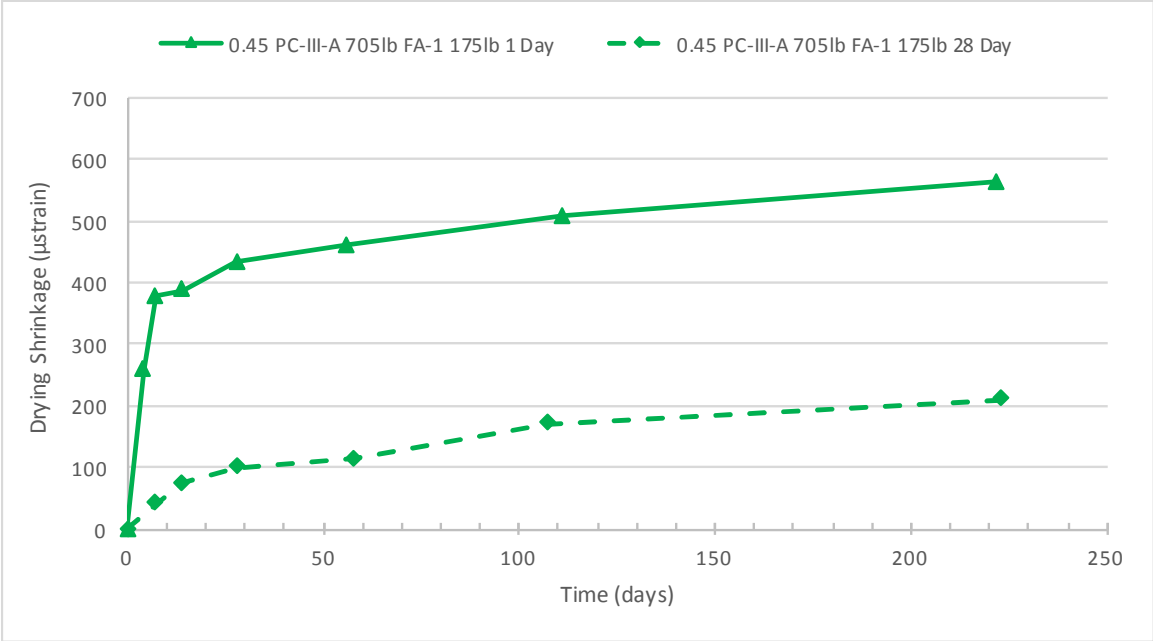

Figure 148: Drying Shrinkage 0.45 PC-III-A 705lb FA-1 175lb

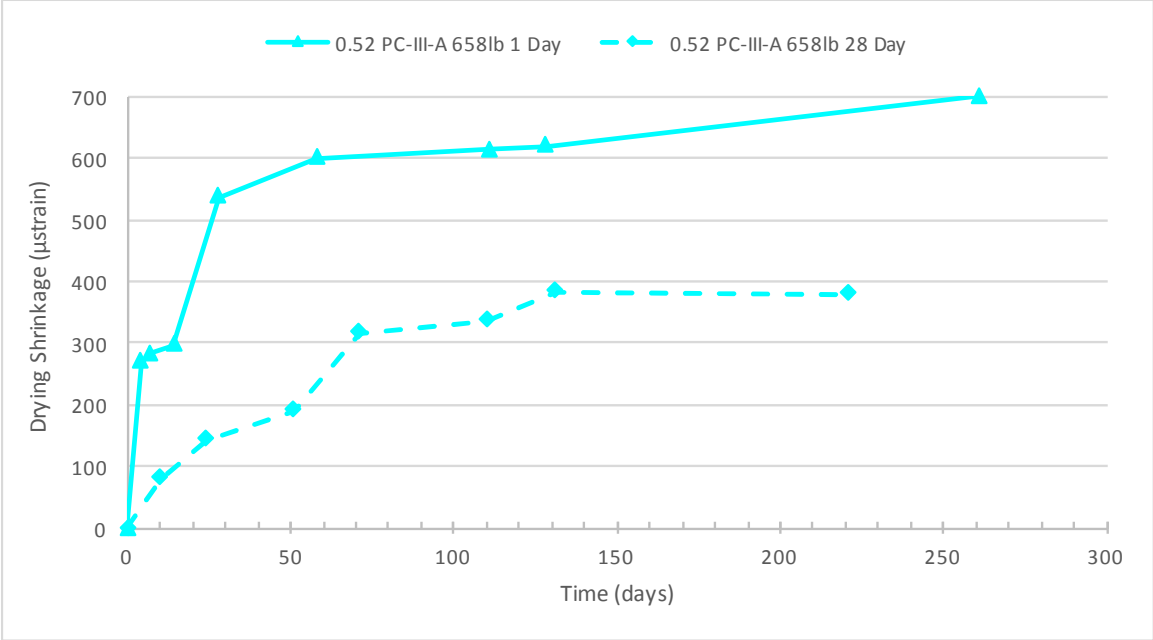

Figure 149: Drying Shrinkage 0.52 PC-III-A 658lb

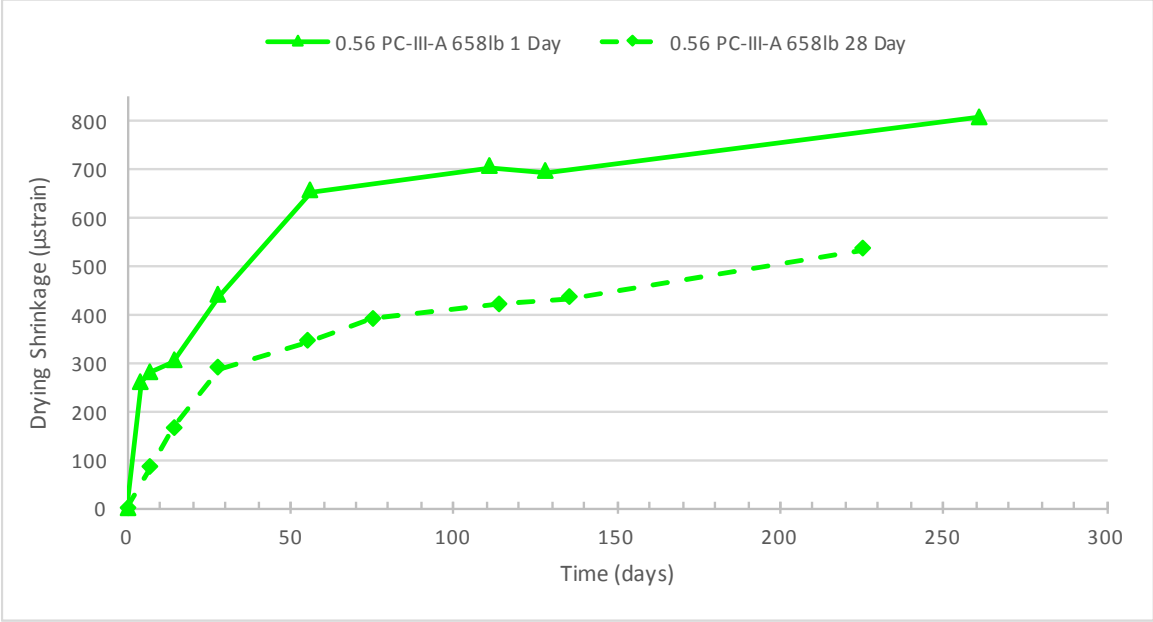

Figure 150: Drying Shrinkage 0.56 PC-III-A 658lb

Appendix VI: Restrained Shrinkage Ring Program

```
'CR5000
'Created by Stephen Stacey 2015

'Declare Variables and Units
Public BattV
Public FCLoaded
Public PTemp_C
Public CReps
Public ZMode
Public QBSSMode
Public CIndex
Public CAvg
Public LCount
Public Strain(16)
Public Vr1000(16)
Public GFAdj(16)
Public BrZero(16)
Public CKnown(16)
Public CReps_2
Public ZMode_2
Public QBSSMode_2
Public CIndex_2
Public CAvg_2
Public LCount_2
Public Strain_2(16)
Public Vr1000_2(16)
Public GFAdj_2(16)
Public BrZero_2(16)
Public CKnown_2(16)
Public CReps_3
Public ZMode_3
Public QBSSMode_3
Public CIndex_3
Public CAvg_3
Public LCount_3
Public Strain_3(16)
Public Vr1000_3(16)
Public GFAdj_3(16)
Public BrZero_3(16)
Public CKnown_3(16)
Public CReps_4
Public ZMode_4
Public QBSSMode_4
Public CIndex_4
Public CAvg_4
Public LCount_4
Public Strain_4(16)
Public Vr1000_4(16)
Public GFAdj_4(16)
Public BrZero_4(16)
```

Figure 151: CR Basic restrained shrinkage program for mixtures (5-8)

```
Public CKnown_4(16)
Public CReps_5
Public ZMode_5
Public QBSSMode_5
Public CIndex_5
Public CAvg_5
Public LCount_5
Public Strain_5(16)
Public Vr1000_5(16)
Public GFAdj_5(16)
Public BrZero_5(16)
Public CKnown_5(16)
Public
GFsRaw(16)={2.13,2.13,2.13,2.13,2.12,2.12,2.12,2.12,2.12,2.12,2.12,2.1
2,2.12,2.12,2.12,2.12}
Public
GFsRaw_2(16)={2.13,2.13,2.13,2.13,2.12,2.12,2.12,2.12,2.13,2.12,2.13,2
.12,2.12,2.12,2.12,2.12}
Public
GFsRaw_3(16)={2.12,2.12,2.12,2.12,2.12,2.12,2.12,2.12,2.12,2.12,2.12,2
.12,2.12,2.12,2.12,2.12}
Public
GFsRaw_4(16)={2.13,2.13,2.13,2.13,2.13,2.12,2.13,2.12,2.12,2.12,2.12,2
.12,2.12,2.12,2.12,2.12}


Units BattV=Volts
Units PTemp_C=Deg C
Units Strain=mic
Units Vr1000=mV/V
Units GFAdj=unitless
Units BrZero=mV/V
Units Strain_2=mic
Units Vr1000_2=mV/V
Units GFAdj_2=unitless
Units BrZero_2=mV/V
Units Strain_3=mic
Units Vr1000_3=mV/V
Units GFAdj_3=unitless
Units BrZero_3=mV/V
Units Strain_4=mic
Units Vr1000_4=mV/V
Units GFAdj_4=unitless
Units BrZero_4=mV/V


'Define Data Tables Simply Change the Mix_XX to a new number each
time.
'Check How data is stored after in collection.
```

Figure 151 (cont.): CR Basic restrained shrinkage program for mixtures (5-8)

```
DataTable(Mix_7,True,-1)
        DataInterval(0,5,Min,10)

        Sample(1,Strain_3(5),IEEE4)
        Sample(1,Strain_3(6),IEEE4)
        Sample(1,Strain_3(7),IEEE4)
        Sample(1,Strain_3(8),IEEE4)
        Sample(1,Strain_3(9),IEEE4)
        Sample(1,Strain_3(10),IEEE4)
        Sample(1,Strain_3(11),IEEE4)
        Sample(1,Strain_3(12),IEEE4)
        Sample(1,Strain_3(13),IEEE4)
        Sample(1,Strain_3(14),IEEE4)
        Sample(1,Strain_3(15),IEEE4)
        Sample(1,Strain_3(16),IEEE4)
EndTable

DataTable(Mix_6,True,-1)
        DataInterval(0,5,Min,10)

        Sample(1,Strain_4(1),IEEE4)
        Sample(1,Strain_4(2),IEEE4)
        Sample(1,Strain_4(3),IEEE4)
        Sample(1,Strain_4(4),IEEE4)
        Sample(1,Strain_4(5),IEEE4)
        Sample(1,Strain_4(6),IEEE4)
        Sample(1,Strain_4(7),IEEE4)
        Sample(1,Strain_4(8),IEEE4)
        Sample(1,Strain_4(9),IEEE4)
        Sample(1,Strain_4(10),IEEE4)
        Sample(1,Strain_4(15),IEEE4)
        Sample(1,Strain_4(16),IEEE4)
EndTable

DataTable(Extra_Ring,True,-1)
        DataInterval(0,5,min,10)

        Sample(1,Strain_4(11),IEEE4)
        Sample(1,Strain_4(12),IEEE4)
        Sample(1,Strain_4(13),IEEE4)
        Sample(1,Strain_4(14),IEEE4)
EndTable

'Main Program
BeginProg
        'Initialize calibration variables for
        'Full Bridge Strain, 120 ohm measurement 'Vr1000()'
        CIndex=1 : CAvg=1 : CReps=16
        For LCount = 1 To 16
```

Figure 151 (cont.): CR Basic restrained shrinkage program for mixtures (5-8)

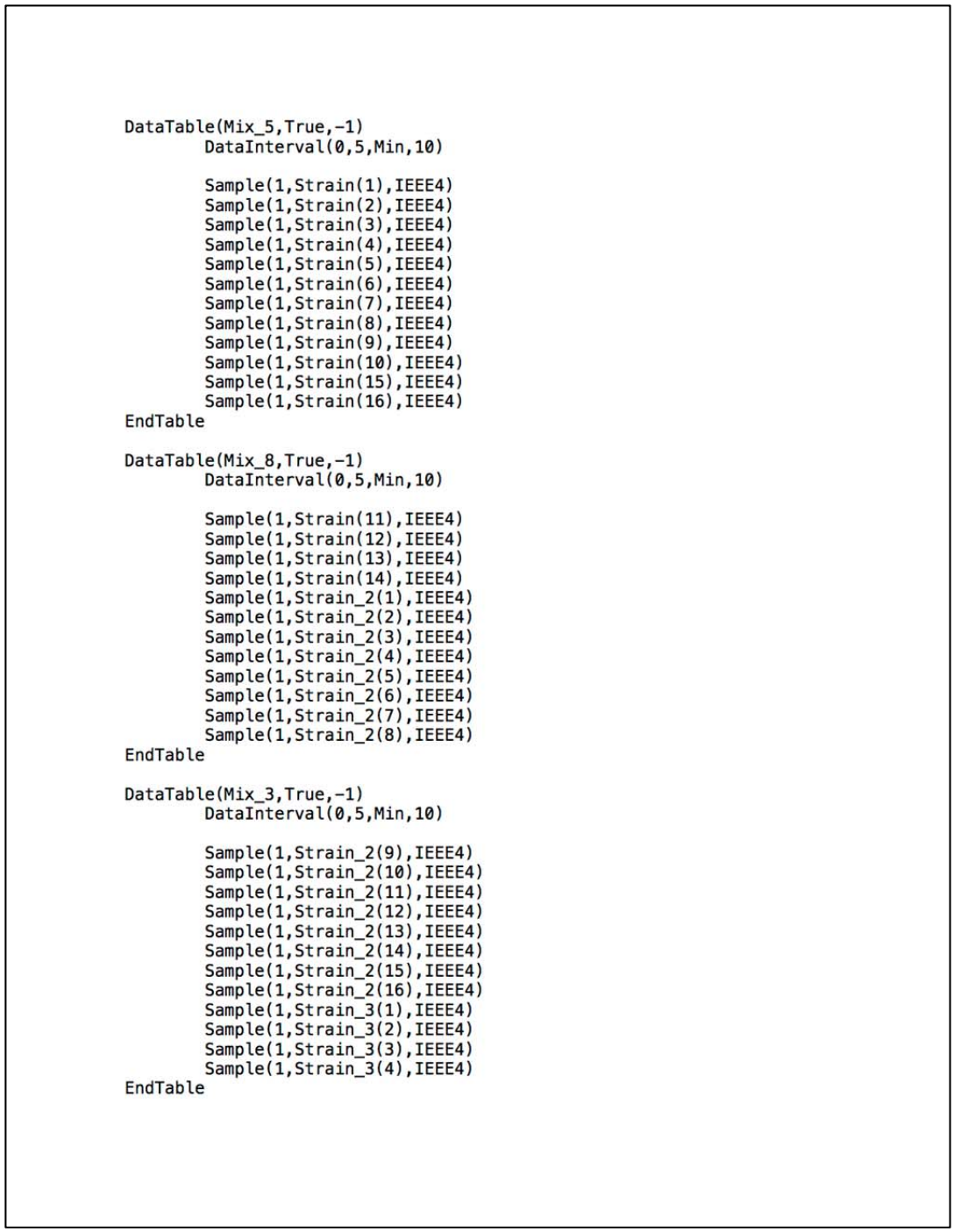

```
DataTable(Mix_5,True,-1)
        DataInterval(0,5,Min,10)

        Sample(1,Strain(1),IEEE4)
        Sample(1,Strain(2),IEEE4)
        Sample(1,Strain(3),IEEE4)
        Sample(1,Strain(4),IEEE4)
        Sample(1,Strain(5),IEEE4)
        Sample(1,Strain(6),IEEE4)
        Sample(1,Strain(7),IEEE4)
        Sample(1,Strain(8),IEEE4)
        Sample(1,Strain(9),IEEE4)
        Sample(1,Strain(10),IEEE4)
        Sample(1,Strain(15),IEEE4)
        Sample(1,Strain(16),IEEE4)
EndTable

DataTable(Mix_8,True,-1)
        DataInterval(0,5,Min,10)

        Sample(1,Strain(11),IEEE4)
        Sample(1,Strain(12),IEEE4)
        Sample(1,Strain(13),IEEE4)
        Sample(1,Strain(14),IEEE4)
        Sample(1,Strain_2(1),IEEE4)
        Sample(1,Strain_2(2),IEEE4)
        Sample(1,Strain_2(3),IEEE4)
        Sample(1,Strain_2(4),IEEE4)
        Sample(1,Strain_2(5),IEEE4)
        Sample(1,Strain_2(6),IEEE4)
        Sample(1,Strain_2(7),IEEE4)
        Sample(1,Strain_2(8),IEEE4)
EndTable

DataTable(Mix_3,True,-1)
        DataInterval(0,5,Min,10)

        Sample(1,Strain_2(9),IEEE4)
        Sample(1,Strain_2(10),IEEE4)
        Sample(1,Strain_2(11),IEEE4)
        Sample(1,Strain_2(12),IEEE4)
        Sample(1,Strain_2(13),IEEE4)
        Sample(1,Strain_2(14),IEEE4)
        Sample(1,Strain_2(15),IEEE4)
        Sample(1,Strain_2(16),IEEE4)
        Sample(1,Strain_3(1),IEEE4)
        Sample(1,Strain_3(2),IEEE4)
        Sample(1,Strain_3(3),IEEE4)
        Sample(1,Strain_3(4),IEEE4)
EndTable
```

Figure 151 (cont.): CR Basic restrained shrinkage program for mixtures (5-8)

```
                GFAdj(LCount)=GFsRaw(LCount)
        Next
        'Initialize calibration variables for
        'Full Bridge Strain, 120 ohm measurement 'Vr1000_2()'
        CIndex_2=1 : CAvg_2=1 : CReps_2=16
        For LCount_2 = 1 To 16
                GFAdj_2(LCount_2)=GFsRaw_2(LCount_2)
        Next
        'Initialize calibration variables for
        'Full Bridge Strain, 120 ohm measurement 'Vr1000_3()'
        CIndex_3=1 : CAvg_3=1 : CReps_3=16
        For LCount_3 = 1 To 16
                GFAdj_3(LCount_3)=GFsRaw_3(LCount_3)
        Next
        'Initialize calibration variables for
        'Full Bridge Strain, 120 ohm measurement 'Vr1000_4()'
        CIndex_4=1 : CAvg_4=1 : CReps_4=16
        For LCount_4 = 1 To 16
                GFAdj_4(LCount_4)=GFsRaw_4(LCount_4)


        Next
        'Load the most recent calibration values from the CalHist
table
        FCLoaded=LoadFieldCal(True)
        'Main Scan
        Scan(1,Min,1,0)
                'Default Datalogger Battery Voltage measurement
'BattV'
                Battery(BattV)
                'Default Wiring Panel Temperature measurement
'PTemp_C'
                PanelTemp(PTemp_C,_60Hz)
                'Turn AM16/32 Multiplexer On
                PortSet(2,1)
                Delay(0,1,mSec)
                LCount=1
                SubScan(0,uSec,16)
                        'Switch to next AM16/32 Multiplexer channel
                        PortSet(1,1)
                        Delay(0,1,mSec)
                        PortSet(1,0)
                        Delay(0,1,mSec)
                        'Full Bridge Strain, 120 ohm measurement
'Vr1000()'
                        BrFull(Vr1000(LCount),
1,mV20,1,Vx1,1,5000,True,True,50000,_60Hz,1,0)
                        LCount=LCount+1
                NextSubScan
                'Calculated strain result 'Strain()' for
```

Figure 151 (cont.): CR Basic restrained shrinkage program for mixtures (5-8)

```
                'Full Bridge Strain, 120 ohm measurement 'Vr1000()'
                StrainCalc(Strain(),16,Vr1000(),BrZero(),-1,GFAdj(),0)
                'Bending full bridge strain shunt calibration for
                'Full Bridge Strain, 120 ohm measurement 'Vr1000()'
                FieldCalStrain(13,Strain(),1,GFAdj(),
0,QBSSMode,CKnown(),CIndex,CAvg,GFsRaw(),0)
                'Zeroing calibration for
                'Full Bridge Strain, 120 ohm measurement 'Vr1000()'
                FieldCalStrain(10,Vr1000(),CReps,0,BrZero(),ZMode,
0,CIndex,CAvg,0,Strain())
                'Turn AM16/32 Multiplexer Off
                PortSet(2,0)
                Delay(0,1,mSec)
                'Turn AM16/32 Multiplexer On
                PortSet(4,1)
                Delay(0,1,mSec)
                LCount_2=1
                SubScan(0,uSec,16)
                        'Switch to next AM16/32 Multiplexer channel
                        PortSet(3,1)
                        Delay(0,1,mSec)
                        PortSet(3,0)
                        Delay(0,1,mSec)
                        'Full Bridge Strain, 120 ohm measurement
'Vr1000_2()'
                        BrFull(Vr1000_2(LCount_2),
1,mV20,2,Vx2,1,5000,True,True,50000,_60Hz,1,0)
                        LCount_2=LCount_2+1
                NextSubScan
                'Calculated strain result 'Strain_2()' for
                'Full Bridge Strain, 120 ohm measurement 'Vr1000_2()'
                StrainCalc(Strain_2(),
16,Vr1000_2(),BrZero_2(),-1,GFAdj_2(),0)
                'Bending full bridge strain shunt calibration for
                'Full Bridge Strain, 120 ohm measurement 'Vr1000_2()'
                FieldCalStrain(43,Strain_2(),1,GFAdj_2(),
0,QBSSMode_2,CKnown_2(),CIndex_2,CAvg_2,GFsRaw_2(),0)
                'Zeroing calibration for
                'Full Bridge Strain, 120 ohm measurement 'Vr1000_2()'

FieldCalStrain(10,Vr1000_2(),CReps_2,0,BrZero_2(),ZMode_2,0,CIndex_2,C
Avg_2,0,Strain_2())
                'Turn AM16/32 Multiplexer Off
                PortSet(4,0)
                Delay(0,1,mSec)
                'Turn AM16/32 Multiplexer On
                PortSet(6,1)
                Delay(0,1,mSec)
                LCount_3=1
                SubScan(0,uSec,16)
```

Figure 151 (cont.): CR Basic restrained shrinkage program for mixtures (5-8)

```
                        'Switch to next AM16/32 Multiplexer channel
                        PortSet(5,1)
                        Delay(0,1,mSec)
                        PortSet(5,0)
                        Delay(0,1,mSec)
                        'Full Bridge Strain, 120 ohm measurement
'Vr1000_3()'
                        BrFull(Vr1000_3(LCount_3),
1,mV20,3,Vx3,1,5000,True,True,50000,_60Hz,1,0)
                        LCount_3=LCount_3+1
                NextSubScan
                'Calculated strain result 'Strain_3()' for
                'Full Bridge Strain, 120 ohm measurement 'Vr1000_3()'
                StrainCalc(Strain_3(),
16,Vr1000_3(),BrZero_3(),-1,GFAdj_3(),0)
                'Bending full bridge strain shunt calibration for
                'Full Bridge Strain, 120 ohm measurement 'Vr1000_3()'
                FieldCalStrain(43,Strain_3(),1,GFAdj_3(),
0,QBSSMode_3,CKnown_3(),CIndex_3,CAvg_3,GFsRaw_3(),0)
                'Zeroing calibration for
                'Full Bridge Strain, 120 ohm measurement 'Vr1000_3()'

FieldCalStrain(10,Vr1000_3(),CReps_3,0,BrZero_3(),ZMode_3,0,CIndex_3,C
Avg_3,0,Strain_3())
                'Turn AM16/32 Multiplexer Off
                PortSet(6,0)
                Delay(0,1,mSec)
                'Turn AM16/32 Multiplexer On
                PortSet(8,1)
                Delay(0,1,mSec)
                LCount_4=1
                SubScan(0,uSec,16)
                        'Switch to next AM16/32 Multiplexer channel
                        PortSet(7,1)
                        Delay(0,1,mSec)
                        PortSet(7,0)
                        Delay(0,1,mSec)
                        'Full Bridge Strain, 120 ohm measurement
'Vr1000_4()'
                        BrFull(Vr1000_4(LCount_4),
1,mV20,4,Vx4,1,5000,True,True,50000,_60Hz,1,0)
                        LCount_4=LCount_4+1
                NextSubScan
                'Calculated strain result 'Strain_4()' for
                'Full Bridge Strain, 120 ohm measurement 'Vr1000_4()'
                StrainCalc(Strain_4(),
16,Vr1000_4(),BrZero_4(),-1,GFAdj_4(),0)
                'Bending full bridge strain shunt calibration for
                'Full Bridge Strain, 120 ohm measurement 'Vr1000_4()'
                FieldCalStrain(43,Strain_4(),1,GFAdj_4(),
```

Figure 151 (cont.): CR Basic restrained shrinkage program for mixtures (5-8)

```
0,QBSSMode_4,CKnown_4(),CIndex_4,CAvg_4,GFsRaw_4(),0)
                'Zeroing calibration for
                'Full Bridge Strain, 120 ohm measurement 'Vr1000_4()'

FieldCalStrain(10,Vr1000_4(),CReps_4,0,BrZero_4(),ZMode_4,0,CIndex_4,C
Avg_4,0,Strain_4())
                'Turn AM16/32 Multiplexer Off
                PortSet(8,0)
                Delay(0,1,mSec)

                'Call Data Tables and Store Data
                CallTable Mix_5
                CallTable Mix_8
                CallTable Mix_3
                CallTable Mix_7
                CallTable Mix_6
                CallTable Extra_Ring

        NextScan
EndProg
```

Figure 151 (cont.): CR Basic restrained shrinkage program for mixtures (5-8)

Appendix VII: Restrained Shrinkage Ring Data

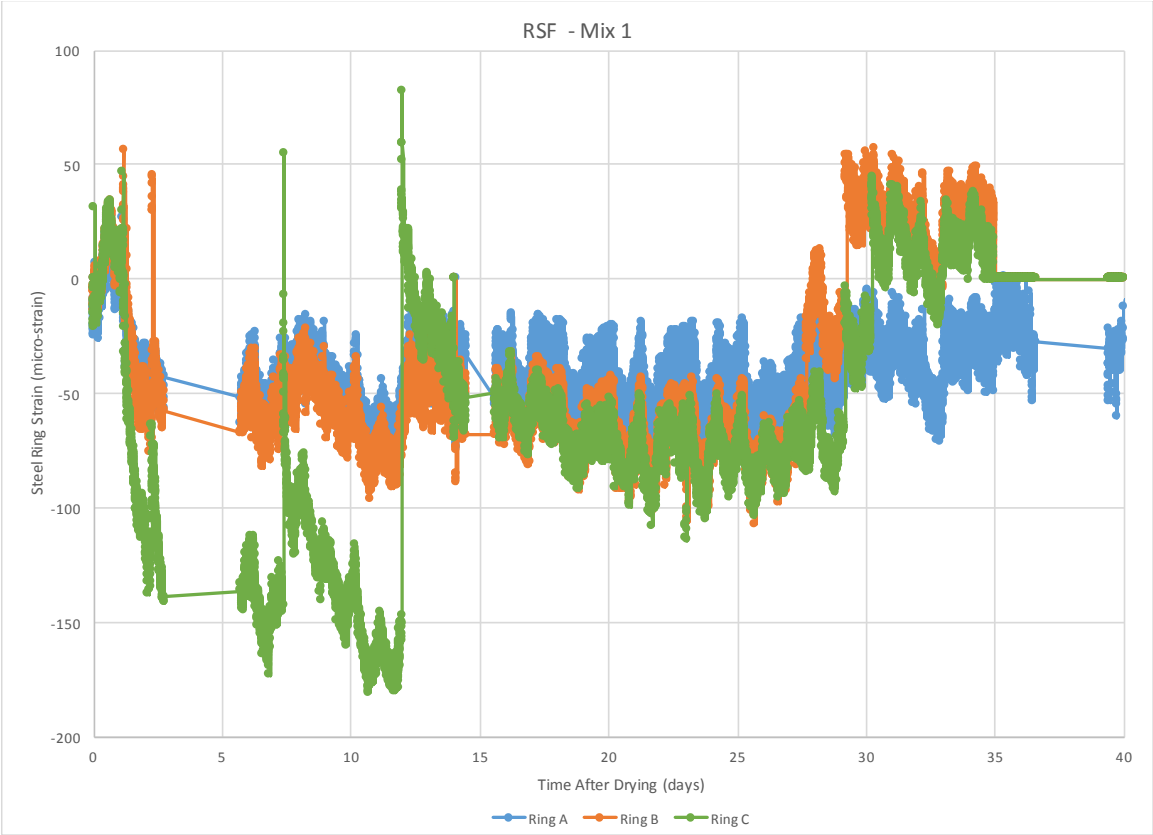

Figure 152: Net strain vs time (days) for rings A, B and C for Mixture 1

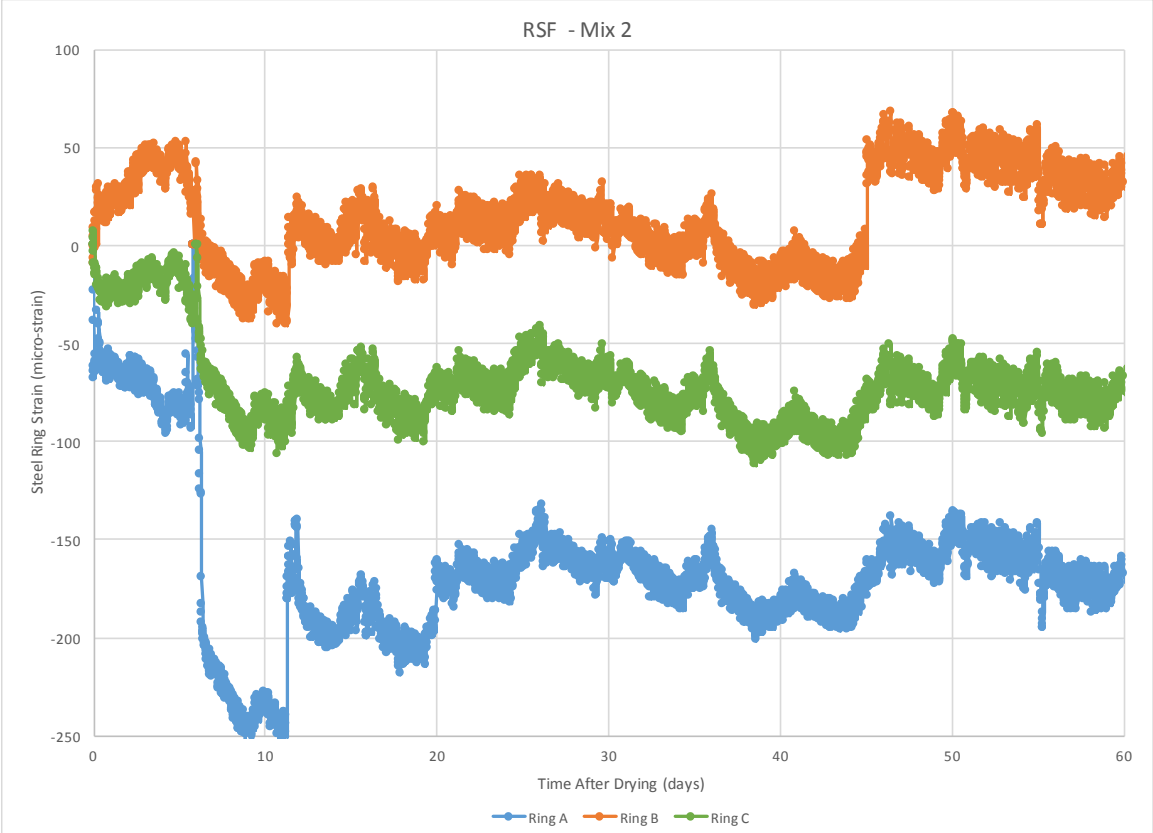

Figure 153: Net strain vs time (days) for rings A, B and C for Mixture 2

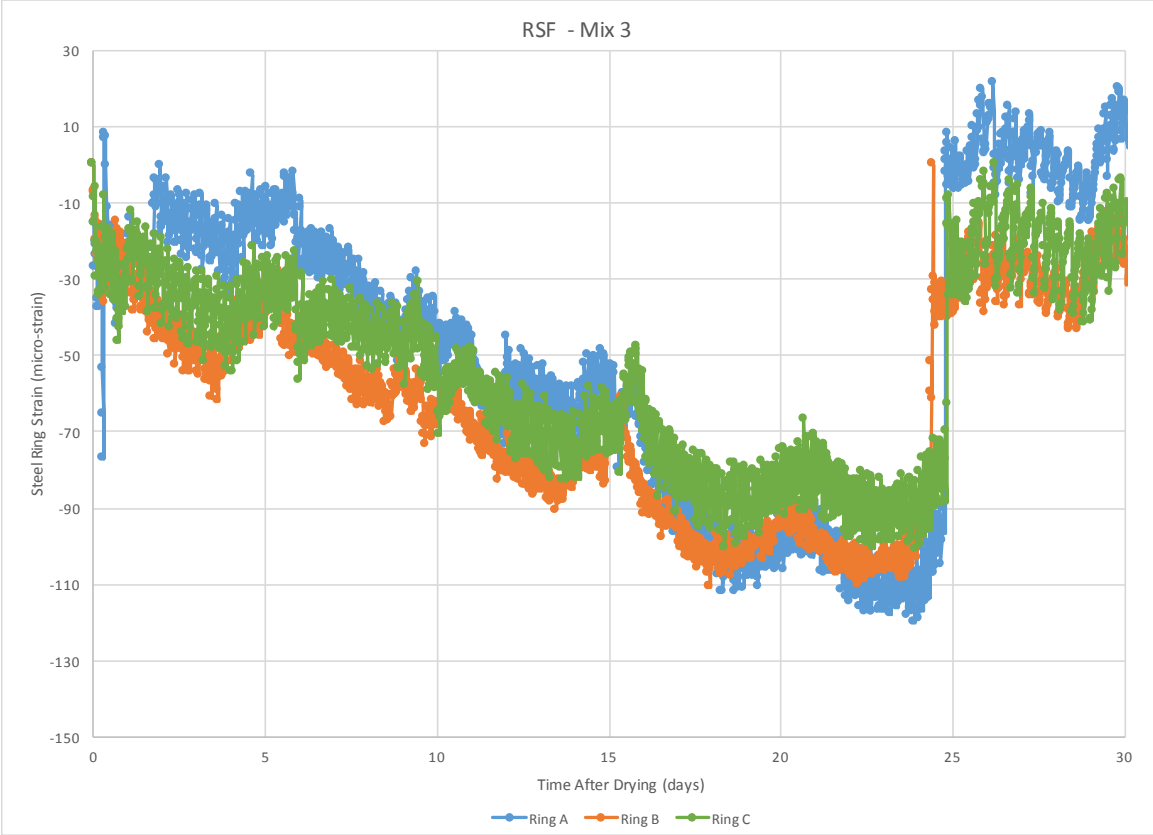

Figure 154: Net strain vs time (days) for rings A, B and C for Mixture 3

Figure 155: Net strain vs time (days) for rings A, B and C for Mixture 4

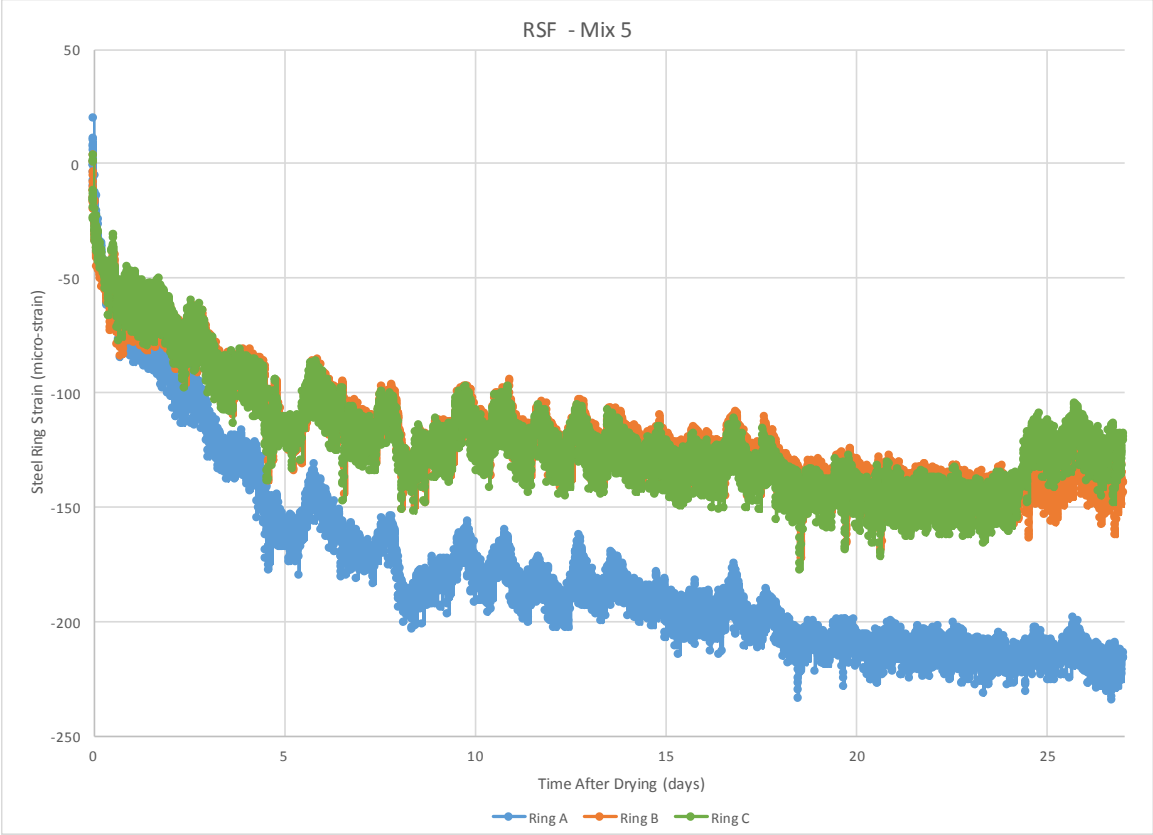

Figure 156: Net strain vs time (days) for rings A, B and C for Mixture 5

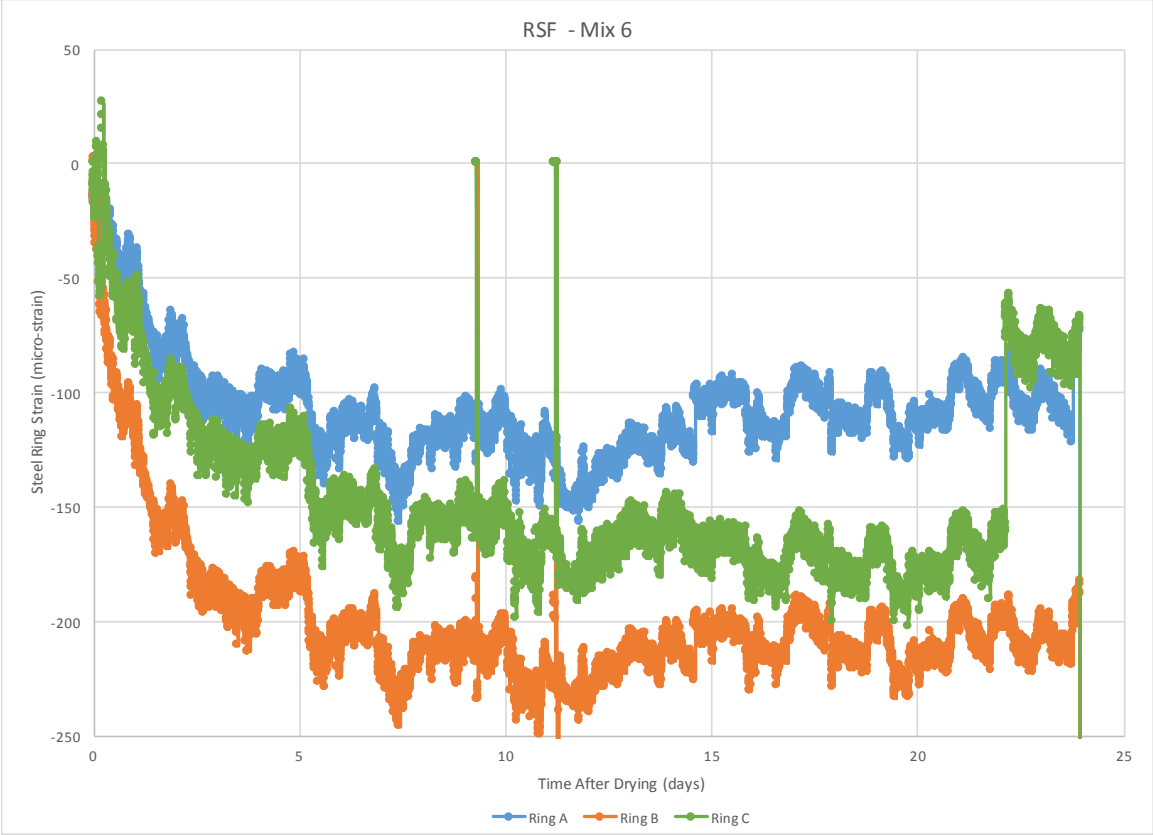

Figure 157: Net strain vs time (days) for rings A, B and C for Mixture 6

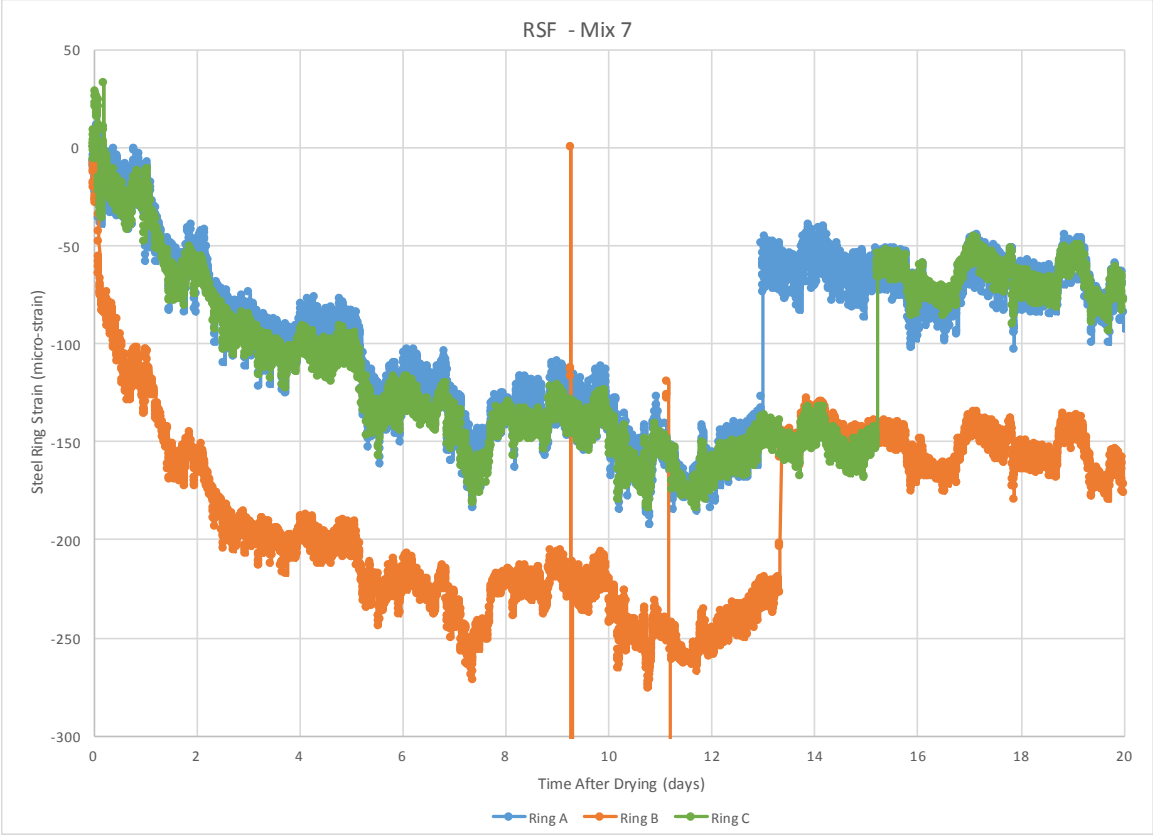

Figure 158: Net strain vs time (days) for rings A, B and C for Mixture 7

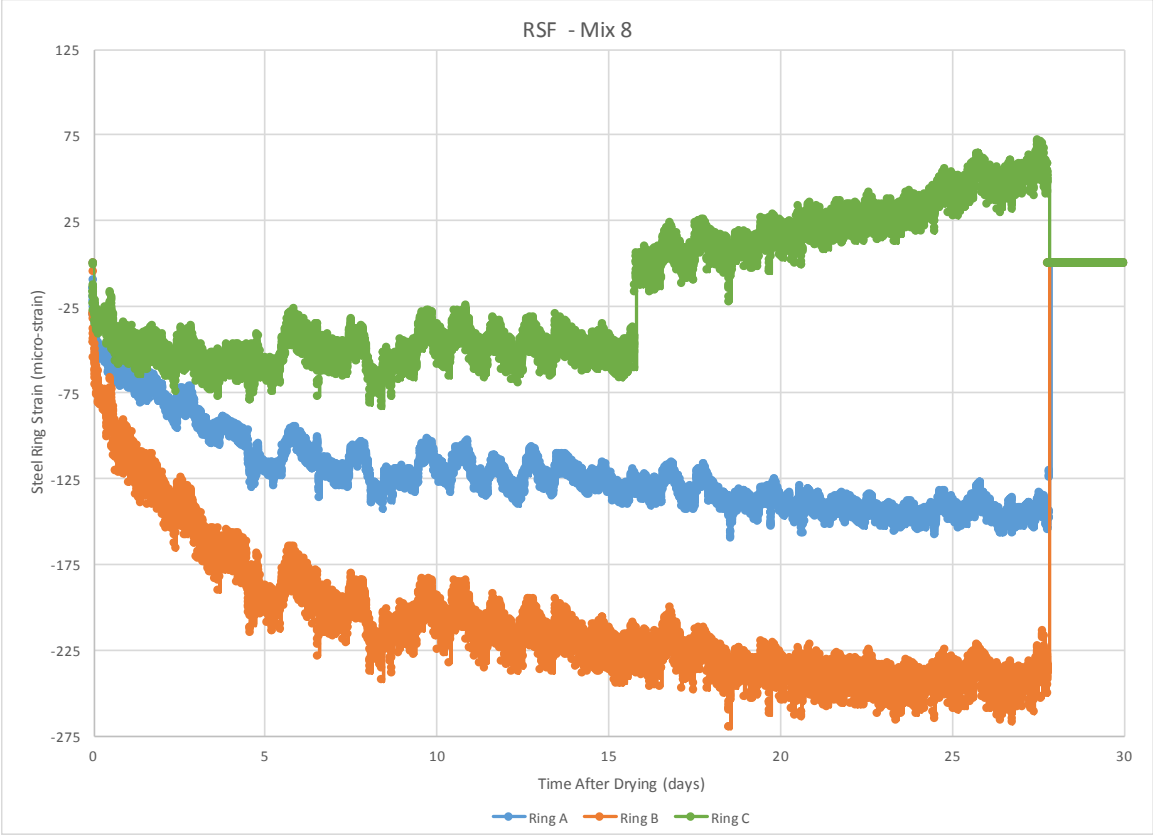

Figure 159: Net strain vs time (days) for rings A, B and C for Mixture 8

Appendix VIII: Buoyancy Test Data

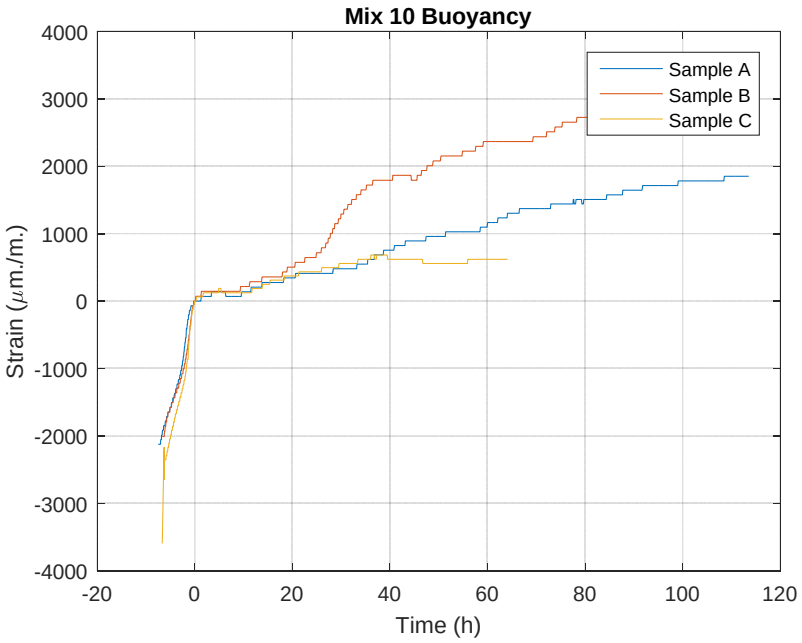

Figure 160: Buoyancy Strain 0.31 PC-III-A HR-P1 6.5 fl oz/100lb

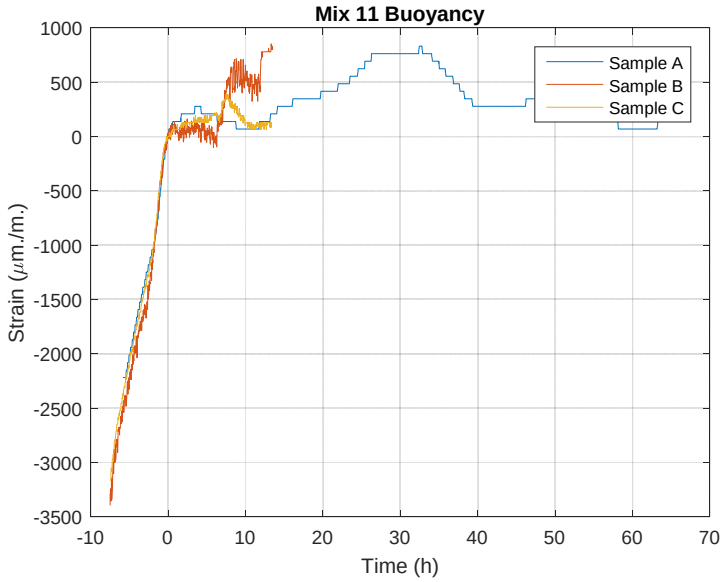

Figure 161: Buoyancy Strain 0.31 PC-III-A HR-P1 8.25 fl oz/100lb

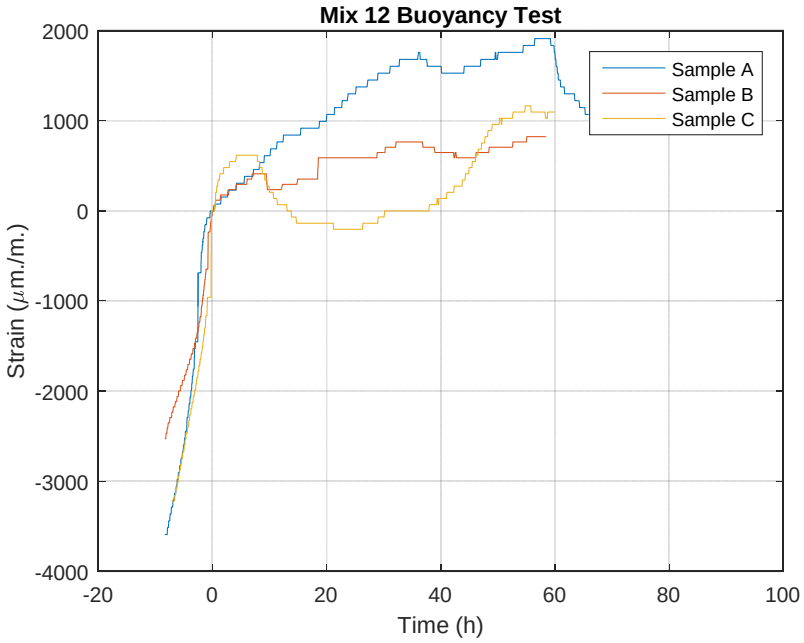

Figure 162: Buoyancy Strain 0.31 PC-III-A HR-P1 12 fl oz/100lb

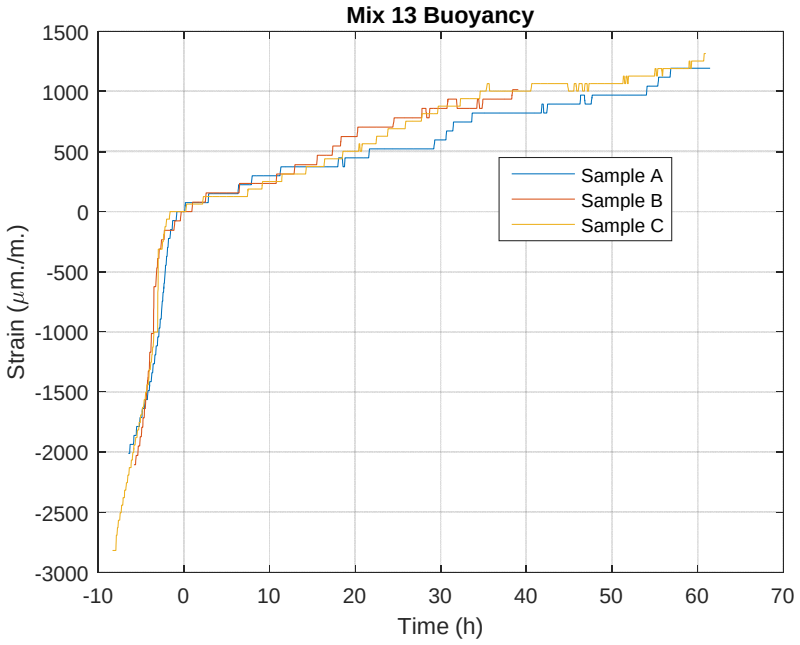

Figure 163: Buoyancy Strain 0.31 PC-III-A HR-P2 6.5 fl oz/100lb

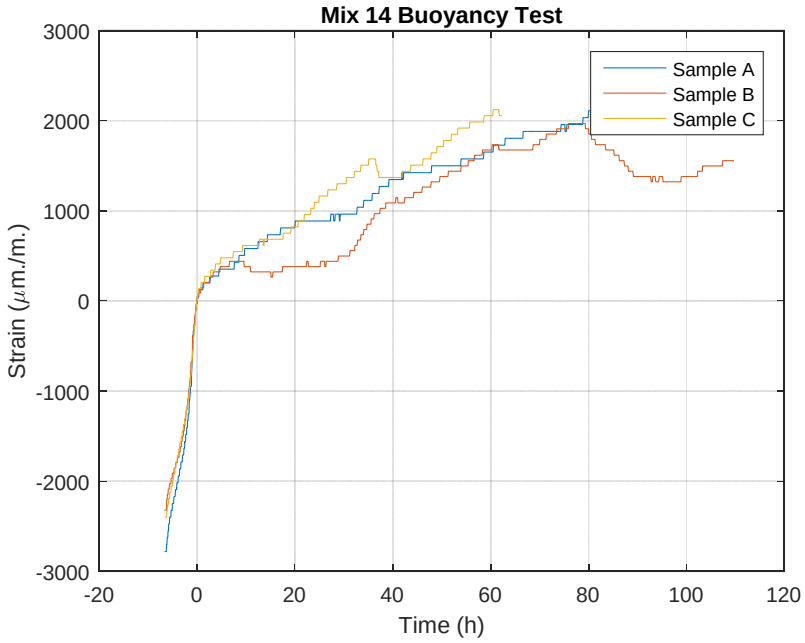

Figure 164: Buoyancy Strain 0.31 PC-III-A HR-P2 8.25 fl oz/100lb

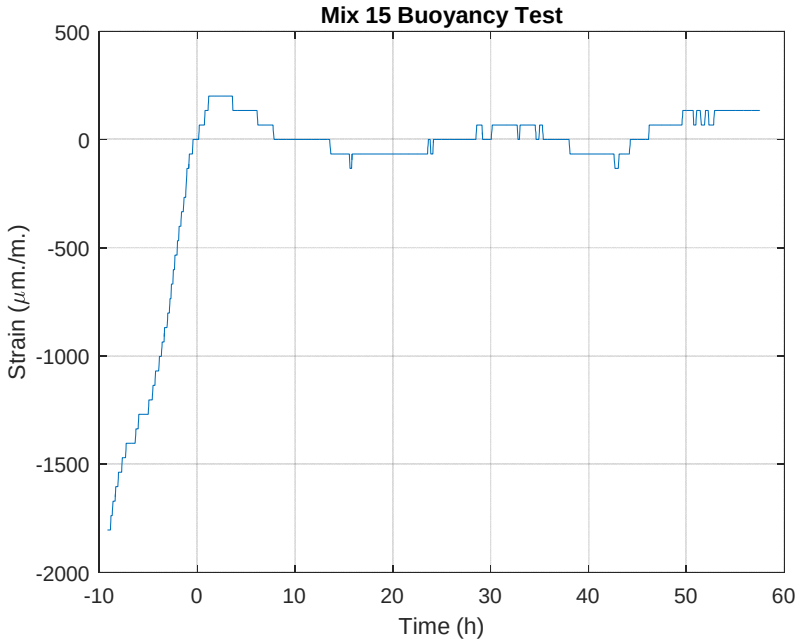

Figure 165: Buoyancy Strain 0.31 PC-III-A HR-P2 12 fl oz/100lb

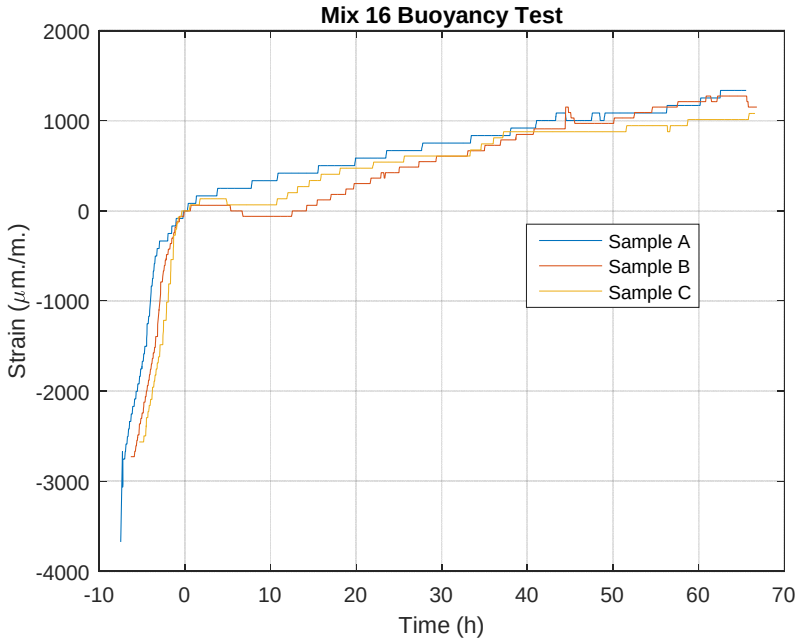

Figure 166: Buoyancy Strain 0.31 PC-III-A HR-P3 6.5 fl oz/100lb

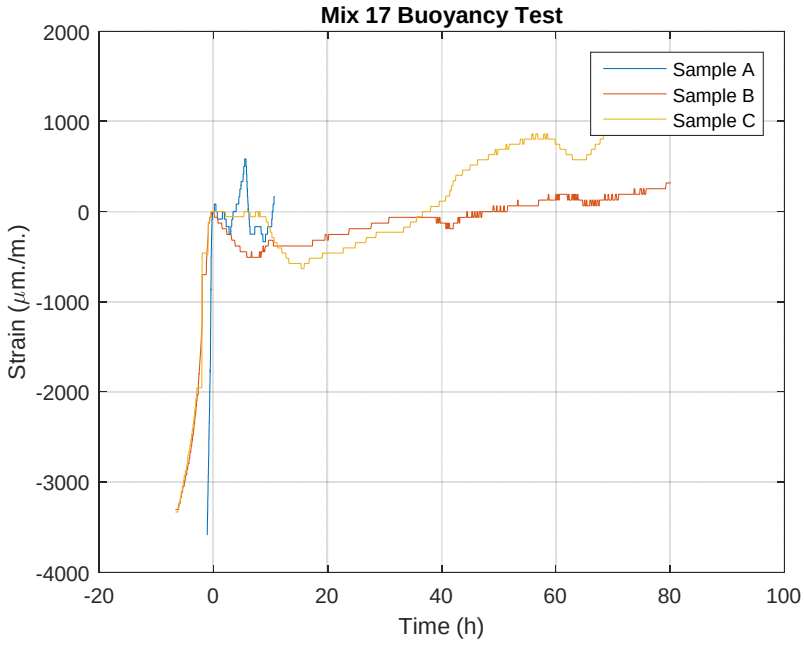

Figure 167: Buoyancy Strain 0.31 PC-III-A HR-P3 8.25 fl oz/100lb

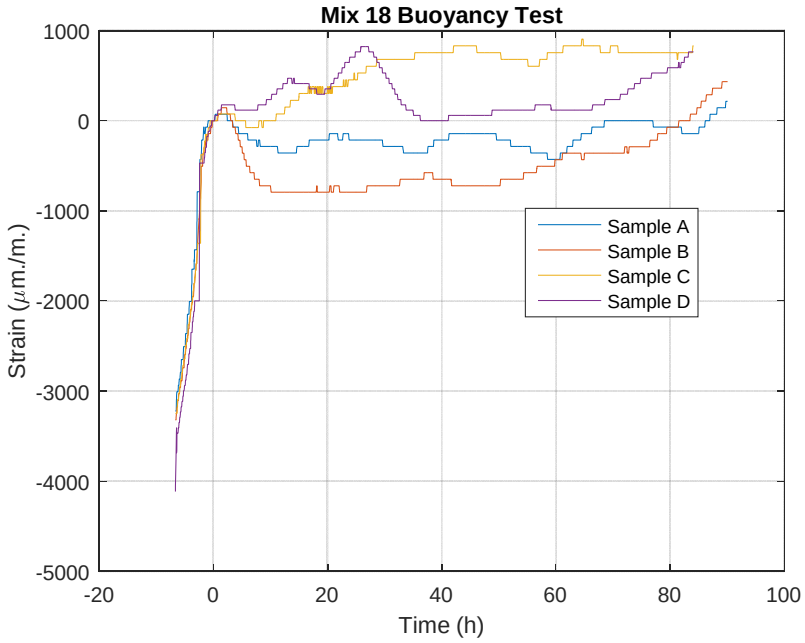

Figure 168: Buoyancy Strain 0.31 PC-III-A HR-P3 12 fl oz/100lb

Appendix IX: LVDT Test Data

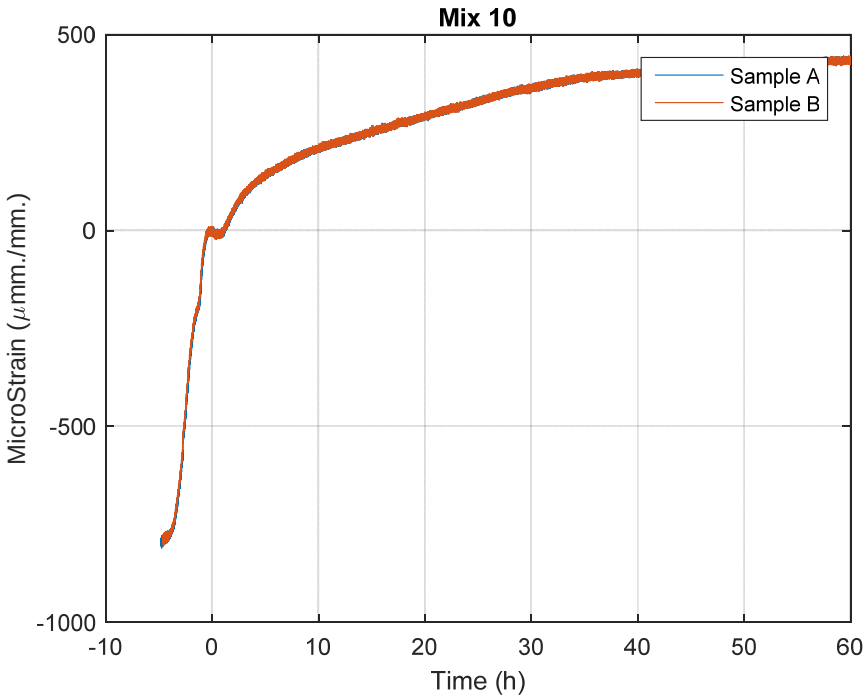

Figure 169: LVDT Strain 0.31 PC-III-A HR-P1 6 fl oz/100lb

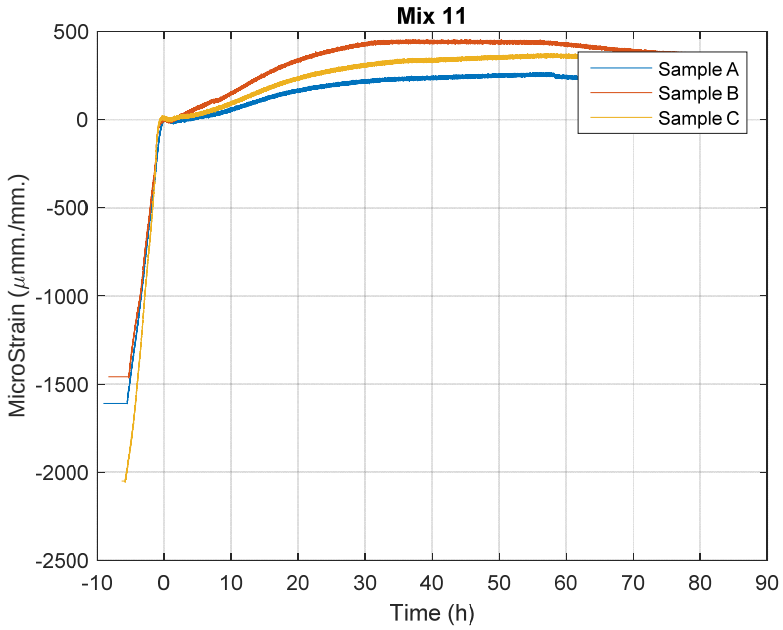

Figure 170: LVDT Strain 0.31 PC-III-A HR-P1 8.25 fl oz/100lb

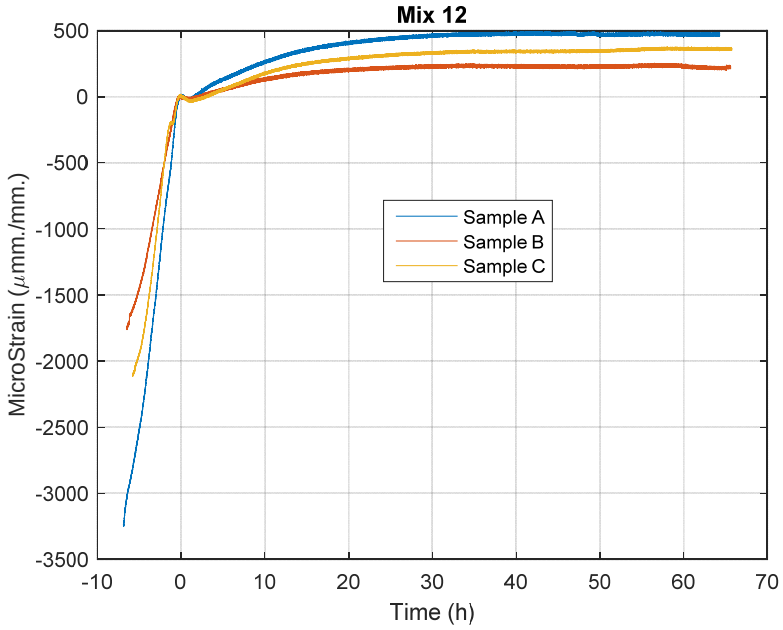

Figure 171: LVDT Strain 0.31 PC-III-A HR-P1 12 fl oz/100lb

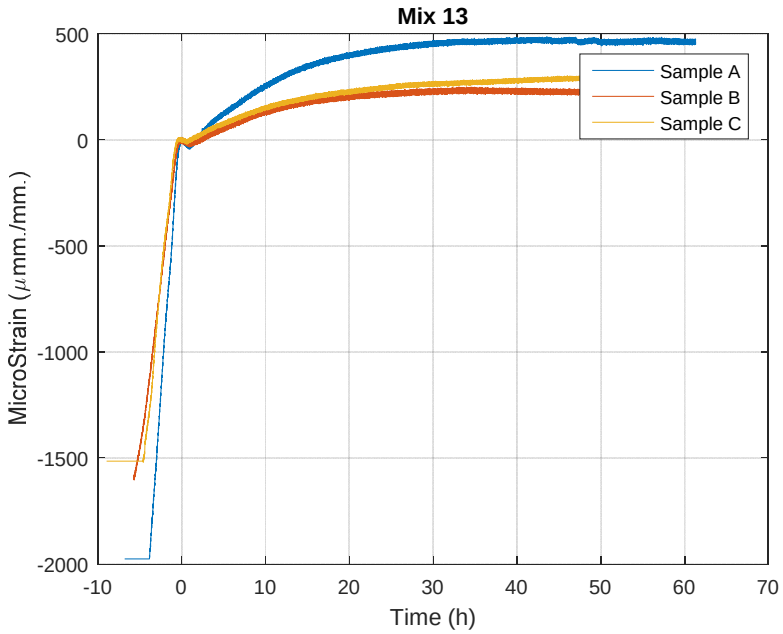

Figure 172: LVDT Strain 0.31 PC-III-A HR-P2 6.5 fl oz/100lb

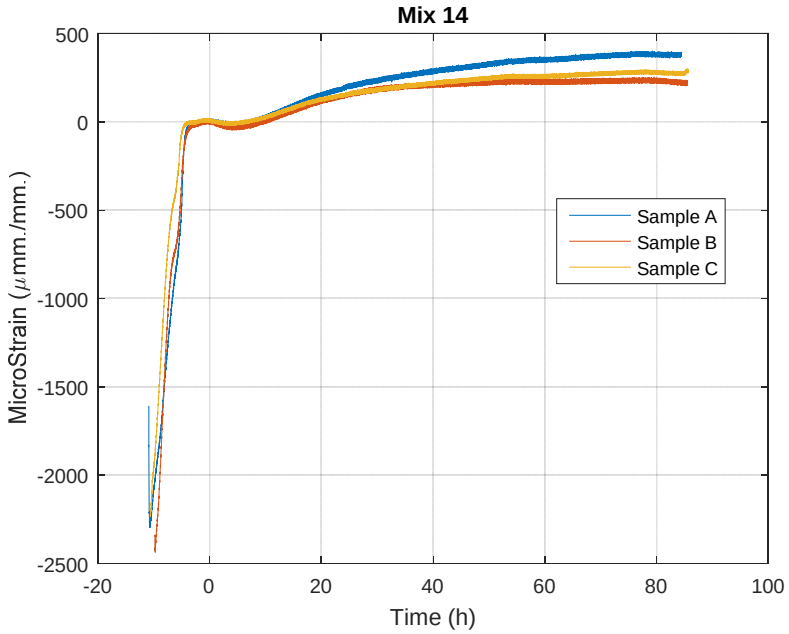

Figure 173: LVDT Strain 0.31 PC-III-A HR-P2 8.25 fl oz/100lb

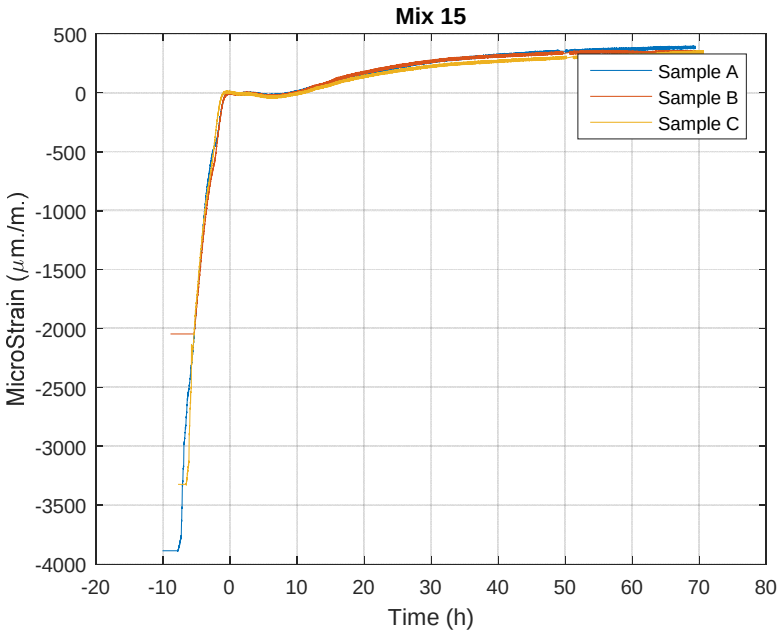

Figure 174: LVDT Strain 0.31 PC-III-A HR-P2 12 fl oz/100lb

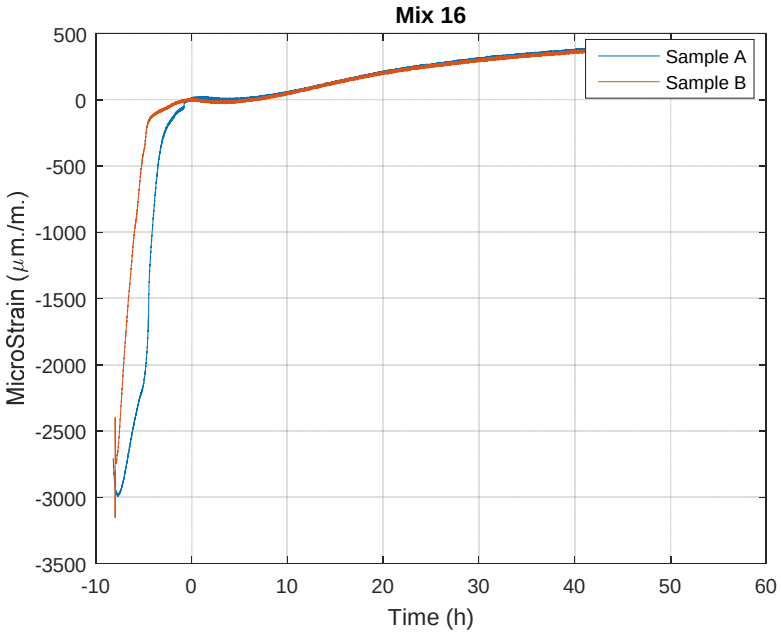

Figure 175: LVDT Strain 0.31 PC-III-A HR-P3 6.5 fl oz/100lb

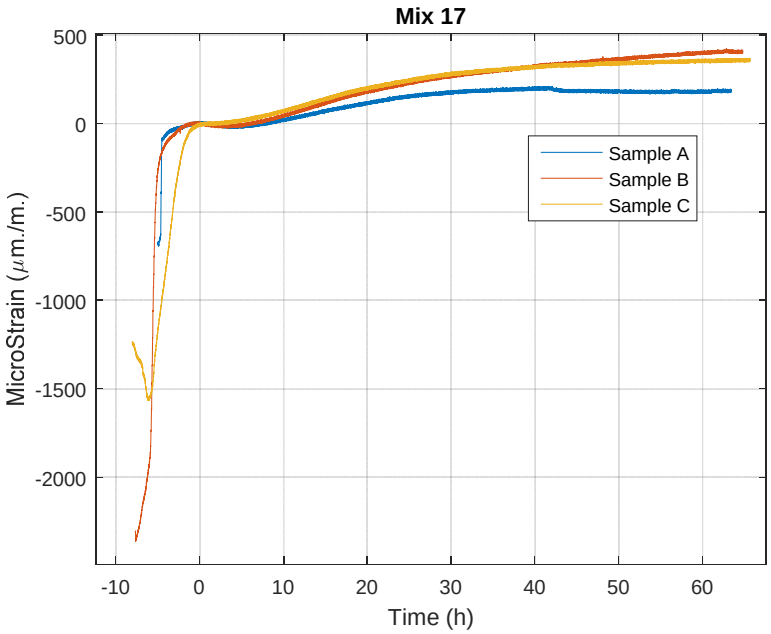

Figure 176: LVDT Strain 0.31 PC-III-A HR-P3 8.25 fl oz/100lb

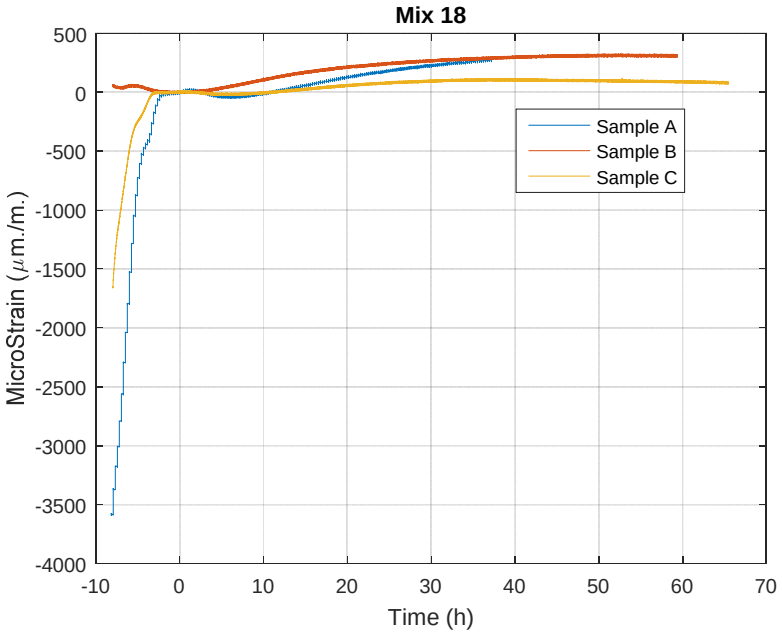

Figure 177: LVDT Strain 0.31 PC-III-A HR-P3 12 fl oz/100lb

Appendix X: UT Exposure Site Map

G-1		
w/cm:	0.28	9/20/15
PC-III-A:	705	lbs
Fly Ash:	-	lbs
CA/FA:	FA-R	CA-R
HR-P1	12.0	floz/100 lb
NR-1	3.0	cement

G-2		
w/cm:	0.28	2/27/15
PC-III-A:	705	lbs
Fly Ash:	-	lbs
CA/FA:	FA-R	CA-R
HR-P1	12.0	floz/100 lb
NR-1	3.0	cement

G-3		
w/cm:	0.28	1/26/15
PC-III-A:	705	lbs
Fly Ash:	-	lbs
CA/FA:	FA-R	CA-L
HR-P2	12.5	floz/100 lb
NR-1	3.0	cement

G-7		
w/cm:	0.24	2/19/15
PC-III-A:	705	lbs
Fly Ash:	-	lbs
CA/FA:	FA-R	CA-L
HR-P4	12.0	floz/100 lb
NR-2	3.0	cement

G-6		
w/cm:	0.28	3/19/15
PC-III-A:	705	lbs
Fly Ash:	-	lbs
CA/FA:	FA-R	CA-L
HR-P3	12.0	floz/100 lb
NR-2	3.0	cement

G-5		
w/cm:	0.28	2/27/15
PC-III-A:	705	lbs
Fly Ash:	-	lbs
CA/FA:	FA-R	CA-R
HR-P3	12.0	floz/100 lb
NR-2	3.0	cement

PP-A		
w/cm:	0.31	3/5/15
PC-III-A:	663	lbs
Fly Ash:	271	lbs
CA/FA:	FA-R	CA-R
HR-P4	5.5	floz/100 lb
NR-2	0.5	cement

G-8		
w/cm:	0.24	2/24/15
PC-III-A:	705	lbs
Fly Ash:	-	lbs
CA/FA:	FA-R	CA-R
HR-P2	15.0	floz/100 lb
NR-1	3.0	cement

PP-B LAB		
w/cm:	0.30	5/25/15
PC-III-A:	564	lbs
Fly Ash:	188	lbs
CA/FA:	FA-RII	CA-RII
HR-P3	8.0	floz/100 lb
NR-2	0.5	cement

PP-B		
w/cm:	0.30	3/12/15
PC-III-A:	564	lbs
Fly Ash:	188	lbs
CA/FA:	FA-RII	CA-RII
HR-P3	8.0	floz/100 lb
NR-2	2.0	cement

G-11		
w/cm:	0.28	5/26/15
PC-III-B:	705	lbs
Fly Ash:	-	lbs
CA/FA:	FA-R	CA-L
HR-P1	12.0	floz/100 lb
NR-1	3.0	cement

G-4		
w/cm:	0.28	1/27/15
PC-III-A:	705	lbs
Fly Ash:	-	lbs
CA/FA:	FA-R	CA-L
HR-P2	12.0	floz/100 lb
NR-1	3.0	cement

PP-A LAB NC		
w/cm:	0.26	6/9/15
PC-III-A:	705	lbs
Fly Ash:	-	lbs
CA/FA:	FA-R	CA-R
HR-P2	6.5	floz/100 lb
NR-1	3.0	cement

PP-A LAB SCC		
w/cm:	0.31	6/9/15
PC-III-A:	663	lbs
Fly Ash:	271	lbs
CA/FA:	FA-R	CA-R
HR-P2	5.5	floz/100 lb
NR-1	2.5	cement

Figure 178: UT Exposure Site Map (Blocks)

B-1		
w/cm:	0.28	9/20/15
PC-III-A:	705	lbs
Fly Ash:	-	lbs
CA/FA:	FA-R	CA-R
HR-P1	12.0	floz/100 lb
NR-1	3.0	cement

B2-A		
w/cm:	0.28	2/27/15
PC-III-A:	705	lbs
Fly Ash:	-	lbs
CA/FA:	FA-R	CA-R
HR-P1	12.5	floz/100 lb
NR-1	3.0	cement

B2-B		
w/cm:	0.28	2/27/15
PC-III-A:	705	lbs
Fly Ash:	-	lbs
CA/FA:	FA-R	CA-R
HR-P1	12.5	floz/100 lb
NR-1	3.0	cement

B-3		
w/cm:	0.24	1/26/15
PC-III-A:	705	lbs
Fly Ash:	-	lbs
CA/FA:	FA-R	CA-L
HR-P2	12.0	floz/100 lb
NR-1	3.0	cement

B-5		
w/cm:	0.28	2/27/15
PC-III-A:	705	lbs
Fly Ash:	-	lbs
CA/FA:	FA-R	CA-R
HR-P3	12.0	floz/100 lb
NR-2	3.0	cement

B-7		
w/cm:	0.24	2/19/15
PC-III-A:	705	lbs
Fly Ash:	-	lbs
CA/FA:	FA-R	CA-L
HR-P4	12.0	floz/100 lb
NR-2	3.0	cement

B-4		
w/cm:	0.28	1/27/15
PC-III-A:	705	lbs
Fly Ash:	-	lbs
CA/FA:	FA-R	CA-L
HR-P2	12.0	floz/100 lb
NR-1	3.0	cement

B-6		
w/cm:	0.28	3/19/15
PC-III-A:	705	lbs
Fly Ash:	-	lbs
CA/FA:	FA-R	CA-L
HR-P3	12.0	floz/100 lb
NR-2	3.0	cement

PP-A		
w/cm:	0.31	3/5/15
PC-III-A:	663	lbs
Fly Ash:	271	lbs
CA/FA:	FA-R	CA-R
HR-P4	5.5	floz/100 lb
NR-2	0.5	cement

B-8		
w/cm:	0.24	2/24/15
PC-III-A:	705	lbs
Fly Ash:	-	lbs
CA/FA:	FA-R	CA-R
HR-P3	15.0	floz/100 lb
NR-2	3.0	cement

PP-B LAB		
w/cm:	0.30	5/25/15
PC-III-A:	564	lbs
Fly Ash:	188	lbs
CA/FA:	FA-RII	CA-RII
HR-P3	8.0	floz/100 lb
NR-2	0.5	cement

PP-B-A		
w/cm:	0.30	3/12/15
PC-III-A:	564	lbs
Fly Ash:	188	lbs
CA/FA:	FA-RII	CA-RII
HR-P3	8.0	floz/100 lb
NR-2	2.0	cement

B-11		
w/cm:	0.28	5/26/15
PC-III-B:	705	lbs
Fly Ash:	-	lbs
CA/FA:	FA-R	CA-L
HR-P1	12.0	floz/100 lb
NR-1	3.0	cement

PP-B-B		
w/cm:	0.30	3/12/15
PC-III-A:	564	lbs
Fly Ash:	188	lbs
CA/FA:	FA-RII	CA-RII
HR-P3	8.0	floz/100 lb
NR-2	2.0	cement

PP-A LAB NC		
w/cm:	0.26	6/9/15
PC-III-A:	705	lbs
Fly Ash:	-	lbs
CA/FA:	FA-R	CA-R
HR-P2	6.5	floz/100 lb
NR-1	3.0	cement

PP-A LAB SCC		
w/cm:	0.31	6/9/15
PC-III-A:	663	lbs
Fly Ash:	271	lbs
CA/FA:	FA-R	CA-R
HR-P2	5.5	floz/100 lb
NR-1	2.5	cement

BP-1		
w/cm:	0.28	3/19/15
PC-III-A:	705	lbs
Fly Ash:	-	lbs
CA/FA:	FA-R	CA-L
HR-P3	12.0	floz/100 lb
NR-2	3.0	cement

BP-2		
w/cm:	0.33	9/20/15
PC-III-A:	658	lbs
Fly Ash:	-	lbs
CA/FA:	FA-R	CA-R
HR-P1	12.0	floz/100 lb
NR-1	3.0	cement

BP-3		
w/cm:	0.28	9/20/15
PC-I-A:	700	lbs
Fly Ash:	-	lbs
CA/FA:	FA-R	CA-R
HR-P1	12.0	floz/100 lb
NR-1	3.0	cement

BP-4		
w/cm:	0.30	9/20/15
PC-III-A:	564	lbs
Fly Ash:	188	lbs
CA/FA:	FA-R	CA-R
HR-P3	8.00	floz/100 lb
NR-2	2.0	cement

BP-5		
w/cm:	0.26	9/20/15
PC-III-A:	700	lbs
Fly Ash:	175	lbs
CA/FA:	FA-R	CA-R
HR-P2	8.25	floz/100 lb
NR-1	3.0	cement

BP-6		
w/cm:	0.26	9/20/15
PC-III-A:	700	lbs
Fly Ash:	175	lbs
CA/FA:	FA-R	CA-R
HR-P3	10.00	floz/100 lb
NR-2	3.0	cement

BP-7		
w/cm:	0.26	9/20/15
PC-III-B:	700	lbs
Fly Ash:	271	lbs
CA/FA:	FA-R	CA-R
HR-P1	8.25	floz/100 lb
NR-1	3.0	cement

BP-8		
w/cm:	0.31	9/20/15
PC-III-A:	663	lbs
Fly Ash:	271	lbs
CA/FA:	FA-R	CA-R
HR-P2	7.25	floz/100 lb
NR-2	2.5	cement

BP-9		
w/cm:	0.31	9/20/15
PC-III-A:	663	lbs
Fly Ash:	271	lbs
CA/FA:	FA-R	CA-R
HR-P3	7.25	floz/100 lb
NR-2	2.5	cement

BP-10		
w/cm:	0.31	9/20/15
PC-III-B:	663	lbs
Fly Ash:	271	lbs
CA/FA:	FA-R	CA-R
HR-P1	7.25	floz/100 lb
NR-1	2.5	cement

Figure 179: UT Exposure Site Map (Girders)

REFERENCES

Acker 2004 - Acker, P. "Swelling, Shrinkage and Creep: A Mechanical Approach to Cement Hydration." Mat. Struct. Materials and Structures 37.4 (2004): 237-43. Web.

Adam Neville symposium: Creep and Shrinkage – structural design effects, ACI SP-194, (2002)

Ai, Hua, J. Francis Young, and George W. Scherer. "Thermal expansion kinetics: method to measure permeability of cementitious materials: II, application to hardened cement pastes." Journal of the American Ceramic Society 84.2 (2001): 385-91.

Al-Fadhala, Manal, and Kenneth C. Hover. "Rapid evaporation from freshly cast concrete and the Gulf environment." Construction and Building Materials15.1 (2001): 1-7.

Almusallam, A. A., et al. "Effect of mixture proportions on plastic shrinkage cracking of concrete in hot environments." Construction and Building Materials 12.6 (1998): 353-358.

Altoubat, Salah A., and David A. Lange. "Creep, shrinkage, and cracking of restrained concrete at early age." ACI Materials Journal 98.4 (2001): 323-331.

ASTM C 192, Standard Practice for Making and Curing Concrete Test Specimens in the Laboratory, American Society of Testing and Materials, (2015)

ASTM C150, Standard Specification for Portland Cement, American Society of Testing and Materials, (2012).

ASTM C157, Standard Test Method for Length Change of Hardened Hydraulic-Cement Mortar and Concrete, American Society of Testing and Materials, (2008).

ASTM C1579, Standard Test Method for Evaluating Plastic Shrinkage Cracking of Restrained Fiber Reinforced Concrete (Using a Steel Form Insert), American Society of Testing and Materials, (2013).

ASTM C1581, Standard Test Method for Determining Age at Cracking and Induced Tensile Stress Characteristics of Mortar and Concrete under Restrained Shrinkage, (2009).

ASTM C1608, Standard Test Method for Chemical Shrinkage of Hydraulic Cement Paste, American Society of Testing and Materials, (2012).

ASTM C1679, Standard Practice for Measuring Hydration Kinetics of Hydraulic Cementitious Mixtures Using Isothermal Calorimetry, American Society of Testing and Materials, (2014).

ASTM C305, Standard Practice for Mechanical Mixing of Hydraulic Cement Pastes and Mortars of Plastic Consistency, American Society of Testing and Materials, (2014).

ASTM C33, Standard Specification for Concrete Aggregates, American Society of Testing and Materials, (2013).

ASTM C39, Standard Test Method for Compressive Strength of Cylindrical Concrete Specimens, American Society of Testing and Materials, (2014).

ASTM C403, Test Method for Time of Setting of Concrete Mixtures by Penetration Resistance, ASTM International, (2008).

ASTM C469, Standard Test Method for Static Modulus of Elasticity and Poisson's Ratio of Concrete in Compression, American Society of Testing and Materials, (2010).

ASTM C494, Standard Specification for Chemical Admixtures for Concrete, American Society of Testing and Materials, (2013).

ASTM C496, Standard Test Method for Splitting Tensile Strength of Cylindrical Concrete Specimens, American Society of Testing and Materials, (2011).

ASTM C511, Standard Specification for Mixing Rooms, Moist Cabinets, Moist Rooms, and Water Storage Tanks Used in the Testing of Hydraulic Cements and Concretes, American Society of Testing and Materials, (2013).

ASTM C618, Standard Specification for Coal Fly Ash and Raw or Calcined Natural Pozzolan for Use in Concrete, American Society of Testing and Materials, (2012).

Barcelo, Laurent, Micheline Moranville, and Bernard Clavaud. "Autogenous shrinkage of concrete: a balance between autogenous swelling and self-desiccation." Cement and Concrete Research 35.1 (2005): 177-183.

Bažant, Z. P. "Delayed thermal dilatations of cement paste and concrete due to mass transport." Nuclear Engineering and Design 14.2 (1970): 308-318.

Bazant, Zdenek P., and Yunping Xi. "Continuous retardation spectrum for solidification theory of concrete creep." Journal of Engineering Mechanics121.2 (1995): 281-288.

Bentur, A., and K. Kovler. "Evaluation of early age cracking characteristics in cementitious systems." Materials and Structures 36.3 (2003): 183-190.

Bentz, D. P., and W. J. Weiss. "REACT: reducing early-age cracking today."Concrete Plant International 3 (2008): 56-61.

Bentz, Dale P., and Ole Mejlhede Jensen. "Mitigation strategies for autogenous shrinkage cracking." Cement and Concrete Composites 26.6 (2004): 677-685.

Bisschop and van Mier 2002 Bisschop, J & Mier, JGM van (2002). Drying shrinkage microcracking in concrete. Heron, 47(3), 163-184.

Bouasker, Marwen, et al. "Chemical shrinkage of cement pastes and mortars at very early age: effect of limestone filler and granular inclusions." Cement and Concrete Composites 30.1 (2008): 13-22.

Cohen, Menashi D., Jan Olek, and William L. Dolch. "Mechanism of plastic shrinkage cracking in portland cement and portland cement-silica fume paste and mortar." Cement and Concrete Research 20.1 (1990): 103-119.

"Concrete Rated Source Quality Catalog." (2016): n. pag.Ftp://ftp.dot.state.tx.us/pub/txdot-info/cmd/mpl/crsqc.pdf. TxDot Construction Division – Materials & Pavements (CST-M&P). Web.

Czernin, Wolfgang. Zementchemie für Bauingenieure. Bau-Verlag, 1977.

Dao, V. T. N., et al. "Plastic shrinkage cracking of concrete." Australian Journal of Structural Engineering 10.3 (2010): 207-214.

Davis H.E. (1940) Autogenous Volume Change of Concrete, Proceedings of the 43rd Annual American Society for Testing Materials, Atlantic City, N.J., June, pp. 1103-1113

Dela Two-dimensional analysis of crack formation around aggregates in high-shrinkage cement paste Birgitte Friis Dela*, Henrik Stang

Dela, Birgitte Friis, and Henrik Stang. "Two-dimensional analysis of crack formation around aggregates in high-shrinkage cement paste." Engineering Fracture Mechanics 65.2 (2000): 149-164.

Douglas KS, Hover KC (2002) Measuring non-drying bulk shrinkage of cement paste and mortar using Archimedes' principle: Part I. In: Jensen OM, Bentz DP, Lura P (eds) Autogenous deformation of con- crete, ACI SP 220, American Concrete Institute, Farmington Hills, Michigan, pp 39–51

Gao, Peng, et al. "Improvement of autogenous shrinkage measurement for cement paste at very early age: Corrugated tube method using non-contact sensors." Construction and Building Materials 55 (2014): 57-62.

Grube, H. Causes of shrinkage of concrete and its effect on concrete structures (In German). Dusseldorf 1991.

Hammer, Tor Ame, O. Bjontegaard, and E. Sellevold. "Measurement methods for testing of early age autogenous strain." RILEM Proceedings of Conference on Early Age Cracking in Cementitious Systems EAC. Vol. 1. 2002.

Hewlett, P. C. Lea's Chemistry of Cmenet and Concrete . 4th Edition. St. Edmundsbury Pres Ltd. , 1998.

Holt, E., and M. Leivo. "Cracking risks associated with early age shrinkage."Cement and Concrete Composites 26.5 (2004): 521-530.

Holt, Erika E. Early age autogenous shrinkage of concrete. Vol. 446. Technical Research Centre of Finland, 2001.

Hossain, Akhter, Brad Pease, and Jason Weiss. "Quantifying early-age stress development and cracking in low water-to-cement concrete: restrained-ring test with acoustic emission." Transportation Research Record: Journal of the Transportation Research Board 1834 (2003): 24-32.

Houst , Y. F. , and F. H. Wittmann. "Depth profileso of carbonate formed during natural carbonation ." Cement and Concrete Research (Pergamon press) 32 (2002): 1923-1930.

Jensen, O. Mejlhede, and P. Freiesleben Hansen. "A dilatometer for measuring autogenous deformation in hardening Portland cement paste."Materials and structures 28.7 (1995): 406-409.

Jensen, O.M., Hansen, P.F.: Autogenous deformation and RH-change in per- spective. In: Cement and Concrete Research 31 (2001), pp. 1859-1865

Jensen, Ole Mejlhede, and Per Freiesleben Hansen. "Autogenous deformation and RH-change in perspective." Cement and Concrete Research31.12 (2001): 1859-1865.

Khunthongkeaw, Jittbodee, Somnuk Tangtermsirikul, and Thatchavee Leelawat. "A study on carbonation depth prediction for fly ash concrete."Construction and Building Materials 20.9 (2006): 744-753.

Kosmatka, S. K. (2008). Design and Control of Concrete Mixtures. Skokie, IL: Portland Cement Association.

Kovler, K. "Testing system for determining the mechanical behaviour of early age concrete under restrained and free uniaxial shrinkage." Materials and Structures 27.6 (1994): 324-330.

Kovler, Konstantin. "Interdependence of creep and shrinkage for concrete under tension." Journal of materials in civil engineering 7.2 (1995): 96-101.

Kronlof, A., Leivo, M., and Sipari, P., (1995), “Experiment study on the basic phenomena of shrinkage and cracking of fresh Mortar”, Cement and Concrete Research, Vol. 25, No.9. pp. 1747-1754.

Kropp et al. 1995 – Kropp, j. And Hilsdorf, H.K. (eds.). 1995: Performance Criteria for Concrete Durability – State of the art Report Prepared by RILEM Report 12, E & F N Spon, Longdon, U.K., (pp Rilem, Paris), 341 pp.

Kwak, H-G., and S-J. Ha. "Plastic shrinkage cracking in concrete slabs. Part I: a numerical model." Magazine of Concrete Research 58.8 (2006): 505-516.

Lam, L., and J. G. Teng. "Ultimate condition of fiber reinforced polymer-confined concrete." Journal of Composites for Construction 8.6 (2004): 539-548.

Le Chatelier, H. "Sur les changements de volume qui accompagnent le durcissement des ciments." Bulletin Societe de l’encouragement pour l’industrie nationale 5 (1900).

Locher, F.W.: Zement - Grundlagen der Herstellung und Verwendung. Düsseldorf, Germany, Verlag Bau und Technik 2000. English: Cement – Principles of production and use. Düsseldorf, Germany, 2006

Lura & Bisschop 2004). - Acker, P. "Swelling, Shrinkage and Creep: A Mechanical Approach to Cement Hydration." Mat. Struct. Materials and Structures 37.4 (2004): 237-43. Web.

Lura, Pietro, and Ole Mejlhede Jensen. Volumetric Measurement in Water Bath-An Inappropriate Method to Measure Autogenous Strain of Cement Paste. No. PCA R&D Serial No. 2925. 2005.

Lura, Pietro, Ole Mejlhede Jensen, and Jason Weiss. "Cracking in cement paste induced by autogenous shrinkage." Materials and structures 42.8 (2009): 1089-1099.

Lura, Pietro, Ole Mejlhede Jensen, and Klaas van Breugel. "Autogenous shrinkage in high-performance cement paste: an evaluation of basic mechanisms." Cement and Concrete Research 33.2 (2003): 223-232.

Lynam, C. G. "Growth and Movement in Portland Cement Paste Concrete, London." (1934): 139.

M. Won, Improvements of Testing Procedures for Concrete Coefficient of Thermal Expansion, Transportation Research Record: Journal of the Transportation Research Board No. 1919, (2005).

Meeks, Corey Franklin. "Implementation of ConcreteWorks software in Texas highway construction." (2011).

Mora-Ruacho, José, Ravindra Gettu, and Antonio Aguado. "Influence of shrinkage-reducing admixtures on the reduction of plastic shrinkage cracking in concrete." Cement and Concrete Research 39.3 (2009): 141-146.

P.K Mehta, P.J.M Monteiro, Concrete: Structure, Properties and Materials, Third Edition, McGraw-Hill, (2006).

Pease, B., Adam Neuwald, and W. J. Weiss. "The influence of aggregates on early age cracking in cementitious systems." Celebrating concrete: role of concrete in sustainable development, International symposium dedicated to Prof. S. Shah, Northwestern University. 2003.

Pease, B., Neuwald, A., and Weiss, W. J., The Influence of Aggregates on Early Age Cracking in Cementitious Systems, Celebrating Concrete: Role of Concrete in Sustainable Development, An International Sympoium dedicated to Professor Surendra Shah, Northwestern University, pp. 329~338, (September 2003)

Persson, Bertil. "Experimental studies on shrinkage of high-performance concrete." Cement and Concrete Research 28.7 (1998): 1023-1036.

Plastic Cracking in Concrete," Technical Information Letter No. 171-NRMCA, Modern Concrete, Oct. 1960, pp. 63-64.

Plastic Cracking in Concrete," Technical Information Letter No. 171-NRMCA, Modern Concrete, Oct. 1960, pp. 63-64.

Powers, T. C. "The thermodynamics of volume change and creep." Matériaux et Construction 1.6 (1968): 487-507.

Powers, T. C. "TL Brownyard Proc. Am. Concrete Institute, 43 (1946–1947)."Proc. Am. Concrete Institute 43 (1946): 149.

Powers, T. C., and T. L. Brownyard. "Studies of the physical properties of hardened Portland cement paste." Bulletin 22 (1946).

Qi, Chengqing, Jason Weiss, and Jan Olek. "Characterization of plastic shrinkage cracking in fiber reinforced concrete using image analysis and a modified Weibull function." Materials and Structures 36.6 (2003): 386-395.

Radjy, Fariborz, Erik J. Sellevold, and Kurt Kielsgaard Hansen. Isoteric vapor pressure: temperature data for water sorption in hardened cement paste: enthalpy, entropy and sorption isotherms at different temperatures. 2003.

Radocea, A. "A model of plastic shrinkage." Magazine of Concrete Research46.167 (1994): 125-132.

Radocea, Adrian. "A new method for studying bleeding of cement paste."Cement and concrete research 22.5 (1992): 855-868.

Roziere, E., A. Loukili, and F. Cussigh. "A performance based approach for durability of concrete exposed to carbonation ." Construction ad Building Materials (Elsevier Ltd.) 23 (2009): 190-199.

Sant, G. L. (2006). A Discusssion of Analysis Approaches for Determining 'Time-zero' from Chemical Shrinakge and Autogenous Strain Measurments in Cement Paste. International Rilem Conference on Volume Changes of Hardening Concrete: Testing and Mitigation (p. 9). Lyngby, Denmark: RILEM.

Sant, G. L. (2006). Measurement of Volume Change in Cementitious Materials at Early Ages. Transportation Research Record, 21-29.

Sant, L. a. (2006). Measurement of Volume Change in Cementitious Materials at Early-ages Review of Testing Protocols and Interpretation of Results. Transportation Research Record: Journal of the Transportation Research Board, 21-29.

Scherer, George W. "Thermal expansion kinetics: method to measure permeability of cementitious materials: I, theory." Journal of the American Ceramic Society 83.11 (2000): 2753-2761.

See HT, Attiogbe EK, Miltenberger MA. Potential for restrained shrinkage cracking of concrete and mortar. In: Proceedings of the ASTM symposium on early-age cracking of concrete, December 2003.

Sellevold, E. J., and Ø. Bjøntegaard. "Coefficient of thermal expansion of cement paste and concrete: Mechanisms of moisture interaction." Materials and Structures 39.9 (2006): 809-815.

Sellevold, E., et al. "High performance concrete: early volume change and cracking tendency." RILEM PROCEEDINGS. CHAPMAN & HALL, 1995.

Shaeles, Christos A., and Kenneth C. Hover. "Influence of mixture proportions and construction operations on plastic shrinkage cracking in thin slabs." ACI Materials Journal 85.6 (1988): 495-504.

Simpkins, P.G., Johnson, D.W., and Fleming, D.A., "Drying Behavior of Colloidal Silica 2 Gels," Journal of the American Ceramic Society, V. 72, No. 10, 1986, pp. 1816-1821.

Slowik, Volker, Markus Schmidt, and Roberto Fritzsch. "Capillary pressure in fresh cement-based materials and identification of the air entry value."Cement and Concrete composites 30.7 (2008): 557-565.

Tazawa, E. "Autoshrink'98." Proc. of the Int. Workshop on Autogenous Shrinkage of Concrete. 1998.

Tazawa, E. And Miyazawa, S. (1992) Autogenous shrinkage of cement paste with condensed silica fume, Proceedings of the 4th CANMET/ACI International Conference on Fly Ash, Silica Fume, Slag and Natural Pozzolans in Concrete, ACI, pp.875-894.

Tazawa, Eiichi. Autogenous Shrinkage of Concrete: Proceedings of the International Workshop, Organized by JCI (Japan Concrete Institute), Hiroshima, June 13-14, 1998. New York: Routledge, 1999. Print.

Thomas, M. D. A., and J. D. Matthews. "Carbonation of fly ash concrete."Magazine of Concrete Research 44.160 (1992): 217-228.

Tian, Qian, and Ole Mejlhede Jensen. "Measuring autogenous strain of concrete with corrugated moulds." Microstructure related durability of cementitious composites (2008): 1501-1511.

Tiburzi, Nicolás Bruno. Evaluation of Volume Changes and Cracking Potential of Low Water-to-cementitious Material Ratio Concrete Mixtures. Thesis. University of Texas at Austin, 2015. N.p.: n.p., n.d. UT Electronic Theses and Dissertations. Web.

Weiss, William Jason. Prediction of early-age shrinkage cracking in concrete elements. 1999.

Weyers, R. E., J. C. Conway, and P. D. Cady. "Photoelastic analysis of rigid inclusions in fresh concrete." Cement and Concrete Research 12.4 (1982): 475-484.

Wittmann, F. H. "On the action of capillary pressure in fresh concrete."Cement and Concrete Research 6.1 (1976): 49-56.

Young, J. Francis, Sidney Mindess, and David Darwin. Concrete. Prentice Hall, 2002.

Zou, Dinghua, and Jason Weiss. "Early age cracking behavior of internally cured mortar restrained by dual rings with different thickness." Construction and Building Materials 66 (2014): 146-153.

12390, CEN/TS. Determination of the Relative Carbonation Resistance of Concrete. 2008.